University of Reading

Attenuation of myostatin/activin signalling delays skeletal muscle ageing signs in a progeric mouse model

Khalid Alyodawi

Thesis submitted for the degree of Doctor of Philosophy

School of Biological Sciences

July 2019

Declaration

I confirm that this is my own work and the use of all material from other sources has been properly and fully acknowledged.

Khalid Alyodawi

Acknowledgement

I want to express my praises and thanks to God for the blessings and give me the ability to complete this work. Then, I would like to give my sincere thanks and gratitude to my supervisor Professor Ketan Patel for giving me this opportunity to do staying PhD and providing invaluable guidance throughout this project. Sincere gratitude for his motivation, encouragement and guidance in all the time of research and writing of this thesis. It was a great privilege and honour to work and study under his supervision. I am incredibly grateful for what he has offered me. My thanks to my sponsor, the Higher Committee for Education Development in Iraq (HCED), for their generous funding for this project. I would also like to send special thanks to Dr. Antonios Matsakas, who helped me a lot and showed me the stunning techniques. I am also grateful for my colleagues Dr. Henry Collins-Hooper and Dr. Robert Mitchell, Dr. Taryn Morash. Dr. Ben Mellows and Danielle Vaughan for the willing to help me with anything. I am very appreciative of the support that was provided by the team that Professor Ketan Patel had around during my PhD. A massive thank you to the following people, Dr. Wilbert Vermeij (Erasmus University, Netherland), Dr. Oliver Kretz (University of Freiburg, Germany), for their collaboration to complete this research work. I am extremely grateful to my parents for their love, prayers, and sacrifices for educating me. I would also like to say a huge thank you to my brothers and sisters for their constant support and encouragement. I am very much thankful to my family (my wife and my kids) for their love, patience, care and continuing support during my PhD. My Special thanks go to my friends Moafaq Samir and Saleh Omairi for their constant support and encouragement.

Abstract

Accumulation of DNA damage with age induces a stress response that shifts cellular resources from growth towards maintenance. A mouse model with defects in DNA damage repair, *Ercc1*$^{\Delta/-}$, has noticeable growth retardation and multisystemic ageing signs. Skeletal muscle wasting, locomotor activity and reduce muscle strength are the most apparent signs of accelerated ageing in this model. Using anti myostatin as a strategy in health and disease condition offer a unique approach to increase muscle mass or prevent muscle loss. However, it might be a conflict with the output of stress response in the aged and progeric muscle.

The hypothesis that we tested here is the maintenance of skeletal muscle growth through attenuation of myostatin/activin signalling in progeric *Ercc1*$^{\Delta/-}$ mice could counteract the effect of DNA damage and stress response and delay signs of ageing.

Eight weeks old male mice FVB/C57/Bl6, before the development of progeric features were injected intraperitoneally with sActRIIB. Animal weights were measured weekly. Life was even terminated at 16 weeks before the onset of premature death or animals leaves until the end of life in life span cohort.

As a result of myostatin (Mstn) antagonism, there was an increase in body mass in *Ercc1* $^{\Delta/-}$ and *Ercc1*$^{+/+}$ mice. All muscles were heavier in treated progeric and control mice. Muscle mass increase due to increase in CSA of all types of fibres. Antagonism of Mstn attenuates the decline in locomotor activity and muscle strength in progeric mice. However, there was a reduction in activity and strength in control treated mice. Antagonism of Mstn attenuates fibre damage and promotes fibre survival in progeric mice. Supra-normalisation of mechanical force transduction apparatus of progeric muscle by sActRIIB. Partial normalisation of progeric muscle stem cells by sActRIIB was noted.

The main findings of this study are the *Ercc1*$^{\Delta/-}$ progeric mouse model shows many features of naturally aged mice in term of sarcopenia. These characteristics were attenuated through the antagonism of Myostatin/Activin signalling, even with a persistent defect in DNA damage repair system. The enhancements were at the level of locomotor activity, muscle strength and delayed parameters of neurodegeneration.

List of abbreviations

4E-BP1	4E-binding protein 1
ACh	Acetylcholine
ActRIIB	Activin A receptor type IIB
ADP	Adenosine diphosphate
AIDS	Acquired immune deficiency syndrome
AKT	Protein kinase B
ALK	Activin receptor-like kinase
AMPK	Adenosine monophosphate kinase
ANOVA	Analysis of Variance
AOE	Antioxidant enzyme
Atg12	Autophagy-related protein 12
ATP	Adenosine Triphosphate
ATPase	Adenosine triphosphatase enzyme
BB	Biceps brachii
BDNF	Brain-derived neurotrophic factor
BMD	Becker muscular dystrophy
BMP4	Bone morphogenic protein-4.
BMRs	Basal metabolic rates
CAT	Catalase
CD31	Cluster of differentiation 31
Cdk2	Cyclin-dependent kinase2
CDK2	Cyclin-dependent kinase 2
cDNA	Complementary DNA
CP	Creatine phosphatase
CR	Caloric restriction
CS	Cockayne syndrome
CSA	Cross-sectional area
DAPI	4, 6-diamidino-2-phenylindole.
DDR	DNA damage response
DGC	Dystrophin-glycoprotein complex

DHE	Dihydroethidium
DMD	Duchene muscular dystrophy
DMEM	Dulbecco's Modified Eagle Medium
DML	Dorsomedial lips
dNTP	Deoxyribonucleotide triphosphate
DR	Dietary restriction
DSB	DNA double-strand break
DSHB	Developmental studies Hybridoma bank
dT	Deoxythymine
ECM	Extracellular matrix
ECRL	Extensor carpi radialis longus
EDL	Extensor Digitorum Longus
ERCC1	Excision repair complementary complex1
Errγ	Estrogen-related receptor gamma
ETC	Electron transport chain
FBS	Foetal bovine serum
FGF	Fibroblast growth factors
FoxO	Forkhead box O
FSTL-1	Follistatin-like-1
FVB/C57/Bl6	Friends virus B/ C57 black 6 (mixed background mice)
GABARAP	γ-aminobutyric-acid-type-A-receptor-associated protein
GATE16	Golgi-associated ATPase enhancer of 16 kDa
GF	Growth factor
GH	Growth hormone
H&E	Haematoxylin and eosin
H_2O_2	Hydrogen peroxide
HA	Hyaluronic acid
HGF	Hepatocyte growth factor
HGF/SF	Hepatocyte growth factor/scatter factor
HGPS	Hutchinson-Gilford progeria syndrome
HPRT	Hypoxanthine Phosphoribosyltransferase

ICL	Interstrand crosslink
IGF	Insulin-like growth factor
IL-6	Interleukin-6
IL-7	Interleukin-7
IP	Intraperitoneal
L530P	Leucine at residue 530
LC3B	Microtubule-associated protein 1 light chain 3B
LIF	Leukaemia inhibitory factor
LMNA	Lamin A
LN2	Liquid nitrogen
MHC	Myosin heavy chain
MMP	Matrix metalloproteinase
MPCs	Myogenic precursor cells
MRFs	Myogenic regulation factors
Msx1	Msh homeobox
mTOR	Mechanistic target of rapamycin
MuRF	Muscle RING finger
Myf	Myogenic determination factors
MyoD	Myogenic Differentiation Antigen
NBT	Nitro blue tetrazolium
N-CAM	Neural cell adhesion molecule
NER	Nucleotide excision repair
NMJ	Neuromuscular junction
nNOS	Neuronal nitric oxide synthase
NO	Nitric oxide
OCR	Oxygen consumption rate
OCT	Optimal Cutting Temperature compound
Pax3	Paired box3
Pax7	Paired box7
PBS	Phosphate buffer saline
PCR	Polymerase chain reaction

PFA	Paraformaldehyde
PGC-1α	Peroxisome proliferator-activated receptor gamma coactivator 1-alpha
PI3K	Phosphoinositide 3-kinase
qPCR	Quantitative polymerase chain reaction
ROS	Reactive oxygen species
sActRIIB	Soluble activin receptor type IIB
SDH	Succinate dehydrogenase
SEM	Scanning electron microscopy
SFCM	Single Fibre Culture Medium
Shh	Sonic hedgehog
SMAD2	Mothers against decapentaplegic 2
SMAD3	Mothers against decapentaplegic 3
SOD	Superoxide dismutase
TA	Tibialis Anterior
TEM	Transmission electron microscopy
TGF-β	Transforming Growth Factor-beta
TNF-α	Tumour necrosis factor alpha
TTD	Trichothiodystrophy
Ub	Ubiquitin
UPP	Ubiquitin-proteasome pathway
UPR^{ER}	Endoplasmic reticulum Unfolded Protein Response
UPR^{MT}	Mitochondrial Unfolded Protein Response
UV	Ultraviolet
VEGF	Vascular endothelial growth factor
VLL	Ventrolateral lips
WRN	Warner protein
WRS	Wiedemann-Rautenstrauch Syndrome
WS	Werner syndrome
WT	Wild type
XP	Xeroderma pigmentosum
Zmpste24	Zinc metalloproteinase STE24

Contents

Figures

Chapter 1

General Introduction

1.1. Muscle tissue

Muscular tissue is formed from subunits, myocytes, and their structure and arrangement define the muscle type. Diversity of muscle tissue includes, smooth, cardiac and skeletal muscle (Clark, 2005) represent one of primary four types of living body tissues together with epithelial, connective and nervous tissues. Skeletal and cardiac muscle are distinguished from smooth muscle tissue by posses of striation of fibres and named after this striation (Pocock et al., 2004). Each type of these three muscles tissue has its unique features that fit their function and therefore, location. Cardiac muscle forms the heart, and smooth muscle is considered as a lining for hollow organs and blood vessels (Campbell et al., 2008). Skeletal muscle named after it attaches to the skeleton and its voluntary contraction result in body movement and stability. However, movement is not its only the function. Skeletal muscles is considered as an energy reservoir and regulatory organ for myokines production. The skeletal muscle will be the focus organ for investigation in this project.

1.1.1 Skeletal muscle

Skeletal muscles represent 40-50% of the total body mass; therefore, consider the most abundant tissue in the human body (Janssen et al., 1985). The skeletal muscles differ in size, shape, attachments, and relative proportions of myosin isoform. They can produce different movements such as a fine movement of the eye by extraocular muscle and gross movement in large muscles such as the thighs quadriceps (Gray et al., 1995). The shape of the skeletal muscles is also very variant, the orbicularis oculi are circular, while the Sartorius that extends along the thigh length is straight. Skeletal muscle performs a wide range of different functions across the body.

The main functions of skeletal muscle include 1. It maintains posture and body position. 2. Their contraction transduced to the skeleton and permits movement through force generation. 3. It provides support to the soft tissues, for example, the muscles of the abdominal wall and pelvic floor. 4. Guards entrances and exits of the mammalian body orifices. 5. Functions as a vital amino acid store and maintains core body temperature through heat production, via the critical role played in metabolism (MacIntosh et al., 2006).

1.1.2 Skeletal muscle formation

1.1.2.1 Embryonic origin of Skeletal muscle

Myogenesis of skeletal muscle is a critical way to understand the restriction of cell fate during embryonic, fetal and post-natal development. Skeletal muscle develops in sequential but overlapping stages (Pedersen et al., 2000). The origin of body muscles is paraxial mesoderm layer, and it arises from segmented structures called somites. Primordial muscle precursor cells differentiate after receiving signals from the adjacent tissues and become committed in a myogenic fate (Borycki and Emerson, 2000). The somite then divides into ventromedial and dorsolateral portions. The ventromedial part forms cartilage of the vertebrae and ribs. The muscle progenitor cells differentiate from dermomyotome, the dorsolateral portion of the somite that is facing the surface ectoderm. The dermomyotome also gives rise to cells of the endothelial, vascular smooth muscles, dermal and brown fat lineages. Dermomyotome also gives rise a muscle of diaphragm and tongue (Tajbakhsh and Buckingham, 2000, Biressi et al., 2007). The dermomyotome is further subdivided into two cell populations, medial and lateral parts that giving rise to the epaxial and hypaxial muscles (Pedersen et al., 2000). However, ocular, mandibular and superficial facial muscles all originate from unsegmented head of mesoderm and prechordal mesoderm (Brand-Saberi and Christ, 2000).

A population of differentiated muscle cells originating from dermomyotomal progenitor responding to signals from adjacent tissues (Tajbakhsh and Buckingham, 2000). Then differentiated cells align and fuse to form the mature multinucleated myotubes. However, a population of undifferentiated cells remained quiescent, to form a resident stem cell and termed as the satellite cells (Seale and Rudnicki, 2000). Differentiation of muscle cells is accomplished by the transcriptional activation of muscle-specific genes encoding for metabolic enzymes, ion channels, neurotransmitter receptors and contractile proteins (Hastings and Emerson, 1982).

The differentiation of skeletal muscle needs to express myogenic determination factors, such as myogenic determination factors Myf5 and Mrf4 (Bajanca et al., 2006). During disintegration the epithelial cells in the central part of mature dermomyotome express Paired box3 (Pax3) and its paralogue Paired box7 (Pax7) (Manceau et al., 2005). These cells

proliferate and do not express myogenic regulatory factors and muscle protein. However, as a result of activation of the myogenic determination factor 5 (Myf5) and myogenic differentiation (MyoD), they can lead to subsequent differentiation of the skeletal muscle (Zammit et al., 2006). Most of the body muscles are derived from highly proliferative Pax3+/Pax7+ cells that derived from the central dermomyotome (Relaix et al., 2005, Gros et al., 2005, Kassar-Duchossoy et al., 2005). The progenitor cells with Pax3+/ Pax7+ profile are able of both proliferation/self-renewal and differentiation along the skeletal muscle lineage (Kang and Krauss, 2010).

1.1.2.2 Satellite cells and muscle regeneration

Earliest electron microscope study described satellite cell as a resident cells located beneath the basal lamina of skeletal muscle fibre (Mauro, 1961) and later considered these cells as a stem cell for its ability to behave as myoblast (Reznik, 1969). Satellite cells are quiescent and have small nuclei compared to adjusting tissue; however, have high nuclear-to-cytoplasm ratio, and upon injury, they appear as a swell on myofibres surface (Schultz and McCormick, 1994). Satellite cells incubated with myofibres extract have more myogenic response compared to cells incubated with serum-containing media, suggested an essential role myofibre to initiate satellite cells activation response, which gives evidence of the vital role of niche environment in regulating satellite cells behaviour (Bischoff, 1990).

A member of the Paired Box family of transcriptional factors Pax3 and Pax7 have an essential role in controlling satellite cell behaviour (Bopp et al., 1986, Goulding et al., 1991). Pax 3 is essential for myoblast migration (Goulding et al., 1994, Epstein et al., 1996) and regulating precursor cells to enter the myogenic lineage via acting upstream of the myogenic regulating factor MyoD (Tajbakhsh et al., 1997). Pax7 is essential for its role in embryogenesis and postnatal in satellite cells lineage specification, as well as renewal and propagation (Seale and Rudnicki, 2000, Oustanina et al., 2004). In response to myogenin, Pax7 is downregulated in order to allow muscle cells differentiation to proceed (Olguin et al., 2007).

The process of regeneration in damaged skeletal muscle fibres is reliant on satellite cells (Moss and Leblond, 1971). Proliferating satellite cells provide both replace damaged fibres

and repopulate its cell pool by self-renewal ability (Collins et al., 2005). Two possible scenarios provide a pool of satellite cell, first, a subpopulation of satellite cells progression down the myogenic lineage and revert to the quiescent state, or, second, the proliferated cells produce two daughters, one for myogenic lineage and others for maintaining stem cell pool (Zammit et al., 2004, Kuang et al., 2008). Satellite cells activated following muscle injury then most of the activated cells switch on the expression of the myogenic regulating factor MyoD, and after that differentiate to repair myofibres damage (Cornelison and Wold, 1997, Zammit et al., 2004).

1.1.2.3. Limb muscle formation

Cells from somites at the levels of forelimbs and hindlimbs undergo an epithelial-to-mesenchymal transition (Brand-Saberi et al., 1993). These cells migrate to their final destination, in the limb, through the action of c-Met (tyrosine kinase receptor) which interact with their ligand, Hepatocyte Growth Factor-1 (HGF-1) (Dietrich et al., 1999). C-met transcription depends on the presence of Paired box3 (Pax3) transcriptional factor (Epstein et al., 1996), and the work of Tajbakhsh group (Tajbakhsh et al., 1997) show the precise relation between Pax3 and migration of myoblast cells. They found that a Pax3 mutant mouse has no limb muscle. Also, Schäfer & Braun defined other factors that affect migration using mutant mice for Lbx1, and the result was the progenitor cells delaminate from somite but do not migrate to the limb (Schäfer and Braun, 1999).

Expression of *MyoD* and Myogenic determination factors (*Myf5*) in the cells that migrate from somite is activated when they reach the final destination in the limbs (Tajbakhsh and Buckingham, 1994). These two genes play a critical role in cell cycle regulation. Thus it is essential in cell proliferation and the maintenance of this either by Pax3 directly or by c-met activation (Buckingham et al., 2003). Houzelstein et al. (Houzelstein et al., 1999) suggest that Msh homeobox 1(Msx1) a homeobox protein, plays a role in proliferation; it keeps the myoblast continually dividing. Odelberg (Odelberg et al., 2000) found that its overexpression restored the ability of proliferation to differentiated cells. Fibroblast growth factors (FGF) family through their receptors also have been implicated in myoblast proliferation in the limb (Edom-Vovard et al., 2001).

Migrating myogenic precursor cells arrange themselves as a dorsal and ventral masses when they reach the limb mesenchyme (Christ et al., 1977) and the muscle pattern is regulated by signals from the mesoderm of the limb bud (Grim and Wachtler, 1991). Growth in muscles results from a balance between proliferation and differentiation (Amthor et al., 1999). Muscle growth and an increase in size are stimulated by increased proliferation rate of muscle precursor cells (Füchtbauer, 2002). Growth is controlled by the action of factors such as FGFs, IGFI (insulin-like growth factor), BMPs (Amthor et al., 1999, Floss et al., 1997, Barton-Davis et al., 1998). In contrast, reducing muscle mass is achieved by factors such as Noggin and Twist (Fuchtbauer, 1995, Amthor et al., 1999). Furthermore, another critical pathway that inhibits muscle differentiation is the Notch axis by promoting continued expression of Myf5 and Pax3 and the down-regulation of MyoD (Delfini et al., 2000) as well as Hepatocyte growth factor/scatter factor (HGF/SF) pathway (Scaal et al., 1999). Myostatin also regulates myogenesis and decreases the number of skeletal muscle cells (McPherron et al., 1997).

Muscle fibres are formed by the fusion of myoblasts (Stockdale and Holtzer, 1961). These multinucleated fibres express specific myosin heavy chain (MHC) (Ontell et al., 1993). There are many types of MHC and can be classified into Iβ, α, extra-ocular, neonatal, embryonic, IIA, IIX, IIM, and IIB which are expressed from a large genes family (Weiss and Leinwand, 1996). The myoblasts will express MyoD and begin to fuse in the limb buds into small primary fibres through the action of surface molecules, which mediate cell-cell recognition such as a neural cell adhesion molecule, N-CAM, and M-cadherin (Arnold and Braun, 2000). M-cadherin mediates terminal differentiation and fusion of myoblasts during morphogenesis and formation of myotube is mediated by N-CAM (Ishido et al., 2006). The most recent discovered factor that controls myoblast fusion is Myomaker; a muscle-specific membrane protein expressed especially on the cell surface during fusion. This protein is expressed in a myotomal portion of the somite, limb bud, and axial skeletal muscle, especially during differentiation (Millay et al., 2013). Intact genome is essential to maintain skeletal muscle formation during myogenesis. For instance, impairment of Pitx2/Pitx3 and downstream antioxidant enzymes was leading to the accumulation of reactive oxygen species (ROS) in skeletal muscle tissue. Increase ROS level resulting in an irreversible oxidative DNA damage and apoptosis that impairing skeletal muscle development in this

model (L'Honore et al., 2014). In this context, it seems to be that impairment of any DNA damage repair mechanisms leads to interfering skeletal muscle myogenesis.

1.1.3 Anatomy of skeletal muscle

1.1.3.1 Gross anatomy

Skeletal muscle consists of muscle fibres, connective tissue, nerves, and blood vessels. Each skeletal muscle contains three layers of connective tissue: (1) epimysium, (2) perimysium, and (3) endomysium. Epimysium is a dense layer of collagen fibres that surrounds entire muscle, while the perimysium divides the muscle into bundles of skeletal muscle fibres called fascicle. Perimysium consists of collagen as well as elastic fibres and contains nerve and blood vessels. Every fibre within the fascicle is surrounded by the loose connective tissue of endomysium that interconnects adjacent fibres (fig. 1.1). This layer is essential for the maintenance of skeletal muscle fibres by providing nutrition via a capillary network, control muscle contraction by nerve supply, and contains an adult skeletal muscle stem cell, satellite cells, that have damage repair ability. The collagen fibres of these three layers at each end of the muscle come together and connect to the bone in a structure called the tendon or aponeurosis (Martini et al., 2018). The main content of collagen in epimysium and perimysium is type I and little amounts of type III. Endomysium is composed mainly of collagen I and III (Light and Champion, 1984).

The primary arteries that supply muscle divide into feed branches inside the epimysium and when they leave this layer, they give rise to a network of arteriole that invade the perimysium. Arterioles then penetrate the perimysium layer and branch to many capillaries embedded in endomysium (Korthuis, 2011). In cross-section, the capillaries are arranged surrounding the fibres in the highly variable way (Poole et al., 2008). This variation is due to differences in capillary circumference and oxygen demand (Berg and Sarelius, 1995).

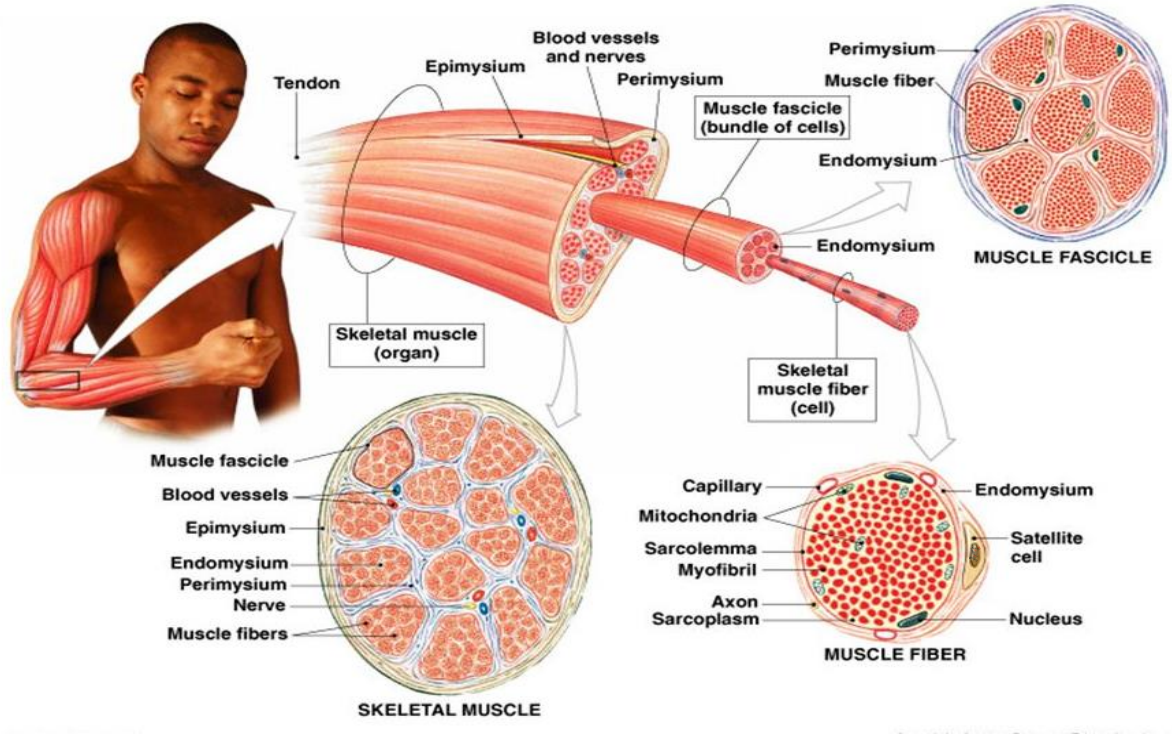

Figure 1.1. The organisation of skeletal muscles. A skeletal muscle consists of bundles of muscle fibres, fascicles, enclosed by the epimysium. Fascicles are separated from each other by the connective tissue of perimysium, and within each bundle, the muscle fibres are surrounded by the endomysium (Martini et al., 2018).

1.1.3.2 Microanatomy (Histology) of skeletal muscle

Each skeletal muscle fibre is a cylindrical-multinucleated cell. The nucleus is long and oval and located peripherally under the sarcolemma, the cell membrane of skeletal muscle fibres. In longitudinal section, skeletal muscle fibre shows a striated pattern, with light and dark bands. The darker bands are called A bands, and the lighter bands called I bands. At the middle of each I bands thartere is a line called the Z line and is considered a landmark of the sarcomere, the contractile apparatus. This apparatus consists mainly of myofibrils, long cylindrical filamentous bundles. The striation of myofibril is due to the regular arrangement of two types of myofilaments, thick and thin, and which lie parallel to the long axis of myofibrils. Thick filaments occupy the A band at the centre of sarcomeres and thin filaments lie between and parallel to thick filaments with one end attached to Z line. I band consists of the thin filament which do not overlap with thick one, while A band composed

mainly of thick and overlapping thin filaments. The lighter area in an A band, H zone, consist of the only thick filament, and lateral connection of these filaments at the middle of zone make, and a dark line called M line (fig. 1.2). Thick and thin filaments consist of protein, myosin, and actin, respectively (Mesher, 2010).

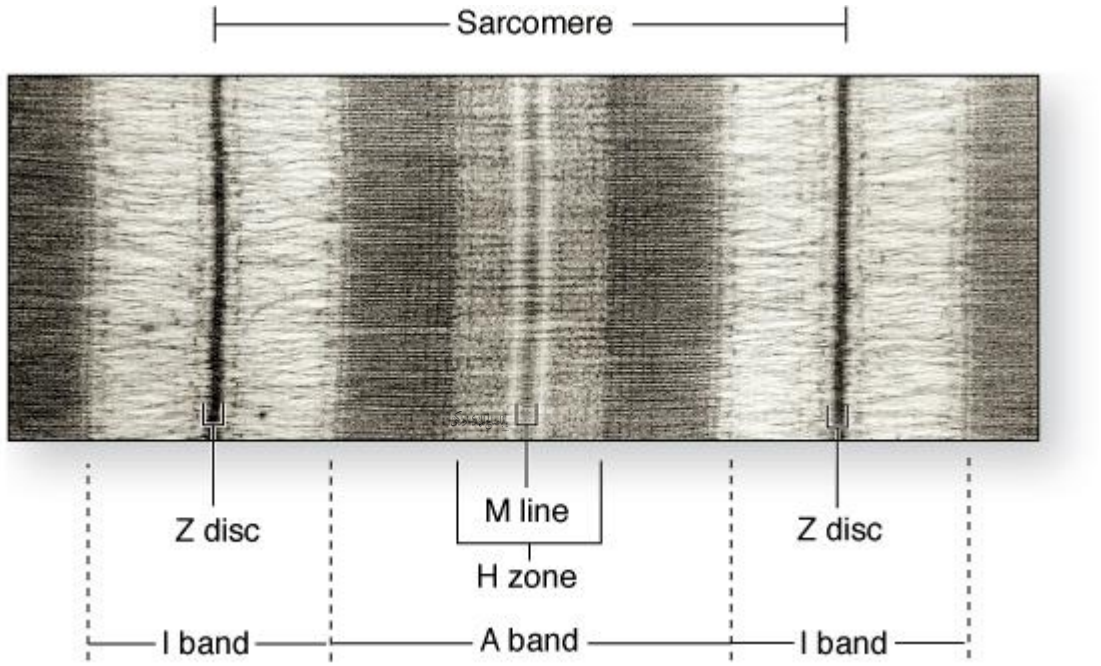

Figure 1.2. Structure of myofibril: a series of sarcomeres. Each myofibril consists of a long series of sarcomeres, which contain thick and thin filaments and are separated from one another by Z disc. Thin filaments are actin; it bound Z line from one end and interacts with myosin; thick filaments, on the other end. Myosin has occupied A band and bound to M line (Mesher, 2010).

The nervous system controls the action of the skeletal muscle systemically. The communication site between the nervous system and skeletal muscle is called neuromuscular junction (NMJ) and is located at the middle of each fibre. Each skeletal muscle fibre is controlled by neurone originate from the axon branches within perimysium. Each branch ends on muscle fibre via an expanded portion called synaptic terminal. The expanded end occurs in the synaptic cleft, a space separating the nerve from sarcolemma. The sarcolemma at this cleft is called motor end plate. The synaptic terminal contains neurotransmitter called acetylcholine (ACh). The release of the ACh at the NMJ increase the permeability of sarcolemma and allow the Sodium ions (Na^+) to enter the sarcoplasm

and generate a membrane action potential. This condition leads to the release of Ca^{+} from cisterna of sarcoplasmic reticulum (Martini et al., 2018).

Sarcoplasmic reticulum, a smooth endoplasmic reticulum of muscle cells, is a specialised Ca^{2+} ion store. The ion is released during depolarising at the site of NMJ at the surface of muscle fibres and diffuses inside the fibre. To ensure that all regions of fibre are activated at the same time and to form a uniform contraction, the muscle cell needs a conducting system. This system is represented by transverse (T) tubule, a network of invaginations of sarcolemma surroundings every myofibril. These tubules with the terminal cisterna, (expansions of the sarcoplasmic reticulum) form the triad. The impulse from nerve at NMJ transduces along muscle fibre towards the triad and leads to release of Ca^{2+} from the sarcoplasmic reticulum. The release of this ion leads to the contraction of muscle fibres. Relaxation occurs when the depolarisations end and cisterna take up Ca^{2+} (Mesher, 2010).

1.1.4 Skeletal muscle Physiology

1.1.4.1 Mechanism of contraction

Muscle contraction occurs under control of the nervous system, via a special connection called neuromuscular junction (NMJ). Excitation of neuron leads to release ACh, a neurotransmitter, and making sarcoplasmic reticulum more permeable to discharge Ca^{2+} and start contraction (Martini et al., 2018). The basis of muscle contraction depended on the sliding of overlapping actin and myosin filament and was first described by Andrew Huxley and Ralph Niedergerke as the sliding filament model in 1954 (HUXLEY and NIEDERGERKE, 1954). The sliding of actin and myosin during contraction shortens the sarcomere and brings Z line closer together. Therefore, the fundamental role of muscle contraction depends on the interaction between actin and myosin filaments (Cooper et al., 2007). Myosin filaments in skeletal muscle fibres consist as complex consist of two heavy coiled chains with two light chains. The two heavy chains on one end form a head that can bind actin and have Adenosine Triphosphate (ATP) binding site. During contraction, a myosin heavy chain head interacts with the actin filament by forming a cross-bridge. The cycle of attachment and detachment is performed by the presence of Ca^{2+} and ATP, respectively. Cross bridge cycles are controlled by nerve impulse that activates

sarcoplasmic reticulum to release Ca^{2+} ions, and it will continue until this ion is removed (Mesher, 2010).

Significant ageing-related change occurs in the contraction element, neuron and proteins, resulting in a reduction in contractile speed and force generation capacity of the muscle fibres (Larsson et al., 2001). This condition leads to reduced physical activity of aged people. Decrease physical activity lead to increase oxidative stress due to the movement of neuronal nitric oxide synthase (nNOS) from the extracellular matrix to the cytosol. Cytosolic nNOS lead to muscle loss by enhancing Forkhead box O3 (FoxO3)-mediated transcription of atrogin-1 and MuRF1 through the oxidative environment (Suzuki et al., 2007).

1.1.5 Energy uses and muscular activity

The breakdown of ATP molecules powers skeletal muscle contraction by the thick filament. Each muscle fibres may contain 15 million thick filaments, each filament when actively contracting breakdown approximately 2500 ATP molecules per second. Most of these molecules are formed during contraction. At rest, skeletal muscle fibre has a little ATP, and a high-energy compound called creatine phosphate (CP). ATP is an unstable molecule, and its function is to transfer energy inside cells rather than storage. Therefore, the surplus energy of ATP molecules that muscle produces during rest is transferred to CP, and ATP then converts to ADP by releasing a phosphate group. During contraction, ATP molecules are broken down by myosin heavy chain heads and converted to adenosine diphosphate (ADP) that will recharge by phosphate group from CP for reuse. Because the muscle has thousands of fibres, this source is not enough to provide energy for muscle contraction for an extended period. Therefore, the muscle needs to generate ATP on demand. In general, living cells generate ATP by two mechanisms, (1) glycolysis in the cytoplasm and (2) aerobic metabolism in mitochondria (Martini et al., 2018).

1.1.5.1 Glycolysis

Glycolysis occurs in the cytoplasm and produces pyruvic acid by breaking down glucose. It also called anaerobic metabolism because it does not require oxygen. Although it produces a small amount of energy (2 ATP molecules per 1 glucose molecule), it is vital because it

provides substrates, pyruvic acid, for aerobic metabolism. Furthermore, it is considered the primary source of cell fuel in cases of limited oxygen availability. The glucose molecules needed for this process are obtained from the cell storage of glycogen (Martini et al., 2018).

1.1.5.2 Aerobic metabolism

Aerobic metabolism occurs in mitochondria, by employing oxygen, ADP, phosphate ions, and organic substrate (such as pyruvic acid) from the cytoplasm. The substrate enters an enzymatic pathway called the citric acid cycle, which breaks down the organic molecule, releases carbon dioxide, and uses hydrogen in the respiratory chain. The result of this pathway is a large amount of energy released as ATP (36 molecules) with water as a side product. Skeletal muscle fibres metabolise fatty acid from circulation in the aerobic pathway to generate ATP in resting status. However, the mitochondria in contracting muscle rely on pyruvic acid molecule instead of fatty acid. The Pyruvic acid molecules are produced in the cytoplasm by glycolysis of glucose from surrounding interstitial fluid or the breakdown of glycogen from sarcoplasm (Martini et al., 2018).

1.1.6 Skeletal muscle fibres plasticity

Skeletal muscle is a highly adaptable tissue in term of cells (fibres) number and size, metabolic status and contents, especially proteins (as reviewed by Matsakas and Patel (Matsakas and Patel, 2009)). Fibres change their profile, metabolic, molecular, structural, and contractile properties due to many factors. These factors include innervation, exercise training, mechanical loading/unloading, hormones, and ageing. Based on the contractile profile (Pette and Staron, 2001) oxidative potential (Armstrong and Phelps, 1984), the muscle fibres can be classified into slow-twitch and fast-twitch fibres. Slow-twitch fibres are oxidative while fast-twitch are classified as oxidative glycolytic and glycolytic. The contractile properties depend on the composition in myosin heavy chain isoform (MHC), which combining with actin to form the actomyosin complex (Kammoun et al., 2014). This fibres isoform type subjected to transition from slow to fast vice versa, MHCIβ ↔ MHCIIa ↔ MHCIId ↔ MHCIIb (Pette and Staron, 2001).

The traditional classification of skeletal muscle fibres was based on MHC isoform show many subtypes, Iβ, α, extra-ocular, neonatal, embryonic, IIA, IIB, IIX and IIM (masticatory) (Weiss and Leinwand, 1996). Small mammal limb expresses the MHC IIb, MHC IId/x and MHC IIa as a main fast isoform component and slow MHC Iβ (Pette, 1998). Limb slow twitch isoform is MHCIβ, and fast twitch isoforms are MHC IIa, MHC IIx, and MHC IIb (Lukas et al., 2000). The primary two fibres types, depending on MHC isoform, type I and type II, possess a unique profile. Type I fibres are considered as aerobic with small cross-sectional area enriched with mitochondria and myoglobin. In contrast, anaerobic type II fibres have a large cross-sectional area profuse amount of glycogen and little myoglobin and few mitochondria (Burkitt, 1993). However, a recent study challenges these categories by producing larger muscle fibres with preserve oxidative status (Omairi et al., 2016).

Nerve impulse pattern shows a close relation impact on fibres phenotype. Experimentally, cross-enervation (Buller et al., 1960a) or chronic electrical stimulation with slow or fast motoneuron-specific impulse patterns (Pette and Staron, 2001) converted fibres phenotype from slow to fast and vice versa. Factor, such as myostatin, also control muscle fibre phenotype. The increase of glycolytic and decrease in oxidative fibres have been found in the mouse model with *Myostatin* knockout (Amthor et al., 2007).

As reviewed by Hoppeler, skeletal muscle plasticity has a molecular basis. Maintaining the oxidative status and mitochondrial activity is due to convergence in Ca^{2+} signalling and AMPK. Also, PGC-1α coordinates both transcriptional and post-transcriptional processes to preserve fibres phenotype. On another side, large, glycolytic, and abundant of protein fibres phenotype is preserved by mTORC1, and the latter is regulated by insulin and growth-factor-dependent signalling cascade as well as mechanical and nutritional factors (Hoppeler, 2016).

1.1.7 Skeletal muscle fibres distribution

Muscle type and animal species contribute to the distribution of muscle fibres type. For instance, IIB myofibres consider the largest population of myofibres type in a variety of rat skeletal muscle, however, there were some muscles, such as the Soleus, that contained very few, if any type IIB myofibres (Delp and Duan, 1985). Location of muscle contributes to the distribution of myofibres type since studies including rats, pigs, dogs and cats,

demonstrate a high proportion of type I fibres found in deep muscles compared to superficial that mostly contain type IIB (Ariano et al., 1973, Armstrong and Phelps, 1984, Armstrong et al., 1985, Armstrong et al., 1982). Likewise, the distribution pattern of myofibres within a single limb muscle. For example, the deep region of the muscle composed mainly of type I myofibres, in contrast very few are located superficially, as an alternative in this peripheral region, there is an abundance of type IIB myofibres (Armstrong and Phelps, 1984, Fuentes et al., 1998). Type IIB fibres the most dominant fibres in Extensor Digitorum Longus (EDL) and Tibialis Anterior (TA) from mouse and rat were replaced in rabbit by IIX and no pure type IIB myofibres (Hamalainen and Pette, 1993). In these three species hindlimb muscles, the type I illustrate a proximo-distal distribution. Also, except Soleus muscle, the muscles of the rat hindlimb were all fast muscles and the patterning of type I distribution shows trends of declining proximo-distal type I myofibre densities (Wang and Kernell, 2001). The function of muscle have a direct link to the composition and distribution of myofibres. For instance, slow oxidative profile with most dominant type I myofibres were common in muscle anti-gravity or postural muscles such as Soleus whereas the fast glycolytic profile with a large proportion of type IIB fibres is found in locomotor muscle (Suzuki, 1995). Larger mammals and man show a more significant proportion of type I fibres when compared to small animals (Prince et al., 1976, Johnson et al., 1973, Delp and Duan, 1985). The need of faster contraction for faster movement in smaller animals could explain the requirement for the use of type IIB myofibres (Hamalainen and Pette, 1993, Suzuki, 1995, Armstrong et al., 1985). Human skeletal muscle has only three (pure) myofibre types (I, IIA and IIX); however, there was IIB RNA formed in the masseter muscle and external oblique but not protein (Yan et al., 1985, Smerdu et al., 1994, Horton et al., 2001).

1.1.8 Skeletal muscle fibres transitions

The determining factor that commands skeletal muscle to carry out a variety of functions and movements is the diversity of myofibres in their physiological, biochemical and metabolic features. Skeletal muscle is unique in its ability to adapt to environmental, metabolic and functional demands controlled by numerous intrinsic signalling pathways (Bassel-Duby and Olson, 2006). For example, the cross interaction between muscles have

a different profile, slow twitch (soleus) and fast twitch (Flexor digitorum longus), lead to change in contractile speed in both muscles (Buller et al., 1960b). The other study suggests that the shift was due to difference impulse pattern, it shows the denervated muscles received electrical stimulations that mimic patterns of high (intermittent short bursts) and low (prolonged) frequency activities determine the contractile properties of fast and slow muscles, respectively (Lomo et al., 1974, Salmons and Vrbova, 1969). Unloading and hyperthyroidism were reported as another factor of slow to fast switch in myofibre type (Caiozzo et al., 1985). In contrast, muscle overloading and hypothyroidism were considered fast to slow types inducer (Nwoye and Mommaerts, 1981, Schiaffino and Reggiani, 2011).

Furthermore, conditions like chronic diseases, such as obesity, ageing, and physical activity promote skeletal muscle myofibres to undergo phenotypic transitions (Hickey et al., 1995, Inbar et al., 1981, Yan et al., 1985). For example, the transformation of myofibres from those more glycolytic to an oxidative phenotype within fast fibres type have notice specifically with endurance exercise (Green et al., 1979, Andersen and Henriksson, 1977, Schiaffino and Reggiani, 2011). In contrast, a higher proportion of type IIA and IIX are observed in more sedentary humans (Klitgaard et al., 1990).

On molecular level, the AMP-activated protein kinase (AMPK) and peroxisome proliferator-activated receptor gamma coactivator 1-alpha (PGC-1α) interactions (AMPK/ PGC-1α), as well as the mitogen-activated protein kinase (MAPK)/PGC-1α signalling pathways, in the response to metabolic stress and energy deficiency, have an ability to increase contractile activity, by segmentally initiating exercise-induced myofibre transitions and mitochondrial biogenesis, respectively (Röckl et al., 2007, Garcia-Roves et al., 2008, Lin et al., 2002, Pogozelski et al., 2009).

1.1.9 Skeletal muscle supporting tissue

1.1.9.1 Skeletal muscle capillarization

The density of blood vessels in skeletal muscle has a direct effect on many physiological prosses since it considers the port for delivering oxygen, substrates and hormones (Gudbjornsdottir et al., 2003).

The capillaries organised into microvascular units surrounding fibres and originate from the terminal arterioles (Lund et al., 1987) and branched initially from conduit arteries that are positioned to control the amount of blood entering the muscle (Segal, 2005). Capillary density has been demonstrated to match the muscle fibres need for metabolite under resting conditions and during exercise (Mortensen and Saltin, 2014). Furthermore, the abundance of the capillary is positively correlated to oxidative phenotype since the later express high level of angiogenic factors which is not the case in glycolytic phenotypes (Annex et al., 1998, Hudlicka et al., 1992, Cherwek et al., 2000). Besides, not only do the oxidative fibres have a high ability to produce angiogenic factor but also several transcriptional regulators that determine the oxidative phenotype of fibres, which also can stimulate angiogenesis. Nuclear receptor PPARgamma-coactivator-1α (PGC-1α) a critical regulator of oxidative fibre type (Arany et al., 2008), and peroxisomal proliferator activator receptor (PPARδ) are known to promote angiogenic genes expression in skeletal muscle (Narkar et al., 2008, Gaudel et al., 2008).

1.1.9.1 Skeletal muscle connective tissue

The fibroblast cell is the chief cells to produce, maintain and repair connective tissue in muscle and tendon (Kuhl et al., 1984, Gatchalian et al., 1989). Although collagen is mainly produced by myocyte, its proper assembly into the functional extracellular matrix (ECM) require the presence of fibroblast (Lipton, 1977). The main component of ECM is collagens or non-collagenous components such as glycoproteins, proteoglycans and elastin. Collagen occurs in two primary forms: fibrillar and non-fibrillar collagen. Collagen I and III represent the fibrillar form where their high-stress tolerant properties provide ECM with the capacity to transmit muscle contraction force to the bone via the tendons. Collagen IV is considered a non-fibrillar form of collagen and resident in the basement membrane (Kjaer, 2004). Along with other ECM proteins such as laminin represent a unique bind to dystrophin-glycoprotein complex (DGC). DGC composed of three sub-complexes: (1) the sarcoglycans (α, β, γ, and δ); (2) syntrophin, nNOS, and dystrobrevin; and (3) α and β dystroglycan (Matsumura et al., 1993). The leading role of DGC is to linking cytoskeleton, the sarcolemma, and the ECM into a functional unit that maintains muscle integrity (Ohlendieck et al., 1991). Furthermore, ECM is considered a niche for resident stem cell,

satellite cell, and plays a crucial role in regulating its activity including self-renewal (Calve et al., 2010), proliferation and migration (Gillies and Lieber, 2011) thereby muscle regeneration process.

The connective tissue enclosed the skeletal muscle in three levels (Gillies and Lieber, 2011). The first innermost level is represented by a layer of collagen I and collagen III surrounding individual muscle fibres, and it called the endomysium. It works as a transducer and load bearing structure upon myofibre contraction. The endomysium connecting to the sarcolemma via basement membrane that formed from two layers, internal basal lamina connects directly to the sarcolemma, and the external reticular lamina (Sanes, 2003, Campbell and Stull, 2003, Trotter and Purslow, 1992). The second level of connective tissue wrapping, that mainly collagen I and the proteoglycan decorin, is called perimysium and surround bundle of fibres or what is term as fascicle. Perimysium is continuous with the tendon, so it is responsible for transmitting force from muscle to bone to create movement. Blood vessels and nerves are contained within the perimysium tissue (Passerieux et al., 2007, Gillies and Lieber, 2011). The outer most third layer of connective tissue of skeletal muscle is called epimysium and surrounds the entire muscle (Gillies et al., 2014). The components of the epimysium layer are more similar to the endomysium; however, the collagen patterning more similar to the perimysium and tendon (Gillies and Lieber, 2011).

The ECM deposition is affected by muscle phenotype; for example, the fast muscle has lower ECM component compared to muscle with the slow phenotype (Kovanen et al., 1980). On the level of single fibres, the endomysium and perimysium connective tissue are higher between slow type I than the fast type II myofibres (Kovanen et al., 1984).

1.1.9.1.1 Collagen synthesis and degradation

ECM, in response to external stimuli, changes its deposition pattern and thickness. The synthesis and degradation of the main component of ECM, collagen, is regulated in some aspect by mechanical loading. This muscle activity provoked signalling cascades regulating molecular gene expression, transcription, translation, as well as post-translational modifications collagens (Yasuda et al., 1996). Exercise can increase the releasing of TGF-β and IGF-1 and results in an increased procollagen expression and collagen synthesis (Yang et al., 1997, Kjaer et al., 2009). Procollagen is a molecule produced by fibroblast in ECM and

cleaved by proteases and assembled into collagen fibrils. Ageing could modulate post-translational modifications of collagen include enzymatic cross-linking (Zimmerman et al., 1985, Haus et al., 1985, Wood et al., 1985). Matrix metalloproteinase (MMP) activity has an essential role in remodelling and degradation of ECM component in both physiological and pathological conditions. For instance, the activity of MMP-2, MMP-9, as well as tumour necrosis factor (TNF-α) are increased during degeneration-associated ECM remodelling in *mdx* mice (Bani et al., 2008). Furthermore, increased proliferation of muscle resident stromal cells and enhancement in collagen deposition are enhanced through increases in Wnt signalling (Trensz et al., 2010).

1.1.9.2 Skeletal muscle innervation

The nervous system has an essential role in regulating muscle properties and determination of muscle phenotype (Buller et al., 1960b). Skeletal muscles are under voluntary control; however, some muscle such diaphragm usually works outside conscious alertness (Martini et al., 2018).

The nerves that supply a skeletal muscle called myelinated motor nerve. These nerves enter the muscle and give rise several terminals branched within the perimysium connective tissue layer. The axon loses its myelinated sheath at the site of innervation where it forms a dilated termination situated within a channel on the muscle cell surface, a structure called motor end-plate or the neuromuscular junction (NMJ). Axon terminal contains numerous mitochondria, synaptic vesicles and neurotransmitter acetylcholine (ACh). The space between axon and muscle is called synaptic cleft (Mescher and Junqueira, 2013).

Coordination between a group of motor units, the myofibres and its motor nerve, is fundamental to achieve single muscle contraction (Gutmann and Hanzlikova, 1966). Innervation pattern is considered one of the factors that affect the expression of MHC (Ohira et al., 2006, Patterson et al., 2006).

1.1.10 Skeletal muscle wasting

Skeletal muscle, the most abundant tissue in the living body, is composed mainly of protein. Therefore, the disorders that affect protein production and degradation will lead to a noticeable change in muscle mass. Protein content in the muscular tissue depends on the

balance between synthesis and degradation. Increase degradation at the expense of the synthesis results in conditions such as sarcopenia, cachexia, and muscle disuse lead to muscle wasting (Bowen et al., 2015). Muscle loss also occurs in diseases such as muscular dystrophies, cancer, and AIDS (Mateos-Aierdi et al., 2015, Kazemi-Bajestani et al., 2015, Grinspoon et al., 2003). All of these conditions have altered the metabolic and physiological parameters of muscle and show evidence of progressive weakness.

1.1.10.1 Intracellular Regulators of Protein Homeostasis

Pathways related to skeletal muscle protein synthesis mainly under control of protein kinase B (AKT) insulin-like growth factor 1(IGF-1). Protein synthesis and breakdown are controlled by phosphorylation or dephosphorylation of these factors. In many disorders shows changes in the homeostasis system, the protein will be transported to the ubiquitin-proteasome pathway and end with proteolysis. Furthermore, Myostatin a member of the transforming growth factor β family also consider as a negative regulator of muscle mass by reducing protein contents (Sandri, 2008).

1.1.10.2 Protein synthesis

Protein synthesis is subject to nutrient availability, physical activity, and anabolic signalling. These three elements work together in a compatible way. Availability of nutrient, particularly amino acids and anabolic signalling, increase portion synthesis in the skeletal muscle for a limited period in the absence of physical activity (Atherton and Smith, 2012). Nutrient and exercise participate in protein synthesis by recruiting mechanistic target of the rapamycin (mTOR) signalling pathways (Drummond et al., 2009, Dickinson et al., 2011). mTOR signalling is involved in protein synthesis directly or by biogenesis of ribosomes subunits (Wang and Proud, 2006). Besides, the insulin-like growth factor is an important molecule that stimulates muscle hypertrophy through activation of Phosphoinositide 3-kinase (PI3K)-AKT- mTOR pathway (Bowen et al., 2015). Reduce sensitivity to insulin with ageing (Rasmussen et al., 2006) is the one suggested way, leading to muscle wasting due to blunting of protein synthesis (Volpi et al., 2000). Another key factor in protein synthesis is PGC-1α, a key regulator of mitochondrial biogenesis. Reduction in the signalling of PGC-

1α impairs insulin sensitivity and reduced AKT and mTOR signalling, the main two components in the protein synthesis pathway (Wenz et al., 2009). DNA damage, as a stress condition, may affect the protein synthesis by one of stress response mechanism. REDD1 (regulated in development and DNA damage responses 1) is a gene induced by DNA damage (Ellisen et al., 2002). REDD1 inhibits the mTOR signalling pathway (Brugarolas et al., 2004) and that leads to a suppression of protein synthesis.

1.1.10.3 Protein degradation

Activation of the ubiquitin-proteasome and autophagy-lysosome system lead to muscle wasting resulting from increase muscle protein turnover (Sandri, 2008). Proteins are degrading by proteasome when they enter to the conjugation status and then became polyubiquitinated, which activates the ubiquitin-proteasome pathway (UPP) by enzymes activation system (Lecker et al., 2006). This pathway consists of a system of concerted enzymes linked to chains of polypeptide co-factor, ubiquitin (Ub), which mark protein for degradation (Glickman and Ciechanover, 2002). There are three components of Ub enzymatic system, E1 (Ub-activating enzyme), E2s (Ub-carrier or conjugating proteins), and E3 (Ub-protein ligase). E1 and E2s prepare Ub for conjugation to protein, while E3 recognise specific substrate and facilitates transfer Ub to protein (Lecker et al., 2006). Tagged protein is recognised by the 26S proteasome, a vast protease complex, and degrades them to small peptides (Baumeister et al., 1998). A malfunction in UPP qualitatively occurs with ageing. The first step of UPP, ubiquitination, is not affected with age, but degradation is affected (Carrard et al., 2002). Another study suggests that the increase in proteasome with age and a decrease in the content of regulatory proteins may lead to insufficient activation of the proteasome (Ferrington et al., 2005). Also, increase oxidation of proteasome subunits with age results in changes in UPP regulation (Carrard et al., 2002). Furthermore, increase proteins oxidation with age can inhibit proteasome activity (Terman and Brunk, 2004a).

The autophagy-lysosome system degrades proteins of cytoplasm by making a double-membrane vesicle called autophagosome (Levine and Kroemer, 2008). Many molecules such as microtubule-associated protein 1 light chain 3B (LC3B), γ-aminobutyric-acid-type-A-receptor-associated protein (GABARAP), Golgi-associated ATPase enhancer of 16 kDa (GATE16), and autophagy-related protein 12 (Atg12), are involved in the formation of

autophagosomes (Bechet et al., 2005). Autophagosome binds the conjugated molecule, organelles and proteins, and moves them to the lysosome for degradation (Vinciguerra et al., 2010). Autophagy is genes regulated pathway; LC3 and GABARAP are main two proteins in this prosses. They are upregulated by atrogenes which encode for proteins presented to lysosomes for degradation when fused with autophagosomes. The foxo3 transcriptional factor is also essential in autophagy by transcription autophagy-related genes such as LC3 (Mammucari et al., 2008). In ageing, the lysosomal system undergoes noticeable changes, such as an increase in lysosome volume, decrease stability, altered some hydrolases activities (Terman and Brunk, 2004a). Such alteration leads to a decrease in rates of degradation long-lived protein, e.g. skeletal muscle protein (Bergamini et al., 2004), and this will contribute to the accumulation of oxidised proteins with age as well as insufficient proteins turnover (Martinez-Vicente et al., 2005).

Calpain is a proteolytic enzyme and also considered as intracellular signal transductor mediated by Ca^{2+} (Croall and Ersfeld, 2007). Calpain has many isoforms, but one that is important in skeletal muscle proteolytic is calpain3 (Sorimachi et al., 1989). Activation of this enzyme by changes in Ca^{2+} homoeostasis, resulting in changes in muscle fibres and organelles such as sarcoplasmic reticulum vacuolization and mitochondrial swelling (Armstrong et al., 1991). Calpain is located at the Z line and its proteolytic activity lead to complete disassembly between myofibrils and loss of connection between adjacent sarcomeres (Huang and Forsberg, 1998). This enzyme is also responsible for cleavage of one of the cytoskeleton proteins called fodrin and is accompanied by apoptosis (Martin et al., 1995). Calpain activity in some muscle diseases such as Duchene and Becker muscular dystrophies lead to muscle fibres degradation (Kumamoto et al., 2000).

1.1.10.4 Mitochondrial dysfunction

The alteration in mitochondrial morphology and function associated with muscle loss in many disease conditions, such as cancer cachexia and neuromuscular disorder (Antunes et al., 2014, Katsetos et al., 2013), and muscle loss with ageing (Carnio et al., 2014). Maintenance of mitochondrial integrity seems to have a significant effect on muscle tissue since the genetic disruption of proteins involved in mitochondrial maintenance resulting in muscle atrophy phenotype (Cipolat et al., 2006). On another hand, the overexpression of

proteins involved in mitochondrial biogenesis can protect muscle from atrophy. For example, overexpression of Opa1, a protein associated with inner mitochondrial membrane fusion and function, preserve muscle from atrophy in a condition known of its muscle loss phenotype such as denervation and myopathy (Civiletto et al., 2015). In the same context, the starvation-induced muscle loss was wildly protected in mouse with downregulated Mul1, a FoxO-dependent ubiquitin-ligase involved in the ubiquitination and degradation of Mfn2, the protein involved in mitochondrial integrity (Lokireddy et al., 2012). On another hand, deficiency in Mfn2 in muscle leading to mitochondrial dysfunction and ROS production (Sebastian et al., 2012). The accumulation of ROS accelerates skeletal muscle proteolysis (Powers et al., 2012). Negative feedback of accumulation of ROS will provoke signalling for mitochondrial dysfunction and muscle atrophy (Talbert et al., 1985). Oxidative stress could accelerate muscle atrophy in many ways. First, ROS can regulate atrophy pathway by modulate NF-kB and FoxO transcriptional factors and activating the autophagy-lysosome and the ubiquitin-proteasome systems (Dodd et al., 2010). Second, disuse atrophy that associated with an increased level of ROS production activates muscle proteases calpain and caspase-3 (McClung et al., 2009, Nelson et al., 2012). Third, the ROS lead to oxidation of muscle proteins and make it more prone to proteolysis and degradation (Smuder et al., 2010).

1.1.10.5. Inflammation

Many inflammatory disorders were resulting in muscle loss. For example, the chronic obstructive pulmonary disorder (COPD), a condition characterises by abnormal lung function and systemic inflammation which results in skeletal muscle dysfunction (Killian et al., 1992). There was clear evidence of the elevation level of inflammatory markers such as IL-6, TNF-α and IL-8 associated with COPD (Londhe and Guttridge, 2015). The other inflammatory disease and associated with skeletal muscle atrophy is Rheumatoid arthritis (RA). The muscle loss in RA disease is termed as rheumatoid cachexia, and it is differing from another type of cachexia since it characterises by loss the muscle tissue only while the other combine with fat loss also. The skeletal muscle loss in this inflammatory disease was linked to increasing the level of inflammatory cytokine, especially the TNF-α and IL-1β, and these two factors work synergistically to provoke muscle wasting (Walsmith and Roubenoff, 2002). On the other hand, the inflammation leads to triggers mitochondrial

abnormalities by impairing mitochondrial biogenesis (Marzetti et al., 2013). Moreover, as we mention in the previous section, there is a relationship between mitochondrial dysfunction and muscle loss.

1.1.10.6. Reduction in satellite cell number and activity

In the human study, there was evidence of a decrease in satellite cell number in atrophied fibres, type IIB with ageing but not the type I (Verdijk et al., 2014). However, genetic depletion of a satellite cell in a mouse model did not affect the skeletal muscle fibres size (Fry et al., 2015). The number of satellite cell, according to these studies, have a specific pattern of effect according to species and fibres types.

The satellite cell activity, proliferation and differentiation, was investigated in a mouse model with evidence of muscle atrophy such as mechanical unloading. The mechanical unloading was achieved by hind limb suspension resulting in rapid atrophy in skeletal muscle. The signs of atrophy have been notced in both type of muscle fibres and was a combine by the reduction in satellite cell content and activity. The study also shows a reduction in MyoD positive and Myogenin positive cells in this mouse model as a marker of proliferating and differentiation, respectively (Nakanishi et al., 2016). Chronic illness-induced atrophy, such as cancer and diabetes, was associated with a change in satellite cell activity. For instance, in cancer patients, there was a reduction in myogenin positive cells, and that means a reduction in satellite cell proliferation capacity (Brzeszczynska et al., 2016).

1.1.10.7. Myostatin

Myostatin via its receptor, activin A receptor type IIB (ActRIIB), inhibits muscle growth through activation transcription factors, the SMAD2 (mothers against decapentaplegic 2) and SMAD3 (mothers against decapentaplegic 3). SMAD2/3 enhance skeletal muscle atrophy by upregulating atrogenes transcription. Suppression of muscle growth by myostatin signalling even due to reduced protein synthesis by inhibition of Akt, increase protein degradation by elevated FoxO transcription (Chen et al., 2017) or by inhibition of satellite cell as mention above. Myostatin blockade or inhibition would increase the skeletal muscle mass in muscle wasting conditions. For instance, a study shows that the

knockout of the myostatin gene leads to an increase in muscle mass compared with wild type (Amthor et al., 2007), and block of myostatin to react with its receptor on skeletal muscle, ActRIIB, by follistatin or by the myostatin propeptide lead to a dramatic increase in muscle mass (Lee and McPherron, 2001). Later, Cadena et al. use a soluble form of ActRIIB, and the result increased in muscle mass by 16% in injected mice compared to untreated mice (Cadena et al., 2010). Therefore, the targeting of myostatin by either method to inhibit its negative regulation of skeletal muscle is considers an essential approach to resolving muscle wasting in many disorders, including progeria syndromes and ageing.

1.3. Ageing

Ageing is a multifactorial process affecting all biological systems in living bodies. To study the causes of ageing, scientists and researchers have put forward many hypothesises. These hypothesises are connected in many aspects. In general, they mentioned that the leading cause of the ageing process is the damage in cell components, especially DNA, nuclear and mitochondrial DNA, and proteins. The common cause of DNA damage in the cells from ageing subjects is increases free radical and its oxidative stress consequence. As reviewed by McCord, the cause of increase free radical is an imbalance between free radical formation and the level of elimination by antioxidants (McCord, 2000). Mitochondria is the primary source of critical members of free radical, H_2O_2 (Boveris et al., 1972) and superoxide anion (Han et al., 2001).

Adelman and his group found that the level of thymine glycol and thymidine glycol in urine, an indicator of oxidative DNA damage, is correlated inversely with life span (Adelman et al., 1988). The DNA damage is reversible, and the cells have many systems to correct such damage. One of the essential types of DNA damage repair is the nucleotide excision repair (NER) mechanism. As reviewed by de Boer and Hoeijmakers, NER can repair a variety of DNA lesions such as damage by ultraviolet (UV) light, chemical damage and also alkaline and oxidative agents induced damage (de Boer and Hoeijmakers, 2000). Thus, any impairment in NER may lead to accelerated ageing as seen by progeria syndrome. In order to study the effect of impairment of DNA repair mechanisms as a particular cause of ageing, the mouse model has been generated. This progeric mouse model lacks the protein involved in NER, the ERCC1 protein. These mice even have the full knockout of ERCC1 gene

and die approximately at four weeks, or hypomorph, *Ercc1*$^{\Delta/-}$ mice, with extended life to 22 weeks.

1.3.1. Sarcopenia

General improvements in health care have increased the number of aged people all over the world. World Health Organization expects that in 2030 would be at least 973 millions of people aged 65 years or older compared to 420 million in 2000. Furthermore, there will be an increase in life expectancy estimated around 80 years in industrial countries (Control and Prevention, 2003). Ageing affects almost all organs in the body, and more pronounced affected tissue is the skeletal muscle. A progressive decrease in this organ size is started at the age of 25 years in both size and number of muscle fibres, at the age of 80 years, it has lost about 30% of its mass (Lexell et al., 1988). This condition is called sarcopenia.

Sarcopenia was first used to describe the loss of body mass during ageing by Rosenberg (Rosenberg, 1997) and previously termed as 'senile muscle atrophy' (Gutman and Hanzlikova, 1972). Sarcopenia can be defined as a syndrome characterised by a progressive loss of skeletal muscle mass and strength (Delmonico et al., 2007). The European Working Group on Sarcopenia in Older People defined criteria of this term. They mention that sarcopenia refers to the presence of lower muscles mass and muscle weakness and impaired performance (Cruz-Jentoft et al., 2010).

The consequences of sarcopenia are reflected on aged people as general health complication and communities as well. People suffering from sarcopenia are considered as public health burden by mean of hospitalisation, nursing home admission, development of physical disability, and even mortality (Guralnik et al., 2000). In particular, sarcopenia is associated with graduate loss of physical activity, decrease in functional performance and physical disability (Tanimoto et al., 2012). Impaired ability to walk (Hardy et al., 2011) and increased falls and fall-related fractures are the prominent determinants of subsequent disability (Tanimoto et al., 2014).

Skeletal muscle is considered as a secretory organ because of its secretion of myokines. They have autocrine, paracrine, or endocrine effects. Myokines, a type of cytokines, consist of several hundred peptides make a communication network with other tissues and organs as well as muscle itself. Autocrine activity is endorsed in factors such as myostatin, leukaemia inhibitory factor (LIF), interleukin-6 (IL-6) and interleukin-7 (IL-7) as they are

involved in muscle hypertrophy, myogenesis. Also, a Brain-derived neurotrophic factor (BDNF) and IL-6 as they involved in Adenosine monophosphate kinase (AMPK)-mediated fat oxidation. The endocrine activity of skeletal muscle represented by IL-6 and has an effect on the liver, adipose tissue, immune system, and mediates crosstalk between intestinal L cells and pancreatic islets. Other myokines impact the endothelial function of the vascular system, are the insulin-like growth factors (IGF-1), fibroblast growth factor (FGF-2), follistatin-like-1 (FSTL-1), and Peroxisome proliferator-activated receptor gamma coactivator 1-alpha (PGC-1α)-dependent myokine irisin. The imbalance between these myokines leads to accumulation of fat, especially visceral, and develop cardiovascular diseases, type II diabetes mellitus, and cancer (Pratesi et al., 2013). Production of these factors from skeletal muscle is regulated by contraction (Pedersen and Febbraio, 2012).

A reduction in size characterises aged muscle is mainly due to smaller type II muscle fibres (Nilwik et al., 2013). Not only fibre size is affected by age but also the internal structure of the fibre is changed, such as myofilaments protein content and function (Miller and Toth, 2013). Myosin protein, an essential component of skeletal muscle, is altered and reduced clearly with age (D'Antona et al., 2003). The alteration in this protein, such as oxidation, will disrupt the binding between myosin head and actin filament and reduce contraction efficiency by impair cross-bridges (Moen et al., 2014). This situation will reduce power generation in the whole muscle and affect the overall body strength. Aged skeletal muscle also shows signs of regeneration, including the presence of various fibre size, especially small size, and the presence of a centrally located nucleus (Edström and Ulfhake, 2005). Another sign of muscle regeneration is an expression of embryonic MHC, particularly after degeneration of denervated fibres (Borisov et al., 2001). Furthermore, the mechanical properties of aged muscles also altered. In this context, Ochala et al. reported that the stiffness increases in whole muscle as well as in single fibre with age (Ochala et al., 2007).

At the transcriptional level, aged muscle fibres show incapacitation of the GH-IGF-I axis, and that lead to fibres failing to regenerate in the late phase.

It seems that DNA damage is the primary cause of ageing (Gensler and Bernstein, 1981). There are a variety of DNA damages that accumulate with age as reviewed by Moskalev et al., including single strand and double strand DNA breaks (Moskalev et al., 2013). Lack of DNA repair mechanisms results in accumulation of DNA damages. There are many mouse models with impaired or attenuation of one of these mechanisms with a sign of accelerated

ageing. One of these models is subjected to study by Dollé et al. and it lacked one of essential DNA repair proteins, excision repair complementary complex1 (ERCC1). This model shows signs of multi-organ accelerated ageing (Dollé et al., 2011), including skeletal muscle, sarcopenia (Niedernhofer et al., 2006).

1.3.2. Progeria

Sarcopenia, as mention above, defined as involuntary loss of skeletal muscle mass and function with ageing. However, the conditions and mouse models that show accelerated ageing phenotype also showed a sign of muscle loss and this condition term as progeria. Progeria is a rare genetic disorder that shows the signs of ageing at an early age. There are several syndromes classified as a progeric condition. Progeria has a Greek origin, “pro”, meaning “before”, or “premature”, and “geras” meaning “old age”. Many models mimicking the progeroid syndromes have been developed to build up experimental treatments for these syndromes and natural ageing.

1.3.2.1. Progeria syndrome

1.3.2.1.1. The Cerebro-oculo-facio-skeletal Syndrome

Jaspers et al. have described the first patient with the Cerebro-oculo-facio-skeletal syndrome, with the features of pre- and postnatal growth retardation and death in early infancy. The other features include microcephaly, bilateral microphthalmia, micrognathia, low-set and posterior-rotated ears, arthrogryposis with rocker-bottom feet, flexion contractures of the hands, and bilateral congenital hip dislocation. The death occurred at 14 months due to developed bilateral pneumonia. The patient had a mutation in the ERCC1 gene, and as a result, NER activity reduced to 15% of the average level after UV-induced DNA damage was (Jaspers et al., 2007). ERCC1-XPF is heterodimeric complex that functions as a structure-specific DNA endonuclease participates in NER (Sijbers et al., 1996). Mutation in the ERCC1 gene lead to truncate in the protein encoded by this gene lacks the entire C-terminal domain, which is essential for interaction with XPF (Jaspers et al., 2007). In addition to its function as an endonuclease, ERCC1-XPF also has telomere length maintenance activity (Zhu et al., 2003). As the telomere is essential for normal cell division,

its maintenance defect leads to cell senescence (Bodnar et al., 1998). Cell senescence is one of the essential causes of ageing features in elderly and progeria syndrome.

1.3.2.1.2. Cockayne syndrome

The Cockayne syndrome (CS) first characterise by Cockayne in 1936 as a type of dwarfism with a feature of retinal atrophy and deafness (Cockayne, 1936). As reviewed by Karikkineth et al., CS could be considered as progeria syndrome based on lack of recovery of RNA transcription after UV light-induced DNA damage. CS has many related disorders leading to death at the age of 12 years (Karikkineth et al., 2016). According to a study by Natale V., the death age is variable according to the severity of the syndrome. The study shows that the ranges of death age are 5.0, 16.1, and 30.3 years for severe, moderate, and mild cases, respectively (Natale, 2011). The features of CS were listed by reviewing 25 cases by Ozdirim et al., in addition to dwarfism, CS person has microcephaly, mental retardation, photosensitivity, progeroid appearance (Ozdirim et al., 1996). Moreover, most recently, characterisation of CS reveal severe neurological manifestations, vision disorders, deafness, feeding difficulties, and muscle wasting (Karikkineth et al., 2016).

The mutation in ERCC8 or ERCC6 genes that encoded a protein called CSA and CSB respectively is the leading cause of CS (Natale, 2011, Laugel, 2013). CSB engaged in many DNA damage repair mechanisms. A defect in CSB disrupts RNA polymerase to dealing with transcription blocks (Aamann et al., 2013), base excision repair (Stevnsner et al., 2008), inter-strand crosslink repair (Iyama et al., 2015) and DNA double-strand break repair (Batenburg et al., 2015). CSA has a role in DNA damage repair by involving CSA-associated ligase in the degradation of transcription-coupled repair at the end of repair prosses to allow the resume of transcription (Groisman et al., 2006). CS sharing many features of ageing in an accelerated manner, therefore, is considering as a progeroid syndrome. The underlying cause of CS is the defect in ERCC complex proteins that related to NER of DNA damage. The evidence from this syndrome reveals the relationship between ERCC proteins and the feature of the progeroid syndrome and ageing.

1.3.2.1.3. Trichothiodystrophy

Trichothiodystrophy (TTD) most distinctive feature is brittle hair caused by sulphur-deficiency due to a reduced level of cysteine-rich matrix proteins. Other clinical features include small stature, skin thinning, UV light photosensitivity and decrease muscle tone (Itin et al., 2001, Bergmann and Egly, 2001). TTD is resulting from defects in NER, and it is linked to a mutation in the XPD gene that has a DNA repair activity (Lehmann, 2003). In contrast, non-photosensitive TTD displays a standard NER capacity (Stefanini et al., 1986).

The genetic basis of photosensitive TTD is related to mutations in ERCC2 (XPD) or ERCC3 (XPB) and p8/TTDA; three of ten subunits of TFIIH, a basal transcription/repair factor (Botta et al., 2002). ERCC3 had a helicase activity which opens the DNA surrounding damage site (Guzder et al., 1994). The NER removes DNA damage by ERCC3 ATPase activity in combination with the helicase activity of ERCC2 (Hashimoto and Egly, 2009). Among the many features listed above, the decrease in muscle tone (Itin et al., 2001) may reveal the importance of DNA integrity in maintaining skeletal muscle tissue. Many progeroid syndromes share ERCC group mutant. Therefore, the study of the effect of ERCC mutations and find a therapeutic approach may apply to all these syndromes.

1.3.2.1.4. Xeroderma pigmentosum

Xeroderma pigmentosum (XP) is a disorder characterised by distinctive skin features such as wrinkling, checkered pigmentation, and skin tumour. Other features include neurologic abnormalities, dwarfism, gonadal hypoplasia, and mental deficiency. In addition, XP patients have a high sensitivity to develop skin cancer upon exposure to sunlight (as reviewed by (Black, 2016)). Affected patients may exhibit signs of hearing loss, laryngeal dystonia and peripheral neuropathy (Anttinen et al., 2008).

Xeroderma pigmentosum was the first nucleotide excision repair (NER) deficiency disease to be described (Cleaver, 2004). There are a group of complementation genes participate in this syndrome include *XPA*, *XPB (ERCC3)*, *XPC*, *XPD (ERCC2)*, *XPE (DDB2)*, *XPF (ERCC4)*, *XPG (ERCC5)*, and XP VARIANT (DiGiovanna and Kraemer, 2012). ERCC1-XPF is heterodimeric complex that functions as a structure-specific DNA endonuclease participates in NER (Sijbers et al., 1996). Therefore, any defect in either of these two

components resulting in a defect in DNA damage repair and related features. One of the features of XP that mention above is peripheral neuropathy, and this may lead to a defect in peripheral nerve supplying tissue, including skeletal muscle.

1.3.2.1.5. Hutchinson-Gilford progeria syndrome

Hutchinson-Gilford progeria syndrome (HGPS) is a rare genetic disorder characterised by accelerated ageing. The children affected by HGPS appear normal at birth but within a year start to display signs of ageing. All affected children share the same distinguishing features. Typically facial features include micrognathia (small jaw), the cranium is disproportioned to face, alopecia (loss of hair), and prominent eyes and scalp veins. Furthermore, the affected child has delayed growth, and that leads to short stature and below the average weight. Aged looking skin is due to lack of subcutaneous fat (Sarkar and Shinton, 2001). Death occurs at an average of 13 years because of age-related diseases such as respiratory, cardiovascular, and arthritic conditions (DeBusk, 1972, Baker et al., 1981).

All Hutchinson-Gilford progeria syndrome cases show a sign growth retardation. This condition is related to growth factors imbalance. Even they have a normal level of the growth hormone (GH), but it occurs in an inactive form. Besides, they have deficient insulin-like growth factor with very high basal metabolic rates (BMRs) and increase in hyaluronic acid (HA). These metabolic alterations are closely related to genetic disorders (Brown, 1992).

The genetic basis of HGPS first described by Eriksson groups in 2003; they present evidence of mutation in lamin A (LMNA) gene as a direct cause. This mutation leads to abnormalities in the nuclear membrane, due to abnormal LMNA protein that lacks 50 amino acids at the carboxy terminus. This protein is encoded by the LMNA gene and is considered as a significant component of the inner nuclear membrane lamina (Eriksson et al., 2003). Usually, lamin A is produced as a precursor molecule called prelamin A. This molecule is subjected to farnesylation, a post-translation modification to add farnesyl group. The molecule then undergoes internal proteolytic cleavage to remove 18 coding amino acids to generate mature lamin A (Sinensky et al., 1994). Mutation in the LMNA gene yields prelamin A missing the site of endoproteolytic cleavage. The incompletely processed prelamin A forms a multiprotein complex within the inner nuclear membrane and might

act as a dominant negative factor (Eriksson et al., 2003). Defects in this protein result in disturbance not only in the nuclear membrane but also in the nucleoplasm. A cell that has nuclei with such defective protein will undergo dramatic pathological consequences leading to cell senescence (Cau et al., 2014).

1.3.2.1.6. Werner syndrome

Werner syndrome (WS) is one of the human premature ageing disorders. Patient with this syndrome exhibits many features of ageing in the early stage of life with early onset of age-related diseases. Diseases such as atherosclerosis, osteoporosis cataract and increase susceptibility to cancer are considered the most critical features of WS (Opresko et al., 2003). The symptoms of this syndrome appear in the second or third decade of life (Martin, 1978) and a major cause of death is a myocardial infarction (Opresko et al., 2003).

This condition is accompanied by recombinational changes, chromosomal alteration and attenuated apoptosis. Furthermore, a defect in DNA repair and replication and impaired telomere maintenance also are found in this syndrome (Opresko et al., 2003). Notably, a defect in a gene related to producing Warner protein (WRN) is the leading cause of this syndrome (Yu et al., 1996). The mutation in the gene that cause WS leads to produce WRN lacks the C-terminus, the terminal carboxyl group that enables the protein to transported to the nucleus (Oshima, 2000). This protein has three important enzymes activities, DNA-dependent ATPase (Pichierri et al., 2003), helicase (Gray et al., 1997) and exonuclease (Huang et al., 1998). Therefore, cells, with WR, have unstable genomes.

Inability to repair defects in the genome as well as telomere shortens and dysfunction is a major cause that leads to senescence in this syndrome. In general, telomere-associated senescence can be avoided through the expression of telomerase that extends telomere (Campisi et al., 2001), and more close to resolving the problem of accelerated ageing in WS, exogenous telomerase was expressed in WS fibroblast lead to increase life span (Wyllie et al., 2000).

1.3.2.1.7. Wiedemann-Rautenstrauch syndrome

Wiedemann-Rautenstrauch Syndrome (WRS) is one of the progeroid syndromes in which the newborn show the characteristic of old age at the time of birth. It first described in

1979 by Wiedemann of his two patients, and the other two previously reported patient (Rautenstrauch and Snigula, 1977, Wiedemann, 1979). The WRS consider one of progeroid syndromes because the patient has a characteristic of ageing include age mien, pseudohydrocephaly, general alteration in ossification, subcutaneous tissue atrophy, fat accumulation in flank and phalanxes, biochemical alteration, hypercholesterolemia and hyperinsulinism (Arboleda et al., 1997, Pivnick et al., 2000, Martin, 1978). All patients affected by WRS have limited survival time after birth, with a mean life expectancy of seven months (Arboleda et al., 2007). The newborn with WRS have dentation at birth (Devos et al., 1981), which is related to the alteration of jaws and face (Arboleda and Arboleda, 2005). The two main characteristics of a patient with WRS are an endocrine and metabolic alteration. For example, hyperinsulinism (Arboleda and Arboleda, 2005), and it may reflect on insulin resistant that associated with lipodystrophy (Najjar et al., 1975).

The cause of WRS not clearly understood. However, it suggested the most important causes are factors involved in cellular metabolism such as adipose tissue atrophy, hyperinsulinism and lipid alteration. In healthy cells, Akt mediates modulation of many molecules involved in the regulation of cell survival and cell cycle (Fresno Vara et al., 2004). Therefore, the alteration in PI3K/AKT signalling may have a close relation to this syndrome disorders (Arboleda et al., 2007).

1.3.2.2. Progeria models

Developing mammalian progeria models comes from the need to study and characterise progeria syndromes. However, progeria models can be used to study ageing as these models share many signs with naturally aged mice. Furthermore, using a mouse model of progeria will compress the time for experiments, and it will be easier to design and see the effects of treatment in a shorter time. Reducing the time of experiments will reduce the cost of animal housing and fit the duration of the most research project.

1.3.2.2.1 Mouse model of HGPS

Hutchinson-Gilford progeria syndrome (HGPS) is a rare accelerating ageing disease. As mentioned above the patients with syndrome display signs of ageing such as micrognathia, alopecia, delayed growth and aged looking skin (Sarkar and Shinton, 2001). Besides, the

patients die at an average of 13 years because of respiratory, cardiovascular, and arthritic conditions (DeBusk, 1972, Baker et al., 1981). The mouse model has been generated with a mutation in the A-type lamin gene, a significant component of the nuclear lamina to mimic this syndrome (Burke and Stewart, 2002). Mice with homozygous show defects as that noticed in HGPS, including reduce growth rate and die by four weeks of age.

Furthermore, skin, bone, and muscle also display the same pathologies of progeria. On the cellular level, mouse mutation of LMNA leads to a defect in nuclear morphology, particularly the change in the nuclear lamina (Mounkes et al., 2003). A defect in the lamina will affect the nucleus through chromatin organisation, DNA replication, and gene expression (Spann et al., 2002, Hutchison, 2002). The mouse model that displays this disorder, also called laminopathy, has a genotype of $Lmna^{L530P/L530P}$ mutant (Mounkes et al., 2003). To produce this model, the nucleotide base was changed in the LMNA gene, resulting in proline substitution for leucine at residue 530 (L530P) (Bonne et al., 1999). This mouse model appears normal at birth, but within 4-6 days developed growth retardation, and the average of death is 4-5 weeks. This mouse model also shows other signs of progeria patients, such as micrognathia and abnormal dentition. However, some phenotypes are displayed by progeria syndrome but not in $Lmna^{L530P/L530P}$ mouse, such as osteolysis of terminal digit and atherosclerosis (Mounkes et al., 2003).

1.3.2.2.2 Mouse model deficient in Zmpste24

This mouse model is deficient in zinc metalloproteinase STE24 (Zmpste24), the metalloproteinase that involved in posttranslational maturation of lamin A protein. This protein is considered an essential nuclear envelope component. $Zmpste24^{-/-}$ mice display nuclear abnormalities and show accelerating ageing (Pendas et al., 2002) as seen in humans with a mutation in *Zmpste24* (Agarwal et al., 2003). In addition to disruption of lamin A protein maturation, the mutation of this gene also lead to activated p53 target genes (Varela et al., 2005).

Premature ageing features displayed in mice with the mutant Zmpste24 gene are due to the accumulation of prelamin A. This accumulation cause nuclear abnormalities, decrease longevity, and many ageing related phenotype (Pendas et al., 2002, Bergo et al., 2002). Besides, the activation of p53 targets genes that response to tumour and DNA damage may

lead to apoptosis or cell cycle arrest (cellular senescence). These two processes could attenuate the function and structure of tissue due to depleting of stem cells (Rodier et al., 2007).

1.3.2.2.3 Mouse model with ERCC1 mutation

Longevity is dependent in some aspects, on the genome maintenance. Genome disorders resulting from deficiencies in genome maintenance proteins can lead to reduced lifespan and segmental progeroid syndrome (Hasty et al., 2003). One of the most critical pathways to maintain genome integrity is DNA repair pathways, by which the lesions are removed from DNA. ERCC1 protein complexed with XPF to made up endonuclease (Tripsianes et al., 2005). The activity of this enzyme is essential for correcting damage by nucleotide excision repair (NER) (Aboussekhra et al., 1995). However, this complex also participates in the repair of other DNA damage, namely DNA interstrand crosslink (ICL) (Kuraoka et al., 2000) and DNA double-strand break (DSB) (Ahmad et al., 2008).

The child that born with a defect in NER will suffer from a syndrome called xeroderma pigmentosum (XP), characterised by ultraviolet light (UV) sensitivity, skin pigmentation abnormalities, a strong predisposition to skin cancer in exposed areas, and frequently accelerated neurodegeneration. Other two NER disorder in human is the severe neurodevelopmental conditions, Cockayne syndrome (CS), and trichothiodystrophy (TTD) (Edifizi and Schumacher, 2015). In mammals, the NER disorder representative by UV sensitive rodent cell line can be corrected by human ERCC1 (excision repair cross-complementation group 1) gene. The protein that encoded in ERCC1 gene, complexed with XPF (ERCC4) products and forms the structure-specific endonuclease, which is responsible for the incision in damaged strand 5` of the lesion (Sijbers et al., 1996).

Experimentally, the mutation has been made in the ERCC1 gene in mice. Targeting the ERCC1 gene by knock-out protocol was achieved by subcloning a ~9.5 kb HindIII/SalI fragment containing murine ERCC1 exons 6–10 into pBR322 (Weeda et al., 1997). A unique ClaI restriction site was generated in exon seven by uracil-DNA-mediated mutagenesis (Kunkel et al., 1987). Insertion of the pMC1-neo resistance gene (Thomas and Capecchi, 1987), containing a diagnostic BamHI restriction site, into the unique ClaI site, yielding pE1NEO7 (Weeda et al., 1997). To generate ERCC1 gene with moderate effect, also refer as delta (Δ), Weeda et al., 1997 introduced the following procedure, and produced ERCC^{*292}

strain. They subcloned a 2.8 kb KpnI/XbaI fragment containing ERCC1 murine exons 7–10 into pTZ19 (Pharmacia) then they introduce a stop codon into mouse ERCC1 exon 10, deleting the amino-terminal seven amino acids. To insert the pMC1-neo resistance gene, they introduced a unique ClaI restriction site in intron 9, approximately 350 bp upstream of exon 10 using primer p82 (5`TAGTACATCGATGGGCGG) (Weeda et al., 1997). Breeding of these two genotypes with wild type ($ERCC^{+/+}$) resulting in genotypes related to ERCC1 gene. Full knockout mice of ERCC1 ($ERCC1^{-/-}$) gene are runted at birth and die before weaning (20-28 days) due to liver failure. These mice show evidence of polyploidy in perinatal liver and aneuploidy by three weeks of age. Besides, they show an elevation in p53 in many tissues (McWhir et al., 1993). The mouse model with *Ercc1*$^{-/-}$ genotype is short-lived mice. To generate mice with longer lifespan; Dolle´ et al. bred heterogeneous $ERCC1^{+/-}$ mice with $ERCC1^{+/\Delta}$ mice yielding mice with $ERCC1^{\Delta/-}$ genotype. Life spans of $ERCC1^{\Delta/-}$ mice are 19-26 weeks in male and 21-29 weeks in the female, therefore shorter compared to wild type 111-156 weeks in male and 119-146 weeks in the female, but still more than $ERCC1^{-/-}$. The maximum body weight that $ERCC1^{\Delta/-}$ mice reach for male and female is about 16.7 g and 14.8g respectively at 8-9 weeks of age, comparing to 29.8 g and 21 g for wild type. Also, they show organs weight loss. Liver lesions have been found in both wild type and $ERCC1^{\Delta/-}$ at the end of life. However, renal lesions and lymphoid depletion were more prominent in $ERCC1^{\Delta/-}$ compared to wild type. Dolle´ et al. noticed in general that the changes in aged subjects are comparable to $ERCC1^{\Delta/-}$ mice on biological age scale, i.e. occur at the same point in their lifespan (Dollé et al., 2011). Therefore, this genotype might be considered an excellent accelerated ageing model to study the progeroid syndrome related to DNA repair mechanism deficiencies and the effect of ageing in many organs as well.

1.4. Myostatin

Myostatin is a member of the Transforming Growth Factor-β (TGF-β) superfamily, is mainly secreted by skeletal muscle to negatively regulate its growth and development. Myostatin is an autocrine/paracrine inhibitor of muscle growth that expressed in cells of the skeletal muscle lineage from embryonic to mature cells (McPherron et al., 1997). Overexpression of myostatin results in a decrease in muscle fibre cross-sectional area (CSA) and subsequently, reduction in muscle mass (Durieux et al., 2007). On the contrary, deletion of

myostatin gene produces mice with a phenotype exhibiting a dramatic increase in skeletal muscle mass due to hyperplasia, an increase in the absolute number of muscle fibres, and hypertrophy, an increase in the cross-sectional area of individual muscle fibre (McPherron et al., 1997, Mendias et al., 1985). Myostatin has an inhibitory effect on protein synthesis in both myoblast and myotubes (Taylor et al., 2001). It increases the deposition of ECM components by inducing proliferation of muscle fibroblast (Li et al., 2008). Myostatin also involves in myofibres metabolic profile since its absence leads to loss of oxidative properties, with impaired in oxidative enzymes activity, and a reduction in muscle capillary density (Savage and McPherron, 2010, Amthor et al., 2007, Lipina et al., 2010). Myostatin deletion leads to perturbations in the intermyofibrillar mitochondrial respiration, and that was associated with an increase in muscle fatigability (Ploquin et al., 2012) and decline in muscle force generation, as well as specific tetanic tension (Amthor et al., 2007). Myostatin KO also affects the MHC profile by increase proportion of fast fibres on the expense of slow one (Amthor et al., 2007). Not only myofibres affect by myostatin signalling, but satellite cells also affected in term of proliferation and differentiation (McCroskery et al., 2003, Thomas et al., 2000).

1.4.1 Myostatin signalling pathway

Mechanism of Myostatin signal initiates an intracellular signalling cascade by binding its receptor, the activin type II receptor (ActRIIB), which leads to the recruitment and activation of the activin receptor-like kinase 4 and 5 (ALK4 and ALK5) to form a heterotetrameric receptor complex (Shi and Massague, 2003). Formation of receptor complex was followed by two intracellular signalling cascades activated through phosphorylation. One of these signalling start with phosphorylation of Smad2 and Smad3 and submit them to interact to form a complex with Smad4 that translocates into the nucleus, where it is involved in regulating the transcription of target genes (Shi and Massague, 2003, Feldman et al., 2006). Another signalling pathway is by inhibiting Akt through preventing its phosphorylation, which in turn results in activation of FoxO that leads to protein degradation, and hence muscle atrophy through either proteasome or autophagy mechanisms (Trendelenburg et al., 2009). In turn, FoxO itself interact with myostatin signalling pathway. FoxO1, a member of the Forkhead box O (Fox O)

transcription factor family (Murray et al., 2013) have been characterised in the mouse Myostatin promoter.

1.4.2 Post-developmental blocking of Myostatin

Skeletal muscle wasting occurs in a diversity of pathological conditions. Increase in Myostatin expression in disease states causing muscle wasting has been well documented in many studies. Previous studies have found an increase in Myostatin level in ageing subjects (Yarasheski et al., 2002), as well as due to immobilisation or prolonged bed rest (Reardon et al., 2001, Zachwieja et al., 1999). Numerous studies have revealed a notable increase in muscle mass of a range of species due to Myostatin ablation (McPherron and Lee, 1997, Schuelke et al., 2004, Mosher et al., 2007). Therefore, several approaches to inhibit Myostatin signalling has been suggested, for the therapeutic potential of stimulating muscle growth or preventing muscle loss in settings of conditions that induce muscle wasting. For example, Myostatin propeptide which blocks Myostatin signalling was used to enhance muscle growth in normal mice and amend the dystrophic characteristics of the mdx mice (Matsakas et al., 2009, Bogdanovich et al., 2005). Follistatin, a secreted glycoprotein that can bind Myostatin and inhibit its interaction with ActRIIB, has also been used and induce muscle mass (Haidet et al., 2008, Nakatani et al., 2008). Moreover, neutralising Myostatin by using antibody was able to induce muscle growth (Krivickas et al., 2009, Wagner et al., 2008). Interestingly, administration of soluble ActRIIB causes an increase in muscle mass of wild type and Myostatin null mice, indicating that in addition to Myostatin, there are other ligands bind activin receptor and limit muscle development (Lee et al., 2005). Post-natal block of myostatin unlike Myostatin genetic deletion, characterised by hypertrophy without hyperplasia (Girgenrath et al., 2005, Lee et al., 2005, Whittemore et al., 2003, Zhu et al., 2000).

Hypothesis, aims and objectives

First hypothesis

The acceleration of ageing in progeric mouse model (*Ercc1*$^{\Delta/-}$) mice was facilitated by accumulation of DNA damage through attenuation of ERCC1 protein, the essential protein for the primary DNA repair mechanism. We hypothesise that this progeric mouse model to be an excellent platform to studying ageing specifically ageing related loss of muscle mass and function, sarcopenia.

Aims and objectives

1. **To determine whether disruption of ERCC1 causes the muscle to undergo mass loss.**
2. **To determine whether the acceleration of ageing signs in *Ercc1*$^{\Delta/-}$ mice lead to loss of muscle activity.**
3. **To determine whether the sarcopenic phenotype of skeletal muscle of *Ercc1*$^{\Delta/-}$ mice harbour any metabolic alteration and MHC profile shifting.**
4. **To determine whether the *Ercc1*$^{\Delta/-}$ progeric phenotype affect satellite cells parameters.**

Second hypothesis

The second hypothesis of this project is that antagonising of myostatin/activin signalling in *Ercc1*$^{\Delta/-}$ progeric mice could overcome the skeletal muscle ageing signs due do accumulation DNA damage via attenuation of DNA damage repair ability of ERCC1 protein.

Aims and objectives

1. **To determine whether constraint between maintenance and growth can be broken, thereby promote growth with the persistence of DNA damage.**

   Therefore, we postulated three possible outcomes of the introducing of sActRIIB into *Ercc1*$^{\Delta/-}$ mice:

   a. Mstn blockage cannot prevent muscle wasting in the presence of DNA damage.
   b. Inducing muscle growth in progeric mice accelerates the development of age-related pathology.

c. sActRIIB can prevent muscle loss in *Ercc1*$^{\Delta/-}$.

To test this hypothesis and the outcome possibilities, I aim to utilise a panel of assays to investigate muscle mass, muscle fibre size, and muscle fibre number.

2. **To determine if antagonising of myostatin/activin signalling can emhance specific muscle force generation capacity and physical performance of the progeric animal animals.**
3. **To determine whether the sActRIIB treatment enhances mechanical force transduction apparatus and satellite cells parameters in *Ercc1*$^{\Delta/-}$ progeric mice.**
4. **To determine whether the sActRIIB treatment enhance organismal activity and affect lifespan in *Ercc1*$^{\Delta/-}$ progeric mice.**

Third hypothesis

I hypothesis that use of inbred control (*Ercc1*$^{+/+}$) treated with sActRIIB will behave as same as wild type animal with blocking myostatin signalling.

Aims and objectives

- **To determine whether the outcome of introducing sActRIIB to *Ercc1*$^{+/+}$ mice will be comparable to those in wild type mice.**

Chapter 2

Methods

2.1. Animal maintenance

The deletion of the ERCC1 gene was considered as embryonically lethal on the inbred mouse (Weeda et al., 1997). Control (*Ercc1*$^{+/+}$) and transgenic (*Ercc1*$^{\Delta/-}$) mice were bred as previously described (Dollé et al., 2011, Weeda et al., 1997). The mutation has been made in the ERCC1 gene in mice. Targeting the ERCC1 gene by knock-out protocol was achieved by subcloning a ~9.5 kb HindIII/SalI fragment containing murine ERCC1 exons 6–10 into pBR322 (Weeda et al., 1997). A unique ClaI restriction site was generated in exon seven by uracil-DNA-mediated mutagenesis (Kunkel et al., 1987). Insertion of the pMC1-neo resistance gene (Thomas and Capecchi, 1987), containing a diagnostic BamHI restriction site, into the unique ClaI site, yielding pE1NEO7 (Weeda et al., 1997). To generate ERCC1 gene with moderate effect, also refer as delta (Δ), Weeda et al., 1997 introduced the following procedure, and produced ERCC^{*292} strain. They subcloned a 2.8 kb KpnI/XbaI fragment containing ERCC1 murine exons 7–10 into pTZ19 (Pharmacia) then they introduce a stop codon into mouse ERCC1 exon 10, deleting the amino-terminal seven amino acids. To insert the pMC1-neo resistance gene, they introduced a unique ClaI restriction site in intron 9, approximately 350 bp upstream of exon 10 using primer p82 (5`TAGTACATCGATGGGCGG) (Weeda et al., 1997). Breeding of these two genotypes with wild type (ERCC$^{+/+}$) resulting in genotypes related to ERCC1 gene. These animals were maintained by the Animals (Scientific Procedures) Act 1986 (UK) and approved by the Biological Resource Unit of Reading University or the Dutch Ethical Committee at Erasmus MC. Mice have housed in individually ventilated cages under specific pathogen-free conditions (20–22°C, 12–12 hr light-dark cycle) and provided food and water ad libitum. Because the *Ercc1*$^{\Delta/-}$ mice were smaller than the wild type, food was administered within the cages, and water bottles with long nozzles were used from around two weeks of age. Animals were bred and maintained (for the lifespan cohort) on AIN93G synthetic pellets (Research Diet Services B. V.; gross energy content 4.9 kcal/g dry mass, digestible energy 3.97 kcal/g). Post-natal myostatin/activin block was induced in 7-week-old male mice, through intraperitoneal (IP) injection with 10 mg/kg of sActRIIB-Fc every week, two times till week 16 (Omairi et al., 2016). Each experimental group consisted of a minimum of five male mice. The University of Reading experiments were performed on 12 controls, 9 *Ercc1*$^{\Delta/-}$, and 14 sActRIIB treated *Ercc1*$^{\Delta/-}$ mice (all male mice). Lifespan experiments were

performed on both genders, with five male and five females *Ercc1*$^{\Delta/-}$ mice per treatment condition and four males and four female littermate wild-type controls. End-of-life *Ercc1*$^{\Delta/-}$ animals, both sActRIIB and mock treated, were post-mortem investigated and scored negative for visible tumours, signs of internal bleedings, enlarged spleen size, or abnormally coloured heart or enlarged heart size.

2.2. Open Field Animal Activity Monitoring system

Mice locomotor activity and behavioural pattern were monitored and assessed using an Open Field Animal Activity Monitoring system (Linton Instrumentation AM548). Two grids of the infrared light beam were produced in two levels by photocells, emitters and receptors, set up on an open field chamber. The lower grid measured standard X, Y movement, while the upper grid measured rearing movement. Animals activity were captured using AMON software, running on Windows PCs. Signals from photocell receptors resulted from infrared beam break were recorded due to animal movements. Acclimatisation of animals was performed for 30 minutes before recording data. The data were collected in an undisrupted environment on three occasions at one-day intervals. The total recorded data ware 60 minutes and automatically saved on the computer. Saved data were converted to an Excel sheet before analysing it.

2.3. Rotarod

Rotarod machine (Panlab Harvard Apparatus LE8500) was used for motor activity and fatigue characterisation. Mice were held manually by the tail and placed on the central rod that rotated at the minimum speed for acclimatisation for one minute. After that the rotation rate of the central rod was increased to a maximum of 40 rpm. The mice fall due to loose of coordination or fatigue the machine stopped. The rotation rate and time mice stayed on the central rod was recorded.

2.4. Grip strength to assess forelimb muscle strength.

In vivo assessment of forelimb muscle maximum force was performed using a force transducer (Chatillon DFM-2, Ontario, Canada). All tested animal brought in cages to the experimental room ~20 min before testing to ensure calamities, and they are properly awake. The grip strength meter was fixed adequately on a desk in a vertical position. Before taking each animal measurement, the meter was set to zero. The meter was set to record the maximal grip strength in gram. The animal was held by a tail base and lowered to a metal bar on a meter to allow the animal to grab the bar by front paws. Once the animal grabs the triangular bar, it pulled backwards in the horizontal plane. The strength of grip was recorded as a maximal force applying to the meter once the animal releases the bar. The measurements were taken just if the animal uses both front paws to grip, otherwise, if it uses one front paw or held by hind limb, the record was discard and repeated. The test was repeated in two sessions with three trials for each animal to ensure accurate measurements. The rest for one minute was allowed between the three trials for each animal to allow recovery, and the highest record was taken. Because of differences in body weight between animals and to ensure the objectivity of measurement, the grip values were normalised to the animal's body weight that was taken before each measurement.

2.5. Mice euthanasia

The animals that subjected to dissection in this study were humanely sacrificed via Schedule 1 killing by carbon dioxide asphyxiation followed by cervical dislocation.

2.6. Muscle tension measurements

Dissection of the hind limb was carried out under oxygenated Krebs solution (95% O_2 and 5% CO_2). One end of a silk suture was attached to the distal tendon of the EDL and the other to a force transducer (FT03). The proximal tendon remained attached to the tibial bone. The leg was secured in the experimental chamber. Silver electrodes were positioned on either side of the EDL. A constant voltage stimulator was used to directly stimulate the EDL, which was stretched to attain the optimal muscle length to produced maximum twitch tension (P_t). Tetanic contractions were provoked by stimulus trains of 500 ms duration at,

10, 20, 50, 100 and 200 Hz. The maximum tetanic tension (P_o) was determined from the plateau of the frequency-tension curve.

2.7. Skeletal muscles dissection

2.7.1. Hind limb muscles dissection

A group of hind limb muscle including Tibialis anterior (TA), Extensor Digitorum Longus (EDL) and Soleus muscles for morphological and cellular features investigation were selected because of their fibres type diversity and their ideal anatomical location.

A circular incision was made through the skin around the proximal end of the thigh to expose the hindlimb muscle; then the skin was pulled down to a removed by carefully slicing the footplate and pulling the skin distally free by hand.

2.7.1.1. Tibialis Anterior (TA) muscle dissection

Tibialis anterior is one of medial aspect of anterior surface muscles of the hind limb. The covering connective tissue, the fascia layer, was removed, pulling it toward the knee joint. Then the distal tendon of TA was cut from the insertion point at the dorsal surface of the tarsal and metatarsal bones. The muscle was pulled by the distal tendon until the proximal attachment to the tibial tuberosity using the tendon. The TA muscle then removed by cutting it at its origin.

2.7.1.2. Extensor Digitorum Longus (EDL) muscle dissection

The anatomical location of EDL is on the lateral part of the anterior surface of the hindlimb. On its proximal end, EDL has two tendons attached to the lateral condyle of the tibia and the head and anterior surface of the fibula, however, they appear as one tendon run laterally to the knee joint. The EDL muscle itself lies laterally and under the TA muscle. The tendon of the EDL has four parts on the distal end, which then run down to insert on the dorsal surface of phalanges of the four digits. The four distal EDL tendons were cut and pulled proximally to the knee, and then the two proximal tendons of the EDL were cut.

2.7.1.3. Gastrocnemius and Soleus muscles dissection

The gastrocnemius and the soleus muscles lie at the posterior side of the hindlimb. The gastrocnemius two heads originate from the lateral and medial condyle of the femur. Whereas the Soleus muscle attached to the head of the fibula and the medial side of the tibia bone shaft. The fascia layer and Biceps femoris covering gastrocnemius muscle were removed, thus exposing it. The distal tendons of both gastrocnemius and the soleus were cut, and the muscles were pulled together proximally to the knee. The proximal tendon was cut for both muscles after separating them by forceps.

2.7.2. Forelimb muscles dissection

Biceps brachii (BB) and Extensor carpi radialis longus (ECRL) muscles were dissected to be used in transmission electron microscopy (TEM) technique for investigating ultra-structures of skeletal muscle. After dissection, both muscles were placed directly into fixative solution (2.5% Glut in 0.1 M Na-Cacodylate pH 7.4).

2.7.2.1. Biceps brachii (BB) muscle dissection

Biceps brachii lies anteriorly to the humerus bone and covered with a layer of the fascia. This layer was removed with part of the pectoral muscle to expose the origin of the tendon. The proximal and distal tendons of BB muscle were cut, and the whole muscle was released. The Biceps Brachii muscle then transferred immediately into fixative solution (2.5% Glut in 0.1 M Na-Cacodylate pH 7.4).

2.7.2.2. Extensor Carpi Radialis Longus (ECRL) muscle dissection

Extensor Carpi Radialis Longus muscle lies on the medial side of the arm, the ulna bone. In order to expose the ECRL muscle, the covering fascia layer was removed, and the muscle was detached from all surrounding muscles. The proximal tendon severed from the lateral condyle of the humorous and the distal then cut from the lateral dorsal surface of the base of the third metacarpal bone and ECRL muscle was removed and transferred immediately into the fixative solution.

2.8. Ex vivo skeletal myofibre experimentation

2.8.1. Isolation of intact single myofibres of EDL muscle

The EDL muscle was subjected to use in single fibres experiment since it is relatively easy to get entire muscle with a long tendon from both sides. The EDL was placed after dissection in 1ml of 2% type 1 collagenase (2mg/ml). Then the muscles were incubated at 37°C, 5% CO_2 in the same solution. The individual muscle fibre is beginning to peel away from the muscle after approximately 30 minutes. The majority of myofibres were separated from muscle after incubated for 1.5 - 2 hours. Myofibres then transfer to a Petri dish and visualise with a stereomicroscope (Nikon SMZ1500). The myofibres were washed twice in Dulbecco's Modified Eagle Medium (DMEM), and twice with Single Fibre Culture Medium (SFCM). Then the myofibres even fixed for start point analysis, time zero (T0), or for 72 hr, however, a time point of 12, 24 and 48 hr were also fixed to follow up the progression of stem cell profile. Paraformaldehyde 2% were used to fix myofibres and kept at 4°C.

2.8.2. Satellite cell culture

Single myofibres were cultured in SFCM in a humid incubator at 37°C, 5% CO_2 and incubated for the required time. After incubation for 12, 24, 48 and 72 hr, each time point myofibres then fixed with PFA and keep at 4°C for immunocytochemistry.

2.9. Tissue freezing and preparing for cryosectioning

Dissected muscles were weighed, and slow freeze using the frozen surface of isopentane by liquid nitrogen (LN2) then kept in a tube in -80°C. The muscle was blocked in cryo-embedding medium (Optimal Cutting Temperature compound (OCT) (TAAB O023)) and freeze by half immersed in prechilled alcohol. By using cryostat, a 10 µm transverse sections for each muscle were obtained and transferred to poly-L-Lysine coated slides.

2.10. Haematoxylin & Eosin

Muscle sections were dewaxed in xylene and rehydration in ethanol before incubation with Harris Haematoxylin solution (Sigma HHS16) for 30 seconds to visualised nuclei. After that transfer to Eosin solution (Sigma-Aldrich 318906) for 2 minutes to stain cytoplasmic protein materials. The sections were then dehydrating in ascending ethanol concentrations, cleared with xylene and mounting by DPX medium.

2.11. Histological analysis and immunohistochemistry

Following dissection, the muscle was immediately frozen in liquid nitrogen-cooled isopentane and mounted in Optimal Cutting Temperature compound (OCT) (TAAB O023) cooled by dry ice/ethanol. Immunohistochemistry was performed on 10 µm cryosections that were air-dried at RT for 30 min before the application of block wash buffer (PBS with 5% foetal calf serum (v/v), 0.05% Triton X-100). Antibodies were diluted in wash buffer 30 min before using. Fluorescence-based secondary antibodies were used to detect all primary antibodies except for CD-31 where the Vectastain ABC-HRP kit was deployed (Vector PK-6100) with an avidin/biotin-based peroxidase system and DAB peroxidase (HRP) substrate (Vector SK-4100). Morphometric analysis of muscle fibre size was performed as previously described (Matsakas et al., 2012). Details of primary and secondary antibodies are given in Appendix 1.

2.12. Succinate dehydrogenase staining (SDH)

Muscle cryo-sections were incubated for 3 min at room temperature in a sodium phosphate buffer containing 75 mM sodium succinate, 1.1 mM Nitroblue Tetrazolium (Sigma-Aldrich) and 1.03 mM Phenazine Methosulphate (Sigma-Aldrich). Samples were then fixed in 10% formal-calcium finally applied hydro mount and coverslip.

2.13. Dihydroethidium (DHE) staining

Sectioned slides were dried for 30 minutes at room temperature. The sections were rehydrated using PBS then incubated with DHE (50 µmol/L in PBS Sigma D7008) for 30

minutes at 37°C in the dark. Counterstain for nuclei was DAPI-containing fluorescent mounting medium.

2.14. Transmission electron microscopy

This work has been done by Oliver Kretz, University of Freiburg, Germany.
Biceps muscle was briefly fixed with 4% Paraformaldehyde (PFA) and 2.5% glutaraldehyde in 0.1 M cacodylate buffer pH 7.4 in-situ at RT then dissected, removed and cut into pieces of 1 mm^3 and fixed for 48h in the same solution at 4°C. Tissue blocks were contrasted using 0.5% OsO_4 (Roth, Germany; RT, 1.5 hr) and 1% uranyl acetate (Polysciences, Germany) in 70% ethanol (RT, 1 hr). After dehydration, tissue blocks were embedded in epoxy resin (Durcupan, Roth, Germany) and ultrathin sections of 40 nm thickness were cut using a Leica UC6 ultramicrotome (Leica, Wetzlar, Germany). Sections were imaged using a Zeiss 906 TEM (Zeiss, Oberkochen, Germany) and analysed using ITEM software (Olympus, Germany).

2.15. Protein expression by immunoblotting

Frozen muscles were pulverised with pestle and mortar. Then the muscle powder solubilised in 50 mM Tris, pH7.5, 150 mM NaCl, 5 mM MgCl2, 1 mM DTT, 10% glycerol, 1%SDS, 1%Triton X-100, 1XRoche Complete Protease Inhibitor Cocktail, 1X Sigma-Aldrich Phosphatase Inhibitor Cocktail 1 and 3. Proteins were denatured in Laemmli buffer and resolved on 10% SDS-PAGs before immunoblotting and probing with antibodies and the SuperSignal West Pico Chemiluminescent substrate (Pierce). Details of antibodies are given in Appendix 1.

2.16. Quantitative PCR

50-100mg of Gastrocnemius muscle was solubilised in TRIzol (Fisher) using a tissue homogeniser. Total RNA was prepared using the RNeasy Mini Kit (Qiagen, Manchester, UK). 5µg RNA was reverse-transcribed to cDNA with SuperScript II Reverse Transcriptase (Invitrogen), and analysed by quantitative real-time RT-PCR on a StepOne Plus cycler, using

the Applied Biosystems SYBR-Green PCR Master Mix. Primers were designed using the software Primer Express 3.0 (Applied Biosystems). Relative expression was calculated using the ΔΔCt method and normalised to cyclophilin-B and Hypoxanthine-Guanine phosphoribosyl Transferase (HPRT). Primers sequences are given in Appendix 3.

2.17. Protein Synthesis measure

The relative rate of protein synthesis was measured using the surface sensing of translation method (SUnSET). Mice were injected precisely 30 minutes before tissue collection with 0.04 µmol/g body mass puromycin into the peritoneal cavity and then returned to their cages. After tissue collection, muscles were solubilised as for Western blotting and then pulled through a slot blotting chamber facilitating the transfer of protein onto a nylon membrane. After that the membrane was processed ideally to a Western blot.

2.18. In vivo Post-natal blocking of Myostatin

2.18.1. Intraperitoneal injection of soluble activin receptor IIB (sActRIIB)

Seven weeks-old males' control (*Ercc1*$^{+/+}$) and *Ercc1*$^{\Delta/-}$ mice were injected intraperitoneally twice weekly with 10 mg/kg of the soluble activin receptor IIB (sActRIIB) for a total period eight weeks before culling. To exact dosage, the animals were weighed before injection. The sActRIIB was administrated intraperitoneally using 30G, 8 mm long 1 mL insulin needles (Insumed 3079264). The animals were monitoring at the day of injection, and the day after to ensure they are not developing post-injection bleeding or reaction.

2.19. Imaging and analysis

Zeiss Axioskope2 microscope was used in Haematoxylin and Eosin (H&E), Succinate Dehydrogenase (SDH) and CD31 stained sections and images were captured using an Axiocam digital camera with Zeiss Axiovision computer software version 4.8. Fluorescence microscope (Zeiss AxioImegar A1) was used to examine immunofluorescent stained sections, and images were captured using an Axiocam digital camera with Zeiss Axiovision computer software version 4.8. Photoshop CS3 was used to merge and reconstructed

image for to examine entire muscle, then ImageJ software was used for counting and thickness analysis and Axiovison software version 4.8 was used for measure the myofibres cross-sectional area (CSA).

2.19. Statistical analysis

Data are presented as mean ± SE. The D'Agostino-Pearson omnibus test checked data normal distribution. Significant differences between two groups were performed by the Student's t-test for independent variables. Differences among groups were analysed by one-way analysis of variance followed by Bonferroni's multiple comparison tests or the non-parametric Kruskal–Wallis test followed by the Dunn's multiple comparisons as appropriate. Statistical analysis was performed on GraphPad Prism 5 (La Jolla, USA). Lifespan, onset of neurological phenotypes, and body weight decline were statistically analysed with the survival curve analysis using the product-limit method of Kaplan and Meier with Log-rank Mantel-Cox test in GraphPad Prism. Differences were considered statistically significant at $P < 0.05$.

Chapter 3 Results

Characterisation of skeletal muscle in the *Ercc1*$^{\Delta/-}$ progeric mouse

3.1. Introduction

The skeletal muscle has been extensively studied for its adaptation ability in term of qualitative and quantitative changes in response to physiological and environmental stimuli. These factors include innervation, genetic background, neuromuscular activity, exercise training, mechanical loading/unloading, and ageing (Pette and Staron, 2001). Further investigations focusing on skeletal muscle protein expression profile in responce to changed in fibres size and metabolic properties (Matsakas and Patel, 2009).

In human at middle age the skeletal muscle lost about 0.5-1% of mass per year, which dramatically increases in the seventh decade (Nair, 2005). Age-related muscle loss (sarcopenia) leads to a disproportionate decrease in strength (1.5-5%/year), implying a reduction in both the quality and quantity of the tissue (Keller and Engelhardt, 2013). Sarcopenia invariably leads to a reduced quality of life by impacting on mobility and stability, which leads to an increase in the incidence of fall-related injuries. Moreover, sarcopenia predisposes individuals to adverse disease outcomes (cardiovascular and metabolic diseases) and mortality (Srikanthan and Karlamangla, 2014, Kim et al., 2015).

Increase in the mass of skeletal muscle is dependent on the fibre number (hyperplasia) and fibre size (hypertrophy). However, genetic background and animal breed are significant factors that determine muscle mass (Martyn et al., 2004). As skeletal muscle makes up about 40% of live animal body mass, therfore decrease and increase in skeletal muscle mass is reflected on animal body weight. Change in skeletal muscle fibres number or cross-sectional area (CSA) of fibres affects muscle mass and body weight. As the myofibres numbers are defined at the prenatal stage, the post-natal muscle growth is accomplished by a fusion of skeletal muscle resident stem cells, satellite cells, to the existing myofibres (Sandri, 2008). Upon fibres growth, the newly formed myonuclei differentiated from satellite cells move to the centre of myofibres (Cadot et al., 2012); however, the centrally located fibres are evidence for some disease and physiological conditions such as degeneration-regeneration process (Duddy et al., 2015).

Skeletal muscle differs in term of a specific protein expressing, including myosin heavy chain (MHC), and each muscle is composed of a mixture of these proteins. Fibres expressing different myosin heavy chains have various metabolic requirements and contractile speeds.

The size of fibres has an inverse relationship with the oxidative capacity, explaining why the small fibres are oxidative and large fibres glycolytic (van Wessel et al., 2010).

Developing mouse models that undergo accelerating ageing allows to design experiments and investigate the effect of treatment in short time since these animals living entire life spam in the shortened period. The reduction in time also compress the cost of housing animal till late ages, and it is a relatively long period. Investigating the hallmark of ageing in the progeric mouse and does it mimicking the natural ageing or not to approve the use of this model as a platform for ageing studies.

The platform mouse model that we use in this study, *Ercc1*$^{\Delta/-}$, show accelerated ageing phenotype, however, that in some aspects are much more severe than in geriatric wild-type mice (Dolle et al., 2011, Gregg et al., 2012, Vermeij et al., 2016b). This phenotype is related to accelerate the rate of accumulation of DNA damage due to attenuation of the essential element in the DNA repair mechanism. Particularly, attenuation of Excision repair cross-complementation 1 activity, a key component of several DNA repair pathways including nucleotide excision repair (NER) (Sijbers et al., 1996), in this hypomorphic mutant mice lead to progressively show signs of ageing in all organs from about eight weeks of age. Among these organs, the skeletal muscle, the subject of this chapter, was also affected by genetic disruption of the ERCC1 gene (Dollé et al., 2011).

Here we investigate and describe the main features of skeletal muscles in a male progeric mouse model (*Ercc1*$^{\Delta/-}$) in comparison to control (*Ercc1*$^{+/+}$) group to show its similarities to aged sarcopenic skeletal muscle in its reliability as an ageing model.

Two cohorts of male mice (Control (*Ercc1*$^{+/+}$) and *Ercc1*$^{\Delta/-}$) were bred, housed under standard environmental conditions and provided food and water ad libitum in the Biological Resource Unit, University of Reading. Mice have housed in individually ventilated cages under specific pathogen-free conditions (20–22°C, 12–12 hr light-dark cycle) to end of experiments, age of 16 weeks.

The hind limb muscles (Extensor digitorum longus (EDL), Tibialis Anterior (TA), Gastrocnemius, Soleus and plantaris) were isolated and weighed. These muscles have been selected because they represent a spectrum of myofibres composition. Then muscles were frozen, cryosectioned and immunostained using antibodies for myosin heavy chains (MHC) (types I, IIA and IIB) to determine total muscle fibre number and types and size (CSA) of fibres. For the total fibres number count, the sections of mid belly part of all muscles for

both cohorts were analysed. These sections were stained to detect MHC isoform and used to count the total fibre number. Sections also use to determine the oxidative capacity by detecting the level of succinate dehydrogenase (SDH) activity. Additionally, EDL muscles were incubated in collagenase for single fibres isolation and satellite cells experiment. The procedures and technique used in this chapter were explained in detail in the methods chapter.

The main observations of this chapter are, firstly, muscles from *Ercc1*$^{\Delta/-}$ are lighter than the control group, and the CSA of all fibres type from skeletal muscle of progeric mice were less than the control group. Secondly, the skeletal muscle fibres from *Ercc1*$^{\Delta/-}$ tend to shift to glycolytic and fast profile compared to the control group. Finally, the satellite cell number was reduced in freshly isolated fibres and even after 72hr culture in *Ercc1*$^{\Delta/-}$ mice compared to the control group. Moreover, satellite cells from progeric mice do not follow the normal differentiation profile of the control group.

3.2. Body weight and skeletal muscle mass in an *Ercc1*$^{\Delta/-}$ mice.

Body weight was recorded in two-time points in both control and *Ercc1*$^{\Delta/-}$ group. As early as the 4-week-old, there was a significant difference between the control group and *Ercc1*$^{\Delta/-}$ group. The body weight was less by about 50% in *Ercc1*$^{\Delta/-}$ mice compared to the control group (Figure 3.1. A). Thene the mice grow, and at the age of 16 weeks, the body weight of progeric mice just increased by 23% of 4 weeks old and was still lower than the control group. The control group increased by 45% of their weight at four weeks (Figure 3.1. B).

Fresh muscles weight was taken directly after dissection. Five muscle group were weighed (including EDL, TA, Gastrocnemius, Soleus, and Plantaris). The progeric muscle was significantly lighter by 52%, 51%, 54%, 40% and 50% in EDL, TA, Gastrocnemius, Soleus, and Plantaris than control group respectively (Figure 3.2. A-E).

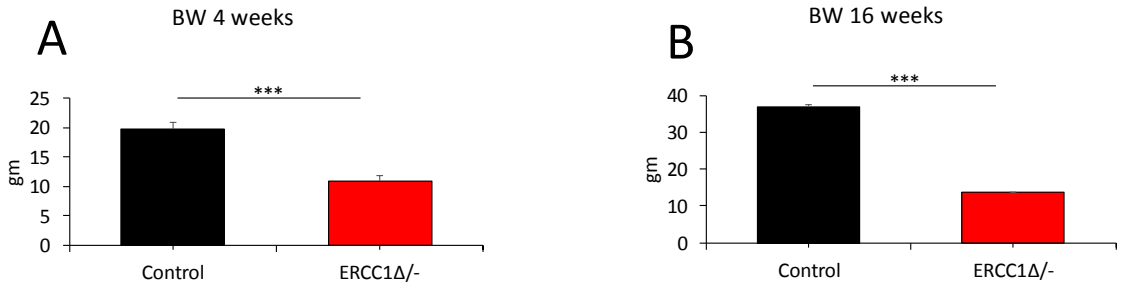

Figure 3.1. The disruption of ERCC1 gene lead to runted phenotype.

Body weight in Control and *Ercc1*$^{\Delta/-}$ group (A) at early as 4 weeks old and (B) at 16 weeks old.

n= 6 male mice from each cohort. Student's t-test, *<0.05,**<0.01, ***p<0.001.

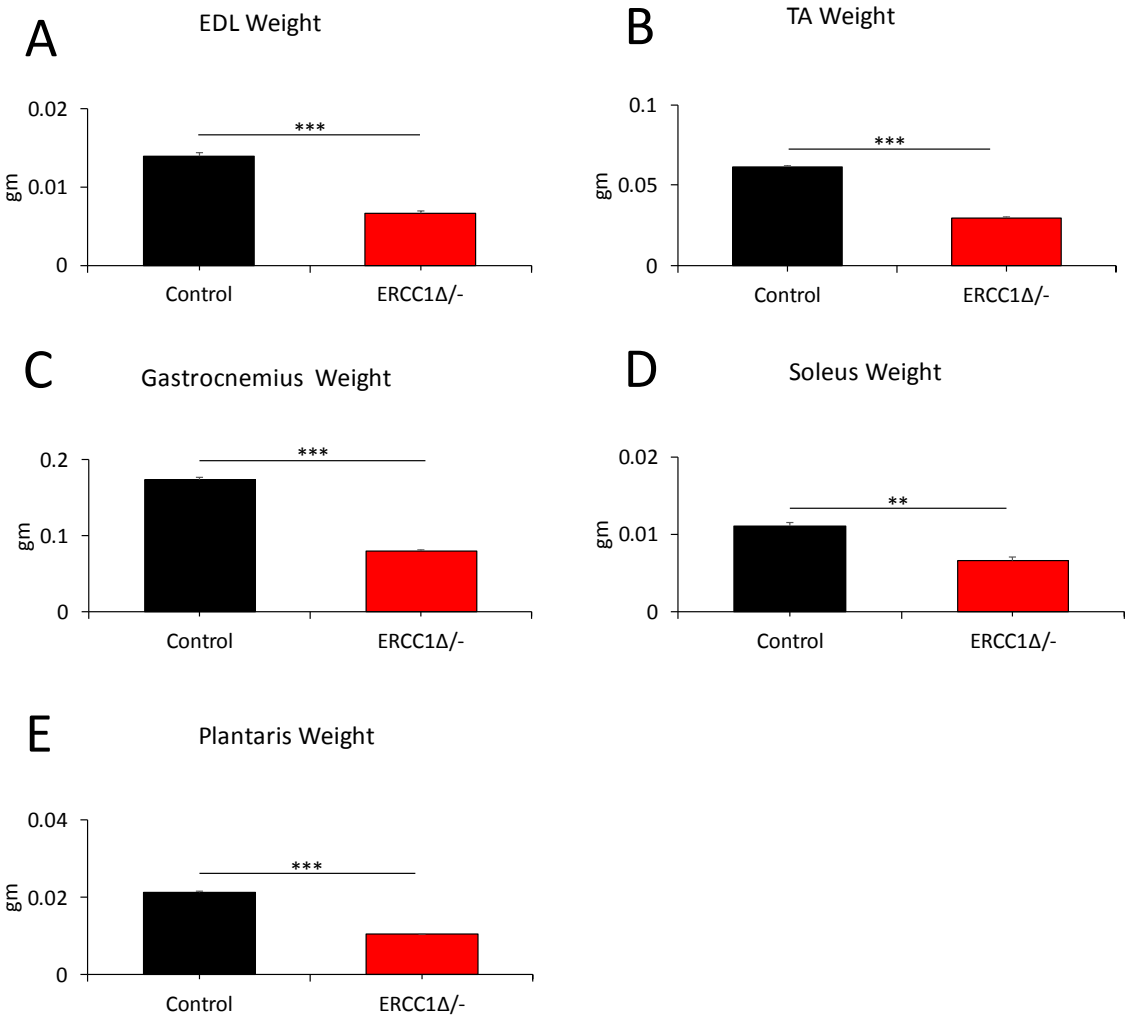

Figure 3.2. *Ercc1*$^{\Delta/-}$ hind limb skeletal muscles show reduces in weight compared to control group.

Muscle weight of 16-week old male *Ercc1*$^{\Delta/-}$ mice. (A) extensor digitorum longus (EDL), (B) tibialis anterior(TA), (C) Gastrocnemius, (D) Soleus and (E) Plantaris. All animals were 16 weeks old at the time of dissection from both cohorts. n= 6 male mice from each cohort. Student's t-test, *<0.05,**<0.01, ***p<0.001.

As the *Ercc1*$^{\Delta/-}$ mice have a runt phenotype and to make more reliant comparsion between progeric and control mice, we did a normalisation to muscle weight. The normalisation in many studies performed related to body weight; however, here we did normalise to tibia length. The body weight fluctuated with ageing and so in progeric mice, making it an unreliable reference for normalising. In contrast, the tibial length, which remains constant after maturity (Yin et al., 1982). Therefore, we normalised the muscle weight to tibia length in both control and *Ercc1*$^{\Delta/-}$ in EDL, TA, Gastrocnemius, Soleus, and Plantaris. All normalised *Ercc1*$^{\Delta/-}$ muscles were significantly lower than the control group by 41%, 39%, 45%, 40% and 46% in EDL, TA, Gastrocnemius, Soleus, and Plantaris respectively (Figure 3.3. A-E).
Taken together, these data show that the progeric phenotype resulting from disrupting ERCC1 gene accompanied by sarcopenia, loss of muscle mass, in all examined muscle. The sarcopenic muscles contributed significantly to body weight loss.

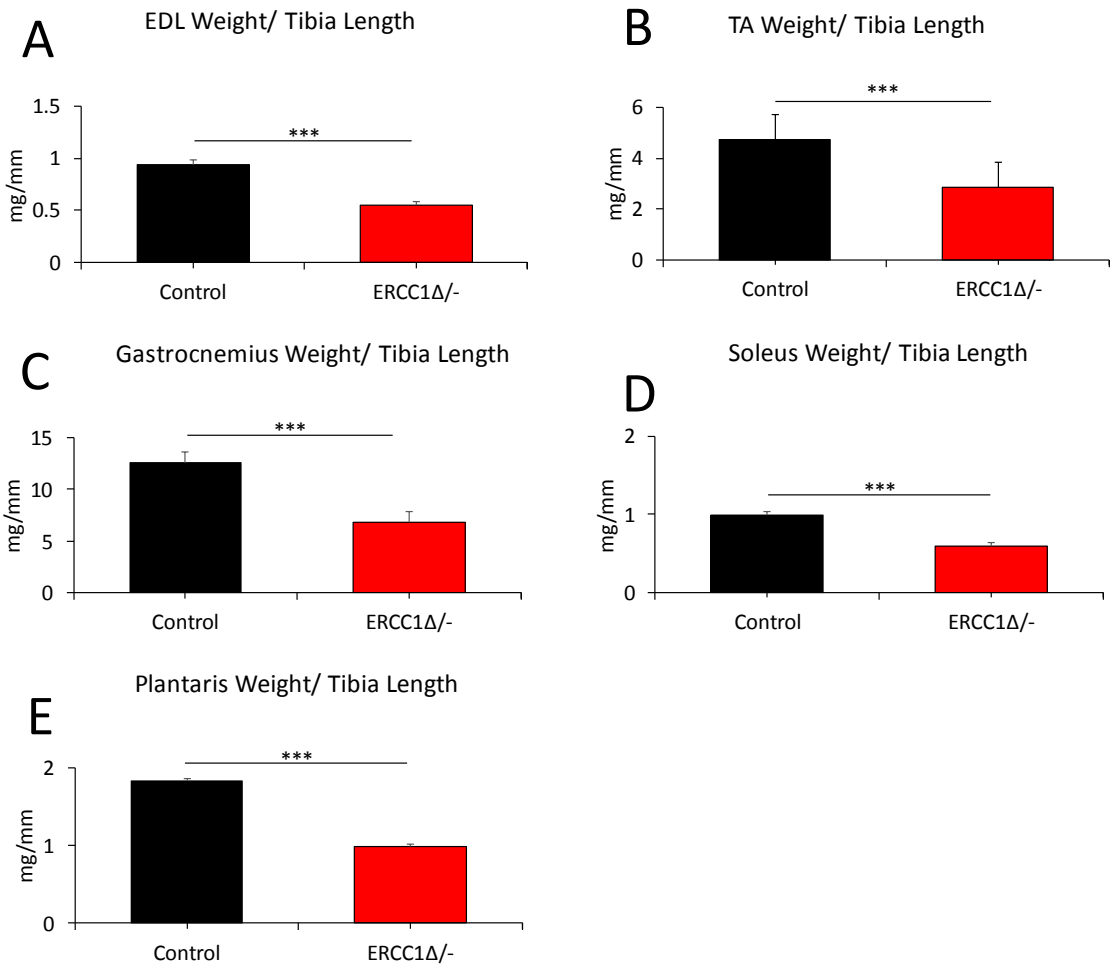

Figure 3.3. Hind limb skeletal muscle weight of progeric mice still lower than the control group. Normalized muscle weight to tibia length of 16-week old male *Ercc1*$^{\Delta/-}$ mice. (A) EDL, (B) TA, (C) Gastrocnemius, (D) Soleus and (E) Plantaris. All animals were 16 weeks old at the time of dissection from both cohorts. n= 6 male mice from each cohort. Student's t-test, *<0.05,**<0.01, ***p<0.001.

3.3. Fibres size and fibres number in an *Ercc1*$^{\Delta/-}$ mice.

Loss of muscle mass in mutant mice was not related to hypoplasia (decrease the fibre number). Surprisingly we found an increase in fibre count in EDL and Soleus muscle. In EDL muscle, the fibre number was significantly higher in *Ercc1*$^{\Delta/-}$ group compared to the control group (Figure 3.4. A) and the same trend found in Soleus albeit was not significant (Figure 3.4. B). As the centrally located nuclei is a sign of newly formed fibre, damage and repair processes, we count the percentage of the centrally located nucleus. EDL centrally located nuclei fibres in *Ercc1*$^{\Delta/-}$ were twofold more significant than the control group and three-fold in Soleus muscle (Figure 3.5. A-B).

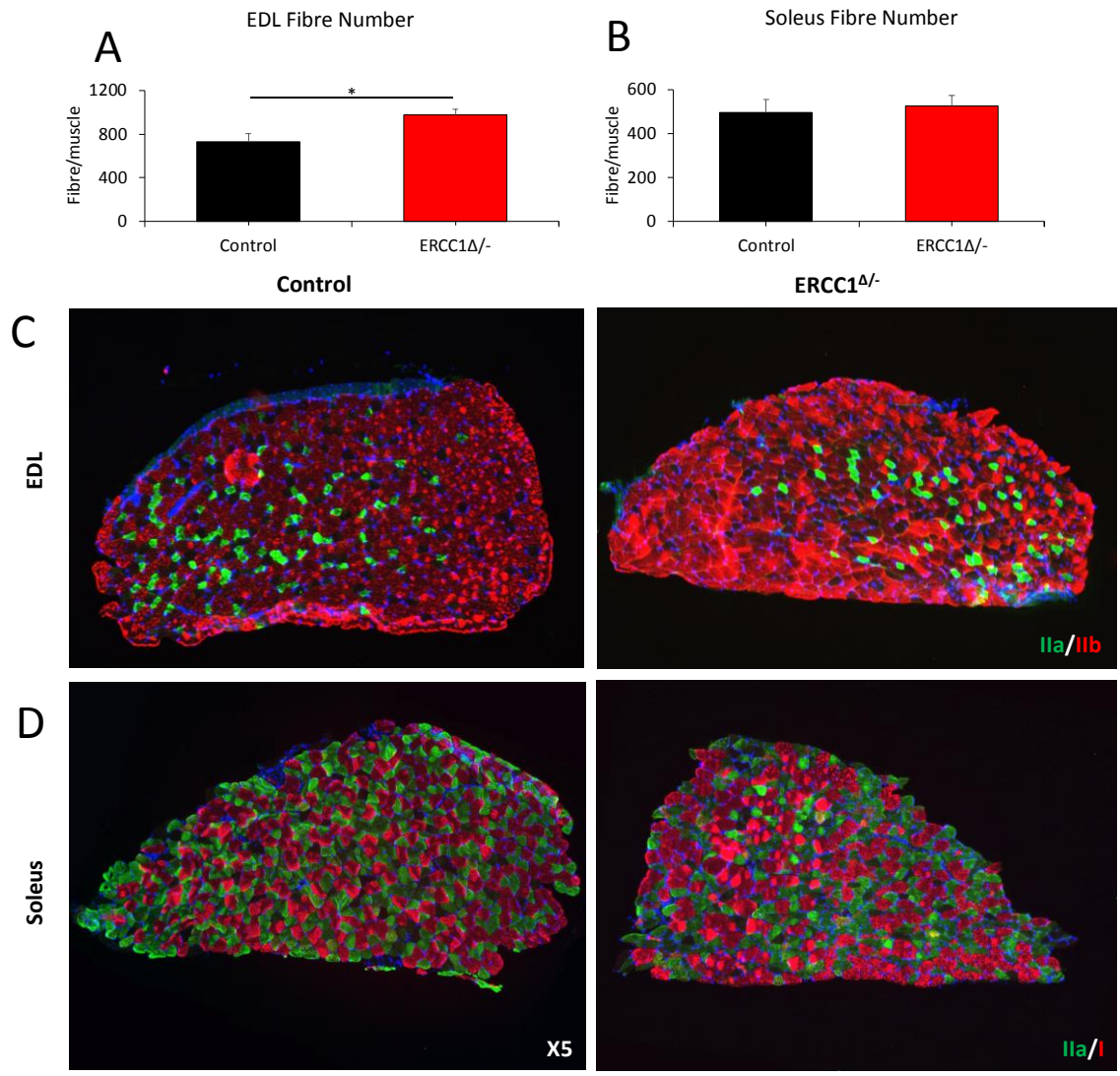

Figure 3.4. ERCC1 disruption increase fibres number in progeric mouse model.

Muscle fibres count. (A) EDL and (B) soleus fibre number count. (C) Representative image of EDL muscle immunostained against MHC IIb and IIa for control and *Ercc1*$^{\Delta/-}$ mice. (D) Representative image of Soleus muscle immunostained against MHC IIb and I for control and *Ercc1*$^{\Delta/-}$ mice. Whole muscle sections were counted for EDL and soleus muscles in both cohorts. All animals were 16 weeks old at the time of dissection from both cohorts. n= 6 male mice from each cohort. Student's t-test, *<0.05,**<0.01, ***p<0.001.

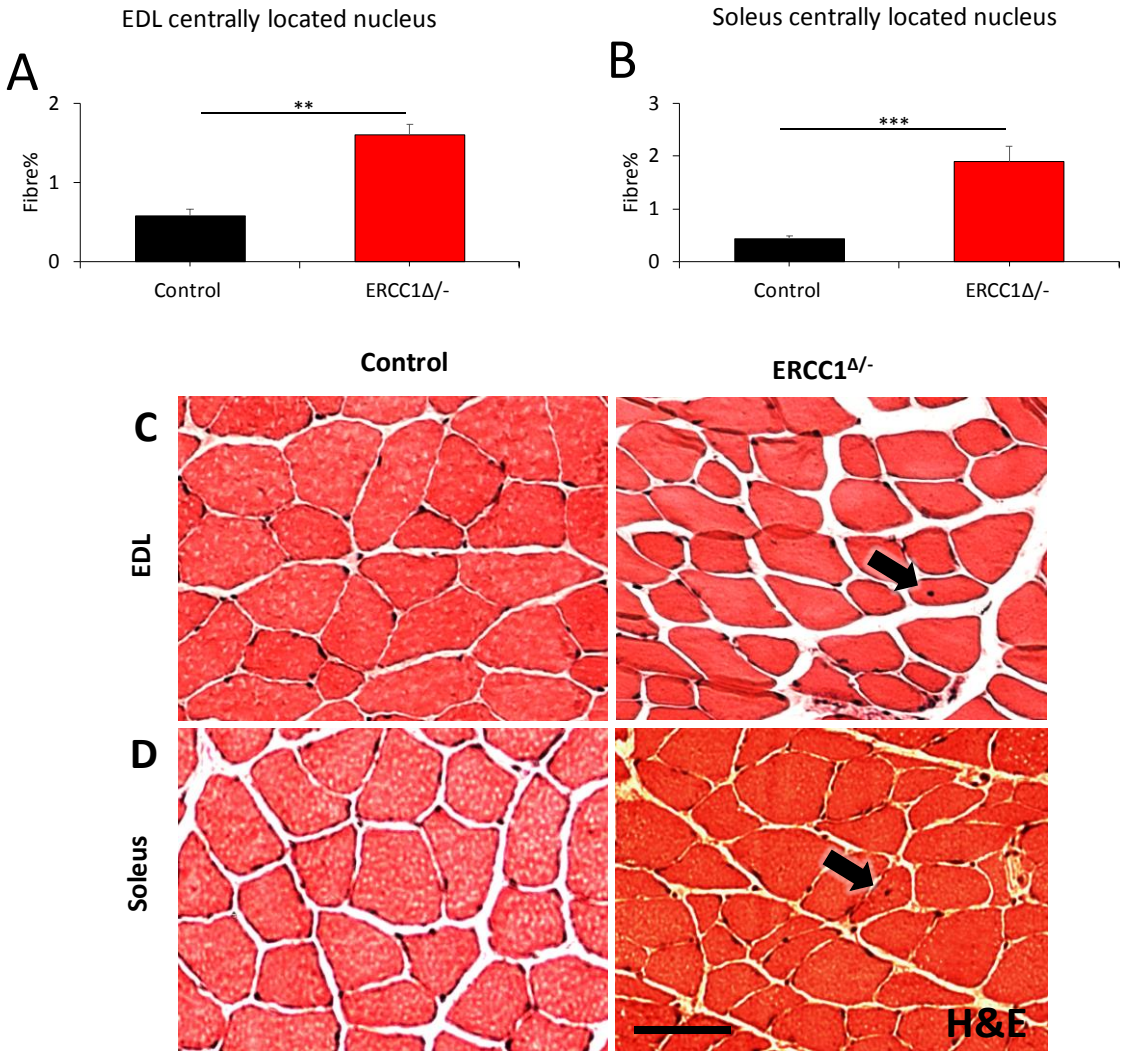

Figure 3.5. Abundance of centrally located nuclei in EDL and Soleus muscle from *Ercc1*$^{\Delta/-}$ mice. Frequency of centrally located nuclei in the (A) EDL and (B) soleus at 16 weeks. (C) representative images of EDL muscle for both progeric and control stained with H&E to detect centrally located nuclei. (C) representative images of Soleus muscle for both progeric and control stained with H&E to detect centrally located nuclei. The black arrows indicate the centrally located nuclie. Whole muscle sections were counted for EDL and soleus muscles in both cohorts and centrally located nucleuses presented as percentage regarding total fibres number. All animals were 16 weeks old at the time of dissection from both cohorts. Scale is 200µm. n= 6 male mice from each cohort. Student's t-test, *<0.05,**<0.01, ***p<0.001.

The decrease in muscle weight in progeric mice resulted from a decrease in fibre size, not the fibre number in all analysed muscles. The decrease in the cross-sectional area was noted in all fibres types (I, IIa, IIx, and IIb), where the CSA was less in *Ercc1*$^{\Delta/-}$ group in EDL, Soleus and TA, compared to control group. In EDL muscle, a glycolytic muscle, the CSA area for all three types of fibres IIa, IIx and IIb were significantly less in *Ercc1*$^{\Delta/-}$ compared to the control group (Figure 3.6. A). The trend was the same for CSA in the oxidative muscle, Soleus, especially in fibres type IIa and IIx, they were significantly lower compared to the control group. The most oxidative fibres in Soleus muscle, type I, were smaller but did not reach statistical significance (Figure 3.6. B). Lastly, for fibres area, we analysed the TA muscle as two areas as it has a superficial glycolytic (fast) and deeper oxidative (slow) areas. The primary two fibres type in the TA superficial area, IIx, and IIb were smaller in *Ercc1*$^{\Delta/-}$ compared to the control group, however type IIx fibres did not reach statistical significance (Figure 3.6. C). The cross-sectional area in the deep oxidative area of TA followed the trend of fibres in other muscle. The CSA area of the primary three fibres types in TA deep area, IIa, IIx, and IIb, were significantly smaller in the progeric group compared to the control group (Figure 3.6. D).

These data, in general, show that the decrease in muscle weight resulted from a decrease in the cross-sectional area of all fibres type in all examined muscle. However, hyperplasia was found in EDL, and Soleus muscle did not rescue the muscle loss.

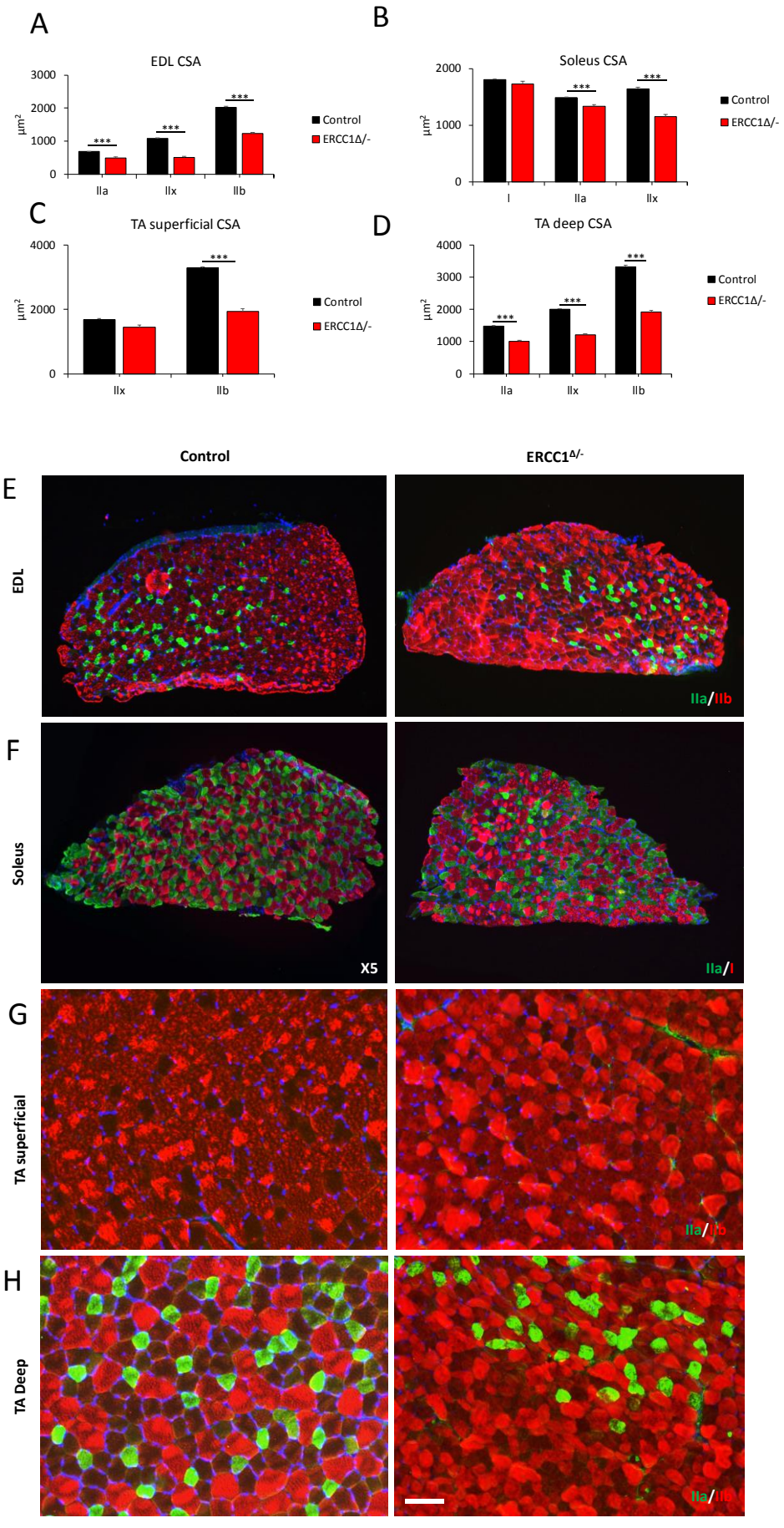
A
EDL CSA
3000
2000
1000
0
µm²
***
***
***
IIa
IIx
IIb
Control
ERCC1Δ/-
B
Soleus CSA
2000
1000
0
µm²
***
***
I
IIa
IIx
Control
ERCC1Δ/-
C
TA superficial CSA
4000
2000
0
µm²
***
IIx
IIb
Control
ERCC1Δ/-
D
TA deep CSA
4000
3000
2000
1000
0
µm²
***
***
***
IIa
IIx
IIb
Control
ERCC1Δ/-
Control
ERCC1Δ/-
E
EDL
IIa/IIb
F
Soleus
X5
IIa/I
G
TA superficial
IIa/IIb
H
TA Deep
IIa/IIb

Figure 3.6. Myofibres of hind limb muscle from *Ercc1*$^{\Delta/-}$ mice show smaller CSA than their counterpart myofibres from control mice.

Skeletal muscle fibre CSA of type I, IIa, IIx and IIb in (A) EDL, (B) soleus and the (C) deep and (D) superficial regions of the TA in relation of MHCs isoform expression. (E) Representative image of EDL immunostained against MHC proteins, green is IIa, red is IIb and nonstained is IIx fibres for both progeric and control mice. (F) Representative image of soleus muscle immunostained against MHC proteins, green is IIa, red is I and nonstained is IIx fibres for both progeric and control mice. Representative image of (G) TA superficial and (H) TA deep muscle immunostained against MHC proteins, green is IIa, red is IIb and nonstained is IIx fibres for both progeric and control mice. Whole muscle sections were counted for EDL and soleus muscles in both cohorts, and 100 fibres were measure for TA muscle CSA in each parts, superficial and deep, in both cohorts. All animals were 16 weeks old at the time of dissection from both cohorts. scale bar is 100 μm. n= 6 male mice from each cohort. Student's t-test, *<0.05,**<0.01, ***p<0.001.

3.4. The skeletal muscle fibres MHC profile and metabolic status in an *Ercc1*$^{\Delta/-}$ mice compared to the control group

Next, we investigate the myosin heavy chains (MHCs) expression. EDL muscle mainly expresses the fast type of myosin, IIb, as well as IIa and IIx (21.8%, 16.8% and 61.4% for MHC type IIa, IIx, and IIb) in the control group but this was 14%, 11% and 73% in *Ercc1*$^{\Delta/-}$ group. The dominant fast fibres IIb in EDL were significantly higher in progeric mice with significant decrease proportion in type IIa and a significant increase in type IIx, compared to control group (Figure 3.7. A). The mostly expressed slow fibre (type I) skeletal muscle, Soleus muscle, was showing no significant shifting toward fast fibres profile. The primary slow fibre in this muscle, type I MHCs had not changed with the proportion of 44.6% and 44.2% in the control group and *Ercc1*$^{\Delta/-}$ respectively. The other two fast fibres type, IIa, and IIx also showed no significant differences between *Ercc1*$^{\Delta/-}$ and control group. The fast fibre, IIa, with the proportion of 47% and 44%, and another fast fibre, IIx, was with the proportion of 8% and 11% in control and *Ercc1*$^{\Delta/-}$ group respectively group (Figure 3.7. B). TA muscle was considered has two different areas depending on MHC expression, the superficial and deep areas. The superficial part of TA muscle shows something similar to that reported in natural aged; the MHCs muscle protein was shifted toward the slower profile. The proportion of MHCIIa was 1.8% in control and increased to 12% in *Ercc1*$^{\Delta/-}$ group. In contrast, the proportion of type IIx and type IIb fibres were 17% and 80% in the control group which was decreased to 10.5% and 77% in *Ercc1*$^{\Delta/-}$ group respectively (Figure 3.7. C). In the deep area, there were shifts in the proportion of fibres MHC profile in *Ercc1*$^{\Delta/-}$ compared to the control group. The proportion of type IIa and type IIx fibre was significantly lower in *Ercc1*$^{\Delta/-}$ compared to control group with 12% and 10.6% for the progeric group and 18% and 19% for control group respectively. The most abundance fibre type IIb was significantly higher in *Ercc1*$^{\Delta/-}$ group compared to the control group with a proportion of 77% and 62.3% respectively (Figure 3.7. D).

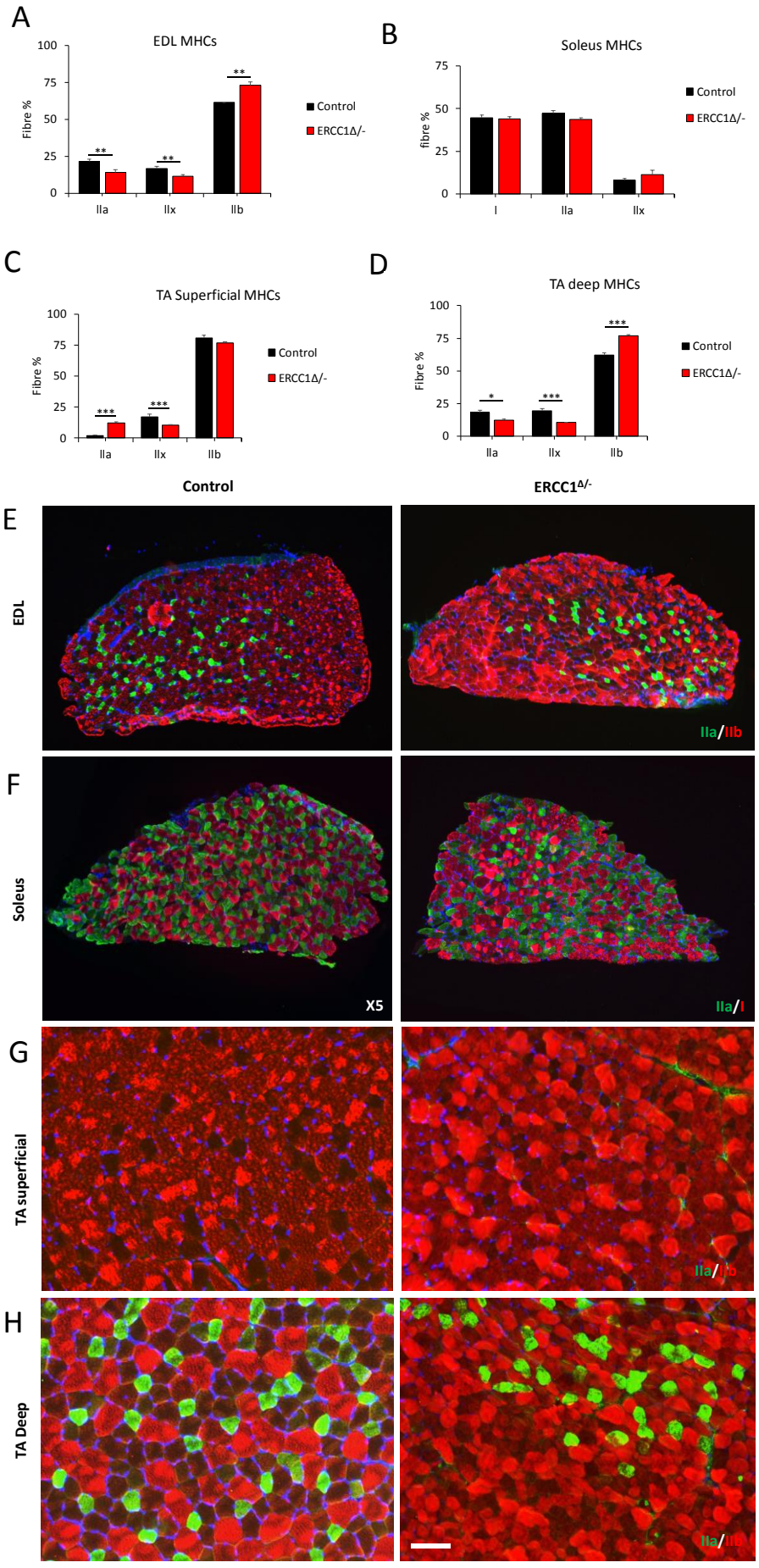
A
EDL MHCs
Fibre %
100
75
50
25
0
IIa
IIx
IIb
Control
ERCC1Δ/-
B
Soleus MHCs
fibre %
I
IIa
IIx
C
TA Superficial MHCs
D
TA deep MHCs
Control
ERCC1Δ/-
Control
ERCC1Δ/-
E
EDL
IIa/IIb
F
Soleus
X5
IIa/I
G
TA superficial
IIa/IIb
H
TA Deep
IIa/IIb

Figure 3.7. Shifting of myosin heavy chain profiling in in *Ercc1*$^{\Delta/-}$ mice hind limb.

MHC isoform (type I, IIa, IIx and IIb) profile detected by immunostaining used specific antibodies for MHC proteins in (A) EDL, (B) Soleus and (C) deep and (D) superficial regions of the TA from control *Ercc1*$^{+/+}$ and progeric *Ercc1*$^{\Delta/-}$ mice. Whole muscle was analysed by counting the specific MHC type and presented as a percentage, however in TA muscle the defined area were choose in deep and superficial area for analyses. (E) Representative image of EDL immunostained against MHC proteins, green is IIa, red is IIb and nonstained is IIx fibres for both progeric and control mice. (F) Representative image of soleus muscle immunostained against MHC proteins, green is IIa, red is I and nonstained is IIx fibres for both progeric and control mice. Representative image of (G) TA superficial and (H) TA deep muscle immunostained against MHC proteins, green is IIa, red is IIb and nonstained is IIx fibres for both progeric and control mice. Whole muscle sections were counted for EDL and soleus muscles in both cohorts and 100 fibres were analyses for TA in superficial and deep regions in both cohorts. All animals were 16 weeks old at the time of dissection from both cohorts. scale bar is 100µm.n= 6 male mice from each cohort. Student's t-test, *<0.05,**<0.01, ***p<0.001.

Next, we investigated the metabolic status by using a biochemical stain, succinate dehydrogenase stain (SDH). Analysing of two muscle, EDL and Soleus revealed a glycolytic shift in the progeric group compared to the control group. In EDL muscle, the percentage of oxidative fibres was significantly less in *Ercc1*$^{\Delta/-}$ group compared to the control group, (38.3% and 49.4%) (Figure 3.8. A). The effect of modulating Ercc1 gene had the same effect in oxidative muscle, soleus muscle. The percentage of oxidative fibre was 55.9% in control group and significantly lower (50.4%) in *Ercc1*$^{\Delta/-}$ (Figure 3.8. B).

Altogether, this set of data shows the trend of skeletal muscle fibres shifting profile regarding contractile speed and metabolic status in the progeric mouse model. There was an overall shift toward fast and more glycolytic profile compared to the control group.

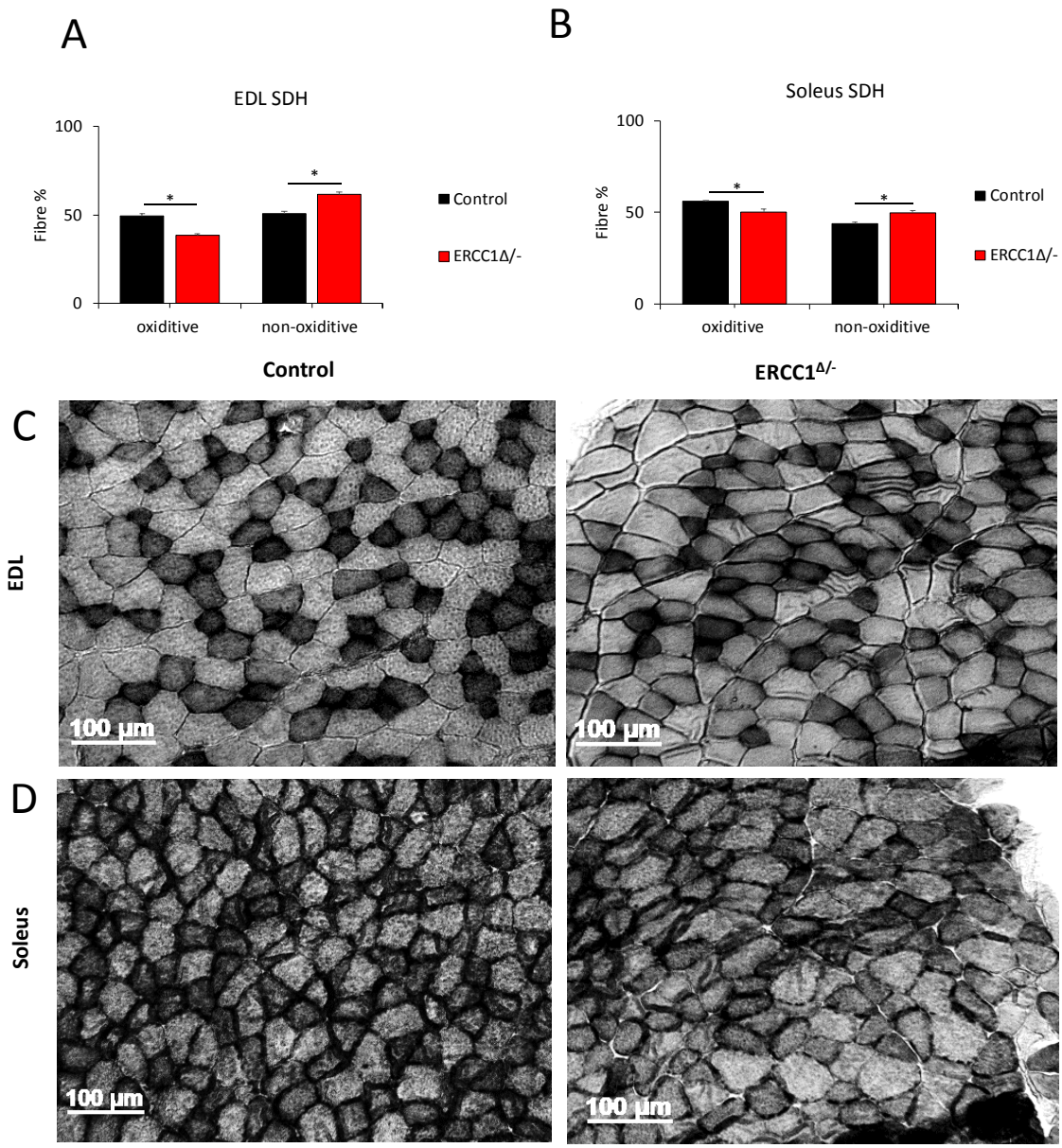
A
EDL SDH
100
50
0
Fibre %
*
*
oxiditive
non-oxiditive
Control
ERCC1Δ/-
B
Soleus SDH
100
50
0
Fibre %
*
*
oxiditive
non-oxiditive
Control
ERCC1Δ/-
Control
ERCC1Δ/-
C
EDL
100 µm
100 µm
D
Soleus
100 µm
100 µm

Figure 3.8. Myofibres from *Ercc1*$^{\Delta/-}$ hind limb skeletal muscle was less oxidative than the control group.

Sections from EDL and Soleus muscle were incubated with succinate dehydrogenase substrate to detect its activity as a marker for oxidative phosphorylation and abundant of mitochondria. Whole muscle sections were analyses and the dark fibres were considered as positive (oxidative) fibres and pale fibres considers as negative (non-oxidative) fibres. (A) Oxidative and non-oxidative fibre percentage detected by SDH activity EDL and (B) soleus. (C) representative images of EDL muscle sections stained with SDH for both control and progeric mice. (D) representative images of soleus muscle sections stained with SDH for both control and progeric mice. Whole muscle sections were counted for EDL and soleus muscles in both cohorts. All animals were 16 weeks old at the time of dissection from both cohorts. n= 6 male mice from each cohort. Student's t-test, *<0.05,**<0.01, ***p<0.001.

3.5. The satellite cell profile and proliferation capacity in the *Ercc1*$^{\Delta/-}$ mice compared to the control group

The muscle growth and regeneration rely in part on skeletal muscle resident stem cell, satellite cell, and its activity. Therefore we analysed the single fibres to investigate the satellite cells number and activity. EDL muscle fibres were isolated as a single fibre and used for analysing. The number of satellite cell that shows positive Pax7 were counted in the fresh sample (T0) and then cultured for 72hr (T72) and investigated at 24hr (T24), 48hr (T48), and T72. For the satellite cell activation and differentiation status, we analyse the cells in T72. For fresh fibres (T0), we counted the number of satellite cell on both control and *Ercc1*$^{\Delta/-}$ groups.

The satellite cells were significantly lower in *Ercc1*$^{\Delta/-}$ group with a mean of 2 satellite cell per fibre compare to 3.65 in the control group (Figure 3.9. A). The proliferation of satellite cell starts as in 24hr in control group, we show it grew up by about a 0.5 cell and reach to 4.13, while in progeric muscle it had just increased by 0.02 and was still significantly different to control group at T24 (Figure 3.9. B). By 48hr of culture, the control group proliferated and increased the number by 2.5-fold, whereas the increase in the *Ercc1*$^{\Delta/-}$ group was 1.75-fold compared to T0. The difference was significant at T48 between control and *Ercc1*$^{\Delta/-}$ group (Figure 3.9. C). After 72 hours of incubation, the satellite cell number in *Ercc1*$^{\Delta/-}$ grew to 2.5 cells per fibre, and it is significantly lower than control that reaches to 11.9 cells per fibres (Figure 3.9. D).

Proliferating stem cell grows as clusters on the surface of the single fibre. Then we counted the clusters per fibres starting from T24. Control group fibres had more clusters per fibre (3.97) than *Ercc1*$^{\Delta/-}$ group (2 clusters per fibre (Figure 3.9. E)). The cluster number doubled in the control group by 48hr culture to reach 6.4 clusters per fibres and it significantly lower in *Ercc1*$^{\Delta/-}$ group with 2.86 clusters per fibre (Figure 3.9. F). By the end of the culture period (T72), the cluster in control group increase by one cell compared to T48 and it was still significantly higher than *Ercc1*$^{\Delta/-}$ fibres that lost some clusters by an average of 1.8 clusters per fibres (Figure 3.9. G). Then we investigate the proliferation of single cell growing to the cluster. At the T24 and T48, there was no significant difference between the control and *Ercc1*$^{\Delta/-}$ group (Figure 3.9. H-I). The proliferation rate of a single cluster was higher in control compared to *Ercc1*$^{\Delta/-}$ mice at T72 with 1.7 and 1.3 cell/cluster, respectively (Figure 3.9. J).

Then we investigate the quiescence/differentiation status of satellite cell at T72 by looking at specific markers (Pax7/Myogenin). We show that about 80% of the satellite cells from the control group had differentiated and were expressing the differentiation marker myogenin (MyoG) and it is significantly at higher levels than the satellite cells from *Ercc1*$^{\Delta/-}$ group which express the marker (57%). The percentage of quiescence marker, Pax7, were significantly more in *Ercc1*$^{\Delta/-}$, 43%, compared to the control group (20%) (Figure 3.9. K).

In summary, the examination of satellite cell on single fibres from EDL muscle shows that the *Ercc1*$^{\Delta/-}$ progeric mice have significantly fewer cells compared the control group. Furthermore, the satellite cell in the progeric group failed to follow the normal proliferation and differentiation regime of the control group.

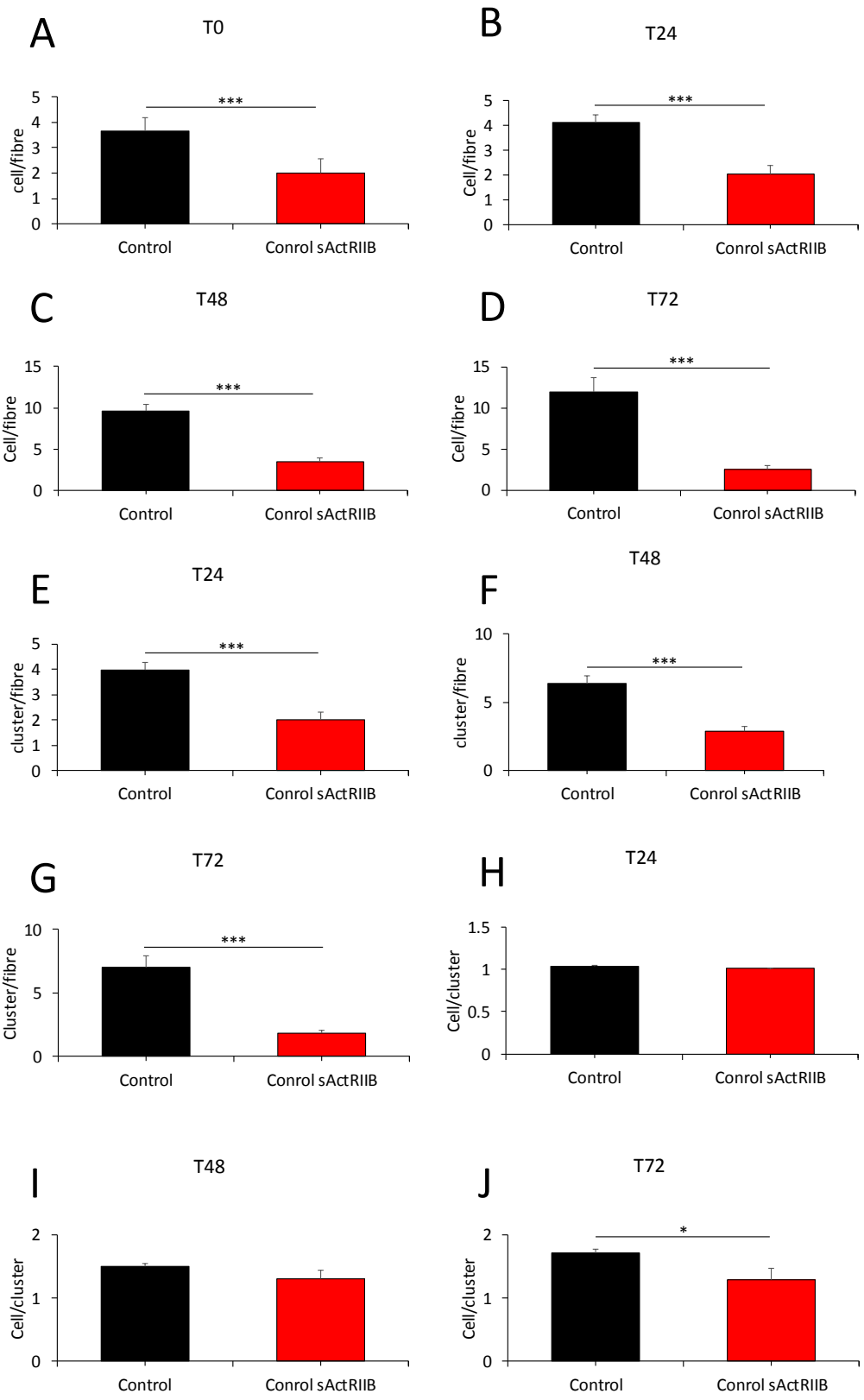
A
T0
cell/fibre
***
Control
Conrol sActRIIB
B
T24
Cell/fibre
***
Control
Conrol sActRIIB
C
T48
Cell/fibre
***
Control
Conrol sActRIIB
D
T72
Cell/fibre
***
Control
Conrol sActRIIB
E
T24
cluster/fibre
***
Control
Conrol sActRIIB
F
T48
cluster/fibre
***
Control
Conrol sActRIIB
G
T72
Cluster/fibre
***
Control
Conrol sActRIIB
H
T24
Cell/cluster
Control
Conrol sActRIIB
I
T48
Cell/cluster
Control
Conrol sActRIIB
J
T72
Cell/cluster
*
Control
Conrol sActRIIB

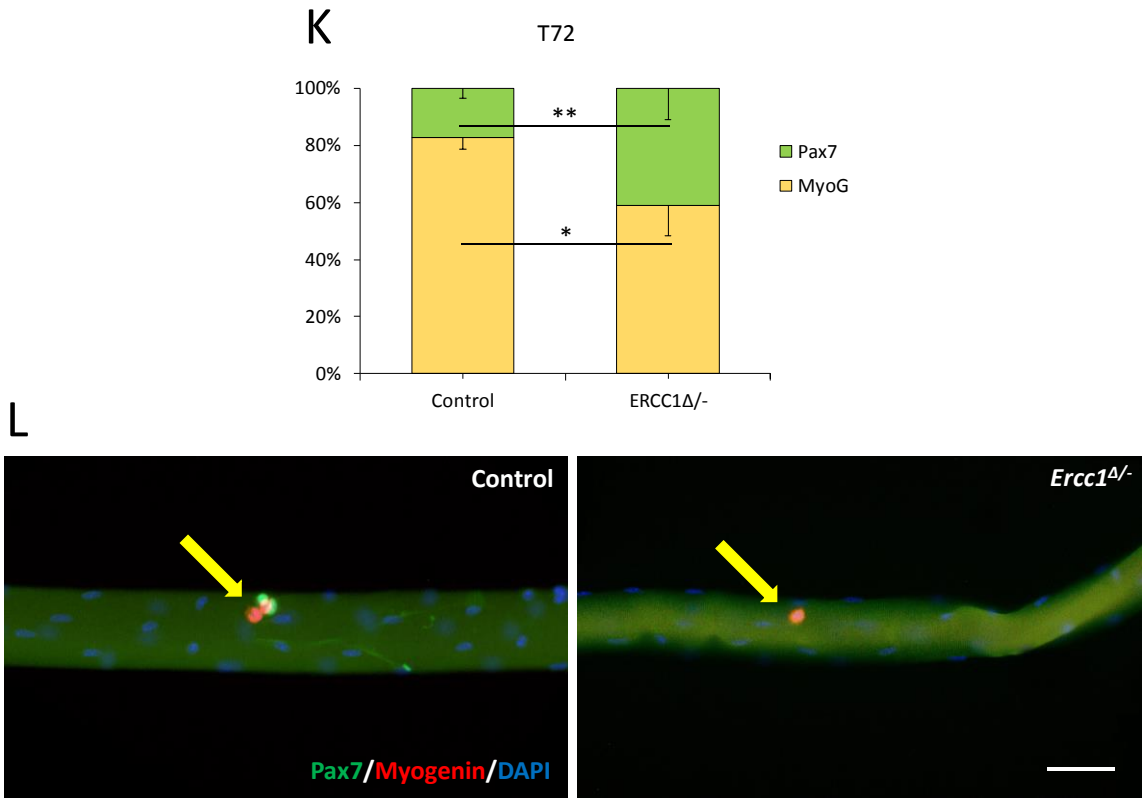

Figure 3.9. Examination of satellite cell number and status in *Ercc1*$^{\Delta/-}$ and control group in fresh and cultured fibres.

Satellite cell and progeny enumeration on (A) fresh and (B-D) cultured EDL fibres over for 72hours. (E-G) Enumeration of satellite cell clusters on cultured EDL fibres. (H-J) number of satellite cell per cluster on cultured EDL fibres. (K) Quantification of proportion of stem cells (Pax7+/Myogenin-) and differentiated cells (Pax7-/Myogenin+) on EDL fibres after 72h culture. (L) Representative images of control and progeric fibres examined at 72 hr for expression of myogenin (red) and Pax7 (green). Arrows indicated satellite cell progeny. Fibres collected from 3 mice from both cohorts and minimum of 20 fibres examined. Scale bar is 50µm. n= 6 male mice from each cohort. Student's t-test, *<0.05, **<0.01, ***p<0.001.

3.6. Discussion

The need for the progeric model to study the changes in ageing phenotype and to develop a suitable cure for diseases and disorders in ageing subjects has grown in the last decades. Designing an experiment and testing a treatment on naturally aged mice is relatively challenging because of time and cost. Furthermore, these models could be used to study both ageing-related diseases and disorders, also progeroid syndrome. Hence one of the essential causes that drive ageing is an accumulation of DNA damage, the mouse model with a defect in DNA damage repair system was therefore generated. We used a mouse model that has increased rate of accumulation of DNA damage due to genetic modification in Ercc1 gene that makes it less active. This mouse model has accelerated ageing phenotype with many similarities with naturally aged mice (Dolle et al., 2011).

We used the *Ercc1*$^{\Delta/-}$ mice as a platform of our experiment, and here we investigated and characterised the changes that are related to sarcopenia.

Ageing, along with factors such as altered neuromuscular activity, exercise training, mechanical loading/unloading, and hormonal profile influence skeletal muscle fibres profile. The changes in MHC isoforms tend to follow a general scheme of sequential transition from fast to slow and from slow to fast: MHCIβ ↔ MHCIIA ↔MHCIID ↔ MHCIIB (Pette and Staron, 2001). There was evidence of MHC profile shifting toward the slow profile with ageing, in fact, it more likely happens because of reduction of type 2 fibres (Lexell et al., 1983) rather than shifting (Aoyagi and Shephard, 1992). Accelerated ageing progeria syndrome patient related to ERCC1 gene, XPF-ERCC1 and progeria mouse model of *Ercc1*$^{-/-}$ both show the signs of sarcopenia (Niedernhofer et al., 2006). In this chapter, we have characterised the features of skeletal muscle from a mouse model of progeria with *Ercc1*$^{\Delta/-}$ genotype compared to *Ercc1*$^{+/+}$ as a control group.

As shown previously, the *Ercc1*$^{\Delta/-}$ mice had a stunted phenotype started at birth with low body weight (Dolle et al., 2011, Weeda et al., 1997). We also found that the body weight was significantly lower in *Ercc1*$^{\Delta/-}$ as early as four weeks of old as well as at the time of culling at 16 weeks compared to the control group. Lower body weight might result from growth arrest; however, it could result from lower organs weight, as shown in a previous study (Dolle et al., 2011). The body weight was about 50% less at four weeks old in *Ercc1*$^{\Delta/-}$ compared to the control group and was 63% less than the control group, at week 16 of age.

The later decrease in body mass could be explained by muscle mass loss, i.e. sarcopenia, as the skeletal muscle comprises 40% of the mouse. We show that all examined skeletal muscle of *Ercc1*$^{\Delta/-}$ mice undergo severe wasting (decreases in hindlimb muscle mass of 40-60% compared to controls). Increase in skeletal muscle mass is dependent mainly on the increase fibre number (hyperplasia) and fibre size (hypertrophy). Surprisingly, we found that the total fibres number in EDL and soleus in *Ercc1*$^{\Delta/-}$ is higher than the control group, even though the soleus does not reach statistically significant. However, the increase in total fibres number in these two muscles did not increase the skeletal muscle mass; on the contrary, the muscle mass was lower *in Ercc1*$^{\Delta/-}$ mice. It is clear that a reduction in skeletal muscle mass in *Ercc1*$^{\Delta/-}$ mice resulted from a decrease in cross-sectional area of all fibres type and the hyperplasia did not rescue the muscle mass loss. We found that the increase in total fibres number in *Ercc1*$^{\Delta/-}$ accompanied by a high number of centrally located nuclei in both EDL and Soleus muscles.

Increase number of myofibres with centrally located nuclei is considered a sign of formation of new fibres (Cadot et al., 2012) or disease such as mdx mice (Duddy et al., 2015) or any myofibres repair (as reviewed by (Folker and Baylies, 2013). We found a decrease in CSA in *Ercc1*$^{\Delta/-}$, so the centrally located nuclei here is not due to growth. The centrally located nuclei are likely to be from the regeneration repair process. Indeed, the growth of muscle, regeneration in the disease condition, and repair in other physiological condition need to recruit proliferating and differentiating satellite cells (Bischoff, 1994, Morgan and Partridge, 2003, Partridge and Davies, 1995). We show that satellite cells number in *Ercc1*$^{\Delta/-}$ was lower in number in freshly isolated fibres and even after 72hr incubation. Furthermore, the well-defined differentiation factor, myogenin (Olguin et al., 2007), was decreased in *Ercc1*$^{\Delta/-}$ compared to the control group. So, we suggest that the increase in centrally located nuclei were resulted from damaged fibres by splitting.

There is evidence of preferable MHCs age-related shifting from fast to slow (Holloszy et al., 1991) and been more oxidative (Smith et al., 2018). Progeric mouse model even follows the same profile shifting with age such mice which mimic Hutchinson–Gilford progeria syndrome (Greising et al., 2012) or in contrary; there was a shift toward fast and slightly more glycolytic in LMN progeria mouse model (Barateau et al., 2017). We show here with *Ercc1*$^{\Delta/-}$ mice, that most of the examined muscle undergone a slow to fast shift and as well as to be more glycolytic than the control group, except for MHCIIa and MHCIIb in the

superficial portion of the TA. A study by Stevenson and his colleagues shows a MHC profile shifting due to disuse in rat skeletal muscle (Stevenson et al., 2003). We could postulate the general preferable fast profile that noticed in the skeletal muscle of this mouse model compared to controls could result from reducing motion and activity related to ageing phenotype in *Ercc1*$^{\Delta/-}$ mice.

Chapter 4 Results

The Activin ligand trap increases body weight and enhances organismal activity and strength in progeric mice.

4.1. Introduction

Many investigations using rodents models suggest that maintaining muscle mass and function not only guards against sarcopenia but also promotes longevity, implying that the entire multi-organ ageing process can be attenuated by such intervention (Lavasani et al., 2012). However, a mechanism that promotes muscle hypertrophy as an anti-ageing regime would seemingly conflict with the intended outcome of the adaptive changes mediated through decreased GH/IGF-1 signalling that focus a body's reserves on tissue maintenance at the expense of growth. Although studies in humans have shown an association between maintaining muscle mass/function and attenuating the impact of sarcopenia (e.g. (Deutz et al., 2014)) and evidence that mass is a predictor for longevity (Srikanthan and Karlamangla, 2014), there is, to my knowledge, no direct evidence that it directly extends lifespan.

Targeting myostatin has been shown to increase muscle mass and strength in disease mouse model such as mdx mice (St Andre et al., 2017), preclinical models of cancer-induced muscle wasting model (Smith et al., 2015), and mouse model of spinal muscular atrophy (Liu et al., 2016). However, myostatin knocks out impaired force generation in wild type background mice (Omairi et al., 2016). As we mentioned above, ageing results in a progressive decline of the skeletal muscle mass and function, term as sarcopenia (Rosenberg, 1997). A study by Siriett et al. shows that prolong absence of myostatin reduce the severity of sarcopenia in aged mice (Siriett et al., 2006).

Myostatin a well-known molecule as its role as negatively regulate skeletal muscle growth and development (McPherron et al., 1997). Many condition that related to growth arrest have been detected with increased level of myostatin, such as immobilization or prolonged bed rest (Reardon et al., 2001, Zachwieja et al., 1999), AIDS, renal failure and heart failure (Gonzalez-Cadavid et al., 1998, Sun et al., 2006, Breitbart et al., 2011). Another study has found an increase in myostatin level with ageing (Yarasheski et al., 2002). Several strategies have been used to inhibit myostatin signalling and reveal enhanced in muscle growth in wild type and disease conditions (McPherron and Lee, 1997, Matsakas et al., 2009). From those, using sActRIIB as an antagonism molecule to myostatin shows an increase in muscle mass in wild type and myostatin null mice (Lee et al., 2005). There were many trail medicines based on the soluble form of Activin receptor type IIB treated different muscular dystrophy conditions; some of them discontinued development and other in on-going

development status. Acceleron Pharma has been producing a ligands trap molecule for TGF-β family called Ramatercept or ACE-031 for muscular dystrophy. This drug was discounted due to safety issues such as nosebleeds and gum bleeding (Saitoh et al., 2017b). The same company has developed another drug called ACE-083 designed for patients they have muscular dystrophy such as facioscapulohumeral muscular dystrophy and it still on-going development and also act as a ligand trap for TGF-β family. This one is different from the ACE-031 because it does not bind the ligands BMP9/10 (Townson et al., 2012).

Previous findings support the notion that an organism slows ageing by remodelling its cellular activity from growth and proliferation to maintenance and repair (Niedernhofer et al., 2006, Garinis et al., 2009, Pinkston et al., 2006). Slowing of ageing can be achieved by attenuating insulin-like growth factor-1 and growth hormone activity which controls the somatic growth axis (Hinkal and Donehower, 2008, Guarente and Kenyon, 2000) and by dietary restriction (DR) (Fontana et al., 2010). Vermeij and his colleagues have shown that DR delays ageing at the organismal level and extends the life and health span of *Ercc1*$^{\Delta/-}$ mice (Vermeij et al., 2016a). These studies advocate that promoting tissue growth in an ageing model might be harmful to the organism.

Here we investigate whether the maintain skeletal muscle growth in *Ercc1*$^{\Delta/-}$ progeric mouse model by injection of sActRIIB confers systemic benefit. Based on the concept that DNA damage induces a survival response that promotes maintenance programmes at the expense of growth one would predict that augmenting muscle growth would, in the long run, exacerbate the pathological features in a progeroid model. What we find is something entirely different; sActRIIB treatment before the onset of progeria can support the growth of skeletal muscle, notwithstanding NER defects.

Three cohorts of male mice (Control (*Ercc1*$^{+/+}$), *Ercc1*$^{\Delta/-}$ and *Ercc1*$^{\Delta/-}$ sActRIIB treated mice) were bred, housed under standard environmental conditions and provided food and water ad libitum in the Biological Resource Unit, University of Reading, or the Dutch Ethical Committee at Erasmus MC. Mice have housed in individually ventilated cages under specific pathogen-free conditions (20–22°C, 12–12 hr light-dark cycle) to end of experiments. Both the control group and *Ercc1*$^{\Delta/-}$ mock treated were IP injected twice a week with a vehicle, PBS, starting from week 7 of age to end of the experiment. The treated mice were also IP injected twice a week with 10 mg/kg sActRIIB starting from week 7 of age to end of the experiment.

Animals' physiological properties including organismal activities, muscle strength and locomotor activities, and ex vivo muscle tension measurement were examined using open field activity monitoring, rotarod and grip strength meter, force measurement device respectively. Glucose levels were measured using a Freestyle mini blood glucose metre. GH, Insulin, and IGF1 levels were measured in serum using ELISA kits. The onset of neurological abnormalities was scored in a blinded manner by experienced research technicians. The procedures and technique used in this chapter were explained in detail in the methods chapter.

The main finding of this section was the decreasing myostatin/activin signalling benefits both skeletal muscle and organismal health. However, we show that treatment with sActRIIB did not induce changes in the circulating levels of growth-related molecules, either GH, glucose, Insulin or IGF1. We show that the treated mice were heavier than nontreated mice, even though treatment with sActRIIB made no change in food consumption rate compared to nontreated mice. Overall, muscle strength parameters were enhanced upon sActRIIB treatment of *Ercc1*$^{\Delta/-}$ compared to the control group. We show a delay in age-related phenotype in treated progeric mice. However, sActRIIB did not affect the survival rate in *Ercc1*$^{\Delta/-}$ mice.

4.2. The Activin ligand trap increases body weight in *Ercc1*$^{\Delta/-}$ mice

The runt phenotype of *Ercc1*$^{\Delta/-}$ accompanied by a decrease in body weight was reported in the previous study (Dolle et al., 2011) and here. Male *Ercc1*$^{\Delta/-}$ mice were IP-injected twice a week with sActRIIB from 7-weeks of age till week 16. Mock-treated *Ercc1*$^{\Delta/-}$ mutants showed no overall body mass gain in 8 weeks, whereas both control and *Ercc1*$^{\Delta/-}$ animals treated with sActRIIB displayed weight increases of 37% and 18% respectively. *Ercc1*$^{\Delta/-}$ mice displayed an increase in body weight from the first week of injection and reached the maximum weight around the age of 14 weeks (35%). Both treated and non-treated *Ercc1*$^{\Delta/-}$ mice show a decline in body weight around week 14 and continue toward the end of the study. By the age of 16 weeks, non-treated *Ercc1*$^{\Delta/-}$ mice weights dropped to starting weight. However, the sActRIIB treated had a 14% increment in body weight (figure 4.1.A). The body weight of progeric mice was the same of treated and treated cohort, and both were less than the control group at the age of 7 weeks, the start points of the experiment (figure 4.1.B). At the end of the experiment, the age of week 15 both treated and non-treated mice still less than the control group. The Ercc1Δ/- treated mice were heavier than non-treated mice, albeit not reach a significant difference (figure 4.1.C). Overall, sActRIIB treatment enhanced the body weight gain in a progeroid mouse model.

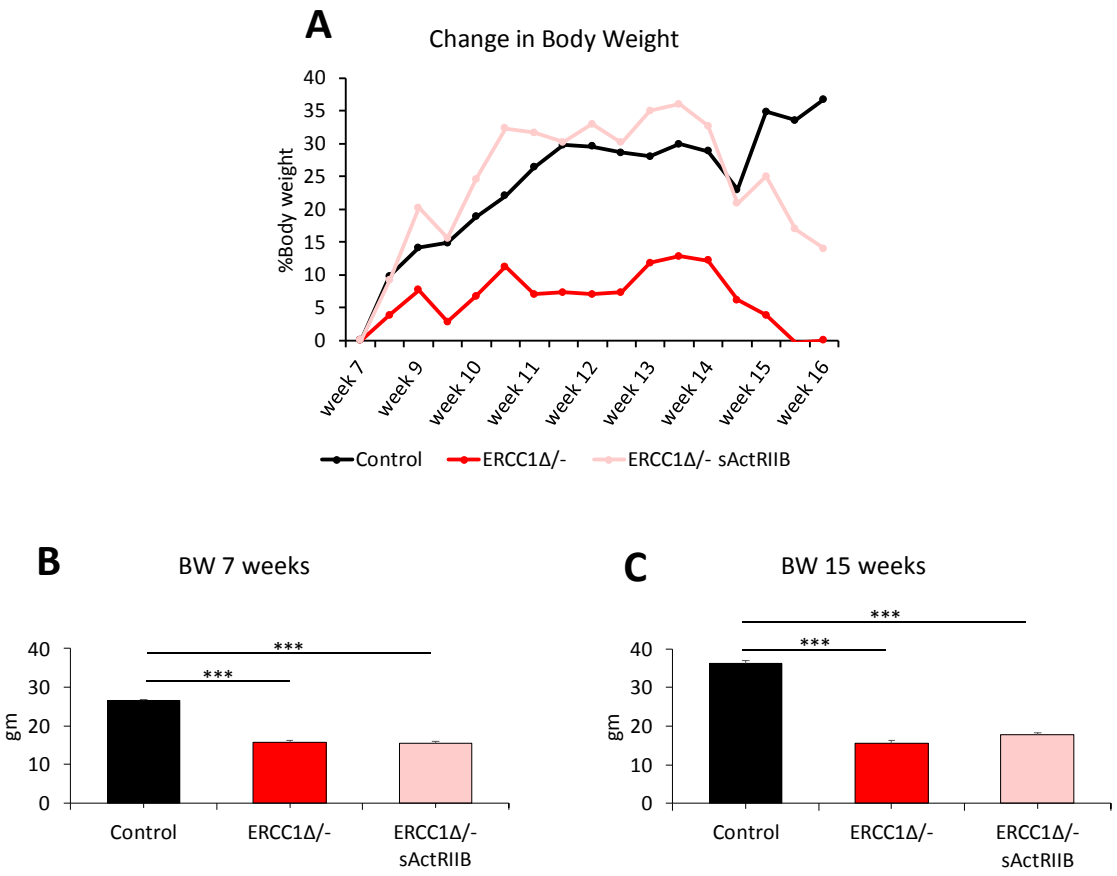

Figure 4.1. sActRIIB treatment mitigates body weight in *Ercc1*$^{\Delta/-}$ mice.

(A) Relative changes in body mass over time. IP injection of *Ercc1*$^{\Delta/-}$ with sActRIIB started at week 7 and tissues collected at the end of week 15. (B) Body weight at the start of experiment, 7 weeks old, in three cohorts, control, *Ercc1*$^{\Delta/-}$ and treated *Ercc1*$^{\Delta/-}$ mice. (C) Body weight at the end of experiment, 15 weeks old, in three cohorts, control, *Ercc1*$^{\Delta/-}$ and treated *Ercc1*$^{\Delta/-}$ mice. The sActRIIB were IP injected starting from week 7 of age to week 15. All mice were at the same age, n=6 control, n=5 *Ercc1*$^{\Delta/-}$ untreated and n=5 *Ercc1*$^{\Delta/-}$ treated males. Statistical analysis performed using one-way ANOVA followed by Bonferroni's multiple comparison tests was used, *p<0.05, **p<0.01, ***p<0.001.

4.3. sActRIIB treatment enhance organismal activity in *Ercc1*$^{\Delta/-}$ mice.

Behavioural and locomotor activity of mice from our three cohorts (Control, *Ercc1*$^{\Delta/-}$, *Ercc1*$^{\Delta/-}$ sActRIIB) were measured using an open field activity monitoring system. The total activity of animal was measured, and the metrics for *Ercc1*$^{\Delta/-}$ treated mice were about double that of non-treated and control group (Figure 4.2.A). sActRIIB treatment-maintained muscle activity in progeroid mice (distance travel per hour 5.6m in untreated mice versus 13.7m in treated). Furthermore, distance travelled of treated *Ercc1*$^{\Delta/-}$ mice not only increased compared to untreated mice but also to control animals (Figure 4.2.B). Total rearing counts and rearing time, measures of locomotor activity as well as exploration and anxiety, were highest in control mice and significantly reduced in *Ercc1*$^{\Delta/-}$ mice. sActRIIB treatment increased these values compared to *Ercc1*$^{\Delta/-}$ but not to normal levels (Figure 4.2.C-D).

Taken together, these data suggest that attenuation of Myostatin/activin by IP administration of sActRIIB to Ercc1$^{\Delta/-}$ mice are efficacious in enhancing behavioural and locomotor characteristics.

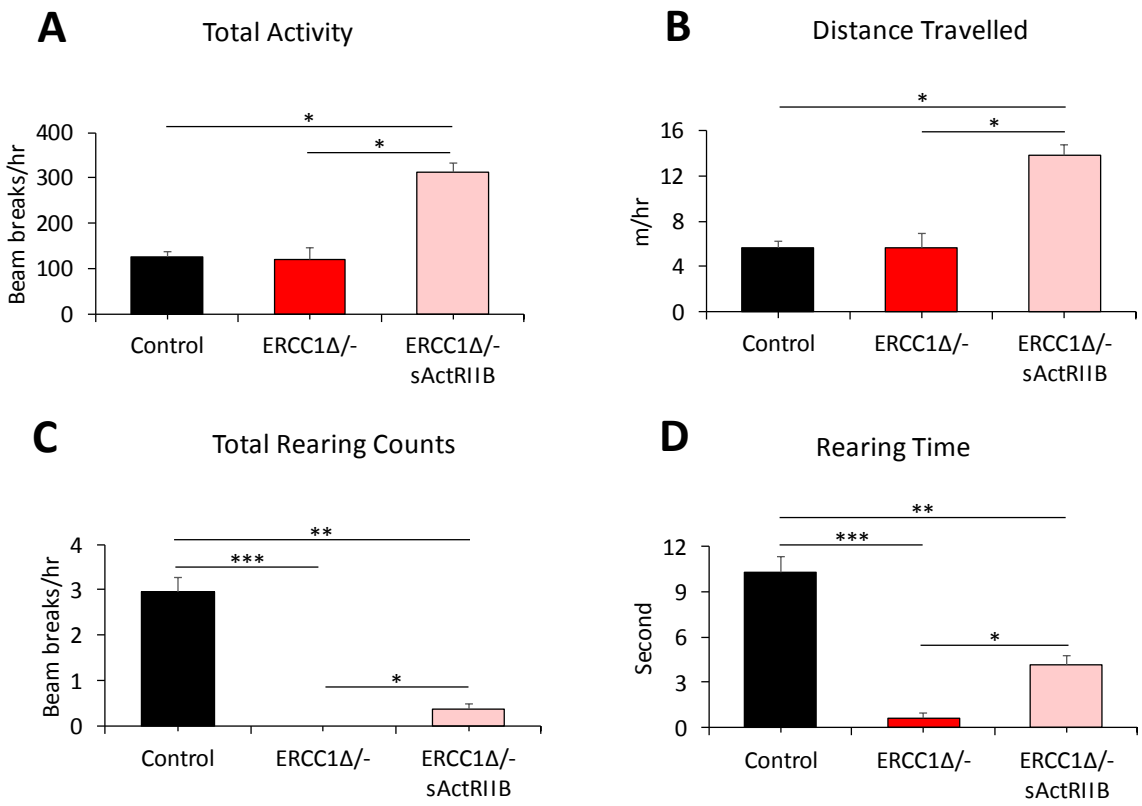

Figure 4.2. sActRIIB treatment enhance organismal activity in *Ercc1*$^{\Delta/-}$ mice.

Organismal activity measurements including (A) total activity, (B) distance travelled (C) total rearing counts and (D) rearing time, through activity cages at the end of week 14. The sActRIIB were IP injected starting from week 7 of age to week 15. All mice were at the same age, n=6 control males, n=5 *Ercc1*$^{\Delta/-}$ untreated males and n=5 *Ercc1*$^{\Delta/-}$ treated males. All analysis performed using nonparametric Kruskal-Wallis test followed by the Dunn's multiple comparisons, *p<0.05, **p<0.01, ***p<0.001.

4.4. sActRIIB enhances motor activity and fatigue characterisation in *Ercc1*$^{\Delta/-}$ mice.

To substantiate the results from the open field system that shows an increase in *Ercc1*$^{\Delta/-}$ activity after treatment with sActRIIB, we perform rotarod tests and measure the hind limb grip strength. Rotarod was used to assess motor activity and fatigue characterisation. Motor coordination, measured using the Rotarod, showed that *Ercc1*$^{\Delta/-}$ mice at the age of 15 weeks had a significant deficit in this skill which was improved, albeit not to normal levels, by sActRIIB treatment (Figure 4.3.A). *In vivo* assessment of forelimb muscle maximum force was enhanced by sActRIIB treatment in *Ercc1*$^{\Delta/-}$ mice. The reduction in progeric mice strength, only 50% of normalised grip strength, compared to control mice was significantly improved in *Ercc1*$^{\Delta/-}$ by sActRIIB (Figure 4.3.B). These data suggest that sActRIIB treatment attenuated the decline of muscle strength in *Ercc1*$^{\Delta/-}$ mice.

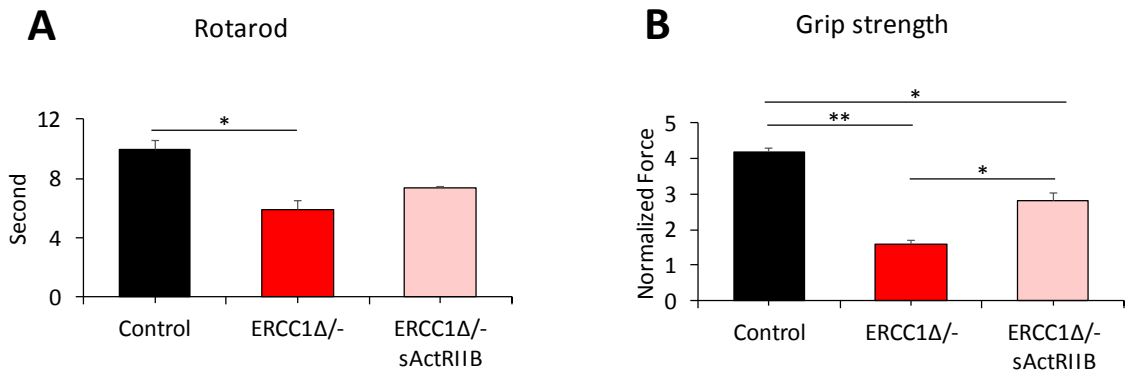

Figure 4.3. Assessment of motor activity and fatigue characterisation using rotarod and forelimb muscle strength using grip strength meter.

(A) Rotarod activity and (B) Muscle contraction measurement through assessment of grip strength at age of 15 weeks. All animal was at the same age at the time of experiment. n=6 control males, n=5 *Ercc1*$^{\Delta/-}$ untreated males and n=5 *Ercc1*$^{\Delta/-}$ treated males. The sActRIIB were IP injected starting from week 7 of age to week 15. All analysis performed using nonparametric Kruskal-Wallis test followed by the Dunn's multiple comparisons, *p<0.05, **p<0.01, ***p<0.001.

4.5. Increased muscle force generation capacity and reduce half relaxation time following sActRIIB injection in *Ercc1*$^{\Delta/-}$

We showed above that *Ercc1*$^{\Delta/-}$ sActRIIB-treated mice enhance behavioural and locomotor characteristics. Furthermore, antagonism of Myostatin/Activins by sActRIIB injection attenuate the decline of muscle strength in *Ercc1*$^{\Delta/-}$ mice. Here, to support these data, we investigate the ex vivo muscle tension measurement of one of hindlimb muscle, EDL, where both force generation and half relaxation time were measured. Previous works show that the targeting myostatin in wild type background mice decreases muscle specific force (Amthor et al., 2007), however, a study on the disease model, *mdx* mice, shows an increase in muscle-specific force after antagonism (Wagner et al., 2002, Bogdanovich et al., 2002). Here we examined the potential of sActRIIB treatment on generating specific force and half relaxation time in *Ercc1*$^{\Delta/-}$ mice. We found that the specific force decreased in *Ercc1*$^{\Delta/-}$ mutants, which were significantly increased by sActRIIB treatment (Figure 4.4.A). The decrease in half relaxation speed was achieved after treated *Ercc1*$^{\Delta/-}$ with sActRIIB, to normalised levels (Figure 4.4.B). Altogether, these data show that antagonise myostatin/activin enhances the contraction force and normalises speeds half relaxation time in *Ercc1*$^{\Delta/-}$.

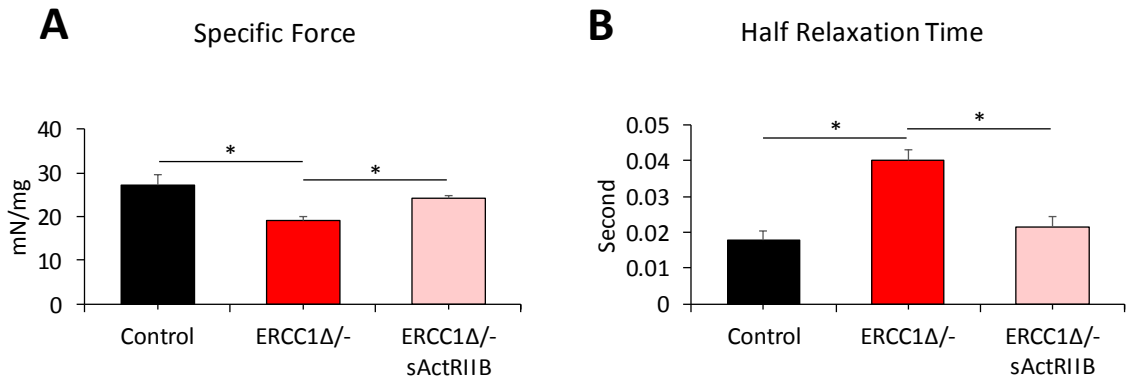

Figure 4.4. Ex-vivo muscle tension measurement.

Ex-vivo assessment of EDL specific force (A) and Half relaxation time (B). All the animals were 15-week-old when these tests were performed. n=6 control males, n=5 *Ercc1*$^{\Delta/-}$ untreated males and n=5 *Ercc1*$^{\Delta/-}$ treated males. The sActRIIB were IP injected starting from week 7 of age to week 15. All analysis performed using nonparametric Kruskal-Wallis test followed by the Dunn's multiple comparisons, *p<0.05, **p<0.01, ***p<0.001.

4.6. The sActRIIB injection does not affect circulating level of growth-related blood parameters in *Ercc1*$^{\Delta/-}$

Many of skeletal muscle parameters related to ageing phenotype in *Ercc1*$^{\Delta/-}$ mice are shown above were enhanced by injection of sActRIIB. Here we show that the growth hormone/ Insulin-like growth factor-1, components of the central genetic axis that controls ageing (Milman et al., 2016), had not changed after sActRIIB treatment in *Ercc1*$^{\Delta/-}$. We measured the level of four molecules known to regulate organismal growth. Blood glucose level was about half of control in *Ercc1*$^{\Delta/-}$ mice, and with treatment with sActRIIB had not changed the level of this molecule (Figure 4.5.A). Analyse another molecule belonging to growth regulated factors, Insulin, showed similar profile of glucose, the blood level of Insulin was less in *Ercc1*$^{\Delta/-}$ compared to the control group; however, the sActRIIB decreased it even further than the *Ercc1*$^{\Delta/-}$ but not reaching a significant difference (Figure 4.5.B).

Antagonise of Myostatin/Activin by sActRIIB injection did not rescue the low level of IGF1 in *Ercc1*$^{\Delta/-}$ compared to the control group (Figure 4.5.C). As previously shown, that prolonged depression of IGF1 gives rise to a feedback mechanism to elevate the level of growth hormone (Niedernhofer et al., 2006). That is what we found; we show the increased level of Growth hormone in *Ercc1*$^{\Delta/-}$ mice compared to an absolute low level in control group, and because of the level of IGF1 did not respond to sActRIIB treated then we found no effect on GH level as well (Figure 4.5.D). However, food intake of *Ercc1*$^{\Delta/-}$ mutants, relative to body weight (but not absolute (Figure 4.6.A)), was higher than control mice but unaffected by sActRIIB treatment (Figure 4.6.B). Overall we found that antagonism of Myostatin/Activin by sActRIIB injection did not induce changes in the circulating levels of either GH, glucose, Insulin or IGF1.

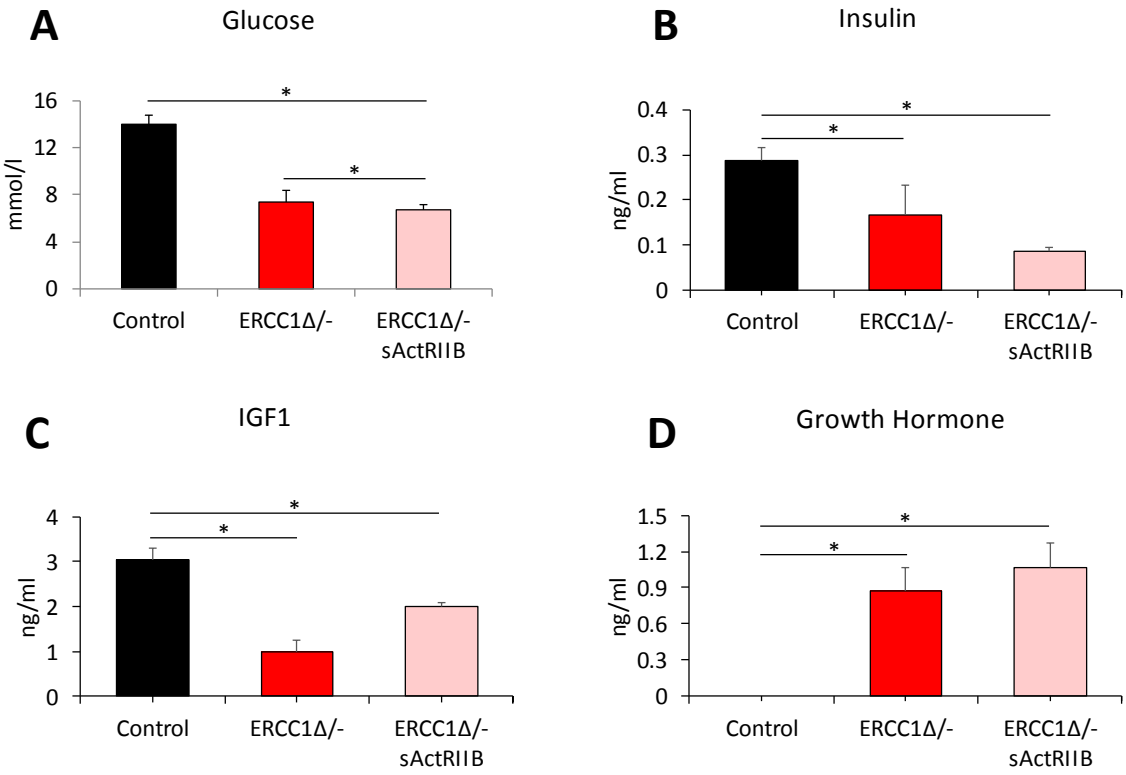

Figure 4.5. Circulating level of growth-related blood parameters.

Levels of (A) Growth hormone (B) Glucose (C) Insulin and (D) IGF1 at beginning of week 15. The sActRIIB were IP injected starting from week 7 of age to week 15. All mice were at the same age, n=6 control males, n=5 *Ercc1* $^{\Delta/-}$ untreated males and n=5 *Ercc1* $^{\Delta/-}$ treated males. All analysis performed using nonparametric Kruskal-Wallis test followed by the Dunn's multiple comparisons except (D) where one-way ANOVA followed by Bonferroni's multiple comparison tests was used, *p<0.05, **p<0.01, ***p<0.001.

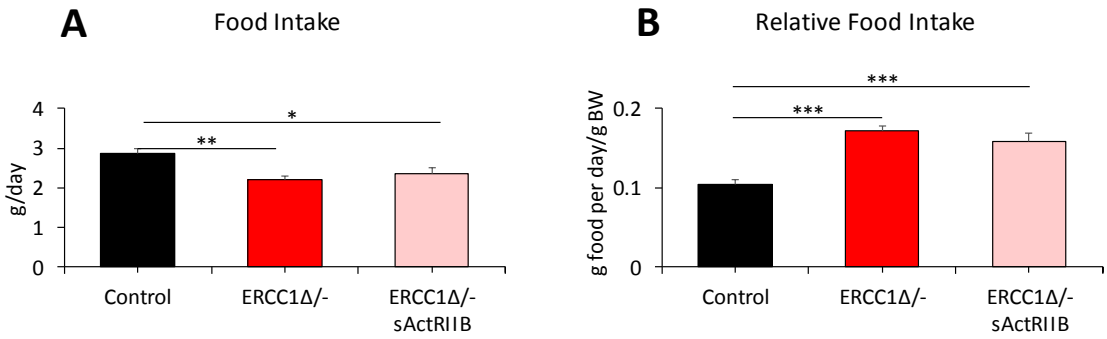

Figure 4.6. Absolute and relative amount of food consumption in Control, *Ercc1*$^{\Delta/-}$ mock and sActRIIB treated mice.

(A) Food intake and (B) Relative food intake at end of week 15. The food pellets were provided in a dish inside the cage and weigh before place in the cage and after one week. The amount of consumption was divided on 7 to work out daily intake. The cage was investigating for any leftover food to consider in calculation of consumption. The food intake was measure by Wilbert Vermeij in Erasmus University, Netherland cohorts. The sActRIIB were IP injected starting from week 7 of age to week 15. All mice were at the same age, n=6 control males, n=5 *Ercc1*$^{\Delta/-}$ untreated males and n=5 *Ercc1*$^{\Delta/-}$treated males. All analysis performed using nonparametric Kruskal-Wallis test followed by the Dunn's multiple comparisons, *p<0.05, **p<0.01, ***p<0.001.

4.7. sActRIIB treatment delayed the onset of neurological abnormalities in *Ercc1*$^{\Delta/-}$ mice.

A longitudinal examination of behavioural abnormalities has performed in the Department of Molecular Genetics, Erasmus University Medical Centre, Rotterdam, The Netherlands. The study was done on three cohorts, control, *Ercc1*$^{\Delta/-}$ and *Ercc1*$^{\Delta/-}$ sActRIIB treated (n=10). The treated cohort had the same sActRIIB injection protocol as in Reading. The characteristic feature of naturally aged and progeric conditions is a neurological disorder. Tremors, severe tremor and imbalance were scored in control and *Ercc1*$^{\Delta/-}$ mock and treated cohorts. We showed that *Ercc1*$^{\Delta/-}$ mice start tremor from week ten before the onset of severe tremor (Figure 4.7.A-B). sActRIIB treatment does not delay tremor in *Ercc1*$^{\Delta/-}$. However, it reduces its severity (Figure 4.7.A-B). The onset of imbalance that noticed on about week 16 in *Ercc1*$^{\Delta/-}$ mice was considerably postponed and frequently absent in treated cohorts (Figure 4.7.C). Nevertheless, sActRIIB treatment of *Ercc1*$^{\Delta/-}$ mice did not extend survival of the animals (Figure 4.7.D). These results show that attenuating Myostatin/Activin signalling prolongs healthspan rather than delaying lifespan.

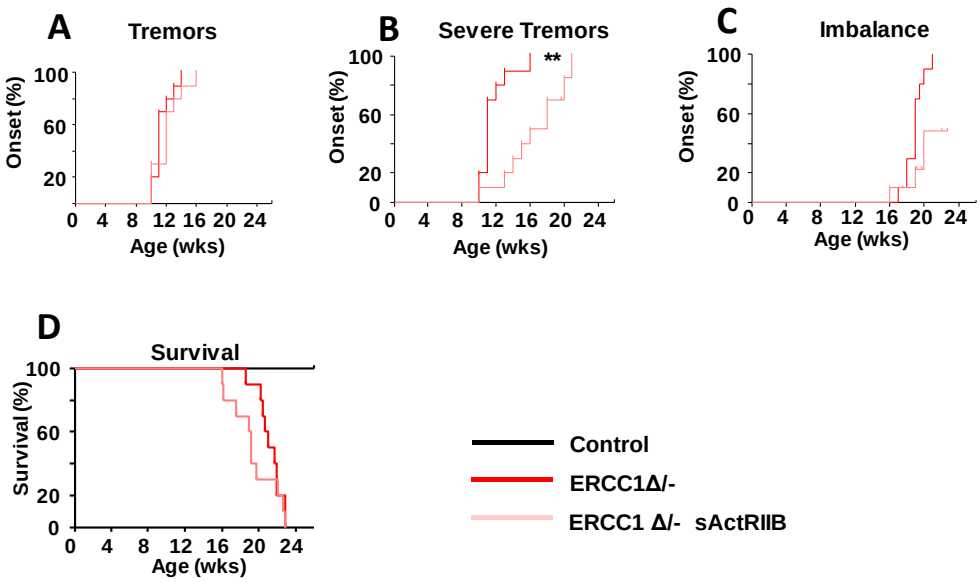

Figure 4.7. Delay of onset of neurological abnormalities in *Ercc1*$^{\Delta/-}$ mice after sActRIIB treatment.

(A) tremors (p=0.28), (B) severe tremors, (p=0.0014), and (C) imbalance (p=0.021) with age. (D) Survival of sActRIIB treated and mock-treated *Ercc1*$^{\Delta/-}$ mice (p=0.27). These parameters were measured by Wilbert Vermeij in Erasmus University, Netherland cohorts. The sActRIIB were IP injected starting from week 7 of age to week 15. n=10 animals per group. Error bars indicate mean ± S.E. Log-rank Mantel-Cox test. *<0.05, **<0.01, ***<0.001.

4.8. Discussion

A segmental progeroid syndrome is a condition characterised by an exhibition of certain features of ageing appear in early life (Ramirez et al., 2007). Many causes of this syndrome have been studied such as abnormal processing of the nuclear envelope protein lamin A as in Hutchinson-Gilford progeria syndrome (Eriksson et al., 2003) or defect in DNA damage repair as in Werner syndrome (WS) (Yu et al., 1996). In both human progeroid syndrome such as a WS and mouse models for progeria as in Zmpste24$^{-/-}$ mice, exhibit muscle weakness and impaired mobility (Greising et al., 2012, Yamaga et al., 2017).

Ageing is controlled in some aspect by GH/IGF-1 axis, as a spectrum of mutations that attenuate components of the GH/IGF-1 signalling cascade resulting in an extended lifespan. The case for a genetic component comes from numerous studies that have defined the Growth Hormone/Insulin-like growth factor-1 (GH/IGF1) as a central genetic axis that controls ageing (Milman et al., 2016). In current models of ageing imply interplay between stochastic and genetic components (Niedernhofer et al., 2006, Garinis et al., 2009). Random damage in DNA represents a stochastic element. Accumulation of DNA damage-induced mutations is considered a significant mediator of cancer, whereas DNA damage-induced cellular functional decline, senescence, and death contribute to ageing (Hoeijmakers, 2009). The different stochastic and genetic components have been reconciled into a unified model of ageing by proposing that accumulation of DNA damage, and after that failure of DNA to accurately replicate or be transcribed leads to activation of a survival response programme that attenuates the GH/IGF-1 activity. The ultimate purpose of dampening GH/IGF-1 signalling is the prioritisation of maintenance mechanisms over those that promote growth (Niedernhofer et al., 2006, Garinis et al., 2009, van der Pluijm et al., 2007).

Here we investigate whether the maintain skeletal muscle growth in *Ercc1*$^{\Delta/-}$ progeric mouse model by injection of sActRIIB confers systemic benefit. Based on the concept that DNA damage induces a survival response that promotes maintenance programmes at the expense of growth one would predict that augmenting muscle growth would, in the long run, exacerbate the pathological features in a progeroid model. What we find is something entirely different; sActRIIB treatment before the onset of progeria can support the growth of skeletal muscle, notwithstanding NER defects.

The key finding of this part was the antagonise myostatin/activin signalling have both skeletal muscle and organismal health benefits. However, we show that treatment with sActRIIB did not induce changes in the circulating levels of growth-related molecules, either GH, glucose, Insulin or IGF1. We show that the treated mice were heavier than nontreated mice, even treatment with sActRIIB made no change in food consumption rate compare to nontreated mice. Overall muscle, strength was enhanced by sActRIIB treatment of *Ercc1*$^{\Delta/-}$ compared to the control group. We show a delay in an age-related sign in treated progeric mice. However, sActRIIB did not affect the survival rate in *Ercc1*$^{\Delta/-}$ mice.

Body weight assessment is considered as an indicator of healthy growth, according to WHO (de Onis, 2015). We show that the *Ercc1*$^{\Delta/-}$ mice had a lower body weight compared to the control group. We show that targeting myostatin/activin signalling increased body weight, as showed before in wild type and diseased (mdx) mice (Relizani et al., 2014).

The need for a cure to prevent or rescue reduction in muscle mass and strength in many diseases and conditions reveal many new techniques. Myostatin antagonism is one of the successful protocols to enhance muscle growth. Injection, an antibody against myostatin in aged mice, lead to reduce muscle fatigue by 30% (LeBrasseur et al., 2009). However, it leads to impaired force generation and muscle fatigability in myostatin null mice (Amthor et al., 2007) and mdx mice (Relizani et al., 2014). We show that attenuation of Myostatin/Activin signalling using sActRIIB maintained muscle health in sActRIIB treated progeroid mice. Indeed, sActRIIB treatment lead to reduce muscle fatigability in *Ercc1*$^{\Delta/-}$ mice as shown by rotarod data. sActRIIB treatment also enhances locomotor activity as well as exploration and anxiety, as shown by open field activity. Enhancement in muscle health by using sActRIIB make the *Ercc1*$^{\Delta/-}$ mice more active, as we were shown by the result of distance travel by activity cage. The movement itself is considered an exercise, and as shown by Bernardo et al., the combination of antagonising myostatin and training lead to enhance in treadmill running time and increased regular activity. (Bernardo et al., 2009). Furthermore, the enhancement ex-vivo measure of specific force and half relaxation time in Ercc1 mutant, and both considered as features of structure alterations (Schwaller et al., 1999), contribute in overall skeletal muscle strength and organismal activity.

Growth retardation in Ercc1 mutant mice could result from activating the survival response, i.e. shift a body's reserves on tissue maintenance at the expense of growth. The case for a genetic component comes from numerous studies that have defined the Growth

Hormone/Insulin-like growth factor-1 (GH/IGF1) as a central genetic axis that controls ageing. A spectrum of mutations that attenuate components of the GH/IGF-1 signalling cascade results in extended lifespan (Milman et al., 2016). The low circulatory level of growth regulatory factor, IGF1, in *Ercc1*$^{\Delta/-}$ mice, was due to activation of stress response in the progeroid mice. However, the increase in Growth hormone in both untreated and sActRIIB treated Ercc1 mutants, are likely as a previously noted feedback mechanism in response to prolonged low IGF1 (Niedernhofer et al., 2006).

Sarcopenia leads to reduce the quality of life by impacting on mobility and stability, which leads to an increase in the incidence of fall-related injury. Moreover, the main signs of sarcopenia in ageing and progeric mouse model is neuromuscular degeneration. A prominent ageing feature of *Ercc1*$^{\Delta/-}$ mice, as shown before, is related to neurodegeneration and the onset of several neuro-muscular phenotypic changes (Vermeij et al., 2016a). The sActRIIB treatment appeared to reduce neurodegeneration in *Ercc1*$^{\Delta/-}$ mice as it reduces the severity of tremor in these progeric mice. Furthermore, the onset of imbalance was considerably postponed and frequently absent by sActRIIB treatment. Nevertheless, sActRIIB treatment of *Ercc1*$^{\Delta/-}$ mice did not extend survival of the animals. These results show that attenuating Myostatin/Activin signalling prolongs healthspan rather than delaying death.

Chapter Results

Quantitative and qualitative improvements to skeletal muscle through sActRIIB treatment in *Ercc1*$^{\Delta/-}$ mice

e

5.1. Introduction

The importance of maintaining muscle mass and function was postulated as its effects on health implications, especially morbidity and mortality. These signs increased with muscle loss and reduced the quality of life (English and Paddon-Jones, 2010, McLeod et al., 2016). Muscle loss is a common sign of many diseases and conditions. Specifically, reduction in muscle mass and function with ageing terms as sarcopenia (Rosenberg, 1997). Sarcopenia invariably leads to a reduced quality of life by impacting on mobility and stability, which leads to an increase in the incidence of fall-related injury. More importantly, sarcopenia predisposes individuals to adverse disease outcomes (cardiovascular and metabolic diseases) and mortality (Srikanthan and Karlamangla, 2014, Kim et al., 2015). Age-related reduction in strength relative to muscle mass loss reveals a reduction in both the quality and quantity of the tissue (Keller and Engelhardt, 2014). This evidence is aligned with an early study by Ansved and Edstrom who demonstrated that ageing results in a change in the skeletal muscle fibres structure such as fibres atrophy, increase in centrally located nuclei and fibres splitting, and ultrastructures such as numerous mitochondria with loss cristae and autophagic vacuoles (Ansved and Edstrom, 1991). However, interference such as exercise could alter the composition and ultrastructure of skeletal muscle (Howald et al., 1985).

One of the mechanisms drives skeletal muscle loss in sarcopenia is decreased protein synthesis (Welle et al., 1993) and decrease in fibres number via activation of the apoptosis pathway (Dirks and Leeuwenburgh, 2002). Reduce in protein synthesis lead to reduced in muscle mass and revealed by a reduction in the cross-sectional area of muscle fibres (Nilwik et al., 2013). The decrease in skeletal muscle fibres number is the leading cause of the reduction in muscle mass in ageing, however in less extend due to a reduction in fibres size (Lexell, 1993). Therefore, any intervention result in increased fibre number or size or both could consider a potential cure for reduction of muscle mass with ageing. Changes in mass and composition could induce in skeletal muscle as an adaptation to various interventions, including exercise and diet (Matsakas and Patel, 2009).

Furthermore, an increase in skeletal mass could be achieved by many non-genetic molecular interventions (Velloso, 2008, Lach-Trifilieff et al., 2014). Myostatin, a member of the Transforming Growth Factor beta (TGF-β) superfamily and well known for its negative

regulation of skeletal muscle growth (McPherron et al., 1997). Lack of myostatin results in an increase in skeletal muscle mass (Amthor et al., 2007). Increase body and muscle mass could be achieved by using one of the most potent reagents including the soluble activin receptor type IIB (sActRIIB) molecule, which acts to neutralise the muscle growth inhibitory properties of myostatin and activin (Relizani et al., 2014). sActRIIB increase muscle mass via modulating signalling pathway responsible for protein synthesis but leads to reduce capillary density in skeletal muscle (Hulmi et al., 2013).

A study suggests that the signs of fibres death through apoptosis and necrosis is considered an important mechanism underlying muscle loss and weakness in aged mice (Cheema et al., 2015). Another study report increase inflammation also drives ageing related phenotype in the muscle (Fagiolo et al., 1993). From these studies, it was concluded that multifactorial reasons caused sarcopenia.

Sarcopenia is also associated with alteration in ultrastructure and organelles in skeletal muscle fibres. For example, a study reported an age-related loss of mitochondrial content and function (Broskey et al., 2014). It concluded that skeletal muscle ageing is driven by aberrant mitochondria resulted from damage in mitochondrial DNA (Hiona and Leeuwenburgh, 2008). It well establishes that the ageing is associated with a fast-to-slow fibre type shifting and to more oxidative instead of glycolytic feature (Gelfi et al., 2006).

Oxidative stress plays a vital role in muscle abnormalities related to sarcopenia (Gomes et al., 2017). Studies have shown the relation between increase myostatin level in aged mice and enhancement of ROS production in skeletal muscle and as a result increase oxidative stress, and aged myostatin null mice show an elevated level basal antioxidant enzyme (AOE), superoxide dismutase (SOD), catalase (CAT), and glutathione peroxidase (GPx), rustling in reducing oxidative stress (Sriram et al., 2011).

Here we investigate the quantitative and qualitative improvement of skeletal muscle in *Ercc1*$^{\Delta/-}$ progeric mouse model by antagonising myostatin/activin. Based on the concept that DNA damage induces a survival response that promotes maintenance programmes at the expense of growth one could expect that augmenting muscle growth would, in the long run, exacerbate the pathological features in a progeroid model. Our result shows that different outcomes; sActRIIB treatment before the onset of progeria can support the growth of skeletal muscle, notwithstanding NER defects. The procedures and technique used in this chapter were explained in detail in the methods chapter.

The main observations of this chapter are, firstly, muscles from *Ercc1*$^{\Delta/-}$ treated mice were heavier than non-treated; however, maintain the same muscle fibre number but have bigger CSA. Secondly, sActRIIB injection mitigates the signs of damage in *Ercc1*$^{\Delta/-}$ mice. Thirdly, we show that the introduction of sActRIIB in *Ercc1*$^{\Delta/-}$ mice maintain fast and glycolytic profile showed in non-treated mice, and their profile became even faster and more glycolytic. TEM work shows that antagonise myostatin/activin signalling protects skeletal muscle from ultrastructure abnormalities found in *Ercc1*$^{\Delta/-}$ mice. Finally, the western blotting result demonstrates that sActRIIB promotes protein synthesis and autophagy but reduce proteasome protein breakdown in *Ercc1*$^{\Delta/-}$ muscle.

5.2. The Activin ligand trap increases muscle weight in *Ercc1*$^{\Delta/-}$ mice.

We determined whether the reduction in muscle mass in *Ercc1* $^{\Delta/-}$ mutants could be prevented by the soluble activin receptor IIB protein (sActRIIB), which were have shown previously to antagonise signalling mediated by Myostatin and related proteins (Omairi et al., 2016). To that end, male, *Ercc1*$^{\Delta/-}$ mice were IP-injected twice a week with sActRIIB from 7-weeks of age till week 16. Previous work has shown that sActRIIB treatment increases muscle mass in wild type mice (Relizani et al., 2014). The increased body weight and grip strength of *Ercc1*$^{\Delta/-}$ mice subjected to sActRIIB that we show in the previous chapter prompted us to examine individual muscles further. Treated *Ercc1*$^{\Delta/-}$ mice revealed that all five groups of hindlimb muscle (EDL, TA, Gastrocnemius, Soleus and Plantaris) showed significantly higher mass compared to those from mock-treated *Ercc1*$^{\Delta/-}$ animals with a range of 30-62% (tibialis anterior and Plantaris respectively, Figure 5.1. A-E). The same outcome was seen after normalising weight to tibia length (Figure 5.2. A-E). Activation of signalling pathways initiated through ActRIIB and via reducing a phosphorylation of key molecule of myostatin signalling pathway, Smad2/3 (Shi and Massague, 2003), were found to be elevated in the muscle of *Ercc1*$^{\Delta/-}$ mice and decreased by sActRIIB treatment, and that represented by an increase in the level of pSmad2/3 in *Ercc1*$^{\Delta/-}$ and reduced after sActRIIB treatment (Figure 5.3. A-C). Importantly, the abundance of DNA breaks, as detected by the level of γH2A.X, a marker of DNA damage (Rogakou et al., 1999), was not changed by sActRIIB treatment (Figure 5.4. A-C).

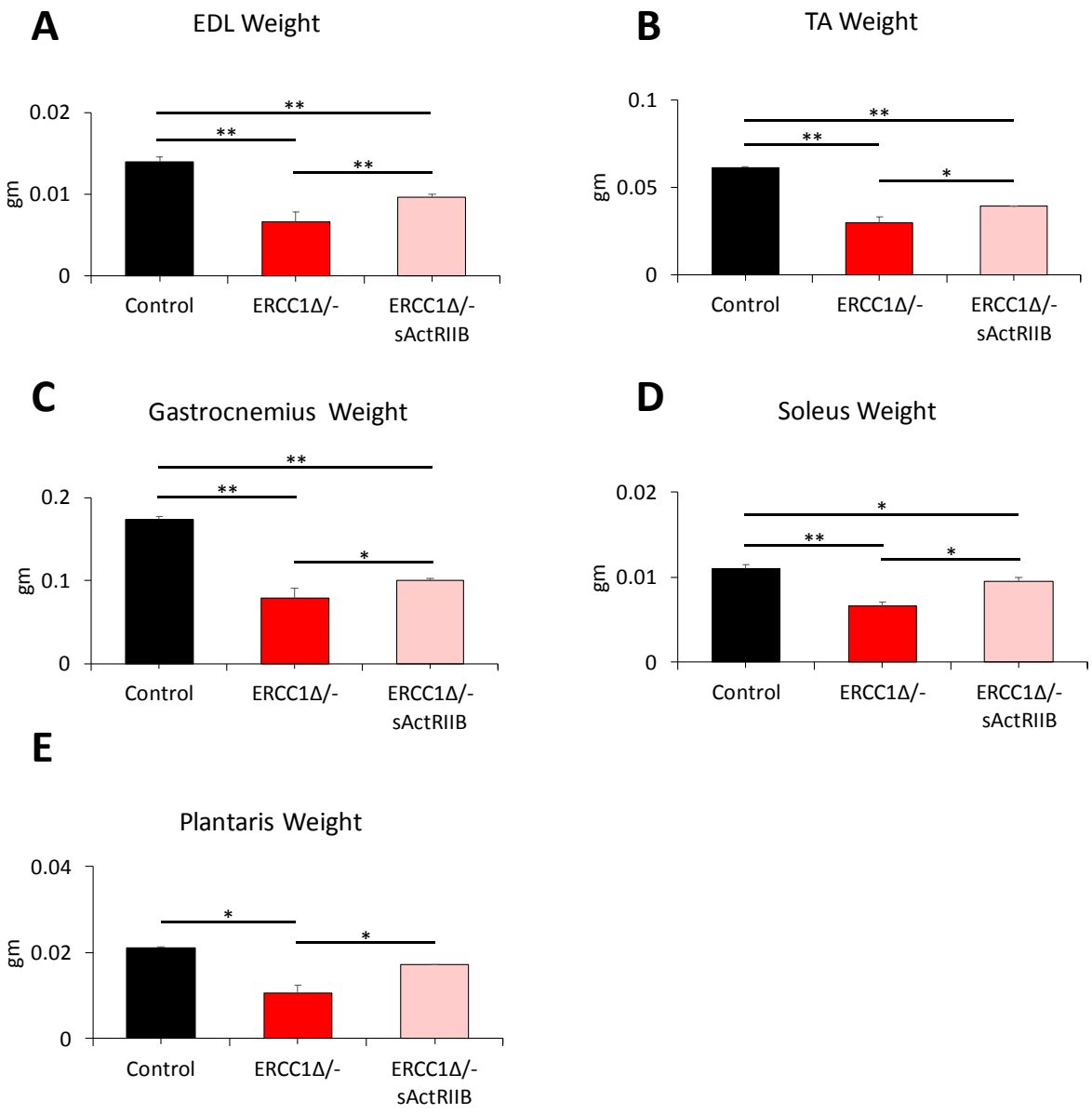

Figure 5.1. sActRIIB treatment increase muscle weight in *Ercc1*$^{\Delta/-}$ mice.

Muscle weight of (A) EDL, (B) TA, (C) Gastrocnemius, (D) Soleus and (E) Plantaris, at the day of dissection at end of week 15. The sActRIIB were IP injected starting from week 7 of age to week 15. All mice were at the same age, n=9 control males, n=8 *Ercc1*$^{\Delta/-}$ untreated males and n=8 *Ercc1*$^{\Delta/-}$ treated males. One-way ANOVA followed by Bonferroni's multiple comparison tests, *p<0.05, **p<0.01.

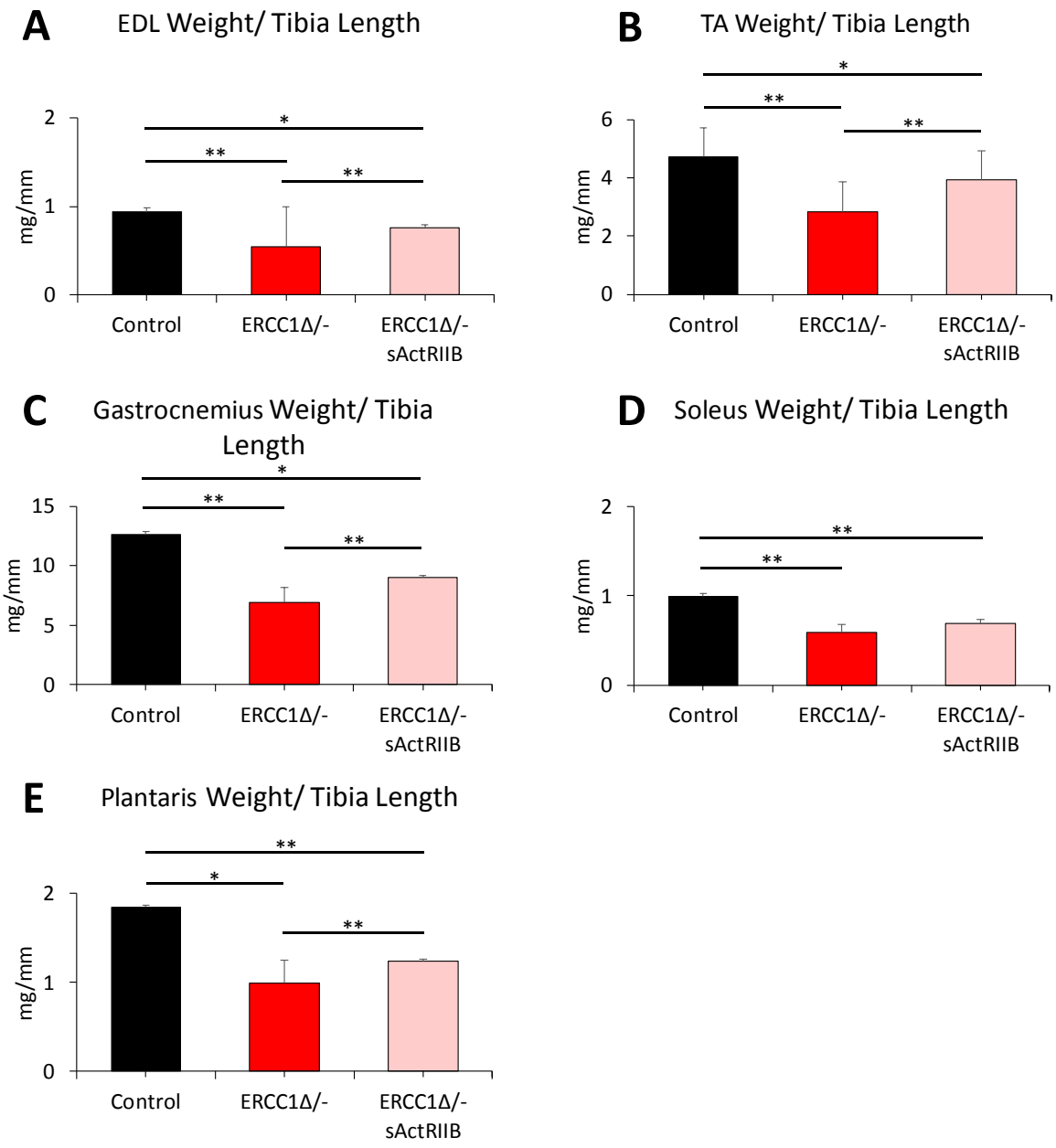

Figure 5.2. Normalise skeletal muscle weight to tibia length show increase in weight after sActRIIB treatment in *Ercc1*$^{\Delta/-}$ mice.

Muscle mass normalised to tibial length for (A) EDL, (B) TA, (C) Gastrocnemius, (D) Soleus and (E) Plantaris, at end of week 15. The sActRIIB were IP injected starting from week 7 of age to week 15. All mice were at the same age, n=9 control males, n=8 *Ercc1*$^{\Delta/-}$ untreated males and n=8 *Ercc1*$^{\Delta/-}$ treated males. One-way ANOVA followed by Bonferroni's multiple comparison tests, *p<0.05, **p<0.01.

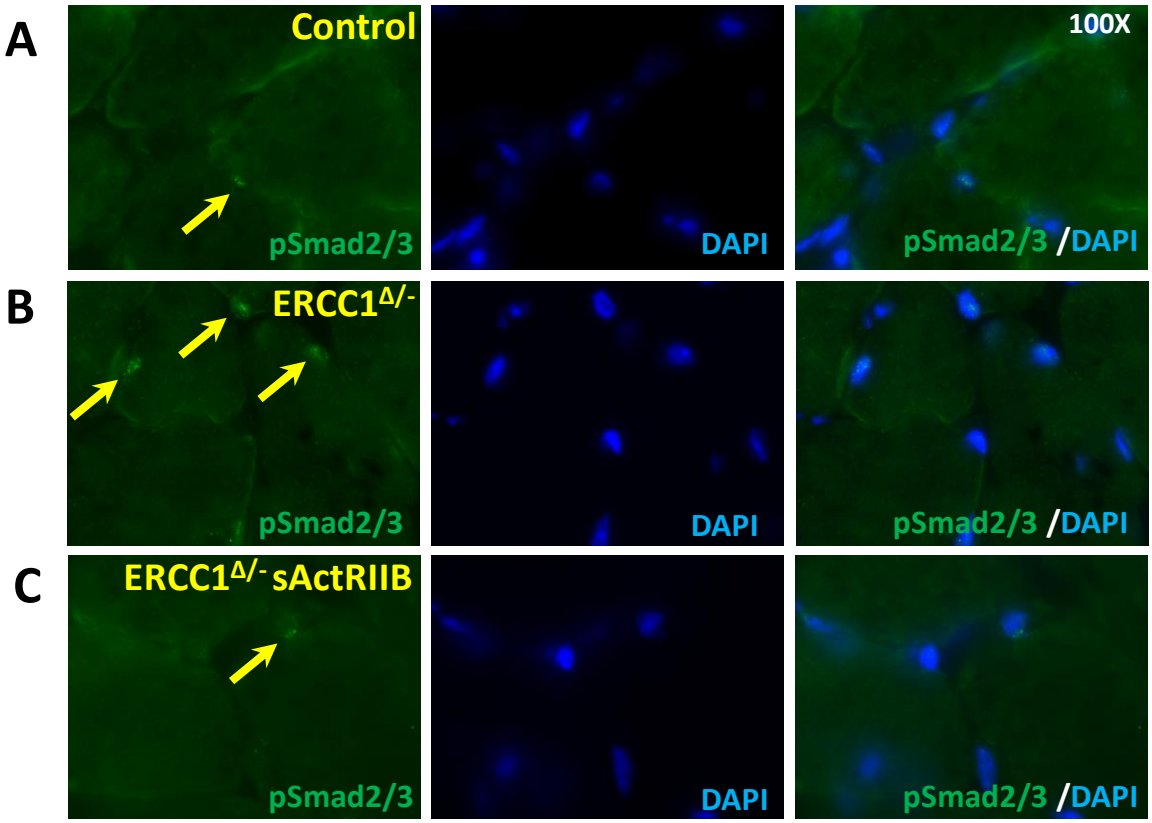

Figure 5.3. Reduce pSmad2/3 signalling after antagonising Myostatin/Activin signalling in *Ercc1*$^{\Delta/-}$ mice.

Immunohistology of pSmad2/3 expression (green) in (A) control, (B) *Ercc1*$^{\Delta/-}$ and (C) *Ercc1*$^{\Delta/-}$ treated in soleus muscle (yellow arrows) at age of 15 weeks. The sActRIIB were IP injected starting from week 7 of age to week 15. n= 8 male mice from each cohort.

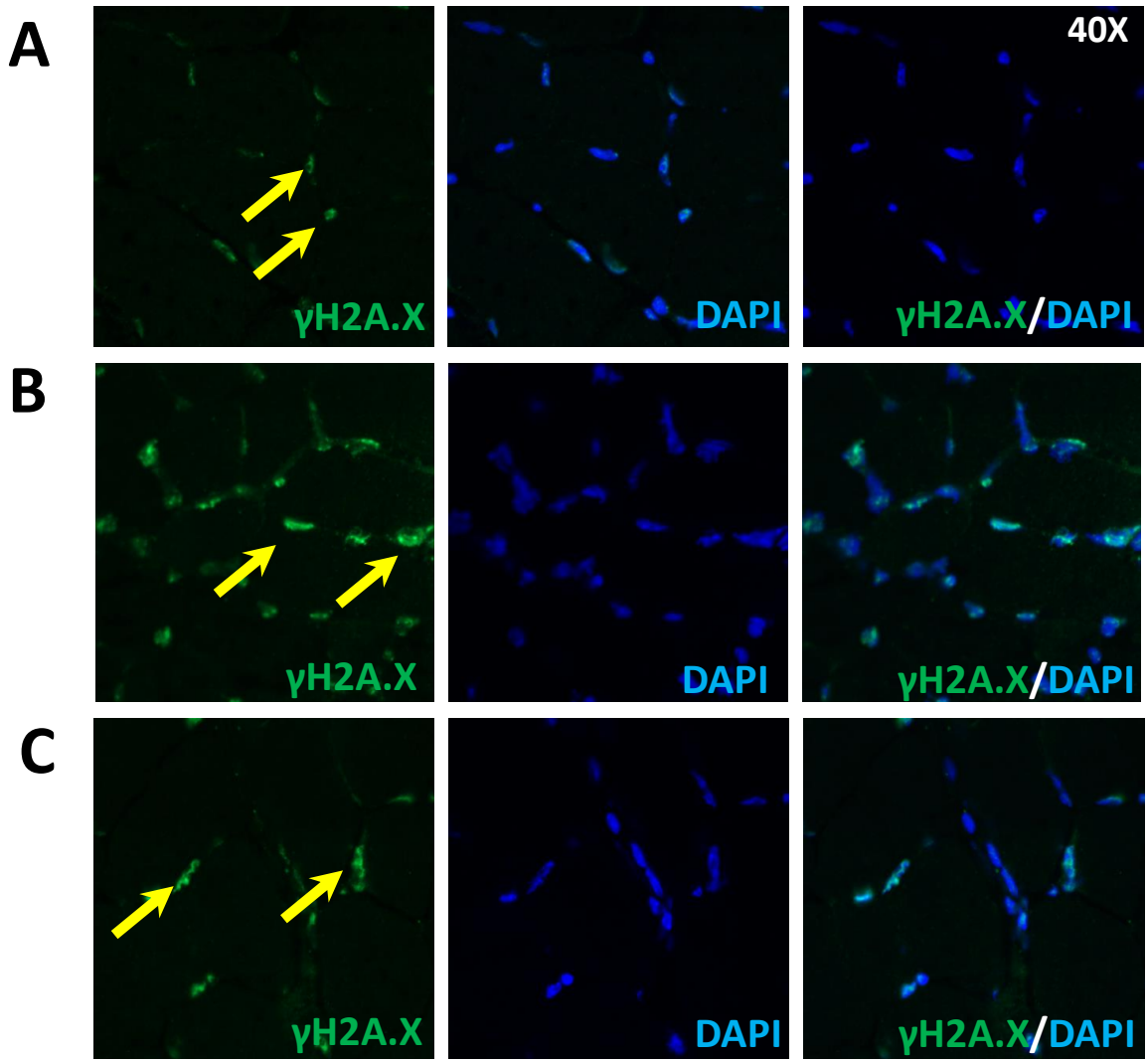

Figure 5.4. DNA damage marker γH2A.X, did not affect by sActRIIB treatment in *Ercc1*$^{\Delta/-}$ mice. Immunohistology of γH2A.X expression (green) in soleus muscle (yellow arrows). (A) control, (B) *Ercc1*$^{\Delta/-}$ and (C) *Ercc1*$^{\Delta/-}$ treated in soleus muscle (yellow arrows) at week 15 of age. The sActRIIB were IP injected starting from week 7 of age to week 15. All mice were at the same age, n= 8 male mice from each cohort.

5.3. The antagonise myostatin/activin increase muscle mass via hypertrophy, not hyperplasia.

We demonstrated that sActRIIB injection rescued the hindlimb muscle mass in progeroid *Ercc1*$^{\Delta/-}$ mice. As shown previously that hind limb muscles of Mtn null mice increase in size (McPherron and Lee, 1997) and the large size of muscles lacking Myostatin is achieved mainly by individual muscle fibre hypertrophy (Amthor et al., 2007). A further study showed an increase in the cross-sectional area of muscle fibre via inactivation of Myostatin (Rodriguez et al., 2014). Here we investigated whether sActRIIB injection increased myofibre size in *Ercc1*$^{\Delta/-}$ mice. Therefore, muscle sections were immunostained using antibodies against MHC isoforms (type I, IIA and IIB). Then the measurements of cross-sectional area (CSA) for myofibres (type I, IIA, IIX and IIB) of hind limb muscles (EDL, soleus and TA) from three cohorts of mice (Control, *Ercc1*$^{\Delta/-}$ and *Ercc1*$^{\Delta/-}$ treated) were taken. A minimum of 150-200 measurements per myofibre type was taken in each muscle section (n=9 control males, n=8 *Ercc1*$^{\Delta/-}$ untreated males and n=8 *Ercc1*$^{\Delta/-}$ treated males).

We found that the fibre sizes were increased upon introducing sActRIIB in *Ercc1*$^{\Delta/-}$ in the EDL muscles compare to non-treated mice. MHCIIX in *Ercc1*$^{\Delta/-}$ treated mice were significantly higher than non-treated mice. However, MHCIIA and MHCIIB did not reach a statistically significant. All types of MHC size did not normalise to the control group (Figure 5.5.A).

Next, we examined myofibre sizes in the soleus muscles. We found that CSA of all MHC types (MHCI, MHCIIX and MHCIIA) increased after sActRIIB treatment in *Ercc1*$^{\Delta/-}$ mice. All examined MHC types in Soleus muscle were smaller in *Ercc1*$^{\Delta/-}$ mice compared to the control group; however, did not reach statistical significance in MHCI. Of particular note was the finding that some types of fibres in the sActRIIB-treated *Ercc1*$^{\Delta/-}$ muscles were significantly larger than even in controls (MHCI and IIA) (Figure 5.5.B).

Finally, myofibres sizes in the TA muscles (superficial and deep regions) from control, *Ercc1*$^{\Delta/-}$ and *Ercc1*$^{\Delta/-}$ treated mice were measured. We found that the size of MHCIIB in the superficial region of TA muscles from *Ercc1*$^{\Delta/-}$ treated mice was significantly larger than non-treated mice that were smaller than the control group. However, the fibre sizes of MHCIIX in this region of TA muscles from control, *Ercc1*$^{\Delta/-}$ treated and non-treated showed no significant changes (Figure 5.5.C).

The deep area of TA muscle sections showed a decrease in CSA of myofibres type IIA in *Ercc1*$^{\Delta/-}$mice compared to the controls were increased after sActRIIB treated. Moreover, fibre sizes of MHCIIX in the deep region of TA muscles from *Ercc1*$^{\Delta/-}$ treated mice were significantly larger than the *Ercc1*$^{\Delta/-}$ non-treated mice. Additionally, the decrease in CSA of most fast MHC, IIB fibres, that were reduced in *Ercc1*$^{\Delta/-}$ mice compared to controls, increased after sActRIIB injection (Figure 5.5.D).

We showed that sActRIIB treated n *Ercc1*$^{\Delta/-}$ mice exhibited a notable increase in muscle mass compared to non-treated mice. It was reported that the increase in muscle mass following Myostatin knock out is due to an increase in muscle fibres size and number (Elashry et al., 2009). In agreement, another study has shown that the increase in muscle mass in the myostatin mutant mouse model was via both hyperplasia and hypertrophy (McPherron et al., 1997).

In the present study, we determined whether the increase in muscle mass of *Ercc1*$^{\Delta/-}$ treated mice was resulted from increased myofibers sizes alone or increase in muscle fibre numbers as well. Therefore, we use the muscle sections of immunohistochemistry stained used for determining the MHC phenotype for count the total fibre number in both EDL and soleus muscles (n=9 control males, n=8 *Ercc1* untreated males and n=8 *Ercc1*$^{\Delta/-}$ treated males) of each genotype (Control, *Ercc1*$^{\Delta/-}$ treated and not treated mice). We did not include the total fibre number of TA muscles in this analysis, as its anatomically heterogeneous in shape and making it difficult to obtain a similar mid-belly section.

Here we examined the effect of a antagonise of myostatin/activin on *Ercc1*$^{\Delta/-}$ EDL and soleus muscles fibre numbers.

Our data showed that total fibres number in EDL muscle from *Ercc1*$^{\Delta/-}$ mice significantly higher than the control group and was not affected by sActRIIB injection (Figure 5.6.A). However, there was no statistical difference in the total fibre number in Soleus muscle between the three cohorts (control, *Ercc1*$^{\Delta/-}$, *Ercc1*$^{\Delta/-}$ treated mice) (Figure 5.6.B).

In summary, these data show that the introduction of sActRIIB induced fibre hypertrophy irrespective of MHC expression. Of particular note was the finding that some types of fibres in the sActRIIB-treated *Ercc1*$^{\Delta/-}$ muscles were significantly larger than even in controls. Importantly, the increase in skeletal muscle mass did not result from hyperplasia as the *Ercc1*$^{\Delta/-}$ muscles have total fibres number more than counterpart muscle in control group and sActRIIB treatment maintain this increment.

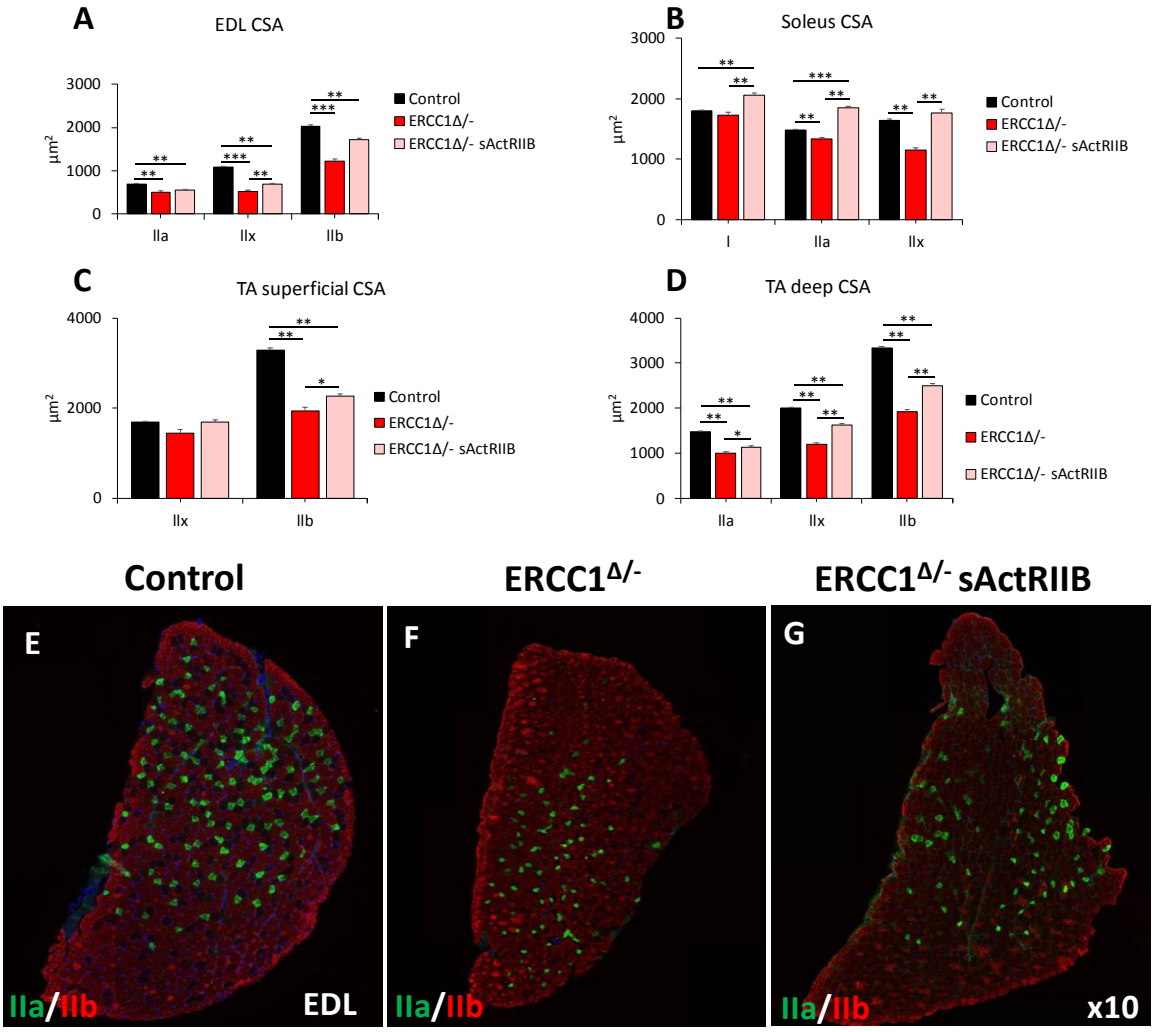

Figure 5.5. Increase fibres cross sectional area in *Ercc1*$^{\Delta/-}$ mice after sActRIIB treatment.

Cross-sectional fibre areas assigned to specific MHC isoforms using antibodies to immunostained the specific MHC proteins in (A) EDL, (B) Soleus, (C) superficial and (D) deep areas of TA. Represenattive images of EDL muscle from (E) control, (F) progeric and (G) sActRIIB treated progeric mice immunustaend agienst MHC. The sActRIIB were IP injected starting from week 7 of age to week 15. Whole muscle sections were counted for EDL and soleus muscles and 100 fibres were analysed for TA in superficial and deep regions in all 3 cohorts. All animals were 16 weeks old at the time of dissection from both cohorts. n=9 control males, n=8 *Ercc1* untreated males and n=8 *Ercc1*$^{\Delta/-}$ treated males. One-way ANOVA followed by Bonferroni's multiple comparison tests, *p<0.05, **p<0.01, ***p<0.001.

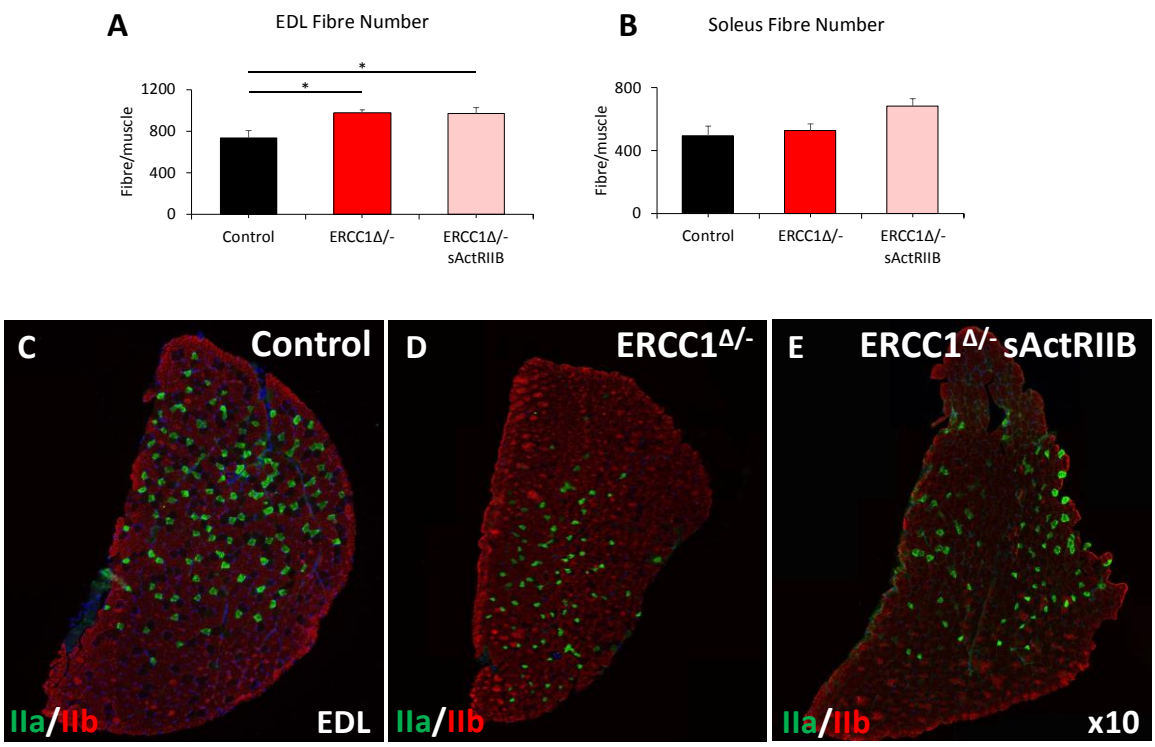

Figure 5.6. Fibres number count did not affect by antagonise of myostatin/activin in *Ercc1*$^{\Delta/-}$ mice.

Fibre number count in (A) EDL and (B) soleus of control, *Ercc1*$^{\Delta/-}$ and mice *Ercc1*$^{\Delta/-}$ treated. Represenattive images of EDL muscle from (C) control, (D) progeric and (E) sActRIIB treated progeric mice immunustaend agienst MHC.The sActRIIB were IP injected starting from week 7 of age to week 15. The sections were used to measure CSA were used here to count the total fibres number in both muscles in all three cohorts. All mice were at the same age, n=9 control males, n=8 *Ercc1* untreated males and n=8 *Ercc1*$^{\Delta/-}$ treated males. One-way ANOVA followed by Bonferroni's multiple comparison tests, *p<0.05, **p<0.01, ***p<0.001.

5.4. Qualitative improvements to *Ercc1*$^{\Delta/-}$ skeletal muscle through sActRIIB treatment.

Antagonise of myostatin/activin signalling was able to rescue muscle mass loss in progeric mice as we showed above. We further investigate the mechanisms underpinning the muscle loss in our progeric mice as an ageing model. As a previous study suggest that the signs of fibres death through apoptosis and necrosis are considered an important mechanism underlying muscle loss and weakness in aged mice (Cheema et al., 2015), we here investigate a fibres damage parameters of our platform mice before and after sActRIIB treatment.

Therefore, EDL single fibres were isolated and immunostained to visualise microdamage. Secondly, muscle sections of EDL and Soleus muscle were immunostained using antibodies against caspase-3 to detect apoptosis activity. Then sections of EDL and Soleus muscle were stained with H & E stain to detect the centrally located nuclei. After that, the EDL muscle section was used to gauge the SDH hyperactivity as an indicator of fibre apoptosis. Finally, a level of ROS was detected in TA muscle sections using the DHE stain. All muscles were hind limb muscles (EDL, soleus and TA) from three cohorts of mice (Control, *Ercc1*$^{\Delta/-}$ and *Ercc1*$^{\Delta/-}$ treated). A minimum of 20 fibres was investigated for single fibres work, and 100 measurements per myofibre type were taken in each muscle section for other stains (n=9 control males, n=8 *Ercc1* untreated males and n=8 *Ercc1*$^{\Delta/-}$ treated males).

Here we examined the effect of a antagonise of myostatin/activin on *Ercc1*$^{\Delta/-}$ muscles fibre in term of integrity and death parameters.

We showed here that a large proportion of fibres has micro-lesions (including tears to the membrane) from the EDL muscle from *Ercc1*$^{\Delta/-}$ animals, which appeared normalised by sActRIIB (Figure 5.7.A-B). Caspase-3 activity as a gauge of apoptosis was significantly elevated in the muscles of *Ercc1*$^{\Delta/-}$ mice and largely normalised by treatment with sActRIIB in both EDL and Soleus muscle (Figure 5.8.A-D). The number of fibres displaying centrally located nuclei was elevated in both the EDL and soleus muscles from *Ercc1*$^{\Delta/-}$ mice compared to controls and became even more abundant following sActRIIB treatment (Figure 5.9.A-D). The fibres showing supra-normal levels of SDH activity, indicative of an abnormal mitochondrial activity that leads to apoptosis (Cheema et al., 2015), were significantly more frequent in both the EDL and soleus of *Ercc1*$^{\Delta/-}$ mice compared to treated mutants (Figure 5.10.A-D). Assessment of ROS activity through DHE intensity showed elevated levels of superoxide in the muscle of *Ercc1*$^{\Delta/-}$ animals which were lowered by

sActRIIB treatment although it did not reach the level of control mice (Figure 5.11.A-D) (Bindokas et al., 1996, Li et al., 2003).

Overall, we show that the abundance of abnormal fibres in *Ercc1*$^{\Delta/-}$ mice identified through central nucleation and dying fibres were largely normalised by antagonising myostatin/activin signalling.

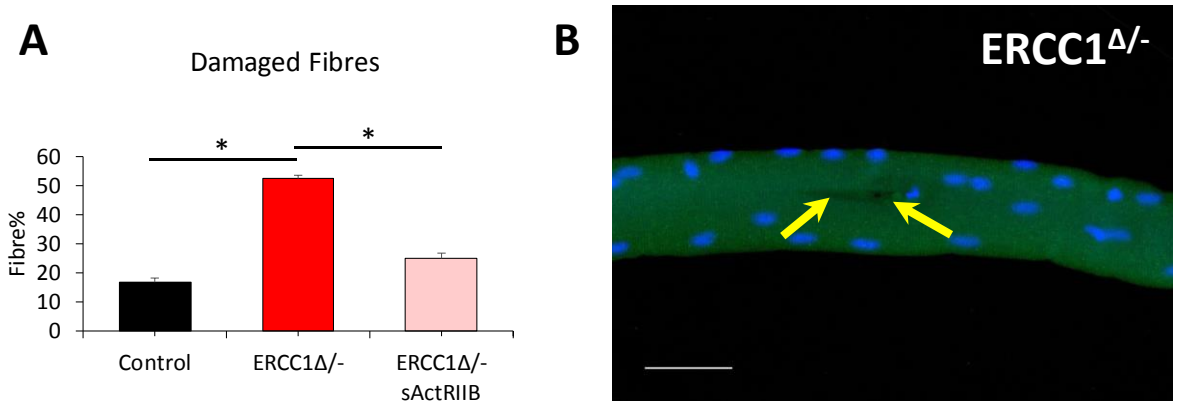

Figure 5.7. Incidence of damaged fibres following single fibre isolation.

(A) Percentage of damage fibres incidence following single fibre isolation in EDL muscle. (B) Example of micro-tear (arrows) in an *Ercc1*$^{\Delta/-}$ EDL fibre. The sActRIIB were IP injected starting from week 7 of age to week 15. Singles fibres were optioned from EDL muscle and immunostained against laminin (green) and DAPI to visualise the nucleus. Total of 20 fibres were analysed from each cohort and the fibres that contain damage including micro tearing, splitting, and wavy fibres were count and represent as a percentage regarding the entre number of fibres in slide. All mice were at the same age, n=9 control males, n=8 *Ercc1* untreated males and n=8 *Ercc1*$^{\Delta/-}$ treated males. Scale 50 µm. One-way ANOVA followed by Bonferroni's multiple comparison tests, *p<0.05.

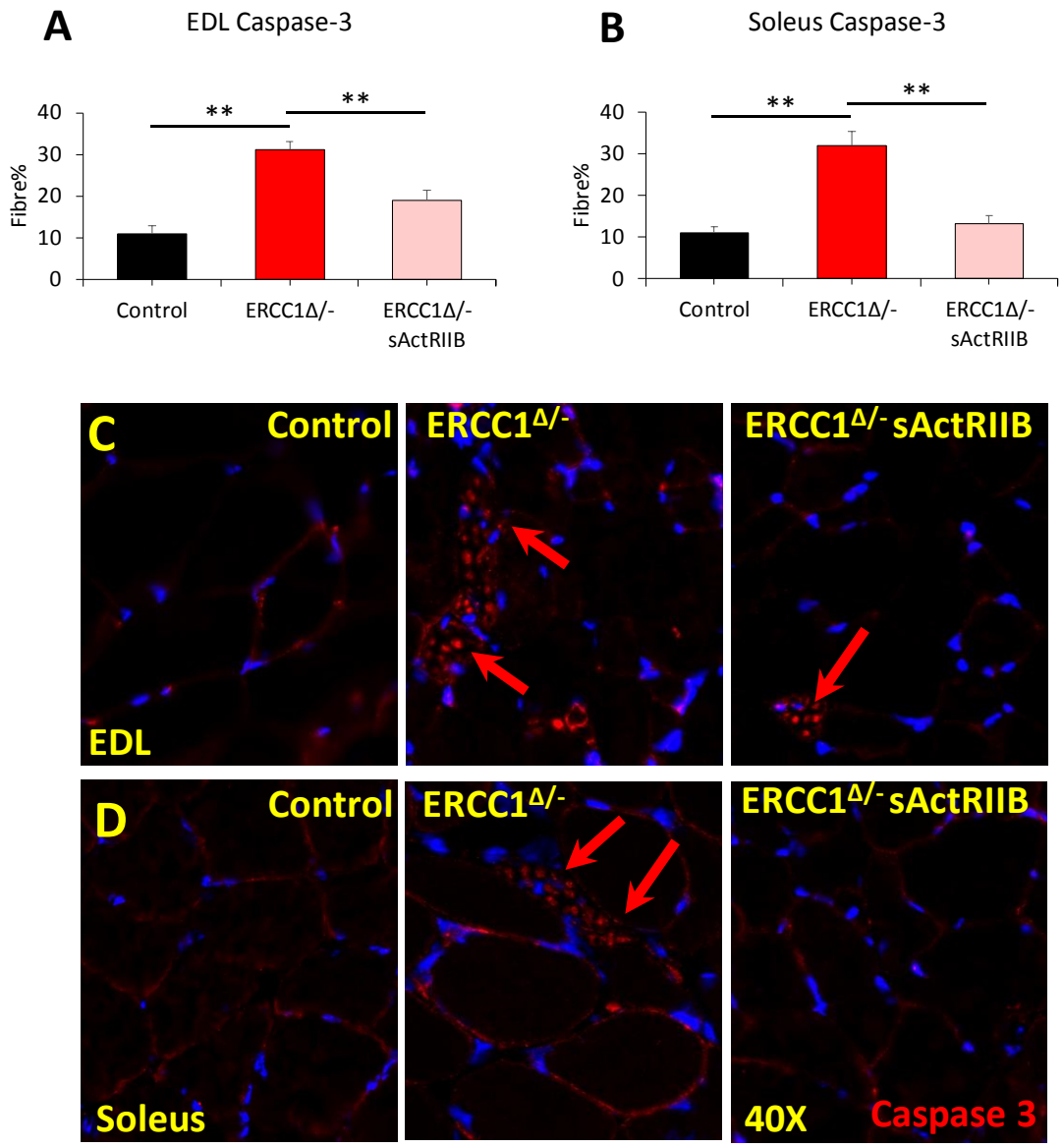

Figure 5.8. Normalise percentage of caspase-3 in *Ercc1*$^{\Delta/-}$ after sActRIIB injection.

Fibres containing caspase 3 epitope as a percentage of (A) EDL and (B) Soleus fibres. (C) representative pictures of EDL muscle immunostained for caspase 3 antibody in control, *Ercc1*$^{\Delta/-}$ and *Ercc1*$^{\Delta/-}$ treated mice. (D) representative pictures of Soleus muscle immunostained for caspase 3 antibody in control, *Ercc1*$^{\Delta/-}$ and *Ercc1*$^{\Delta/-}$ treated mice. Red arrows indicate caspase foci. The sActRIIB were IP injected starting from week 7 of age to week 15. A total of 100 fibres were count for their positive foci of caspase and represented as percentage. All mice were at the same age, n=9 control males, n=8 *Ercc1* untreated males and n=8 *Ercc1*$^{\Delta/-}$ treated males. One-way ANOVA followed by Bonferroni's multiple comparison tests, *p<0.05, **p<0.01.

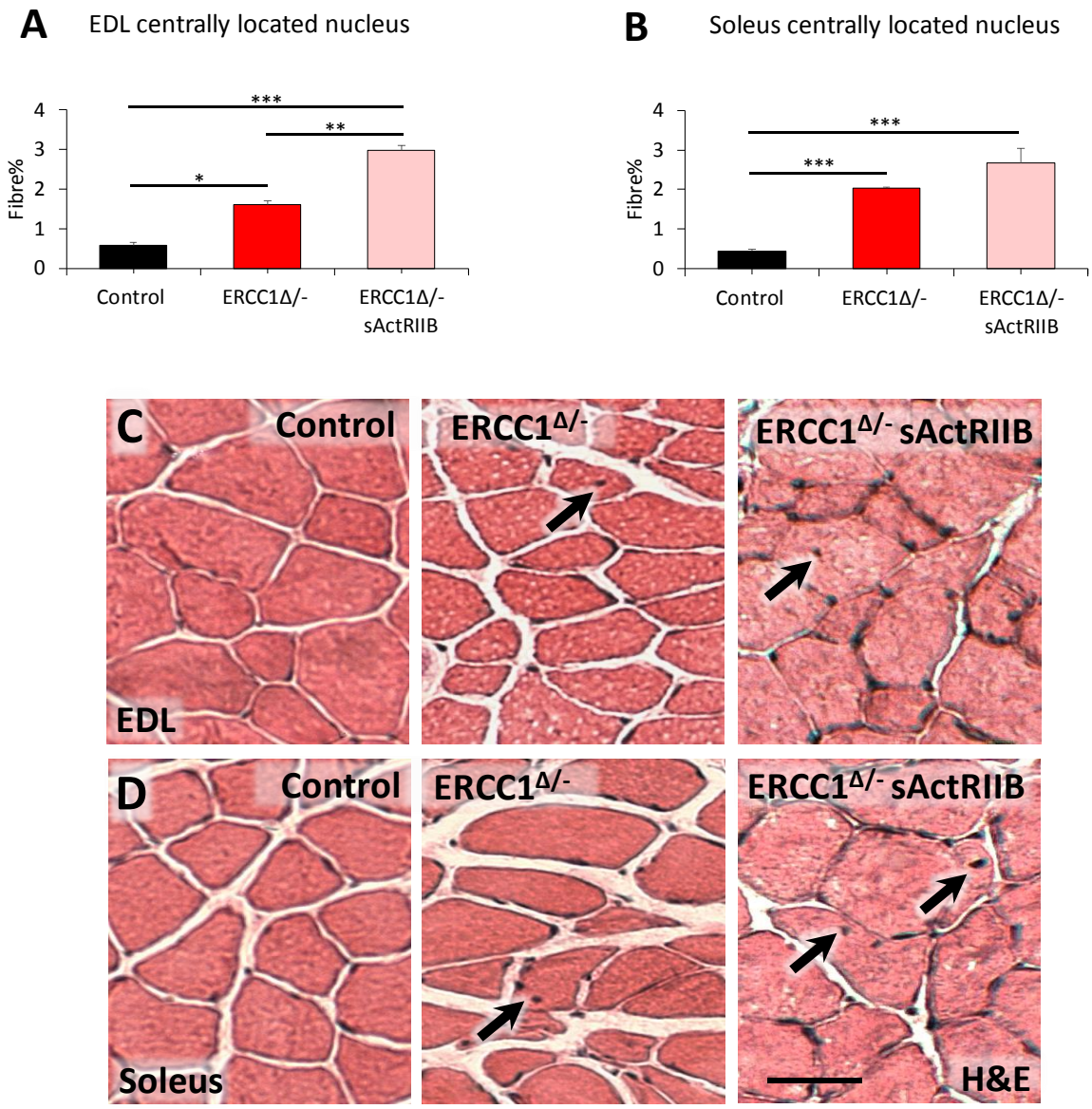

Figure 5.9. sActRIIB injection increase percentage of fibres contain centrally located nucleuses in *Ercc1*$^{\Delta/-}$ mice.

Percentage of fibres with centrally located nuclei in the (A) EDL and (B) Soleus. (C) representative pictures of EDL muscle stained with H and E in control, *Ercc1*$^{\Delta/-}$ and *Ercc1*$^{\Delta/-}$ treated mice. (D) representative pictures of Soleus muscle stained with H and E in control, *Ercc1*$^{\Delta/-}$ and *Ercc1*$^{\Delta/-}$ treated mice. Black arrows indicate centrally located nuclei. Whole muscle section were investigated to detecrt and count the centrally located nucleus in both EDL and soleus muscles and presented as percentage regarding total fibres number in all 3 cohorts. The sActRIIB were IP injected starting from week 7 of age to week 15. All mice were at the same age, n=9 control males, n=8 *Ercc1* untreated males and n=8 *Ercc1*$^{\Delta/-}$ treated males. Scale 50 µm. One-way ANOVA followed by Bonferroni's multiple comparison tests, *p<0.05, **p<0.01, ***p<0.001.

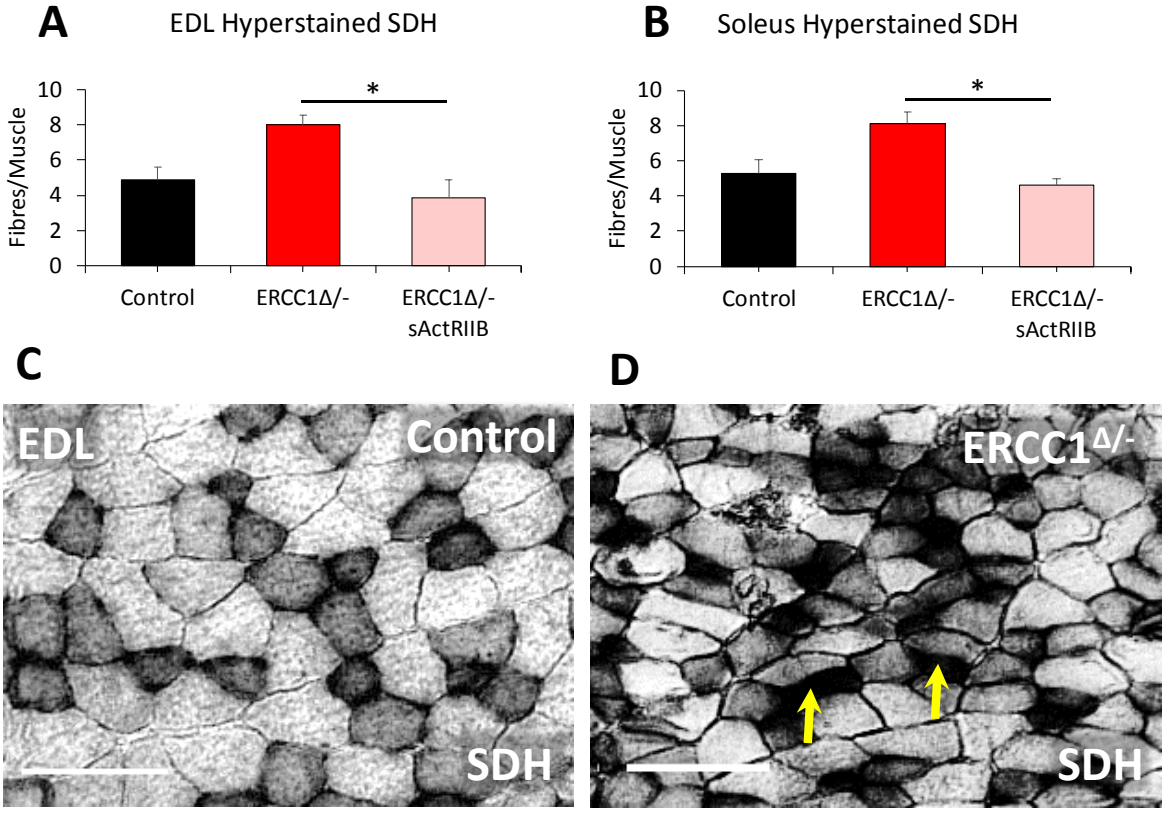

Figure 5.10. sActRIIB treatment normalise hyper-stained SDH in *Ercc1*$^{\Delta/-}$ mice.

Quantification of hyper-stained SDH fibres for (A) EDL and (B) Soleus muscle. (C) SDH in control muscle and (D) *Ercc1*$^{\Delta/-}$ muscle showing hyper-stained fibres (arrows). The extra dark stained fibres were counted in SDH stained section from EDL muscle and whole muscle section were investigated and the positive fibres were presented as a percentage regarding total fibres number. The sActRIIB were IP injected starting from week 7 of age to week 15. All mice were at the same age, n=9 control males, n=8 *Ercc1* untreated males and n=8 *Ercc1*$^{\Delta/-}$ treated males. Scale 100 µm. One-way ANOVA followed by Bonferroni's multiple comparison tests, *p<0.05.

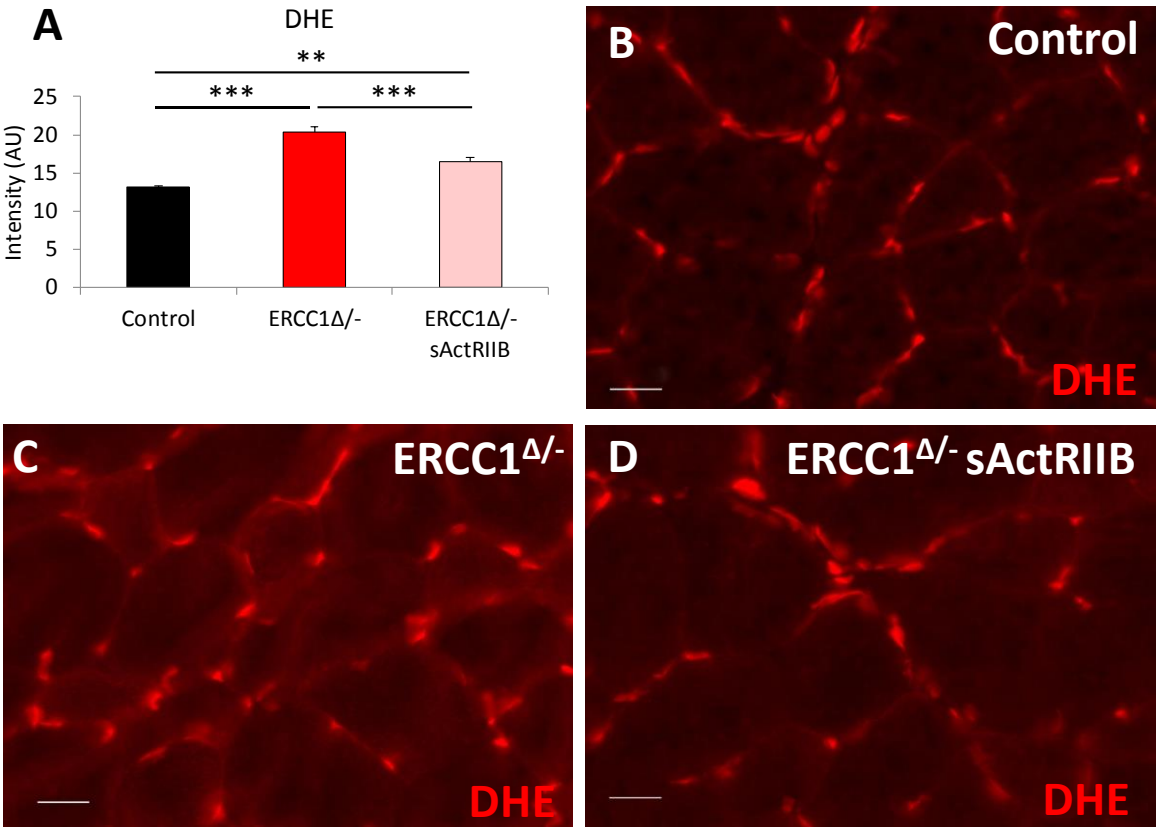

Figure 5.11. Detection of ROS level using DHE staining reveal normalise the ROS level in *Ercc1*$^{\Delta/-}$ mice after sActRIIB injection.

(A) Quantification of DHE fluorescence in TA muscle fibres. (B) Control TA fibres with little DHE fluorescence in the body of control fibres. (C) *Ercc1*$^{\Delta/-}$ TA fibres with elevated DHE fluorescence in the body of control fibres. (D) Treated *Ercc1*$^{\Delta/-}$ TA fibres with little DHE fluorescence in the body of fibres. A total of 100 fibres were analysing to detect the intensity of DHE stain in TA section. The sActRIIB were IP injected starting from week 7 of age to week All mice were at the same age, 15. n=9 control males, n=8 *Ercc1* untreated males and n=8 *Ercc1*$^{\Delta/-}$ treated males. Scale 20 µm. One-way ANOVA followed by Bonferroni's multiple comparison tests, *p<0.05, **p<0.01, ***p<0.001.

5.5. Skeletal muscle fibres metabolic status and MHC profile in *Ercc1*$^{\Delta/-}$ mice after antagonising myostatin/activin signalling.

Sarcopenia is related to change in the profile of skeletal muscle fibres types. There was evidence to profile shift of MHC from fast to slow with advanced in ageing (Narici and Maffulli, 2010). The evidence from other studies shows increase proportion of fibres express the slow type of MHC (type I) at the expense of fibres express fast MHC, (type II) (Andersen, 2003, Lee et al., 2006). As the type II fibres rely mainly on glycolytic metabolism in contrast to type I which mostly depend on oxidative metabolism (Pette and Spamer, 1986), the other study suggests a concomitant shifting from glycolytic to oxidative phenotype during sarcopenia (Fielding et al., 2011). Although there was evidence of higher capillary density related to oxidative fibres (Omairi et al., 2016, Romanul, 1964), the study on older men shows reduces capillary density 70 years old men compared to young (Groen et al., 1985).

Here we examined the effect of a antagonise of myostatin/activin on *Ercc1*$^{\Delta/-}$ muscles fibre MHC profile, oxidative and metabolic status.

Therefore, sections of EDL and Soleus muscle were immunostained using antibodies against myosin heavy chain (MHC), so antibodies were used to detect MHCI, MHCIIa, and MHCIIb for muscle profiling. Also, a section of EDL muscle was stained with SDH to detect the oxidative activity of skeletal muscle fibres. Furthermore, the EDL muscle sections were used to inspect the percentage of capillary per fibres using CD31 antibody. Finally, a level of angiogenesis, PGC1α and fat metabolism genes expression was profiled in gastrocnemius muscle by qPCR. All muscles were hind limb muscles (EDL, soleus and gastrocnemius) from three cohorts of mice (Control, *Ercc1*$^{\Delta/-}$ and *Ercc1*$^{\Delta/-}$ treated), n= 8 each cohort.

Our analysis of MHC distribution revealed that the progeric mice muscle displayed a faster phenotype compared to control muscles. Treatment of progeric animals with sActRIIB resulted in a shift towards an even faster MHC profile. sActRIIB treatment maintains a faster profile in the EDL muscle of *Ercc1*$^{\Delta/-}$ mice. The low proportion of fast MHCIIa and MHCIIx in *Ercc1*$^{\Delta/-}$ mice were maintained after sActRIIB injection. On the contrary, the very fast MHCIIB fibres were in higher proportion in *Ercc1*$^{\Delta/-}$ mice compared to the control group and significantly increased after sActRIIB injection (Figure 5.12.A and C-E). The same trend was found in Soleus muscle after sActRIIB injection. The reduction of the slow MHCI fibres

that we showed in *Ercc1*$^{\Delta/-}$ mice were maintained via antagonising of myostatin/activin signalling and further decrease, not significantly to *Ercc1*$^{\Delta/-}$ mice. The fast MHCIIa were lower in non-treated *Ercc1*$^{\Delta/-}$ mice and further reduce after sActRIIB treatment. The other fast fibre express MHCIIx in the lowest proportion in the control group were shown to a high level in *Ercc1*$^{\Delta/-}$ mice and were decreased after sActRIIB treatment. Of particular note, the Soleus muscle was devoid of very fast MHCIIb in control group, but *Ercc1*$^{\Delta/-}$ had several MHCIIb positive fibres. Surprisingly, the sActRIIB injection increased the proportion of MHCIIb to the level above the usually found MHCIIx (Figure 5.12.B).

To examine the metabolic status of the sActRIIB-treated muscle, we determined the SDH profile in EDL and Soleus muscles. In both muscle group, the number of SDH-positive fibres was decreased in the progeric mice compared to controls (Figure 5.13.A-H). Introduction of sActRIIB treatment further decreased the number of SDH positive fibres, and at the same time increasing the number of SDH negative entities in the EDL (Figure 5.13.A and C-E). Similar changes were also recorded in the soleus; however, not reaching statistical significance (Figure 5.13.B and F-H). Therefore, the sActRIIB treatment further reduces the status of the already diminished oxidative character of *Ercc1*$^{\Delta/-}$ muscles.

Subsequently, we investigated whether changes in the muscle metabolic profile wrought by sActRIIB also induced remodelling of the vasculature. The capillary density profile detected by CD31 antibody on EDL sections indeed showed that the number of blood vessels serving each fibre in *Ercc1*$^{\Delta/-}$ mice were lower than control mice (albeit non-significantly), and further decreased following sActRIIB treatment (Figure 5.13.I-L). These changes of oxidative status and capillary density were underpinned by decreases in the expression of three genes examined that control the development of blood vessels. We show that the gene expression of VEGFa189 and FGF1 genes were lower in *Ercc1*$^{\Delta/-}$ mice and further reduce with treatment. VEGFb gene expression followed the same pattern other angiogenesis genes but not statistically defiance (Figure 5.13.M).

Expression of PGC1α, a key regulator of oxidative properties in muscle was slightly lower in muscle from *Ercc1*$^{\Delta/-}$ mice compared to controls and was even more suppressed following sActRIIB treatment (Figure 5.14.A). Mitochondrial transcript levels mirrored the changes in genes supporting the development of blood vessels. qPCR analysis of eight genes essential for the mitochondrial metabolism revealed that seven had decreased expression in *Ercc1*$^{\Delta/-}$ muscles induced by sActRIIB treatment (Figure 5.14.B). We also investigated genes that

control fat metabolism as there is evidence that increases glycolytic flux decreases fat metabolism (Jeukendrup, 2002). All seven genes examined were significantly reduced in expression by sActRIIB (Figure 5.14.C).

Altogether, the attenuation of myostatin/activin signalling through sActRIIB results in the patterning of muscle towards a fast-contracting status, which has a paucity of oxidative fibres and supporting blood vessels underpinned by changes in the expression of genes that control capillary development and sustain aerobic metabolism.

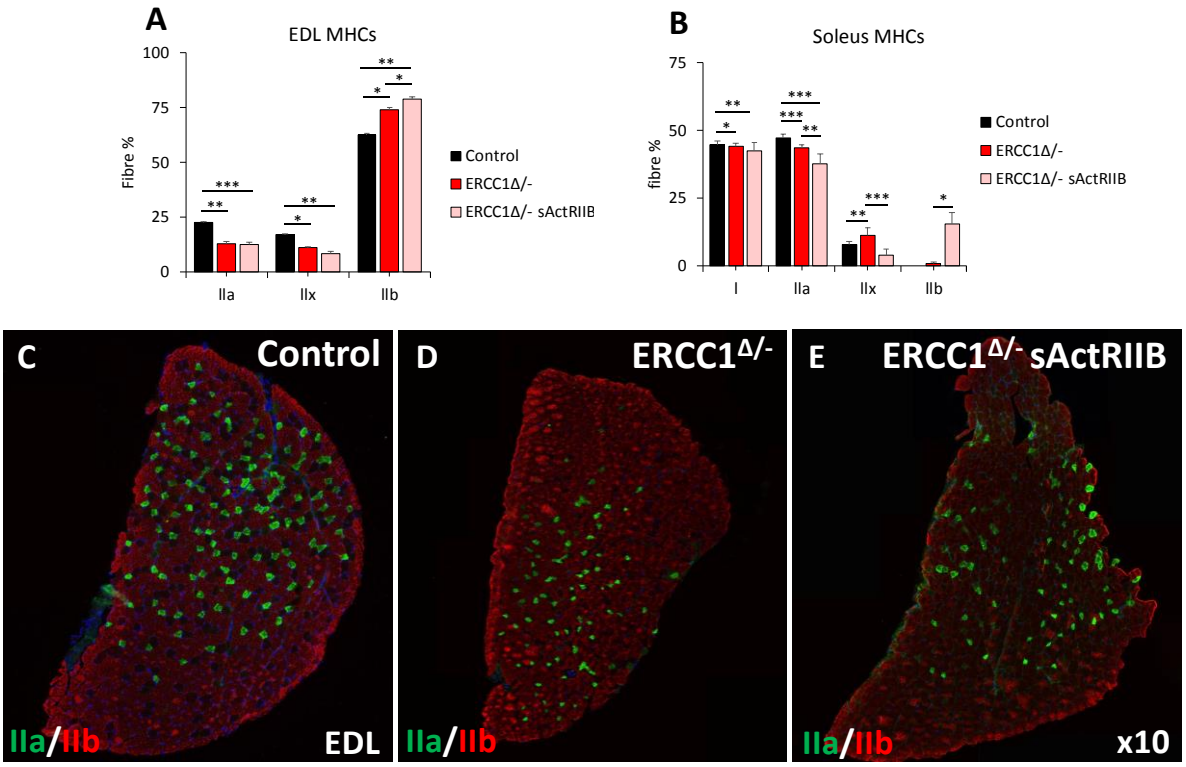

Figure 5.12. Shifting MHCs toward fast profile after sActRIIB injection in *Ercc1*$^{\Delta/-}$ mice.

(A) MHC profile of EDL muscle. (B) MHC profile of Soleus muscle. (C-E) EDL MHCIIA/IIB fibre distribution in the three cohorts, controls, *Ercc1*$^{\Delta/-}$ and *Ercc1*$^{\Delta/-}$ treated with sActRIIB. Whole muscle sections were analysing and counted for fibres typing detected by immunostaining using specific antibody for each MHC type in both EDL and soleus muscle in all 3 cohorts. The fibres type proportion present as a percentage regarding total fibres number. The sActRIIB were IP injected starting from week 7 of age to week 15. All mice were at the same age, n= 8 for all cohorts. One-way ANOVA followed by Bonferroni's multiple comparison tests, *p<0.05, **p<0.01, ***p<0.001.

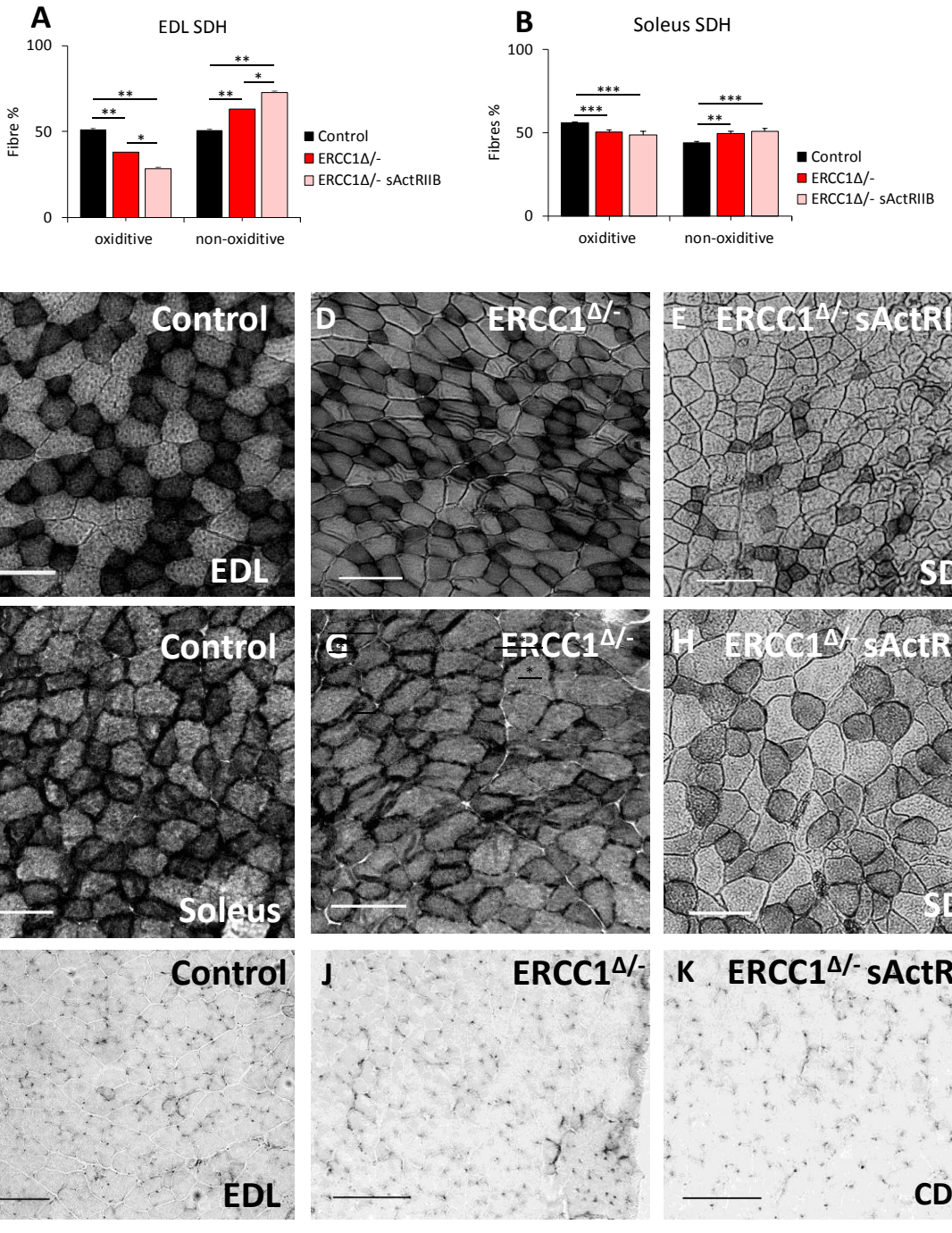
A
EDL SDH
Fibre %
100
50
0
oxiditive
non-oxiditive
Control
ERCC1Δ/-
ERCC1Δ/- sActRIIB
B
Soleus SDH
Fibres %
C Control EDL
D ERCC1Δ/-
E ERCC1Δ/- sActRIIB SDH
F Control Soleus
G ERCC1Δ/-
H ERCC1Δ/- sActRIIB SDH
I Control EDL
J ERCC1Δ/-
K ERCC1Δ/- sActRIIB CD31

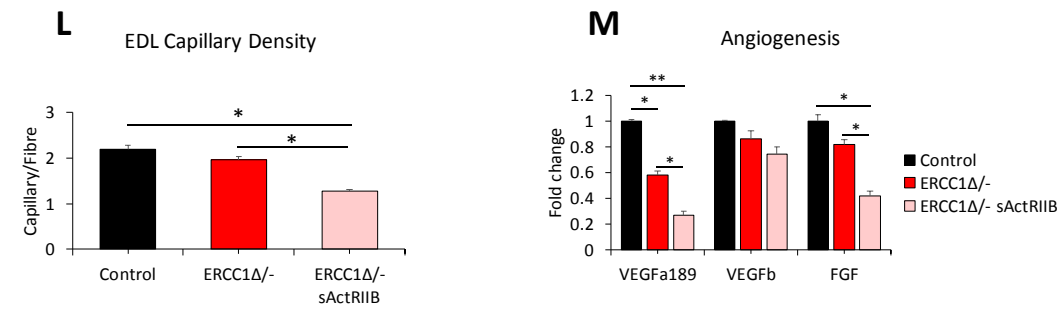
L
EDL Capillary Density
Capillary/Fibre
Control
ERCC1Δ/-
ERCC1Δ/- sActRIIB
M
Angiogenesis
Fold change
VEGFa189
VEGFb
FGF
Control
ERCC1Δ/-
ERCC1Δ/- sActRIIB

Figure 5.13. Reduce oxidative status, capillary density and expression of angiogenesis marker in *Ercc1*$^{\Delta/-}$ mice treated with sActRIIB.

(A) SDH-positive and negative fibre profile of EDL muscle. (B) SDH-positive and negative fibre profile of Soleus muscle. (C-E) representative pictures of SDH stain in EDL muscle of the three cohorts. (F-H) representative pictures of SDH stain in Soleus muscle of the three cohorts. Whole muscle sections were analysing to detect dark (oxidative) and pales stained (non-oxidative) fibres using SDH stain and presented as a percentage regarding total fibres number in EDL and soleus muscle. (I-K) Identification of EDL capillaries with CD-31 in the three cohorts. (L) Quantification of EDL capillary density. Total of 100 fibres in each section of EDL muscle were analyse and capillaries were counted, black dotes, and presented as capillary per fibres in all three cohorts. (M) qPCR profiling of angiogenic genes. The RNA that use in qPCR were obtained from gastrocnemius muscle from all 3 cohorts. The sActRIIB were IP injected starting from week 7 of age to week 15. All mice were at the same age, n= 8 for all cohorts. Scale 100 µm. One-way ANOVA followed by Bonferroni's multiple comparison tests used in all data sets except SDH analysis where non-parametric Kruskal-Wallis test followed by the Dunn's multiple comparison was used, *p<0.05, **p<0.01, ***p <0.001.

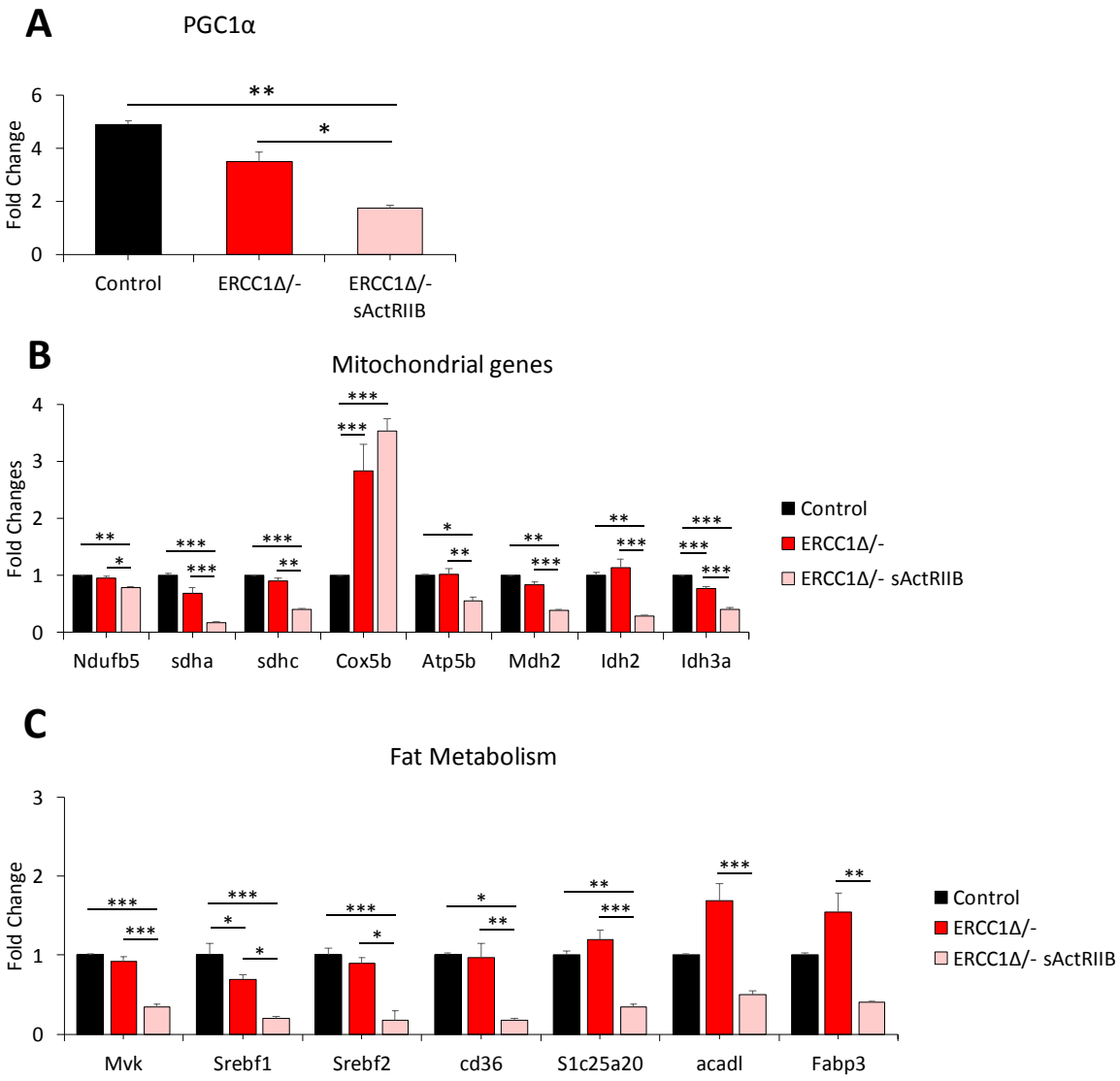

Figure 5.14. Reduce expression of genes regulate mitochondria and fat metabolism in *Ercc1*$^{\Delta/-}$ mice with sActRIIB treatment.

qPCR profiling of (A) PGC1α, (B) mitochondrial genes and (C) regulators of fat metabolism. The RNA that used here were obtained from gastrocnemius muscle from all 3 cohorts. The sActRIIB were IP injected starting from week 7 of age to week 15. All mice were at the same age, n= 8 for all cohorts. One-way ANOVA followed by Bonferroni's multiple comparison tests, *p<0.05, **p<0.01, ***p<0.001.

5.6. sActRIIB normalise ultrastructure abnormalities and mitochondrial characteristics in skeletal muscle of *Ercc1*$^{\Delta/-}$ mice.

We showed that attenuating Ercc1 protein resulted in skeletal muscle loss of mass and activity and change in muscle fibres size and profile in *Ercc1*$^{\Delta/-}$ progeric mice. So far, the antagonising of myostatin/activin signalling rescued most of the sarcopenic phenotype related to *Ercc1*$^{\Delta/-}$ albeit not to control level. It was well established that the maintenance of muscle size and activity is primarily mediated by the maintenance of cell ultrastructure milieu, especially mitochondria (Powers et al., 2012). A study by Merkwirth and Langer has reported that mitochondrial integrity and function were affected by the levels of inflammation and Prohibitin genes (Merkwirth and Langer, 2009). Further studies on cell microenvironment demonstrate the role of epigenetic modification in the maintenance of heterochromatin that changes with age (Benayoun et al., 2015, Liu et al., 2013). Furthermore, the ageing process causes a variable change in the level of histone modifications markers. The ageing progression leads to decrease H3K9me3 but an increase in H4K20me3 (Ocampo et al., 2016).

Therefore, the forelimb Biceps brachii (BB) muscles were isolated, fixed and used for transmission electron microscopy (TEM) work. Secondly, a level of mitochondrial unfolding protein, inflammation markers and Prohibitin genes expression were profiled in gastrocnemius muscle by qPCR. Finally, muscle sections of EDL were immunostained using antibodies against H3K9me3 and H4K20me3 to detect histone modifications.

Hind limb muscles, EDL and Gastrocnemius, and forelimb Biceps brachii from three cohorts of mice (Control, *Ercc1*$^{\Delta/-}$ and *Ercc1*$^{\Delta/-}$ treated) were examined. A minimum of 100 measurements per section was taken in each muscle section for immunostaining work.

We used a transmission electron microscope (TEM) to examine the ultrastructure of skeletal muscle in the three cohorts. We showed the ultrastructure abnormalities were evident in the muscle from *Ercc1*$^{\Delta/-}$ mice including absent and faint Z-lines indicated by blue and black arrows in figures, nonuniform sarcomere indicated by red arrows in figures and large intersarcomeric spaces indicated by black arrowheads in figures compared to controls (Figure 5.15. A, B, D, E, G and H). These abnormalities were mostly absent in muscle from *Ercc1*$^{\Delta/-}$ mice treated with sActRIIB (Figure 5.15. C, F and I). Mitochondrial density was lower in *Ercc1*$^{\Delta/-}$ mice both within the fibre (sarcomeric region) and directly under the sarcolemma compared to control group (Figure 5.15. J-K). Of particular note was the

alteration (swelling) of mitochondria in *Ercc1*$^{\Delta/-}$ mice both within the fibre and immediately under the sarcolemma compared to control group (Figure 5.15. H, L-M). The mitochondrial size was reduced by the treatment with sActRIIB in *Ercc1*$^{\Delta/-}$ mice (Figure 5.15. L-M). Mitochondrial hypertrophy is a protective response to a decrease in mitochondrial function or number or an indicative excessive fusion (Frank et al., 2001, Terman and Brunk, 2004b, Garcia-Prat et al., 2016). It is thought to promote mitochondrial survival by upregulating a stress response programme. Indeed, we found that there was an increase in the expression of critical genes involved in the mitochondrial unfolding protein response (UPR^{mt}) pathway in the muscle from *Ercc1*$^{\Delta/-}$ mice and were normalised to control level after sActRIIB treatment (Figure 5.16. A). We also examined the levels of inflammatory and Prohibitin genes which support the mitochondrial function of ensuring the correct folding of the cristae (Merkwirth and Langer, 2009). Expression of IL6 and IL18, as well as two essential Prohibitin genes (Phb and Phb2), appeared slightly elevated in the muscle of *Ercc1*$^{\Delta/-}$ mice and were normalised to control level after sActRIIB treatment (Figure 5.16.B and C).

Lastly, we examined whether muscle harboured epigenetic modifications involved in the maintenance of heterochromatin that changes with age (Benayoun et al., 2015, Liu et al., 2013). The ageing process causes a decrease in the level of H3K9me3 but an increase in H4K20me3 (Ocampo et al., 2016). H3K9me3 was decreased, and H4K20me3 increased in *Ercc1*$^{\Delta/-}$ animals in keeping with an age-related change (Figure 5.16. D-E). Both features were normalised following sActRIIB treatment (Figure 5.16. D-E). These results demonstrate sub-cellular defects in the *Ercc1*$^{\Delta/-}$ muscle and the expression of genes indicative of on-going stress. The sActRIIB treatment prevented the development of many of these abnormal features.

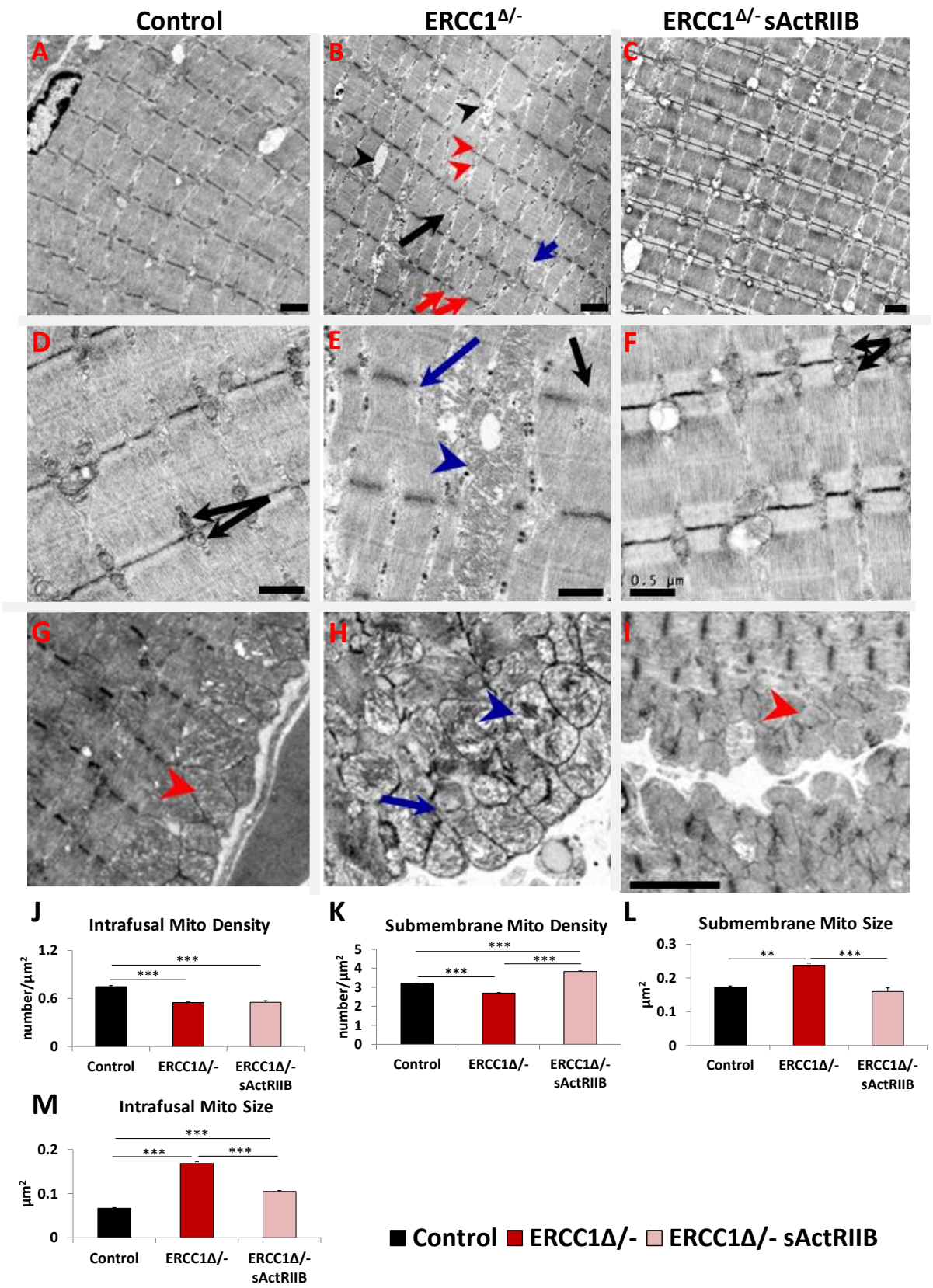
Control
ERCC1Δ/-
ERCC1Δ/- sActRIIB
A
B
C
D
E
F
0.5 µm
G
H
I
J
Intrafusal Mito Density
number/µm²
1.2
0.6
0
***
***
Control
ERCC1Δ/-
ERCC1Δ/- sActRIIB
K
Submembrane Mito Density
number/µm²
5
4
3
2
1
0
***
***
***
Control
ERCC1Δ/-
ERCC1Δ/- sActRIIB
L
Submembrane Mito Size
µm²
0.3
0.2
0.1
0
**
***
Control
ERCC1Δ/-
ERCC1Δ/- sActRIIB
M
Intrafusal Mito Size
µm²
0.2
0.1
0
***
***
***
Control
ERCC1Δ/-
ERCC1Δ/- sActRIIB
Control
ERCC1Δ/-
ERCC1Δ/- sActRIIB

Figure 5.15. Antagonise myostatin/activin signalling enhance microstructures in biceps brachii muscle of *Ercc1*$^{\Delta/-}$ investigated by TEM longitudinal image.

The TEM work has been done by Oliver Kretz, University of Freiburg, Germany.

(A) Low power image of control muscle. (B) Low power image of *Ercc1*$^{\Delta/-}$ muscle. Note large spaces (black arrowheads), non-uniform sarcomere width (red arrows) dilated sarcomeric mitochondria (red arrowheads), split sarcomere (black arrow) and disrupted M-Line (blue arrow). (C) Low power image of sActRIIB-treated *Ercc1*$^{\Delta/-}$ muscle. (D) Higher magnification of sarcomeric region of control muscle showing uniformly sized mitochondria (black arrows). (E) Enlarged mitochondria in sarcomeric region of *Ercc1*$^{\Delta/-}$ muscle (blue arrowhead) and absent (blue arrow) or faint Z-line (black arrow). (F) Higher magnification of sarcomeric region of treated *Ercc1*$^{\Delta/-}$ mice showing smaller sarcomeric mitochondria (black arrows). (G) Sarcolemma region of control muscle showing compact mitochondria (red arrowhead). (H) Dilated (blue arrowhead) and aberrant mitochondria (blue arrow) in sub-sarcolemma region of *Ercc1*$^{\Delta/-}$ muscle. (I) Sarcolemma region of treated *Ercc1*$^{\Delta/-}$ mice showing compact mitochondria (red arrowhead). (J-K) Sarcomeric (intrafusal) and sub-membrane mitochondrial density measurements. (L-M) Sub-membrane and sarcomeric (intrafusal) mitochondrial size measurements. All mice were at the same age, n= 6-7 for all cohorts. The sActRIIB were IP injected starting from week 7 of age to week 15. One-way ANOVA followed by Bonferroni's multiple comparison tests, *p<0.05, **p<0.01, ***p<0.001.

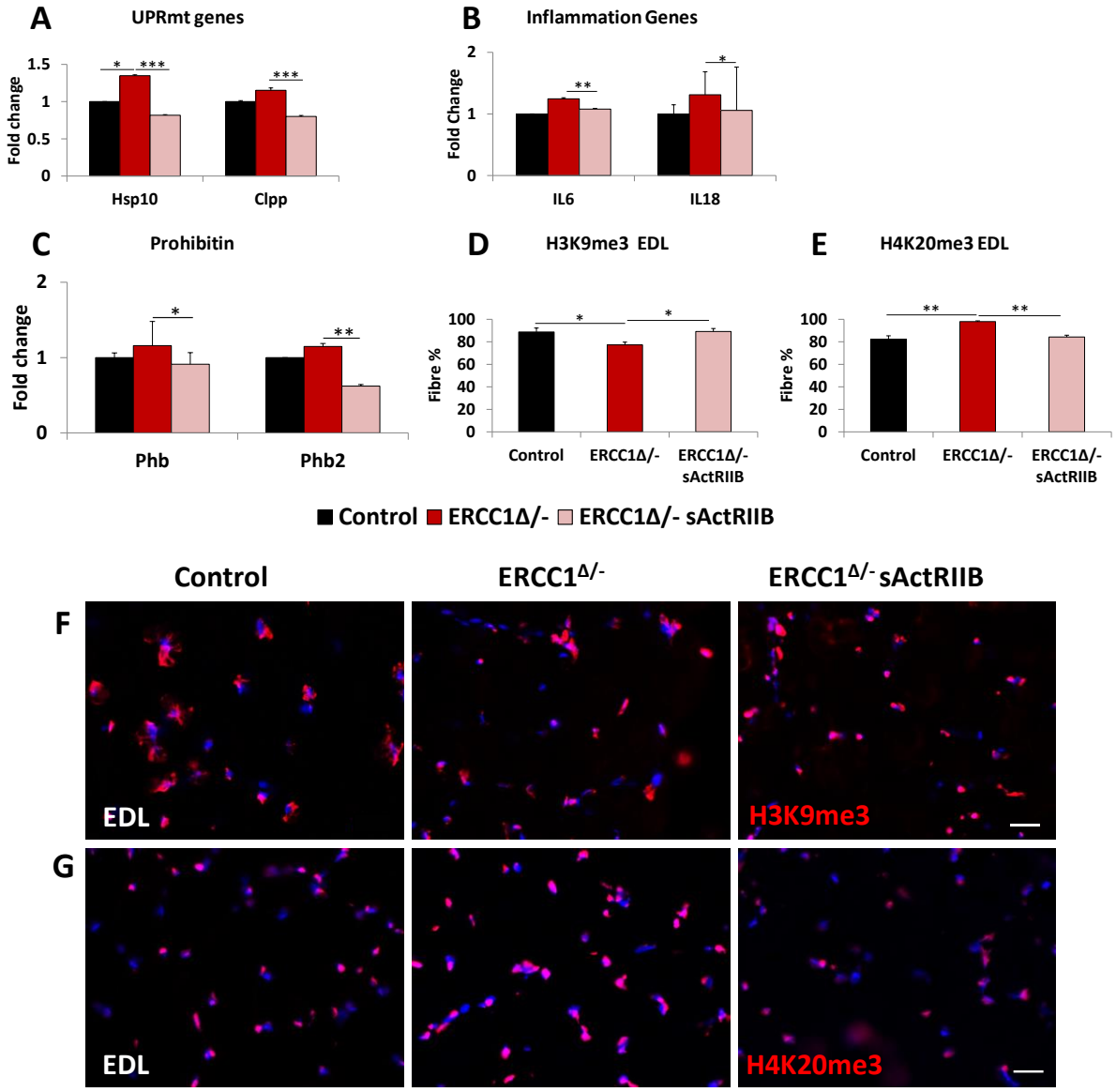
A
UPRmt genes
Fold change
1.5
1
0.5
0
Hsp10
Clpp
B
Inflammation Genes
Fold Change
2
1
0
IL6
IL18
C
Prohibitin
Fold change
2
1
0
Phb
Phb2
D
H3K9me3 EDL
Fibre %
100
80
60
40
20
0
Control
ERCC1Δ/-
ERCC1Δ/- sActRIIB
E
H4K20me3 EDL
Fibre %
100
80
60
40
20
0
Control
ERCC1Δ/-
ERCC1Δ/- sActRIIB
Control
ERCC1Δ/-
ERCC1Δ/- sActRIIB
F
EDL
H3K9me3
G
EDL
H4K20me3

Figure 5.16. Gene expression of ageing key regulator factors.

(A) Expression of Mitochondria Unfolded Protein response gene (UPR^{mt}) in gastrocnemius muscle. (B) Expression of inflammatory genes in gastrocnemius muscle. (C) Expression of prohibitin genes in gastrocnemius muscle. (D) Quantification of EDL fibres expressing H3K9me3 and (E) H4K20me3. (F) Representative images of EDL muscle immunostained against H3K9me3 from all 3 cohorts. The RNA that use here for qPCR were obtained from gastrocnemius muscle for all 3 cohorts. (G) Representative images of EDL muscle immunostained against H4K20me3 from all 3 cohorts. A total of 100 fibres were analysed and the positive nucleus for histone markers were presented as percentage regarding total fibres number. The RNA that use here for qPCR were obtained from gastrocnemius muscle for all 3 cohorts. The sActRIIB were IP injected starting from week 7 of age to week 15. All mice were at the same age, n= 8-9 for all cohorts. Scale is 100 µm. Non-parametric Kruskal-Wallis test followed by the Dunn's multiple comparisons used in (A-B) and rest with one-way ANOVA followed by Bonferroni's multiple comparison tests, *p<0.05, **p<0.01, ***p<0.001.

5.7. Mechanisms underlying fibre size changes before and after sActRIIB treatment in *Ercc1*$^{\Delta/-}$ mice.

We demonstrate that disrupting *Ercc1* gene resulted in a phenotype characterised by skeletal muscle mass loss via reducing fibres size in *Ercc1*$^{\Delta/-}$ progeric mice. However, the antagonising of myostatin/activin signalling rescued most of the sarcopenic phenotype related to *Ercc1*$^{\Delta/-}$ albeit not to control level. We investigated the mechanisms underpinning muscle fibres enlargement resulting from the sActRIIB injection. In general, it is well established that the maintenance of skeletal muscle growth achieved by the dynamic balance between protein synthesis and degradation. Two studies by Sandri and Glass demonstrated that protein synthesis is regulated by AKT/mTOR pathway and protein degradation by the AKT/FoxO pathway (Sandri, 2008, Glass, 2005). The cross talk between Myostatin and AKT/mTOR signalling pathway was also investigated and revealed a central role of Myostatin in regulating muscle protein synthesis and degradation (Elliott et al., 2012).

Therefore, the hindlimb Gastrocnemius muscles were isolated, frozen and used for Western blot and qPCR work. Autophagy marker was detected in muscle sections of EDL muscle via immunostaining using antibodies against p62.

All muscles (hind limb muscles EDL and Gastrocnemius) were from three cohorts of mice (Control, *Ercc1*$^{\Delta/-}$ and *Ercc1*$^{\Delta/-}$ treated). A minimum of 100 measurements per section was taken in each muscle section for immunostaining work. The number of animals was 5 for western blot all cohorts and 8 animals of all cohorts for other work.

We showed, surprisingly, the levels of phosphorylated Akt (an inducer of anabolism) was elevated in the muscle from 16-week old mock-treated *Ercc1*$^{\Delta/-}$ mice (Figure 5.17. A). Next, we examined downstream targets of pAkt and found that there was a slight decrease in the phosphorylation of 4EBP1 at Thr37/46 but none at Ser65 (Figure 5.17. B). However, there was an elevated level of phosphorylation at another pAkt target, S6 (Figure 5.17. C). The effect of sActRIIB on the anabolic programme of *Ercc1*$^{\Delta/-}$ muscle showed a general increase in the level of pAkt, as well as its two downstream targets, 4EBP1 and S6, relative to both mock-treated *Ercc1*$^{\Delta/-}$ and control groups (Figure 5.17. A-C). After that, we probed the catabolic programme and found that activity of FoxO1 and FoxO3a, critical regulators of ubiquitin-mediated protein breakdown (FoxO1 significantly, FoxO3a not so) were generally decreased in the muscle from *Ercc1*$^{\Delta/-}$ mice (Figure 5.17. D-E), and increase after treatment

even to a level exceeding control. Expression of both *MuRF1* and *Atrogin-1,* downstream targets of FoxO1 and FoxO3a, were elevated at the RNA level in the muscle of *Ercc1*$^{\Delta/-}$ mice (Figure 5.17. I-J). The LC3 autophagy activity was suppressed compared to controls (Figure 5.17. F). Treatment with sActRIIB caused an elevation in the levels of inactive FoxO1 and FoxO3a (Figure 5.17. D-E) and a decrease in the expression of *MuRF1* but, surprisingly, not *Atrogin-1*. (Figure 5.17. I-J). Expression of *Mul1*, a key regulator of mitophagy (Rojansky et al., 2016) did not differ between the three groups (Figure 5.17. K). Significantly we found an increase in the level of autophagy gauged by the LC3II/I ratio and levels of p62 following sActRIIB treatment (Figure 5.17. F-G). We quantified the presence of p62 puncta which has been used as an indicator of autophagic flux, with an increase in the numbers of p62 puncta implying a decrease in autophagic activity (Abbey et al., 2004). The number of p62 puncta per given area was higher in *Ercc1*$^{\Delta/-}$ EDL muscle compared to controls, and their levels were reduced by sActRIIB treatment (Figure 5.17. L-M). Treatment of *Ercc1*$^{\Delta/}$ mice with sActRIIB resulted in a non-significant increase in the amount of active eIF2a, a vital regulator of the endoplasmic reticulum Unfolded Protein Response (UPR^{ER}) programme (Figure 5.17. H). At the organismal level, we found that the rate of protein synthesis was elevated (but not to significant levels) in *Ercc1*$^{\Delta/-}$ mice and further elevated by sActRIIB treatment (Figure 5.17. N). The abundance of ubiquitinated proteins was elevated in the muscle of *Ercc1*$^{\Delta/-}$ mice but reduced by sActRIIB treatment (Figure 5.17. O).

These results reveal unique characteristics considering the changes in muscle mass in the progeric mice. The muscle of *Ercc1*$^{\Delta/-}$ mice activates both its protein synthesis pathway and has elevated gene expression of molecules that control protein breakdown. However, autophagy is blunted. Treatment of *Ercc1*$^{\Delta/-}$ with sActRIIB results in an increase in the activity of molecules controlling protein synthesis as well as an overall rate of protein synthesis, a decrease in the abundance of ubiquitinated proteins E3 as well as an increase in key regulators of autophagy.

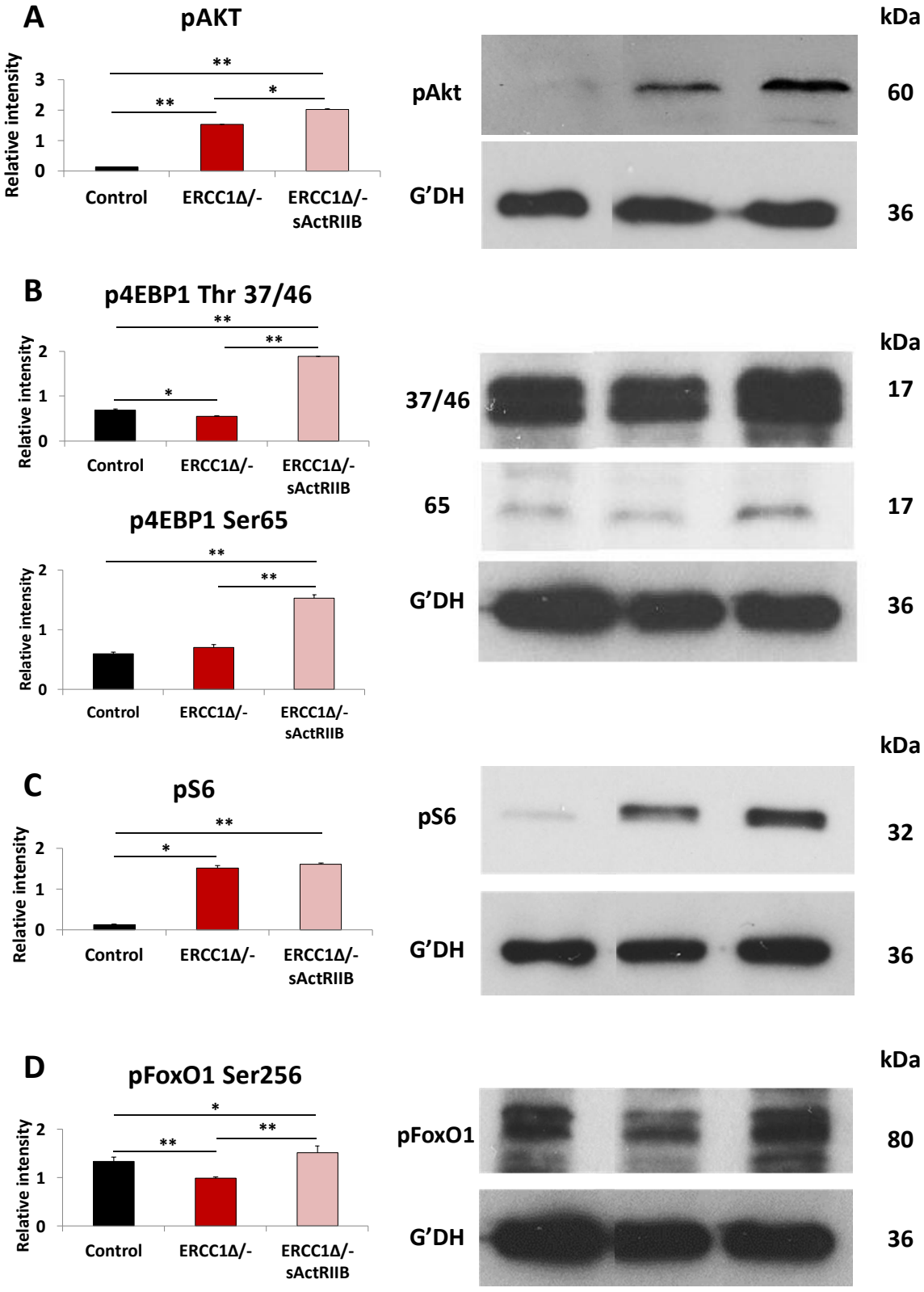
A
pAKT
Relative intensity
3
2
1
0
**
**
*
Control
ERCC1Δ/-
ERCC1Δ/-
sActRIIB
kDa
pAkt
60
G'DH
36
B
p4EBP1 Thr 37/46
Relative intensity
2
1
0
**
**
*
Control
ERCC1Δ/-
ERCC1Δ/-
sActRIIB
kDa
37/46
17
65
17
G'DH
36
p4EBP1 Ser65
Relative intensity
2
1
0
**
**
Control
ERCC1Δ/-
ERCC1Δ/-
sActRIIB
C
pS6
Relative intensity
2
1
0
**
*
Control
ERCC1Δ/-
ERCC1Δ/-
sActRIIB
kDa
pS6
32
G'DH
36
D
pFoxO1 Ser256
Relative intensity
2
1
0
*
**
**
Control
ERCC1Δ/-
ERCC1Δ/-
sActRIIB
kDa
pFoxO1
80
G'DH
36

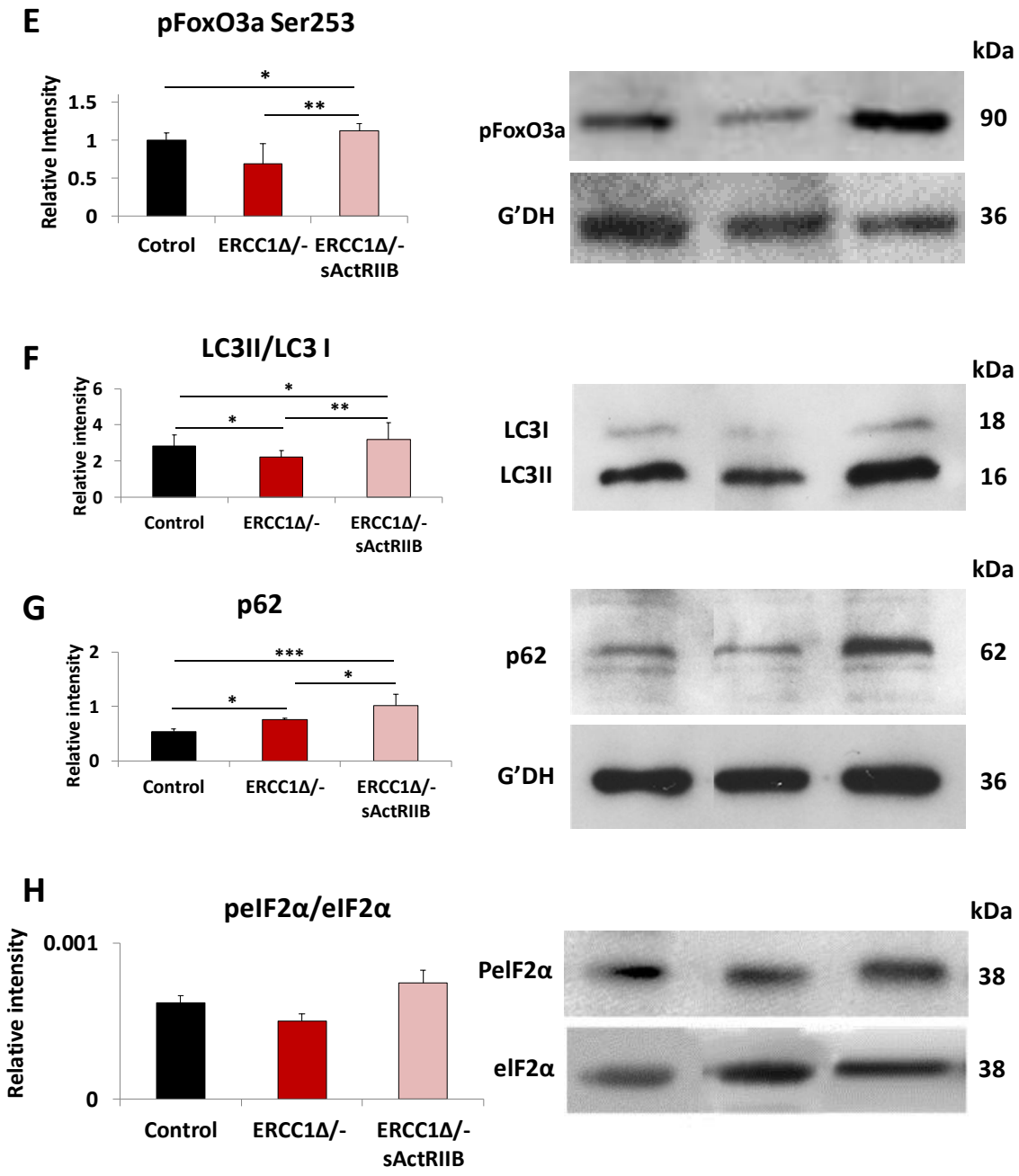
E
pFoxO3a Ser253
Relative Intensity
1.5
1
0.5
0
*
**
Cotrol
ERCC1Δ/-
ERCC1Δ/-
sActRIIB
kDa
pFoxO3a
90
G'DH
36
F
LC3II/LC3 I
Relative intensity
6
4
2
0
*
*
**
Control
ERCC1Δ/-
ERCC1Δ/-
sActRIIB
kDa
LC3I
18
LC3II
16
G
p62
Relative intensity
2
1
0
***
*
*
Control
ERCC1Δ/-
ERCC1Δ/-
sActRIIB
kDa
p62
62
G'DH
36
H
peIF2α/eIF2α
Relative intensity
0.001
0
Control
ERCC1Δ/-
ERCC1Δ/-
sActRIIB
kDa
PeIF2α
38
eIF2α
38

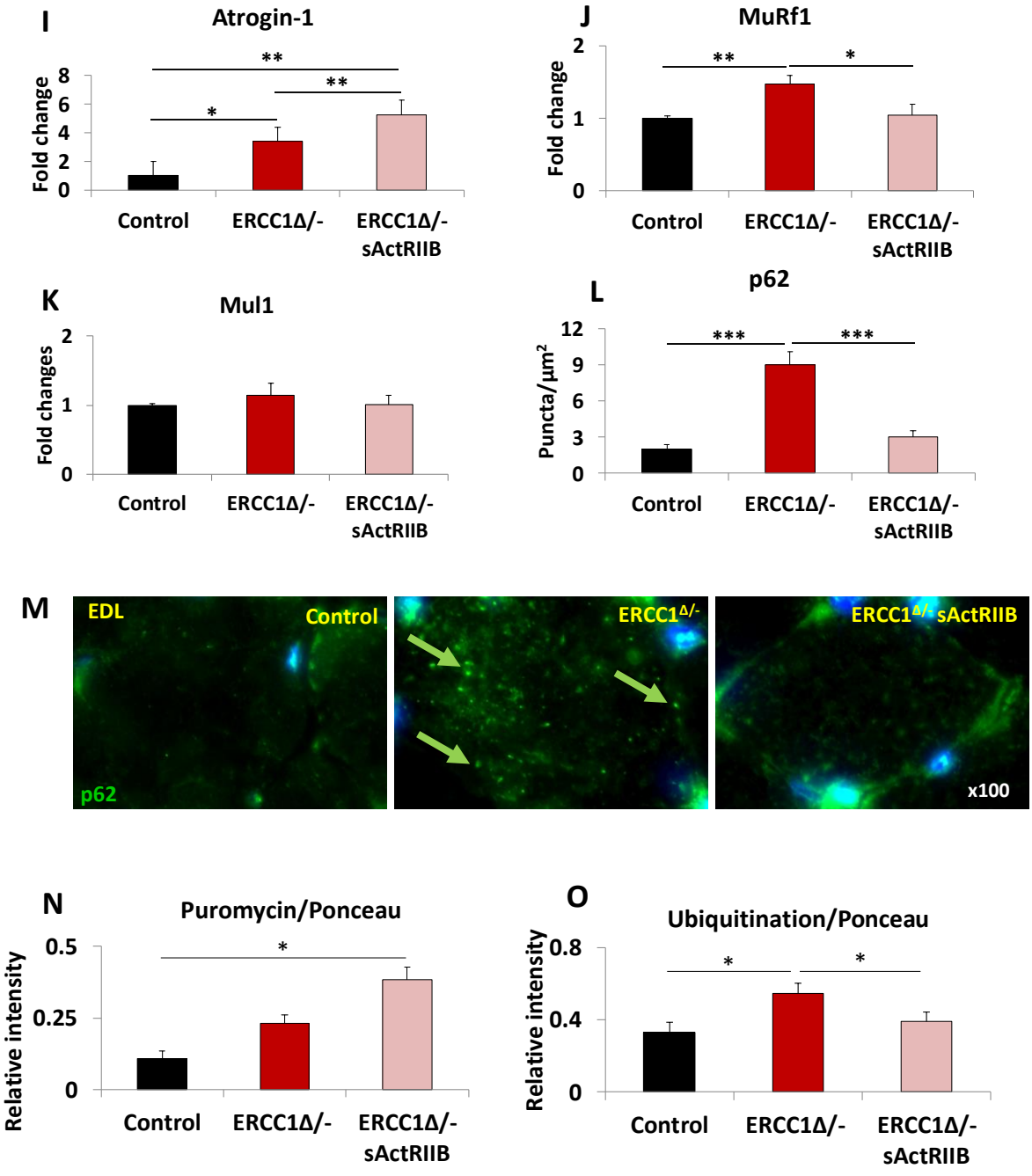
I
Atrogin-1
Fold change
Control
ERCC1Δ/-
ERCC1Δ/-
sActRIIB
J
MuRf1
Fold change
K
Mul1
Fold changes
L
p62
Puncta/µm²
M
EDL
Control
p62
ERCC1Δ/-
ERCC1Δ/- sActRIIB
x100
N
Puromycin/Ponceau
Relative intensity
O
Ubiquitination/Ponceau
Relative intensity

Figure 5.17. Western blotting and qPCR demonstrating that sActRIIB promotes protein synthesis and autophagy but blunts proteasome protein breakdown in *Ercc1*$^{\Delta/-}$ muscle.

Immunoblots and densitometry quantification of (A) pAkt, (B) p4EBPI on Thr37/46 and Ser65, (C) pS6, (D) pFoxO1, (E) pFoxO3a, (F) LC3II/I, (G) p62 and (H) eIF2α. (I-K) qPCR quantification of *Atrogin-1*, *MuRF1*, *Mul1* expression. (L) Quantification of p62 puncta. (M) Immunohistology of p62 puncta in the EDL muscle (green arrows) (N) Densitometry quantification of total puromycin incorporation (protein synthesis rate). (O) Densitometry quantification protein ubiquitination. All western blotting analysis and qPCR done on proteins and RNA from gastrocnemius muscle from all three cohorts. A total of 100 fibres were analysed for p62 and the fibres with positive localisation of this protein represented as a percentage regarding total fibres number. The sActRIIB were IP injected starting from week 7 of age to week 15. All mice were at the same age, n=5 for all western blots and n=8 for rest. Non-parametric Kruskal-Wallis test followed by the Dunn's multiple comparisons used for (A-H and N-O). One-way ANOVA followed by Bonferroni's multiple comparison test used for (I-K). *<0.05, **<0.01, ***p<0.001.

5.8. Discussion

Loss of muscle mass and function with age, i.e. sarcopenia, invariably leads to a reduced quality of life by impacting on mobility and stability, which leads to an increase in the incidence of fall-related injury. More importantly, sarcopenia predisposes individuals to adverse disease outcomes (cardiovascular and metabolic diseases) and mortality (Srikanthan and Karlamangla, 2014, Kim et al., 2015). Exercise, protein intake and calorie restricted were used as a suggested therapy of sarcopenia (McCormick and Vasilaki, 2018). However, enhance muscle growth strategy, such as myostatin inhibitor, have a debate because it conflicts with the theory that shows the tissue with ageing will provoke stress response that shifts the resource from growth to maintenance.

Here we investigated the pathways and mechanisms underpinning increased skeletal muscle mass after treated with sActRIIB in *Ercc1*$^{\Delta/-}$ mice. Based on the concept that DNA damage induces a survival response that promotes maintenance programmes on the expense of growth one would predict that augmenting muscle growth would, in the long run, exacerbate the pathological features in a progeroid model. What we find is something entirely different; sActRIIB treatment before the onset of progeria can scale down the signs of ageing in skeletal muscle, notwithstanding NER defects.

The main finding of this part was the antagonise myostatin/activin signalling enhanced skeletal muscle mass in *Ercc1*$^{\Delta/-}$ progeric mice by increase fibres size and maintained total fibres number. The mechanism underpinning muscle growth was investigated and revealed an increase in protein synthesis markers and reduce protein degradation. The increase in muscle growth was combined by enhancement of fibres condition by reducing the level of fibres damage on both macro and microstructure. However, we show that treatment with sActRIIB intensifies the glycolytic and fast profile of skeletal muscle in *Ercc1*$^{\Delta/-}$ mice. Furthermore, sActRIIB injection reduces capillary density and mitochondrial biogenesis in progeric mice.

One of the most apparent signs of ageing in humans is sarcopenia; the involuntary loss of skeletal muscle mass and function over time (Rosenberg, 1997). It becomes evident at middle age in humans with a loss of 0.5-1% of mass per year, which increases in the seventh decade (Nair, 2005). As a model of accelerated ageing, we show that muscle of *Ercc1*$^{\Delta/-}$ progeroid undergoes severe wasting, compared to controls, hindlimb muscle mass was less than controls of 40-60%. In a previous study, using sActRIIB resulting in induces significant

increases in body mass and muscle weight in less than four weeks in wild-type and disease mouse model (Relizani et al., 2014). Our result shows that the IP-injection of male *Ercc1*$^{\Delta/-}$ mice twice a week with sActRIIB from 7-week of age till week 16 could increase muscle mass by 30-62% compared to untreated progeric. As shown before, the hind limb muscles of Mstn null increase in size and this increment achieved by individual muscle fibre hypertrophy and hyperplasia (Amthor et al., 2007, McPherron and Lee, 1997), we show that the introduction of sActRIIB induced fibre hypertrophy in all fibres type and even larger than control in Soleus's MHCI and MHCIIA. The total fibre number was elevated in *Ercc1*$^{\Delta/-}$ mutants and maintained by sActRIIB. We suggest the higher fibre number in *Ercc1*$^{\Delta/-}$ mice compared to control could be resulting from myofibers splitting. As evidence of branching, we find many damaged fibres, increase in the centrally located nucleus, fibres apoptosis (increase level of caspase-3) and increasing the proportion of fibres with hyper SDH activity, as evidence of abnormal mitochondrial activity that leads to apoptosis (Cheema et al., 2015), in *Ercc1*$^{\Delta/-}$ mice. The same condition was reported in mdx mice were the hyperplasia with a concomitant increase in fibres proportion with centrally nucleated as evidence of fibres branching (Faber et al., 2014).

It has been reported that MHCs profile shows evidence of shifting from fast to slow and shift toward oxidative metabolism with ageing (Doran et al., 2009). One of the limitations of our progeric mice as a model of ageing, the results of the MHC profile shifted from slow to fast and decrease the oxidative activity of fibres. However, MHCIIa and MHCIIb in the superficial portion of the TA follow the same trend of natural age (see figure 3.7.C). Deletion of the myostatin gene leads to a reduction in slow fibres proportion and reduce oxidative property of myofibers in Myostatin null mice (Amthor et al., 2007, Lipina et al., 2010). We find the same results with the *Ercc1*$^{\Delta/-}$ mice after treated with sActRIIB, where the percentage of glycolytic fibres increase in treated mice. Then we investigated the mechanism underpin fibres profile shifting in *Ercc1*$^{\Delta/-}$ mice after sActRIIB injection.

Myostatin is a member of the TGF-β family and its defined as an inhibitor of muscle development and promoter of oxidative metabolism, and mutation of its gene leads to hypertrophic glycolytic fibres (McPherron and Lee, 1997, Amthor et al., 2007). Amthor et al. were showed a reduction in mitochondrial density in myostatin null mice and that could be resulting in increased fatigability of the muscle (Amthor et al., 2007). Beside the mitochondrial density, the oxidative metabolism is relying on mitochondrial activity. A

study by Baligand et al. show alteration in mitochondrial ATP synthesis in the muscle of myostatin null mice (Baligand et al., 2010). Diminishing in mitochondrial activity will affect skeletal muscle contraction properties since mitochondria are the primary source of ATP production in skeletal muscle (Ljubicic et al., 2010). Changes in mitochondrial activity resulting in oxidative stress and lead to impairs muscle contractile properties (Reid et al., 1993).

Furthermore, the myostatin null mice show a reduction in mitochondrial enzyme activity such as succinate dehydrogenase and cytochrome oxidase (Amthor et al., 2007) and that could be interpreted the oxidative profile shifting toward more glycolytic after antagonising myostatin. Maintain the glycolytic profile by sActRIIB injection in progeric mice was with a concomitant decrease in capillary density and angiogenesis factors. Moreover, that was the case in myostatin null mice (Savage and McPherron, 2010, Amthor et al., 2007, Lipina et al., 2010).

Additionally, the expression level of mitochondrial genes was also reduced after sActRIIB treatment in *Ercc1*$^{\Delta/-}$ mice. The principal regulator of oxidative properties in muscle, *PGC1α* (Ploquin et al., 2012), was also reduced after sActRIIB treatment in *Ercc1*$^{\Delta/-}$ mice. Furthermore, the level of fat metabolism markers, that consider a sign of oxidative metabolism (Jeukendrup, 2002), show the low level in *Ercc1*$^{\Delta/-}$ mice after sActRIIB treatment.

Although sActRIIB treated *Ercc1*$^{\Delta/-}$ mice reduced the oxidative metabolism of skeletal muscle, the TEM work showed normalisation in mitochondrial distribution and ultrastructure. We show that the swelling of mitochondria, a protective response in a stress situation (Frank et al., 2001, Terman and Brunk, 2004b, Garcia-Prat et al., 2016), decreased in the sarcomeric region and under the sarcolemma after sActRIIB treatment in *Ercc1*$^{\Delta/-}$ mice. Furthermore, there was a redistribution of mitochondria by an increase in the population of mitochondria in sub sarcolemma region after treatment. A study by Harper et al. demonstrated the dominant role of the mitochondrial electron transport chain (ETC) pathway in the production of Reactive Oxygen Species (ROS) (Harper et al., 2004). A further study documents that the chronic exposure to ROS as a result of mitochondrial dysfunction involved in protein, lipid and DNA damage (Jackson, 2011) and that exuberate the situation in *Ercc1*$^{\Delta/-}$ mice with impaired DNA damage repair. We show that elevated level of ROS in *Ercc1*$^{\Delta/-}$ mice as detected by DHE stain were reduced, although not to control level, after

sActRIIB injection. TEM work that shows normalisation in mitochondria shape and distribution was also revealed an absence of most of the abnormalities in Z-line and sarcomeres after sActRIIB treatment that we find in *Ercc1*$^{\Delta/-}$ mice.

Further investigation revealed qualitative enhancement of sActRIIB's treated progeric mice. As mentioned above the mitochondrial hypertrophy provokes a protective response to promote mitochondrial survival by upregulating a stress response programme. Indeed, we found that there was an increase in the expression of critical genes involved in the mitochondrial unfolding protein response (UPR^{mt}) pathway in the muscle from *Ercc1*$^{\Delta/-}$ mice which are normalising to controls level after sActRIIB treatment. Besides, the levels of inflammatory and Prohibitin genes which support the mitochondrial function of ensuring correct folding of the cristae (Merkwirth and Langer, 2009) were slightly elevated in the muscle of *Ercc1*$^{\Delta/-}$ mice were also reduced to the level of controls in *Ercc1*$^{\Delta/-}$ treated mice. Examination of the level of epigenetic modifications markers, H3K9me3 and H4K20me3 that maintained heterochromatin and changed with age (Benayoun et al., 2015, Liu et al., 2013) showed the same pattern of what has been reported with ageing. The ageing process causes a decrease in the level of H3K9me3 but an increase in H4K20me3 (Ocampo et al., 2016). The sActRIIB injection was largely normalised both features in *Ercc1*$^{\Delta/-}$ mice to controls level.

The antagonising of myostatin/activin signalling, as we mentioned above, protect the progeric mice from loss of skeletal mass. Further investigation shows that the increase in skeletal muscle mass resulted mainly from an increase in cross-sectional area of myofibre. It is well established that muscle myofibers growth depends on the balance between protein synthesis and degradation (Nader, 2005). Surprisingly we found an increase in the level of phosphorylated Akt (pAkt), a key regulator of protein synthesis, and an increase in protein synthesis detected by increase puromycin level as an indicator for newly forming protein, in *Ercc1*$^{\Delta/-}$ mice. However, the downstream target of pAkt, 4EBP1, were slightly reduced at Thr37/46 but none at Ser65. Another pAkt target, S6, was highly phosphorylated in non-treated *Ercc1*$^{\Delta/-}$ mice. The increase in skeletal muscle mass in *Ercc1*$^{\Delta/-}$ treated with sActRIIB resulted from an enhancement of the anabolic programme demonstrated by a dramatic increase in the level of pAkt, as well as its two downstream targets, 4EBP1 and S6, relative to both mock-treated *Ercc1*$^{\Delta/-}$ and control groups. The level of newly formed proteins as detected by puromycin was also elevated in *Ercc1*$^{\Delta/-}$ mice after sActRIIB

treatment. The catabolic programme was generally decreased in *Ercc1*$^{\Delta/-}$, as the activity of FoxO1 and FoxO3a, critical regulators of ubiquitin-mediated protein breakdown were reduced even to a level lower than control. However, the ubiquitinated protein level was increased in *Ercc1*$^{\Delta/-}$ mice with a concomitant increase in the expression level of both *MuRF1* and *Atrogin-1*.

The sActRIIB treatment increased both FoxO1 and FoxO3a and reduced both ubiquitination and *MuRF1* but not *Atrogin-1* in *Ercc1*$^{\Delta/-}$ mice. The FoxO proteins also have an essential role in regulating the autophagy (Bonaldo and Sandri, 2013), the case that leads to an elevated level of abnormal mitochondria and damage to ultrastructure was resulted from reducing autophagy in *Ercc1*$^{\Delta/-}$ mice.

In contrast, Omairi et al. proposed that the role of autophagy is to maintain cellular homeostasis rather than catabolism (Omairi et al., 2016). The LC3 autophagy activity was suppressed in *Ercc1*$^{\Delta/-}$ mice compared to controls and increase after sActRIIB treatment. However, the specific marker for mitochondrial autophagy or mitophagy, *Mul1* (Rojansky et al., 2016), was not changed in 3 cohorts. The quantification of the presence of p62 puncta, which has been used as an indicator of autophagic flux increased, implying a decrease in autophagic activity (Abbey et al., 2004). Treatment of *Ercc1*$^{\Delta/-}$ mice with sActRIIB resulted in a non-significant increase in the amount of active eIF2a, a vital regulator of the endoplasmic reticulum Unfolded Protein Response (UPR^{ER}) programme. These results reveal unique characteristics considering the changes in muscle mass in the progeric mice. The muscle of *Ercc1*$^{\Delta/-}$ mice activates both its protein synthesis pathway and has elevated gene expression of molecules that control protein breakdown. However, autophagy is blunted. Treatment of *Ercc1*$^{\Delta/-}$ with sActRIIB results in an increase in the activity of molecules controlling protein synthesis as well as the overall rate of protein synthesis, a decrease in the abundance of ubiquitinated proteins E3 as well as an increase in key regulators of autophagy.

Chapter 6 Results

The normalisation of *Ercc1*$^{\Delta/-}$ extracellular components by sActRIIB and differentiation and self-renewal of its satellite cells.

6.1. Introduction

Like other organs, skeletal muscle composed of several compartments works coordinately perform to form the tissue. The high-performance action of skeletal muscle needs supporting tissue to maintain muscle structure and function (Gillies and Lieber, 2011). Dystrophin-glycoprotein complex (DGC) play an essential support role by connecting the internal structures of the myofibres, cytoskeleton, to the extracellular matrix (ECM) (Gumerson and Michele, 2011, Gillies and Lieber, 2011). These supportive compartments bind and work together, for instance, component from ECM, such as laminin, bind to the transmembrane compartment, β-Dystroglycan, and also bind to basal lamina member, collagen IV (Allamand et al., 2011). The DGC compartments support skeletal muscle to perform and transmit force to ECM to do the action and protect it from contraction-induced damage (Kjaer, 2004). The importance of supporting compartment in skeletal muscle health is shown as many pathological conditions occur due to mutations in genes of DGC or ECM for example, *Dystrophin* mutation leads to Duchenne Muscular Dystrophy (DMD) and Becker Muscular Dystrophy (BMD) (Kunkel et al., 1989). Dystrophin is a key intercellular component that links the cytoskeleton to the ECM (Hoffman et al., 1987, Ervasti and Campbell, 1993). A physiological condition such as ageing leads to changes in ECM and associated with reducing muscle strength and mechanical properties (Kragstrup et al., 2011). Deposition of proteins such as collagen and laminin are reported to change with ageing (Kovanen et al., 1988). Another study reports the ability of ageing to reduce the gene expression of ECM protein compartments (Pattison et al., 2003). Another study showed a different profile with ageing in different muscles; the amount of dystrophin was increased in EDL and decrease in Soleus with ageing (Rice et al., 2006). Another study report an age-related loss of dystrophin protein in TA muscle (Hughes et al., 2017). Furthermore, many studies show different deposition of another compartment of ECM. A study on rat shows that the level of collagen IV increased with age (Kovanen et al., 1988) however another study in human show increase collagen deposition with peaked in the 50s and reduced at the age of 80s (Inokuchi et al., 1975).

Satellite cells, the myofiber's resident stem cells, mediate skeletal muscle repair and regeneration and are located under the basal lamina (Mauro, 1961, Zammit et al., 2006). Satellite cells have two fates upon activation and proliferation, 1) differentiation and

incorporate into mature muscle fibre for repair or growth, or 2) supply the pole of stem cell (Almeida et al., 2016). Activated satellite cells differentiate to myoblasts and then terminally turned to postmitotic myonuclei (Bischoff and Heintz, 1994). Physiological and disease conditions that change the metabolic properties of skeletal muscle fibres could affect the satellite cells population. Several studies show a positive relationship between the oxidative profile and increase satellite cell presentation (Putman et al., 1985, Christov et al., 2007). For instance, the number of satellite cell was less in the EDL than the Soleus muscle they have glycolytic and oxidative profile, respectively (Gibson and Schultz, 1983). Knocking out the myostatin gene, that results in skeletal muscle hypertrophy with reduced satellite cells population (Amthor et al., 2007).

Myofibers are multinucleated post-mitotic cell form from the fusion of differentiated myoblast (Mauro, 1961). As a big cell, myofibre nuclei abundance provide transcriptional information to cover the whole myofibre (Bruusgaard et al., 2003, van der Meer et al., 2011). Nuclei are distributing throughout the fibres to ensure covering cytosol without challenging of signals transport (Bruusgaard et al., 2003).

The alteration in ECM and DGC proteins deposition and properties in skeletal muscle in ageing was affecting both contraction and satellite cell activity. As the *Ercc1*$^{\Delta/-}$ mice shows many similarities with naturally aged mice, we did investigate the effect of disruption of ERCC1 and the effect of sActRIIB treatment afterwards on the force transduction compartment, satellite cell number and activity, and myonuclei abundant.

Our result shows that sActRIIB treatment before the onset of progeria can change the components of ECM and DGC skeletal muscle and enhance satellite cells proliferation and differentiation, notwithstanding NER defects. However, the sActRIIB treatment did not rescue the reduction in myonuclei number.

One EDL muscle was frozen, cryosectioned and immunostained using antibodies for Dystrophin and Collagen IV to measure these proteins deposition. The other EDL muscle was incubated in collagenase for single fibres isolation and used to detect the satellite cell and myonuclei number. These fibres were incubated for 72 hours to monitor the satellite cell proliferation and differentiation. Antibodies applied on single fibres, against Pax7 and Myogenin, to detect the number, proliferative and differentiation program with counterstain of DAPI to visualise the myonuclei. Gastrocnemius muscle was used for qPCR works. Primers were used to detect the RNA expression for both Dystrophin and collagen

IV. The procedures and technique used in this chapter were explained in detail in the methods chapter.

The main observations of this chapter are, firstly, muscles from *Ercc1*$^{\Delta/-}$ treated mice overexpress level of both Dystrophin and collagen IV and are higher than both *Ercc1*$^{\Delta/-}$ and controls. The reduction in dystrophin thickness in *Ercc1*$^{\Delta/-}$ muscles were enhanced after sActRIIB treatment. Secondly, sActRIIB injection mitigates the reduction in satellite cell ability to proliferate and differentiate in *Ercc1*$^{\Delta/-}$; however, did not rescue the reduction in the number found in freshly isolated fibres. Finally, antagonise, the myostatin/activin signalling did not affect the myonuclei number in *Ercc1*$^{\Delta/-}$ mice.

6.2. The Activin ligand trap normalise extracellular component in *Ercc1*$^{\Delta/-}$ mice

We investigate the extracellular components since skeletal muscle force transmission relies on proteins that link the contractile apparatus to the extracellular matrix (ECM). We examined two of its components and determined how they were modified by the *Ercc1*$^{\Delta/-}$ genotype and after that by sActRIIB treatment. For that, we apply the fluorescence microscopy-based techniques to measure the dystrophin intensity and qPCR to quantify the RNA expression of dystrophin and collagen IV. Firstly, we examined the expression of Dystrophin, and we show that dystrophin RNA expression was decreased in the *Ercc1*$^{\Delta/-}$ muscle, which was subsequently increased to levels higher than controls by sActRIIB (Figure 6.1.A). We measured the amount of Dystrophin located between fibres expressing MHCIIb and also between fibres not express MHCIIb using quantitative immuno-fluorescence and confirmed its reduction in the *Ercc1*$^{\Delta/-}$ muscle compared to controls and was significantly increased by sActRIIB in both sites (Figure 6.1.B and D). After that we examined the expression of Collagen IV as basement membrane component important for force transmission. We found that collagen IV expression was slightly decreased albeit not reaching statistical significance in *Ercc1*$^{\Delta/-}$ muscle (Figure 6.1.C). However, sActRIIB caused its level to increase over both untreated *Ercc1*$^{\Delta/-}$ and control levels (Figure 6.1.C). Collagen IV gene expression levels were reflected at the protein level at the myofibre surface (Figure 6.1.E).

Overall the antagonise myostatin/activin in *Ercc1*$^{\Delta/-}$ mice enhance the level of ECM component the essential parts in the myofibre for both contractile apparatus and stem cell milieu.

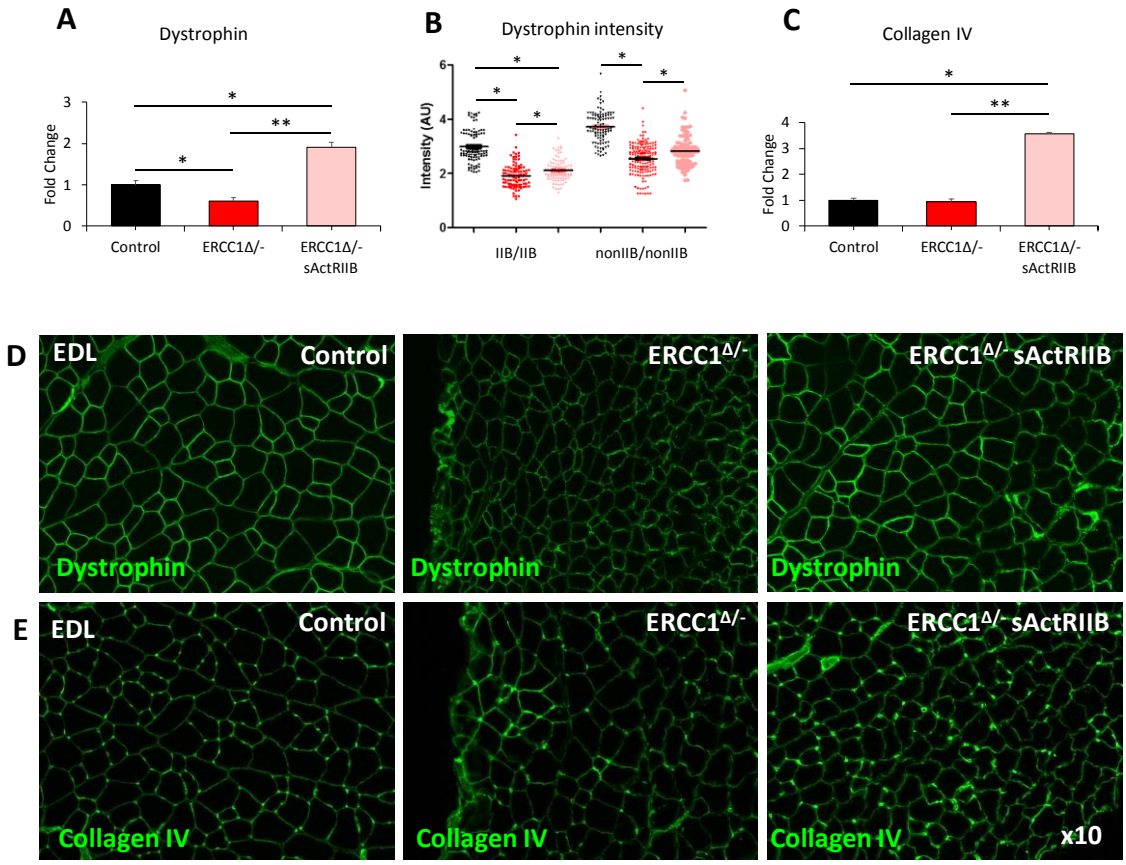

Figure 6.1. Normalisation of *Ercc1*$^{\Delta/-}$ extracellular components by sActRIIB.

(A) *Dystrophin* gene expression measured by qPCR. (B) Measure of Dystrophin in fibre-type-specific manner using quantitative immunofluorescence. (C) Measure of *Collagen IV* expression profiling by qPCR. (D) Representative immunofluorescence image for Dystrophin expression in EDL muscle. (E) Representative immunofluorescence image for Collagen IV expression in EDL muscle. The sActRIIB were IP injected starting from week 7 of age to week 15. A total of 100 measurements were done on EDL muscle sections to measure the thickness of both ECM proteins in all 3 cohorts. All mice were at the same age, n=7 for all cohorts. Non-parametric Kruskal-Wallis test followed by the Dunn's multiple comparisons used. *p<0.05, **p<0.01.

6.3. sActRIIB treatment enhance satellite cell proliferation in *Ercc1*$^{\Delta/-}$ mice.

We showed the antagonise of myostatin/activin in *Ercc1*$^{\Delta/-}$ mice enhance the level of ECM component the essential parts in the myofibre for both contractile apparatus and stem cell milieu. To investigate the effect of ECM modulation by sActRIIB injection on stem cells, we examined features of individual myofibres. A study by Day et al. showed a decrease in the number of satellite cells with ageing (Day et al., 2010). We found the similar result; we show that the number of satellite cells in the freshly isolated fibres (T0) from the EDL from either PBS- or sActRIIB-treated *Ercc1*$^{\Delta/-}$ mutants were significantly lower than the satellite cells number in control mice (Figure 6.2.A). On top of the decline in satellite cell number, it was reported that there is a reduction in proliferative capacity with ageing in wild type mice (Parker, 2015). Here we investigated the proliferative capacity of the satellite cells from the three cohorts and found that after 24 hours, there was no change in satellite cells number in all three cohorts examined (Figure 6.2.B). The cluster of satellite cell per fibres also significantly less in *Ercc1*$^{\Delta/-}$ mice and was not affected by sActRIIB treatment (Figure 6.2.E). The number of satellite cell after 48 hours of incubation proliferated from 4 cells per fibres in control at 24 hours culture to 9.5 cells per fibres, however, in both *Ercc1*$^{\Delta/-}$ treated and non-treated were increase by one cell each compared to 24 hours cultures (Figure 6.2.C). Cluster per cell also increase in control after 48 hours incubation from 4 clusters per fibres in control at 24 hours culture to 6.5 cells per fibres, however, in both *Ercc1*$^{\Delta/-}$ treated and non-treated were increased by one cluster each compared to 24 hours cultures (Figure 6.2.F). After 72 hours of culture, the population from control fibres had undergone a 3-fold increase compared to original numbers (Figure 6.2.D) and cluster increase by about one-fold (Figure 6.2.G). In sharp contrast, the satellite cells from PBS-treated *Ercc1*$^{\Delta/-}$ mice failed to undergo any significant proliferation as cell or cluster. Importantly, sActRIIB treatment of *Ercc1*$^{\Delta/-}$ mice resulted in satellite cells being able to undergo a 2.3-fold increase in a cell per fibre number and increase in the cluster by 1.5 clusters (Figure 6.2.D and G). We then count the ability of a single satellite cell to proliferate and make a nest of cells, so we count a cell per each cluster. As we count the cells per cluster at T24, all cohorts start with one cell per cluster and increase by about 0.5 cells in T48 (Figure 6.2.H and I). At 72 culture, control increase by 1-fold compared to T24, and the treated *Ercc1*$^{\Delta/-}$ have more cell per cluster; however, not significant increase (Figure 6.2.J).

Therefore, sActRIIB treatment mitigates abnormalities in satellite cell proliferation in *Ercc1*$^{\Delta/-}$ animals. However, it did not normalise the low satellite cell number found in mock-treated *Ercc1*$^{\Delta/-}$ mice.

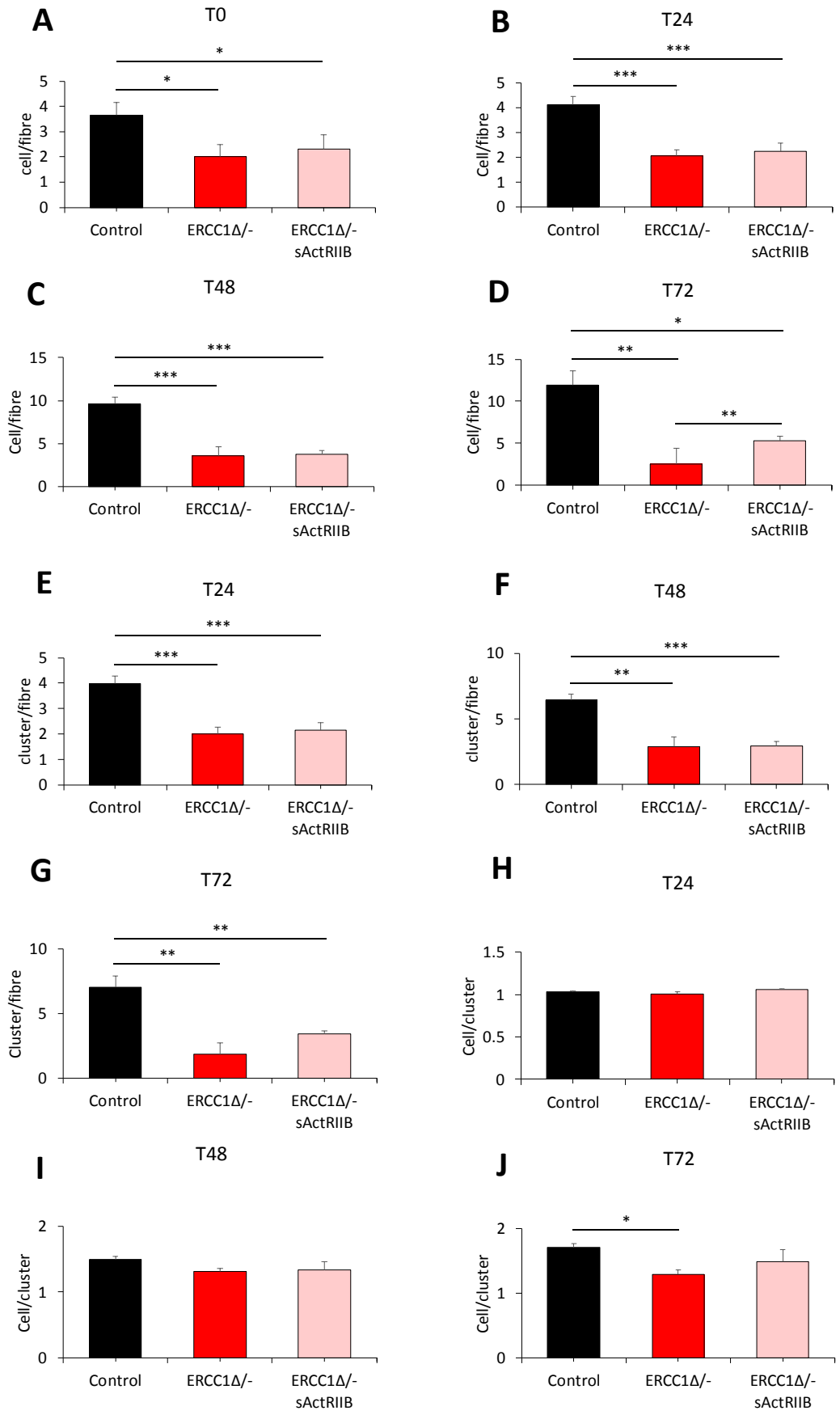
A
T0
cell/fibre
B
T24
Cell/fibre
C
T48
Cell/fibre
D
T72
Cell/fibre
E
T24
cluster/fibre
F
T48
cluster/fibre
G
T72
Cluster/fibre
H
T24
Cell/cluster
I
T48
Cell/cluster
J
T72
Cell/cluster
Control
ERCC1Δ/-
ERCC1Δ/-
sActRIIB

Figure 6.2. Increase satellite cell proliferation in *Ercc1*$^{\Delta/-}$ mice in response to sActRIIB treatment
Quantification of satellite cells on (A) freshly isolated EDL fibres, (B) after 24hr culture, (C) after 48hr culture and (D) after 72hr culture. Quantification of cluster on EDL fibres after (E) 24hr culture, (F) 48hr culture and (G) 72hr culture. Quantification of cell per cluster on EDL fibres after (H) 24hr culture, (I) 48hr culture and (J) 72hr culture. Fibres collected from 3 mice from each cohort and minimum of 25 fibres examined. The sActRIIB were IP injected starting from week 7 of age to week 15. All mice were at the same age. one-way ANOVA followed by Bonferroni's multiple comparison tests was used, *p<0.05, **p<0.01, ***p<0.001.

6.4. The normalisation of satellite cells differentiation and self-renewal in *Ercc1*$^{\Delta/-}$ mice by sActRIIB.

In the previous results, we showed an improvement in satellite cell proliferation in *Ercc1*$^{\Delta/-}$ animals after sActRIIB treatment. Here we examined features of a satellite cell in term of differentiation on individual myofibres to determine the effect of sActRIIB treatment. As a satellite cell differentiates, it downregulates Pax7 and upregulates Myogenin (Zammit et al., 2006). We count the differentiated ($Pax7^-$/$Myogenin^+$) versus quiescent ($Pax7^+$/$Myogenin^-$) after 72h in culture from control, *Ercc1*$^{\Delta/-}$ and *Ercc1*$^{\Delta/-}$ treated. We found that the attenuated differentiation programme of satellite cells from *Ercc1*$^{\Delta/-}$ mice were normalised by sActRIIB treatment (Figure 6.3. A-B).

Overall, sActRIIB treatment mitigates abnormalities in satellite cell differentiation and self-renewal programmes in *Ercc1*$^{\Delta/-}$ animals.

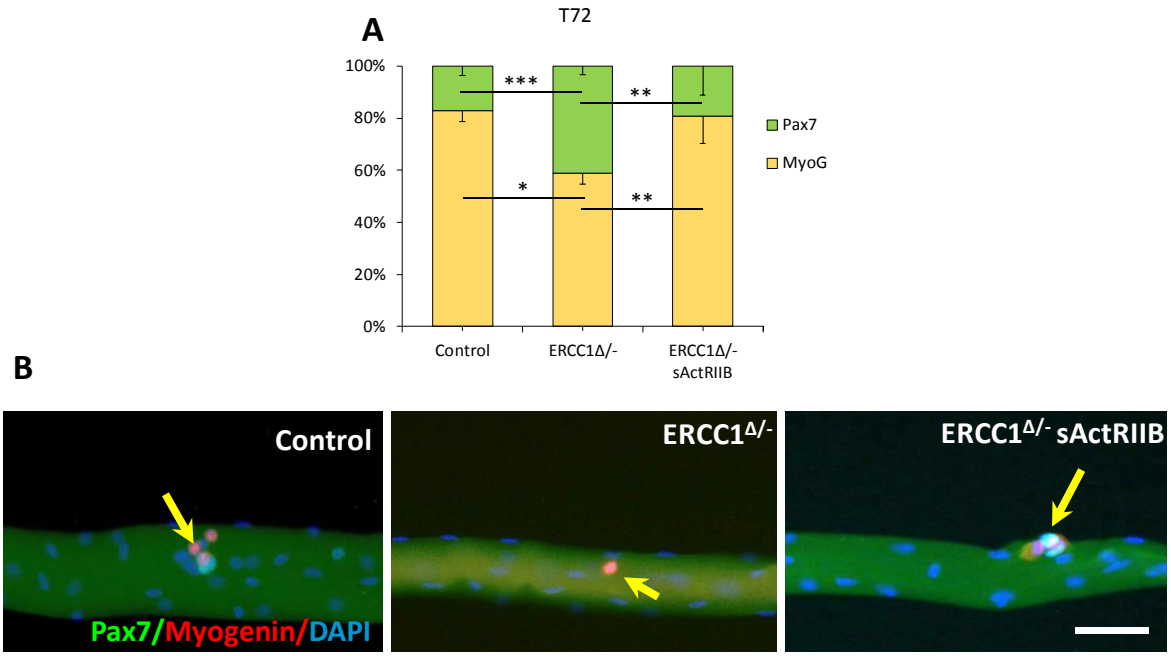

Figure 6.3. Normalisation of *Ercc1*$^{\Delta/-}$ differentiation and self-renewal of its satellite cells by sActRIIB.

(A) Quantification of EDL differentiated (Pax7^{-}/Myogenin^{+}) versus quiescence (Pax7^{+}/Myogenin^{-}) after 72h in culture. Fibres collected from 3 mice from each cohort and minimum of 25 fibres examined. (B) Representative images of control, mock-treated *Ercc1*$^{\Delta/-}$ and sActRIIB-treated *Ercc1*$^{\Delta/-}$ fibre examined at 72h for expression of Myogenin (red) and Pax7 (green). Arrows indicated satellite cell progeny. Fibres collected from 3 mice from each cohort and minimum of 25 fibres examined. The sActRIIB were IP injected starting from week 7 of age to week 15. Scale 50µm. All mice were at the same age. one-way ANOVA followed by Bonferroni's multiple comparison tests was used, *p<0.05, **p<0.01, ***p<0.001

6.5. Antagonise myostatin/activin signalling did not affect the myonuclei number in *Ercc1*$^{\Delta/-}$ mice.

We showed that introduction sActRIIB to *Ercc1*$^{\Delta/-}$ had not changed the satellite cells number; however, it enhances both proliferation and differentiation in stem cell from fibres of EDL muscle. We examined features of individual myofibres to determine the effect of sActRIIB treatment on the number of myonuclei in the fibres from the EDL muscle from control, PBS- and sActRIIB-treated *Ercc1*$^{\Delta/-}$ mutants. A study by Kadi et al. reports that the myonuclei number was lower in old age compared to young in both male and female (Kadi et al., 2004). Another study shows that the myonuclei number did not change in the absence of myostatin, although the fibre size was increased (Qaisar et al., 2012). We found that antagonising of myostatin/activin signalling by sActRIIB did not increase myonuclei in *Ercc1*$^{\Delta/-}$ that was already significantly lower than the number in control mice (Figure 6.4.A-B).

Overall, we show that the sActRIIB treatment enhances both ECM component and satellite cells proliferation and differentiation, however, did not affect the myonuclei number in *Ercc1*$^{\Delta/-}$ progeric mice.

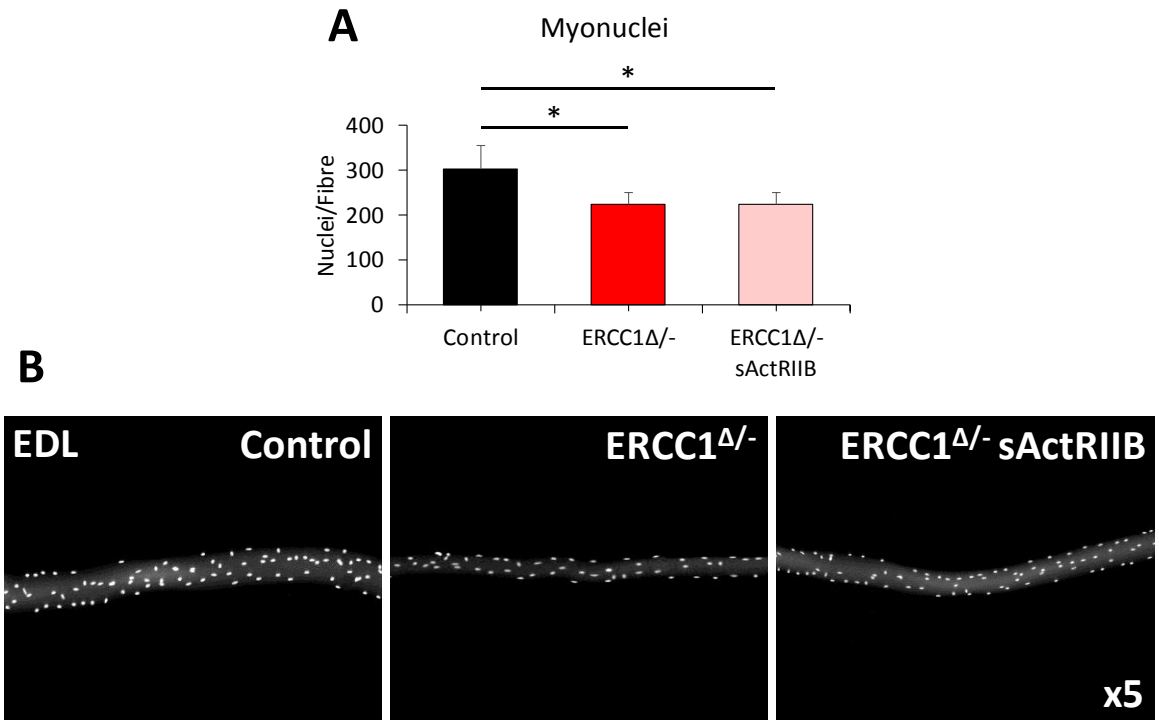

Figure 6.4. Antagonise myostatin/activin signaling did not affect the myonuclie number in *Ercc1*$^{\Delta/-}$ mice.

(A) EDL myonuclei count. (B) Representative single fibres with myonuclie stained with DAPI for control, *Ercc1*$^{\Delta/-}$ and *Ercc1*$^{\Delta/-}$ sActRIIB treated mice. Fibres collected from 3 mice from each cohort and minimum of 25 fibres examined. The sActRIIB were IP injected starting from week 7 of age to week 15. All mice were at the same age, one-way ANOVA followed by Bonferroni's multiple comparison tests was used. *p<0.05.

6.6. Discussion

Loss of muscle mass and function with ageing, sarcopenia (Rosenberg, 1997), is accompanied by a change in ECM. Indeed, the degeneration/regeneration proses in skeletal muscle of both dystrophic and aged mice results in alter the ECM composition and architecture (Kragstrup et al., 2011, Marshall et al., 1989). Furthermore, age-related reduction in force generation ability of skeletal muscle was linked to increasing myofibres stiffness via changes in ECM proteins properties (Haus et al., 1985, Kragstrup et al., 2011, Wood et al., 1985). ECM changes have a direct effect on resident stem cell as the ECM is considered as a niche for satellite cells (Thomas et al., 2015). Consequently, the reduction in satellite cell activity affects the muscle fibre ability to regenerate after injury and damage.

The key finding of this part was the antagonise myostatin/activin signalling have both ECM and satellite cell benefits. However, we show that treatment with sActRIIB did not affect the myonuclei number. We show enhancement in the deposition of dystrophin in treated mice and upregulate RNA expression of both dystrophin and collagen IV. Satellite cell proliferation and self-renewal activity were also enhancing in *Ercc1*$^{\Delta/-}$ treated mice.

Changes in ECM accompany ageing and associated with reducing strength and mechanical properties in skeletal muscle (Kragstrup et al., 2011). A study on ECM in ageing has reported changes in its deposition. Specifically, the concentration of collagen IV was increase with age (Kovanen et al., 1988). Another study reports the age-related reduction in overall gene expression of ECM protein compartments (Pattison et al., 2003). It could be concluded that the thickness of some ECM, i.e. Collagen IV, in ageing is maybe due to the accumulation of this protein over time and reduce the degradation process rather than increase expression. Maintaining a standard ECM component is dependent on the activity of matrix metalloprotease that degrades ECM proteins (Chen and Li, 2009). Indeed the expression of MMP was reported to decrease in samples taken from the elderly compared to young (Wessner et al., 2019). As evidence, Mdx mice, a model of Duchenne muscular dystrophy have a defect in ECM component, were enhanced in term dystrophic characteristic and muscle growth after myostatin antagonise (Matsakas et al., 2009, Bogdanovich et al., 2005). We show an increase in the expression by about 3.5-fold in collagen IV expression in *Ercc1*$^{\Delta/-}$ treated with sActRIIB. We suggest this increase was a compensatory mechanism because we show there was an increase in fibres damage from the progeric group and

normalise after sActRIIB treatment (see Figure 5.7. A-B). We then investigated a member of Dystrophin-glycoprotein complex (DGC), dystrophin, a critical intercellular component that links the cytoskeleton to the ECM (Hoffman et al., 1987, Ervasti and Campbell, 1993). A previous study showed that despite the two-fold increase in mRNA expression of dystrophin, there was a loss of protein with ageing (Hughes et al., 2017). We have seen the similar trend of protein intensity in our progeric mice compared to controls and the sActRIIB treated to increase the intensity in *Ercc1*$^{\Delta/-}$ mice. The RNA expression was less in *Ercc1*$^{\Delta/-}$ and increase even more the controls after sActRIIB treatment.

Satellite cells mediate skeletal muscle repair and regeneration and are located in ECM under the basal lamina (Mauro, 1961, Zammit et al., 2006). As a resident cell in ECM of myofibres, satellite cells would be affected by the changes in this compartment of skeletal muscle fibres. Indeed, satellite cell could be affected by general ageing prosses and by the effect of a change in ECM composition. Satellite cell number has been reported to decrease in number with age (Gibson and Schultz, 1983); however, it does not reflect on its ability to proliferation (Adams, 2006, Schafer et al., 2006). A study by Sadeh shows the effect of age on regeneration ability of satellite cell, where after injection of TA muscle with a myotoxic agent, 3-month-old mice muscle regained their healthy structure but not the two years old mice (Sadeh, 1988). We show a lower number of a satellite cell in *Ercc1*$^{\Delta/-}$ compared to controls. Indeed, the change in satellite cells niche, i.e. ECM, reflect negatively on satellite cell ability to regeneration and repair rather than the number of cells (Hikida, 2011). We show that enhancement in ECM after sActRIIB injection reflects positively on satellite cell ability to proliferate, differentiate and self-renewing. It could be concluded there is a direct effect for injection of sActRIIB since some studies show that the myostatin regulates the activity of satellite cell by upregulation of molecules involve in quiescence status of satellite cells (Thomas et al., 2000, Joulia et al., 2003).

Skeletal muscle fibres are a multinucleated cell and adding new myonuclei achieved by recruiting differentiated satellite cell (Pallafacchina et al., 2013). A study by Kadi reports the decrease in satellite cells in both men and women in old aged compared to young did not affect the myonuclei number on contrary it increased with age (Kadi et al., 2004). However, another study suggests an increase in nucleocytoplasmic ratio due to reducing muscle fibres not to increase myonuclei number, as the myonuclei number did not changes (Manta et al., 1987). Indeed, the aged muscle fibres reach maximum size at a young age by

recruiting new myonuclei over time and then reduced in size with ageing but keep the most of myonuclei. What we show here is different, myonuclei number was not changed after sActRIIB even with enhanced the ability of satellite cell to proliferate an differentiate. The injection of sActRIIB was before the onset of ageing signs in *Ercc1*$^{\Delta/-}$ mice, so it has a protective rather than damage reverse effects. sActRIIB maintains the healthy status of fibres with less injury, and that could be interpreted as to why we did not see any increase in myonuclei in *Ercc1*$^{\Delta/-}$ mice after treatment.

Chapter 7 Results

The effect of antagonising myostatin/activin signalling on *Ercc1*$^{+/+}$ mice

7.1. Introduction

Myostatin is a member of transforming growth factor-β (TGF-β) family and consider a negative regulator of skeletal muscle growth (McPherron et al., 1997). Naturally occur deletion of myostatin gene lead to double muscling phenotype in a cattle species such as Belgium blue and Piedmontese cattle breeds (Kambadur et al., 1997). The same hypertrophic phenotype was reported in a child with natural deletion of myostatin gen with a remarkable increase in muscle strength (Schuelke et al., 2004). However, experimentally deletion of the myostatin gene in a wild type background mouse lead to increase muscle mass but impair muscle force generation (Amthor et al., 2007). Inactivation of myostatin in an animal model with skeletal muscle dystrophy exabit positive effect on disease progression. For example, blocking myostatin signalling by IP injection of anti-myostatin antibody was able to increase muscle mass and strength and reduce muscle degeneration in the mdx mouse model of Duchenne muscular dystrophy (DMD) (Bogdanovich et al., 2002).

The evidence from naturally occurs, and experimentally deletion has been suggested myostatin antagonist as a pharmacological approach in muscular dystrophy. Indeed, there were many trial versions of myostatin intervention and number of it still in on-going development. The first trial of antagonising myostatin was in 2004 by Wyeth company, MYO-029, a myostatin antibody for the muscular dystrophies in subjects with Becker muscular dystrophy, facioscapulohumeral muscular dystrophy, or Limb-girdle muscular dystrophy. This trail has been discontinued development because it failed to increase muscle strength in these subjects. The first pharmaceutical product of a soluble form of ActRIIB was in 2010 by Acceleron under the name of ACE-031. It was developed for muscular dystrophy subjects but stop developed due to safety issue related to nose and gum bleeding. The same company then develop another version of ligand trap, ACE-083, did not bind BMP9/10 and with no bleeding issue, however still in on-going development (Saitoh et al., 2017b).

Considering previous study and trial version of myostatin antagonism, we use the sActRIIB to rescue muscle mass loss in progeric mice. In previous chapters, we show that the IP injection of sActRIIB for eight weeks was able to increase muscle mass and enhance muscle and organism activity in *Ercc1*$^{\Delta/-}$ mice compared to non-traded mice. Here we use sActRIIB

in *Ercc1*$^{+/+}$ group to investigate its effect on the healthy subject and whether it shows the similar phenotype that was previously described. However, the control group used in this study was inbred from a mixed background. The inbred animals provide lower genetic variability and remarkable homogeneous models compared to outbred, highly variable, populations (Casellas, 2011). Both the control and disease model in this study was a sibling and had FVB/C57Bl6 F1 hybrid genetic background. A previous study shows that the uniform background of these inbred mice, *Ercc1*$^{+/+}$, was normal (Dollé et al., 2011).

Here we investigated, to our knowledge for the first time the effect of antagonising of myostatin/activin signalling by injection sActRIIB in *Ercc1*$^{+/+}$ mice. Two cohorts of male mice (*Ercc1*$^{+/+}$ mock and sActRIIB treated mice) used in this part of the study were bred, housed under standard environmental conditions and provided food and water ad libitum in the Biological Resource Unit, University of Reading. The procedures and technique used in this chapter were explained in detail in the methods chapter.

The main finding of this section was that antagonising of myostatin/activin signalling in *Ercc1*$^{+/+}$ mice significantly increase the body and muscle mass. Muscle mass was achieved by increase fibres size rather than fibre number. Increase in skeletal muscle mass was not associated with an increase in satellite cells number and activity. sActRIIB was able to change the skeletal muscle fibres profile as we showed there was a shifting in MHCs from slow to fast and metabolic status toward glycolytic phenotype. The changes in mass and profile affected the force generation in *Ercc1*$^{+/+}$ treated mice; it was reduced in treated mice compared to non-treated mice. However, the assessment of grip strength and motor coordination reveal no change in this parameter related to sActRIIB treatment.

7.2. The effect of antagonises myostatin/activin signalling on body weight and skeletal muscle mass in an *Ercc1*$^{+/+}$ mice.

The effect of injection sActRIIB on body weight in the control group was recorded through the eight weeks of the experiment. Male *Ercc1*$^{+/+}$ mice were IP-injected twice a week with sActRIIB from 7-weeks of age till week 16. As shown previously by Relizani et al. that sActRIIB was able to increase body weight in wild type mice significantly in less than 4 weeks (Relizani et al., 2014), we show here a progressive increase in body weight in sActRIIB treated mice and the difference compared to mock treated mice was started as early as two weeks after injection (Figure 7.1. A). At the end of the experiment, there was a significant increase in body weight in treated mice (Figure 7.1. B).

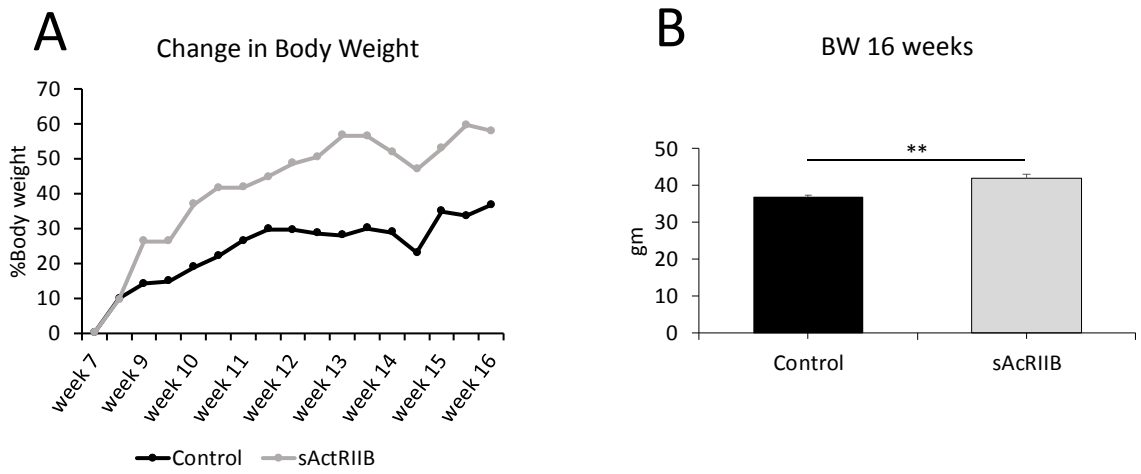

Figure 7.1. sActRIIB treatment increase body weight in *Ercc1*$^{+/+}$ group.

(A) Relative changes in body mass over time. (B) Body weight in control and sActRIIB treated group at 16 weeks old. The sActRIIB were IP injected starting from week 7 of age to week 16. All mice were at the same age, n= 6 male mice *Ercc1*$^{+/+}$ and n=4 *Ercc1*$^{+/+}$ sActRIIB. Student's t-test, **p<0.01.

Hindlimb muscles weight was taken directly after dissection. Five muscle group were weighed (including EDL, TA, Gastrocnemius, Soleus, and Plantaris). The number of studies has shown that a lack of myostatin results in a general increase in skeletal muscle mass (Amthor et al., 2007, McPherron and Lee, 1997). We showed here that muscle from sActRIIB injected mice was heavier than non-treated mice. The increase was 28%, 38.4%, 40%, 34.4%, 48.4% in muscle from sActRIIB treated mice compared to non-treated in EDL, TA, Gastrocnemius, Soleus, and Plantaris respectively (Figure 7.2. A-E). Muscle weight was normalised to tibia length to consider the variance in growth and body mass. Even after normalisation, the muscle from sActRIIB treated mice still heavier than non-treated mice, albeit some of the muscle weight lost the statistical significance (Figure 7.3. A-E).

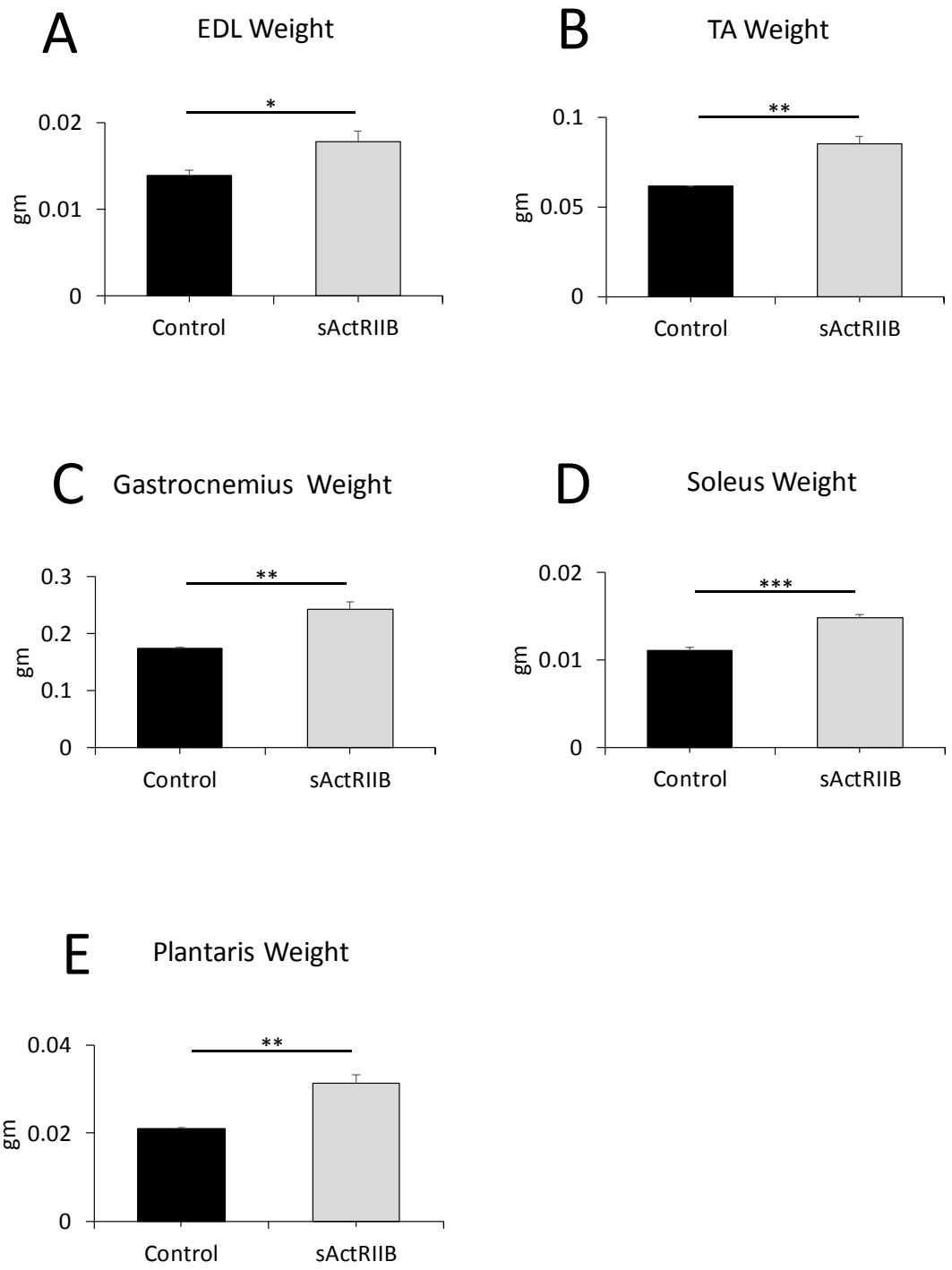

Figure 7.2. *Ercc1*$^{+/+}$ sActRIIB treated hind limb skeletal muscles show increase in weight compared to control group.

Muscle weight of 16-week old male non-treated and treated *Ercc1*$^{+/+}$ mice. (A) EDL, (B) TA, (C) Gastrocnemius, (D) Soleus and (E) Plantaris. The sActRIIB were IP injected starting from week 7 of age to week 16. All mice were at the same age, n= 6 male mice *Ercc1*$^{+/+}$ and n=4 *Ercc1*$^{+/+}$ sActRIIB. Student's t-test, *p<0.05, **p<0.01, ***p<0.001.

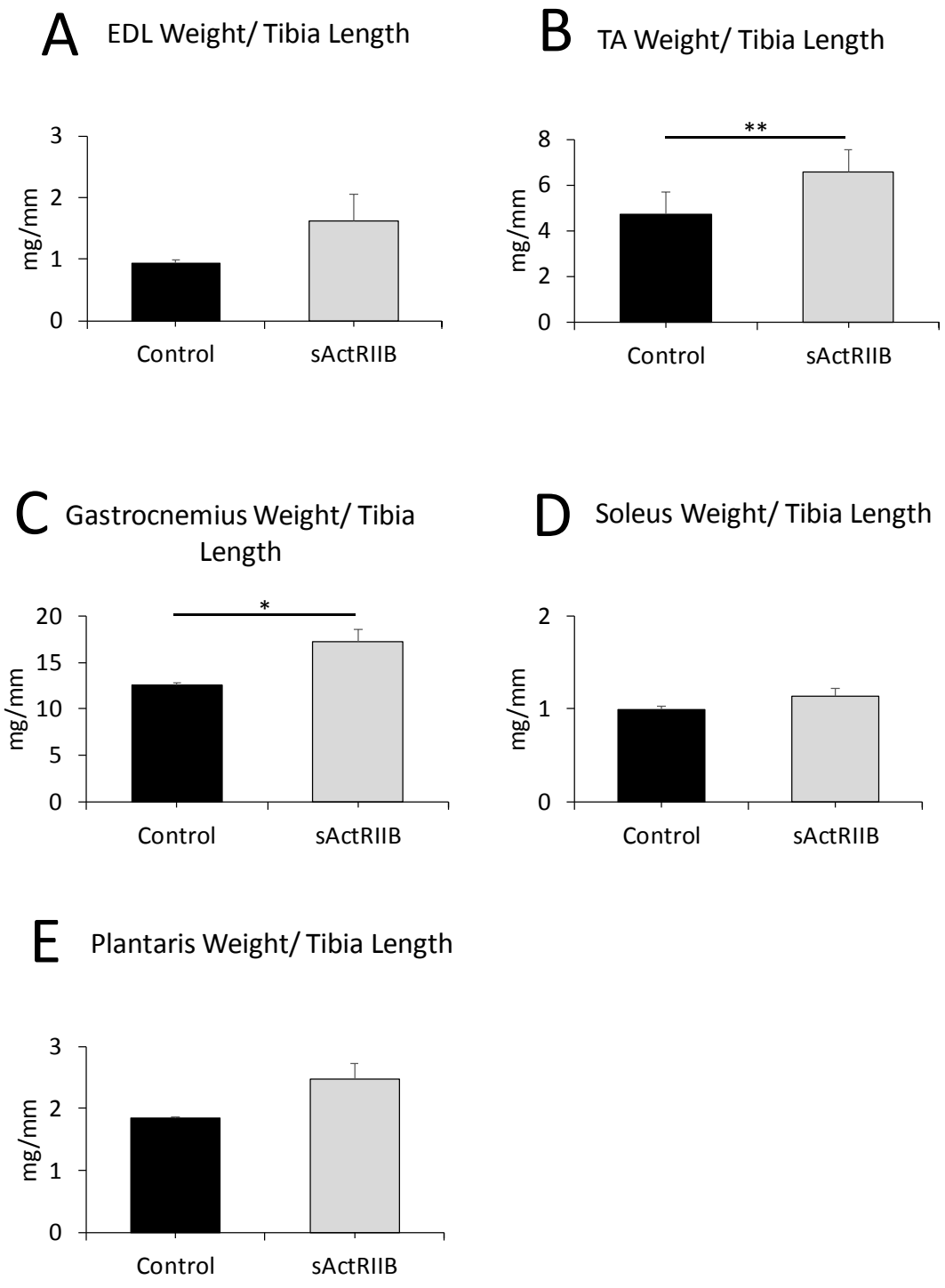

Figure 7.3. Hind limb skeletal muscle weight of *Ercc1*$^{+/+}$ mice non-treated and treated normalise to tibia length.

Normalized muscle weight to tibia length of 16-week old male *Ercc1*$^{+/+}$ non-treated and treated with sActRIIB mice. (A) EDL, (B) TA, (C) Gastrocnemius, (D) Soleus and (E) Plantaris. The sActRIIB were IP injected starting from week 7 of age to week 16. All mice were at the same age, n= 6 male mice *Ercc1*$^{+/+}$ and n=4 *Ercc1*$^{+/+}$ sActRIIB. Student's t-test, *p<0.05, **p<0.01.

7.3. The effect of sActRIIB injection on the fibres size and fibres number in an *Ercc1*$^{+/+}$ mice.

We demonstrated that antagonising myostatin/activin signalling induced muscle growth in *Ercc1*$^{+/+}$ mice. The increase in muscle size has been reported; it is due mainly to individual muscle fibre hypertrophy (Amthor et al., 2007). However, other studies showed that the increase in muscle mass in myostatin null mice was due to both increases in the fibre size and number (Matsakas et al., 2009, McPherron et al., 2009). Here we investigate whether the increase in muscle mass in *Ercc1*$^{+/+}$ after sActRIIB treatment was due to hyperplasia or hypertrophy or both. We found that the number of fibre was increased by 19.5% and 20% in sActRIIB treated EDL and Soleus muscle, respectively, albeit not reach a statistically significant (Figure 7.4. A-B).

Then we investigate the other parameter to gauge the muscle growth, the size of the fibre. We found that the cross-sectional area was increased in sActRIIB treated mice independently of MHCs from hind limb muscle, EDL, Soleus and TA. All muscle fibres type, MHCI, IIa, IIx and IIb, was larger in sActRIIB treated mice in all examined muscle, except the MHCIIx fibres in EDL was not changed (Figure 7.5. A-D).

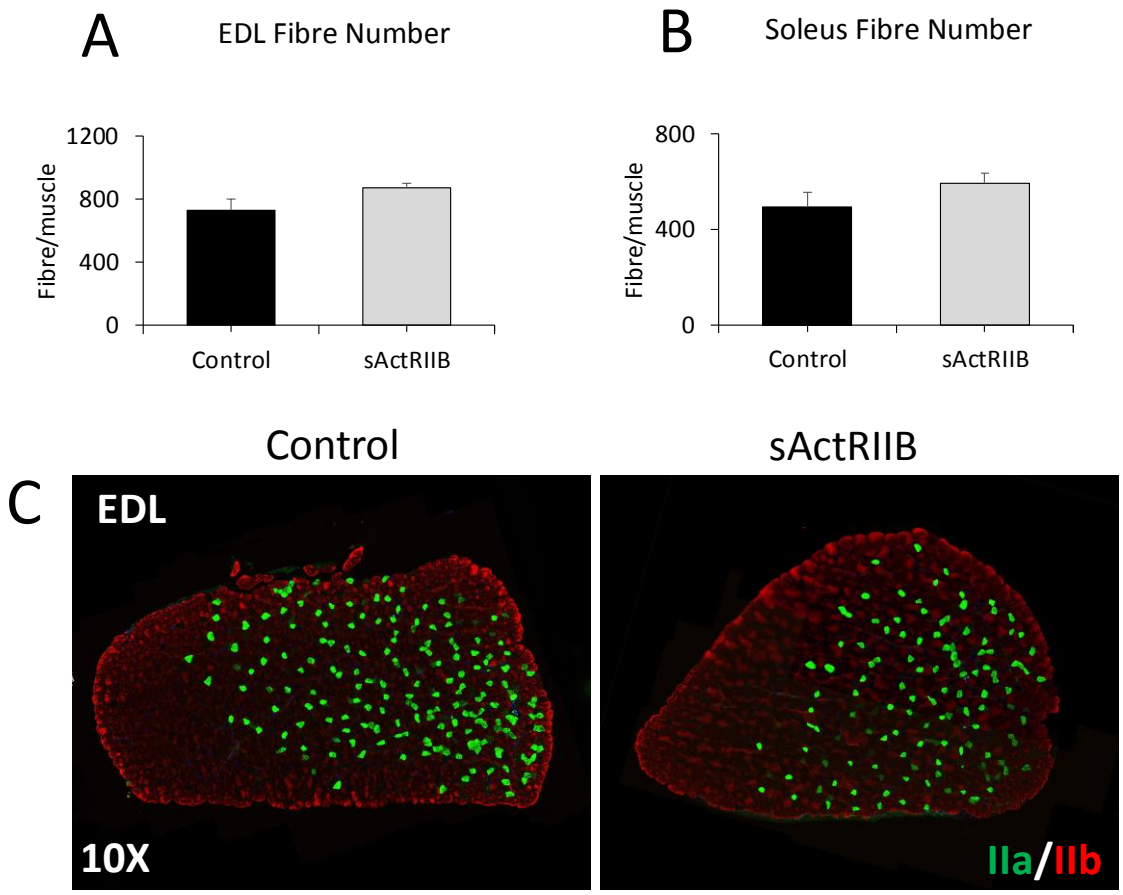

Figure 7.4. sActRIIB injection has no significant effect on fibres number in *Ercc1*$^{+/+}$ group.

Muscle fibres count in (A) EDL and (B) soleus. (C) Representative images of EDL muscle immunostained against MHC proteins, IIa (green) and IIb (red) from control and sActRIIB treated mice. Whole muscle sections were counted for EDL and soleus muscles in both cohorts. All animals were 16 weeks old at the time of dissection from both cohorts. The sActRIIB were IP injected starting from week 7 of age to week 16. n= 6 male mice *Ercc1*$^{+/+}$ and n=4 *Ercc1*$^{+/+}$ sActRIIB. Student's t-test.

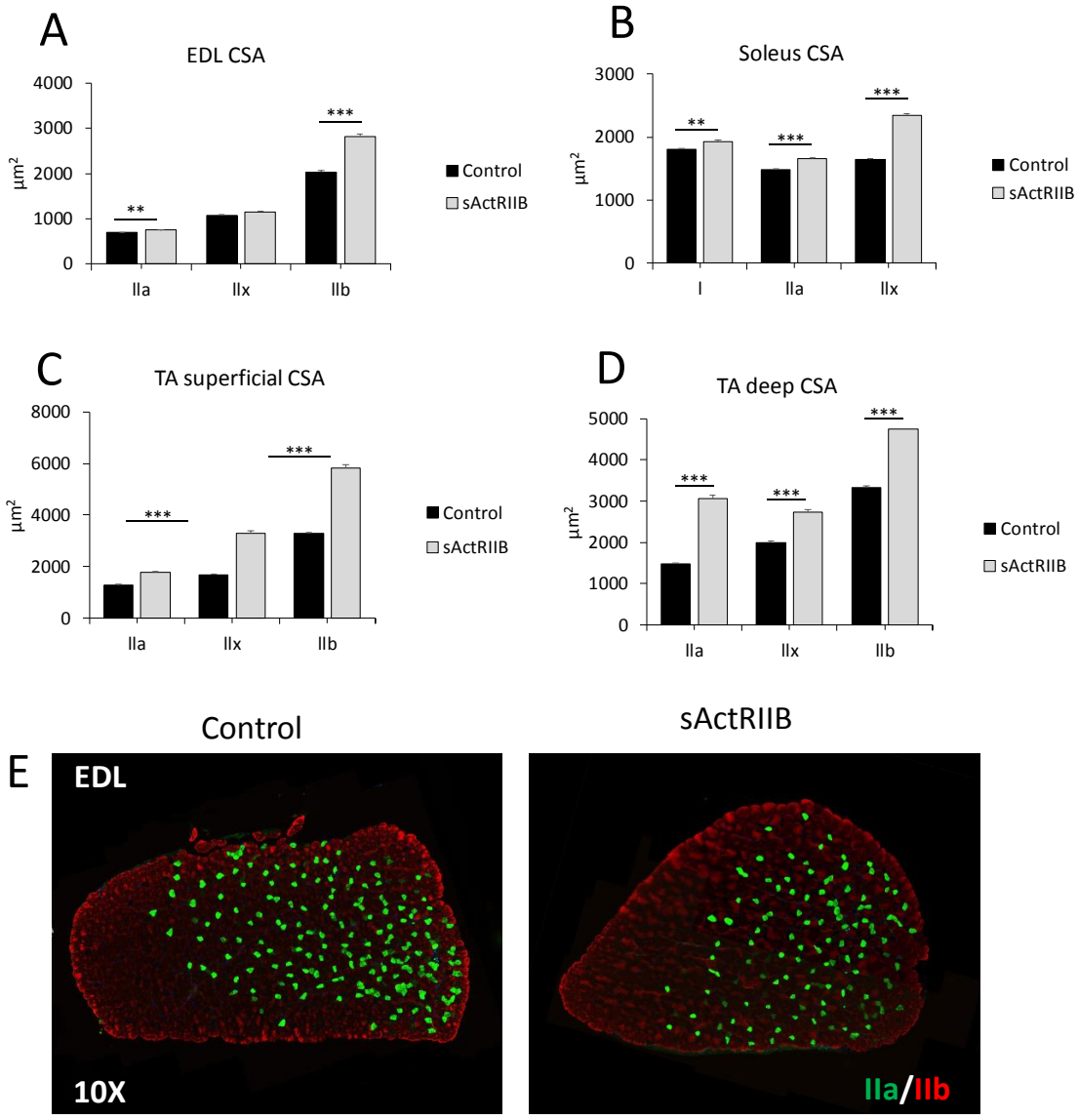

Figure 7.5. myofibres of hind limb muscle from *Ercc1*$^{+/+}$ treated with sActRIIB mice show larger CSA than their counterpart myofibres from non-treated mice.

Skeletal muscle fibre CSA of type I, IIa, IIx and IIb in (A) EDL, (B) soleus and the (C) deep and (D) superficial regions of the TA in relation of MHCs isoform expression. (E) Representative images of EDL muscle immunostained against MHC proteins, IIa (green) and IIb (red) from control and sActRIIB treated mice. Whole muscle sections were counted for EDL and soleus muscles, and 100 fibres were analysed for TA in superficial and deep regions in both cohorts. All animals were 16 weeks old at the time of dissection from both cohorts. The sActRIIB were IP injected starting from week 7 of age to week 16. n= 6 male mice *Ercc1*$^{+/+}$ and n=4 *Ercc1*$^{+/+}$ sActRIIB. Student's t-test, *p<0.05, **p<0.01, ***p<0.001.

7.4. Skeletal muscle fibres metabolic status and MHC profile in *Ercc1*$^{+/+}$mice after antagonising myostatin/activin signalling.

We showed that sActRIIB treatment is efficacious to increase muscle mass in *Ercc1*$^{+/+}$ mice. We speculate that it is necessary to identify whether antagonise myostatin/activin would impact muscle fibres profiling. It well established the ability of skeletal muscle fibre to undergo conversion between different fibre types in response to intrinsic and extrinsic factors. The conversion from the slow (type I and IIA) into fast (type IIX and IIB) phenotypes were reported in mice with myostatin deletion genotype (Girgenrath et al., 2005). Lack of myostatin not only affects the MHC profile but also induce shifting toward glycolytic profile. Amthor et al. have shown decrease the number of succinate dehydrogenase (SDH) positive fibres in mice lacking myostatin, as an indicator of glycolytic status (Amthor et al., 2007). We use an antibody against MHC type I, IIa, IIb to investigate the fibres profile and SDH stain for oxidative status in the muscles from *Ercc1*$^{+/+}$ sActRIIB treated mice. We showed there was an increase in the proportion of fibres express MHCIIb and reduction in fibres express MHCIIa in EDL muscle from *Ercc1*$^{+/+}$ mice compared to mock treated mice and there was no change in MHCIIx express fibres (Figure 7.6. A). The Soleus muscle from sActRIIB treated *Ercc1*$^{+/+}$ mice have a higher proportion of fast fibres MHCIIx compared to the mock-treated group, and less slow fibres MHCI, albeit not reach a significant difference. MHCIIa express fibres show no change between the two groups (Figure 7.6. B). Then we performed staining for the mitochondrion-associate enzyme succinate dehydrogenase (SDH) to investigate whether injection of sActRIIB for eight weeks able to change oxidative status in *Ercc1*$^{+/+}$ mice. We found a decrease in positively dark stained (high SDH activity) and an increase of the proportion of pale stained fibres (low SDH activity) in EDL muscle from sActRIIB treated *Ercc1*$^{+/+}$ mice compared to mock treated mice.

Overall, we agree with what shown before in mice lacking myostatin in term of fibres shifting toward fast profile and being more glycolytic.

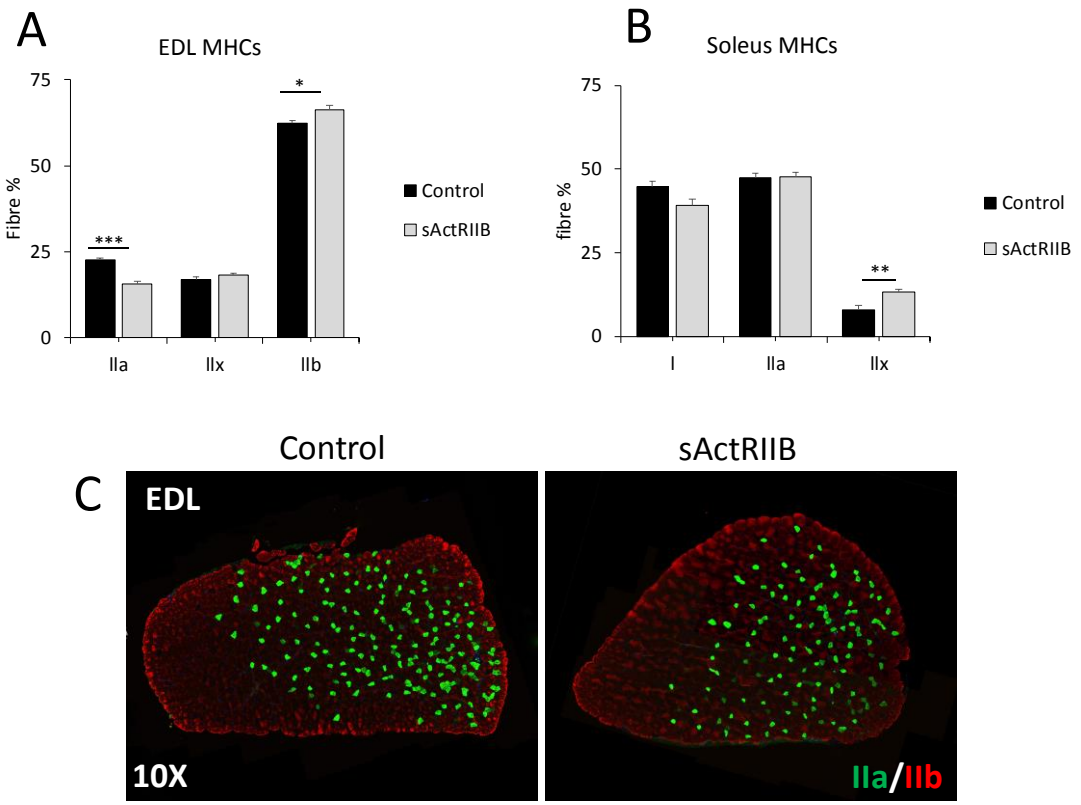

Figure 7.6. Myosin Heavy chain profiling of hind limb muscle affects by sActRIIB injection *Ercc1*$^{+/+}$ mice.

MHC isoform (type I, IIa, IIx and IIb) profile in (A) EDL and (B) Soleus from control and control treated mice. (C) Representative images of EDL muscle immunostained against MHC proteins, IIa (green) and IIb (red) from control and sActRIIB treated mice. Whole muscle sections were counted for EDL and soleus muscles in both cohorts. All animals were 16 weeks old at the time of dissection from both cohorts. The sActRIIB were IP injected starting from week 7 of age to week 16. n= 6 male mice *Ercc1*$^{+/+}$ and n=4 *Ercc1*$^{+/+}$ sActRIIB. Student's t-test, *p<0.05, **p<0.01, ***p<0.001.

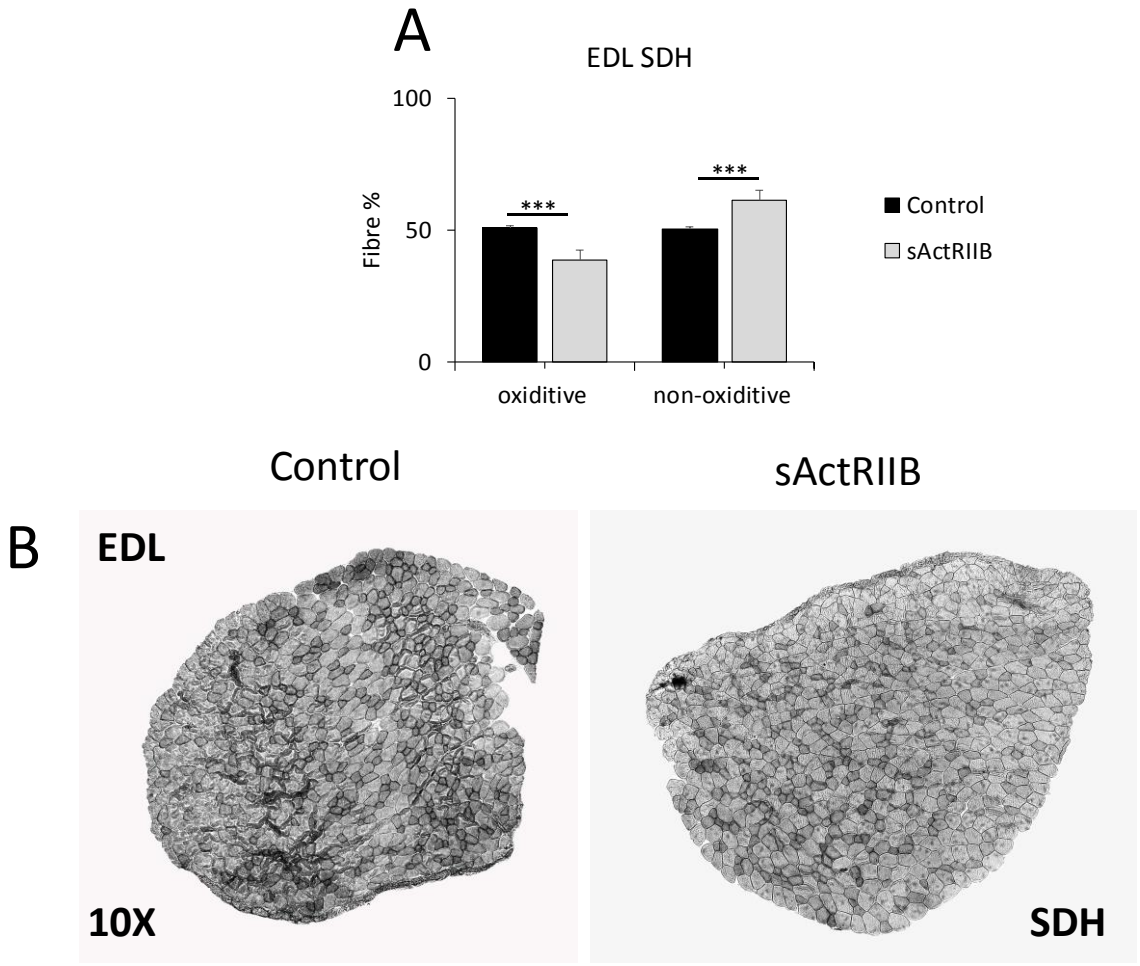

Figure 7.7. Myofibres from sActRIIB treated *Ercc1*$^{+/+}$ hind limb skeletal muscle was less oxidative than the non-treated group.

(A)Oxidative fibre number enumeration through histological SDH activity staining of the EDL muscle. (B) Representative images of succinate dehydrogenase activity in EDL muscle, dark stained fibres consider as oxidative and pale one as a non-oxidative. Whole muscle sections were counted for EDL muscles in both cohorts. All animals were 16 weeks old at the time of dissection from both cohorts. The sActRIIB were IP injected starting from week 7 of age to week 16. n= 6 male mice *Ercc1*$^{+/+}$ and n=4 *Ercc1*$^{+/+}$ sActRIIB. Student's t-test, ***p<0.001.

7.5. The effect of antagonises myostatin/activin on organismal activity and skeletal muscle strength in *Ercc1*$^{+/+}$ mice.

We demonstrated the efficiency of sActRIIB injection to increase skeletal muscle mass in *Ercc1*$^{+/+}$ mice. The increase in muscle mass was accompanied by a shift in MHC profile toward fast profile and concomitant glycolytic status. Here we examined the effect of sActRIIB treatment on *Ercc1*$^{+/+}$ mice organismal activity and skeletal muscle strength. Previous work has shown that myostatin deletion result in reduce muscle function (Matsakas et al., 2012). However, other study demonstrated no significant difference of forelimb gripping strength in Myostatin null mice compared to WT mice (Guo et al., 2016). In term of force generation, antagonise myostatin in the disease condition, mdx mice, lead to increase of muscle-specific force output (Wagner et al., 2002); however, myostatin deletion in WT background decreased muscle force generation (Amthor et al., 2007).

Behavioural and locomotor activity of mice from sActRIIB treated and non-treated *Ercc1*$^{+/+}$ mice were measured using an open field activity monitoring system. The total activity of animal was measured, and the *Ercc1*$^{+/+}$ treated mice were about 50% less than non-treated mice (Figure 7.8.A). sActRIIB treatment reduce muscle activity in *Ercc1*$^{+/+}$ mice (distance travel per hour 5.6m in untreated mice versus 3.4m in treated) (Figure 7.8.B). Total rearing counts and rearing time, measures of locomotor activity, exploration and anxiety, were less in treated mice, albeit not reach statistical difference (Figure 7.8.C-D).

To support the results from an open field system, we perform a rotarod test and measure the hind limb grip strength. Rotarod machine was used for motor activity and fatigue characterisation. Motor coordination, measured using the Rotarod, showed that sActRIIB did not affect this parameter in *Ercc1*$^{+/+}$ mice (Figure 7.9.A). *In vivo* assessment of forelimb muscle maximum force also was not affected by sActRIIB treatment in *Ercc1*$^{+/+}$ mice (Figure 7.9.B).

To endorse the data above, we investigated the ex vivo muscle tension measurement of one of hindlimb muscle, EDL, where both force generation and half relaxation time were measured. We found that the specific force was reduced in *Ercc1*$^{+/+}$ treated mice compared to non-treated (Figure 7.10.A). Furthermore, a reduction in half relaxation speed was resulted from treated *Ercc1*$^{\Delta/-}$ with sActRIIB (Figure 7.10.B).

This set of data show the effect of antagonising of myostatin/activin signalling in *Ercc1*$^{+/+}$ mice. Overall the injection of sActRIIB decreased mice activity and reduce force generation; however, some parameters such as rotarod and grip strength were not affected.

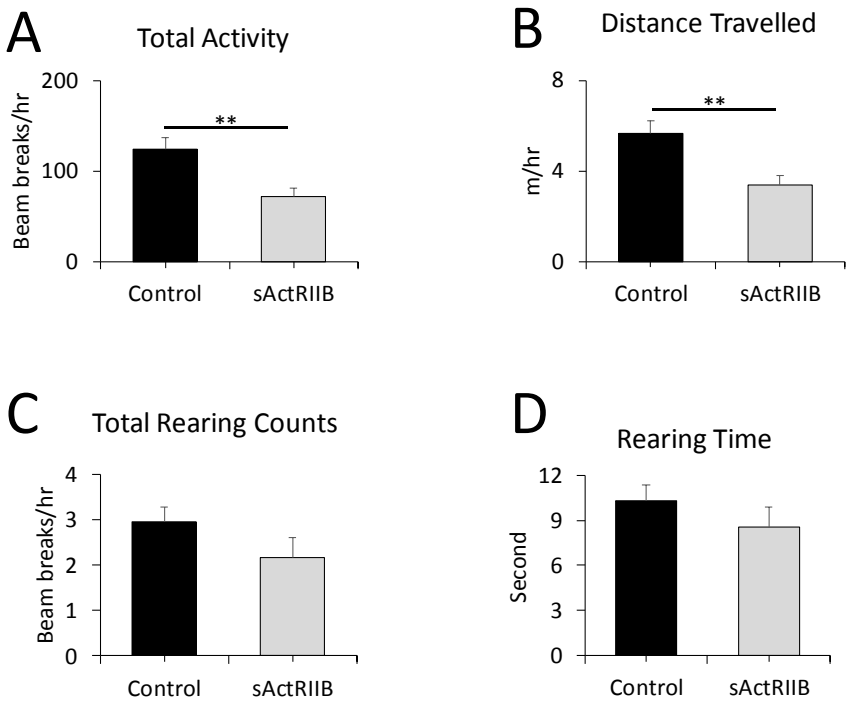

Figure 7.8. The effect of sActRIIB treatment on organismal activity in *Ercc1*$^{+/+}$ mice.
Organismal activity measurements, (A) total activity, (B) distance travelled (C) total rearing counts and (D) rearing time, through activity cages at the end of week. The sActRIIB were IP injected starting from week 7 of age to week 16. All mice were at the same age, 14. n= 6 male mice *Ercc1*$^{+/+}$ and n=4 *Ercc1*$^{+/+}$ sActRIIB. Student's t-test, **p<0.01.

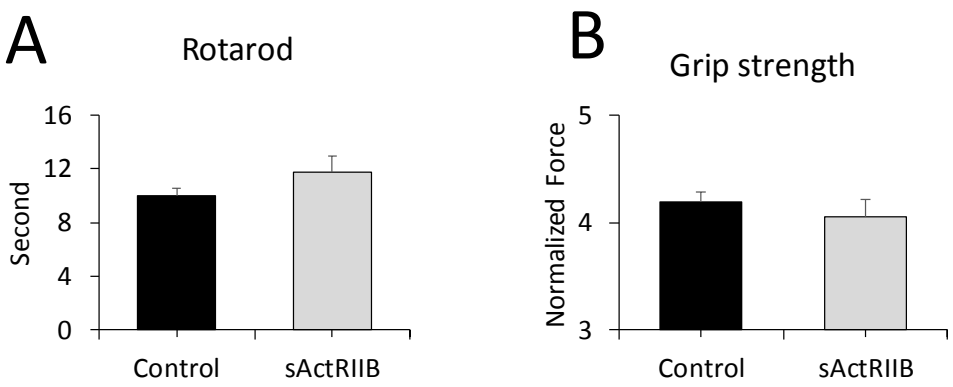

Figure 7.9. Assessment of motor activity and fatigue characterisation using rota rod and forelimb muscle strength using grip strength meter in *Ercc1*$^{+/+}$ after injection of sActRIIB.

(B) Rotarod activity. (B) Muscle contraction measurement through assessment of grip strength. The sActRIIB were IP injected starting from week 7 of age to week 16. All mice were at the same age, n= 6 male mice *Ercc1*$^{+/+}$ and n=4 *Ercc1*$^{+/+}$ sActRIIB. Student's t-test.

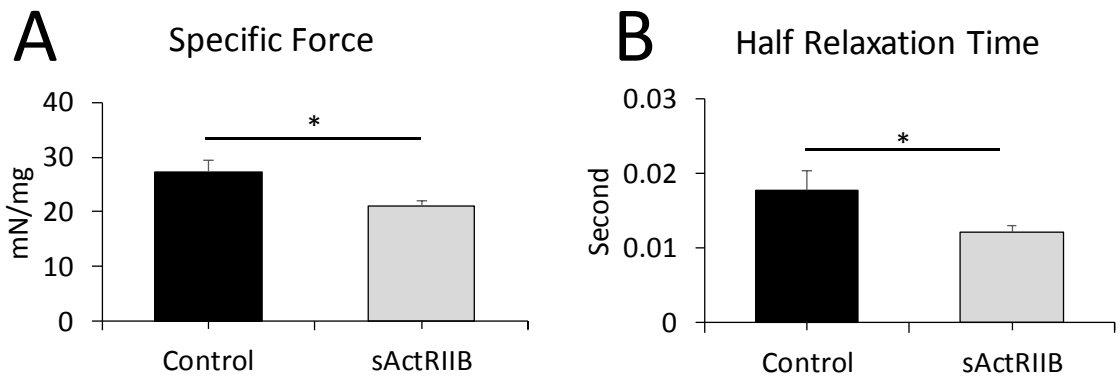

Figure 7.10. Ex-vivo muscle tension measurement *Ercc1*$^{+/+}$ after injection of sActRIIB.

(A) Ex-vivo assessment of EDL specific force. (B) Half relaxation time for the EDL. The sActRIIB were IP injected starting from week 7 of age to week 15. All mice were at the same age, n= 6 male mice *Ercc1*$^{+/+}$ and n=4 *Ercc1*$^{+/+}$ sActRIIB. Student's t-test, *p<0.05.

7.6. The satellite cell profile and proliferation capacity in the *Ercc1*$^{+/+}$ mice treated with sActRIIB.

We show that although increase muscle mass after sActRIIB injection in *Ercc1*$^{+/+}$ mice, there was a reduction in animal activity and specific force generation. Here we examined the consequence of sActRIIB treatment on individual muscle fibres. High numbers of post-mitotic myonuclei achieve the sustainability of myofibres, and myofibres repair and regeneration rely on the pool of satellite cells that located beneath the basal lamina (Mauro, 1961, Zammit and Beauchamp, 2001). A study by Amthor was reported the increase muscle mass in lack of myostatin mice was independent of satellite cell since the number of satellite cell was reduced in myostatin null mice (Amthor et al., 2009). We showed that the number of satellite cells in freshly isolated fibres of EDL muscle from *Ercc1*$^{+/+}$ mice was not changed after sActRIIB treatment (Figure 7.11.A). We investigated activation and proliferation of satellite cell at a different time point, T24, T48 and T72 and revealed no change in the treated group compared to non-treated (Figure 7.11.B-D). The ability of satellite cell to differentiate and self-renewing was detected by using quiescence marker (Pax7) for stem cell pool and Myogenin for differentiated cells. There was no effect of sActRIIB injection on these parameters (Figure 7.11.E). Overall, the number and activity of the satellite cell in *Ercc1*$^{+/+}$ mice were not affected by eight weeks of sActRIIB injection.

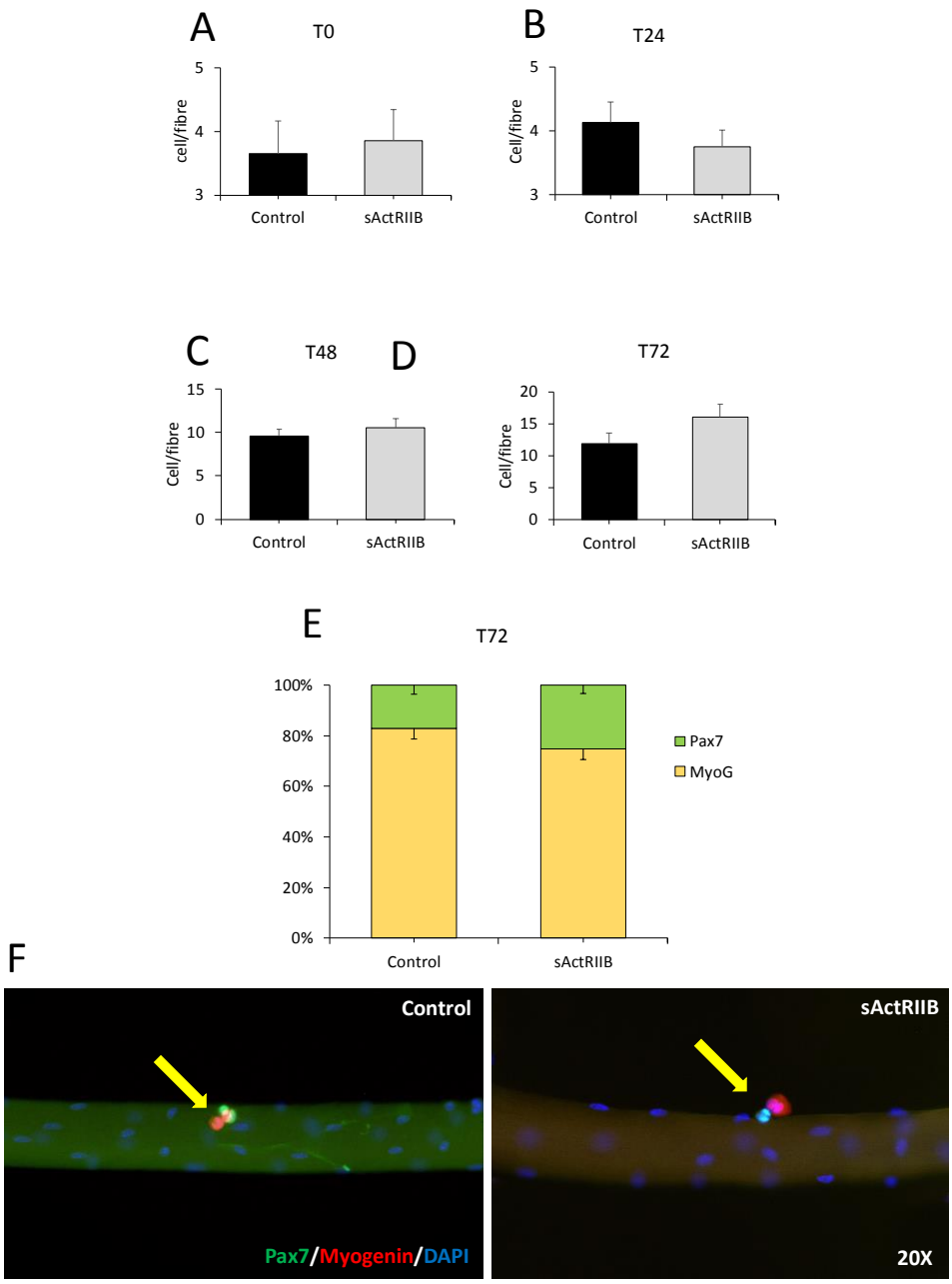

Figure 7.11. Examination of satellite cell number and status in *Ercc1*$^{+/+}$ treated and non-treated with sActRIIB group in fresh and cultured fibres.

Satellite cell and progeny enumeration on (A) fresh and (B-D) cultured EDL fibres over for 72hours. (E) Quantification of proportion of stem cells (Pax7+/Myogenin-) and differentiated cells (Pax7-/Myogenin+) on EDL fibres after 72h culture. (F) Representative images of single fibres stain against Pax7 (green), Myogenin (red) and DAPI (blue). The total of 20 fibres were analysed for both cohort from EDL muscle. The sActRIIB were IP injected starting from week 7 of age to week 16. All mice were at the same age, n= 6 male mice *Ercc1*$^{+/+}$ and n=4 *Ercc1*$^{+/+}$ sActRIIB. Student's t-test.

7.6. Discussion

We performed this experiment to investigate whether the control group (*Ercc1*$^{+/+}$ mice) used in our study show the similar effects of antagonising myostatin signalling in WT mice. Furthermore, the use of inbred mice reduces the genetic variability of outbred WT mice (Casellas, 2011).

Myostatin antagonism has been used for a long time in various conditions and animals yielding increase in muscle mass (Amthor et al., 2007, Puolakkainen et al., 2017, St Andre et al., 2017, Mosher et al., 2007, Saunders et al., 2006, Fiems, 2012). In the agreement, we showed an increase in skeletal muscle mass in *Ercc1*$^{+/+}$ mice after sActRIIB injection. This increase in muscle mass resulted from hypertrophy, an increase in myofibres size, but not fibres number. Prenatal deletion of *Myostatin* increase muscle mass by both hypertrophy and hyperplasia (McPherron et al., 1997, Mendias et al., 1985). However, postnatal blocking of myostatin using sActRIIB, resulting in increasing muscle mass resulting from hypertrophy but not hyperplasia (Omairi et al., 2016). The difference in the mode of increasing muscle mass in postnatal and prenatal could be due to the number of the fibre is defined during muscle formation (Sandri, 2008). We and other (Relizani et al., 2014) showed an increase in body weight after sActRIIB injection. This increase could be due to an increase in muscle mass since the skeletal mass represents about ~40% of animal body mass (Frontera and Ochala, 2015).

Myostatin deletion in mouse model resulting in fibres type shifting toward fast profile. A study by Girgenrath reports conversion from the slow (type I and IIA) into fast (type IIX and IIB) phenotypes in myostatin knock out mice (Girgenrath et al., 2005). However, post-natal antagonise of the myostatin/activin signalling did not affect fibres type distribution in WT and disease mice (Cadena et al., 1985, Morine et al., 2010). The prenatal effect of myostatin blocking on muscle fibres phenotype was due to the particular role of myostatin in fusion myoblast that differentiates to slow fibres (Girgenrath et al., 2005, Stockdale, 1997). However, a study show injection of sActRIIB lead to a reduction in transcription of slow MHCs in Plantaris but not Soleus, yet protein level of MHCs did not change after 28-day treatment (Cadena et al., 1985). We were injected sActRIIB for eight weeks and show some fibres type shifting and was more evident in EDL rather than Soleus. A study showed nuclei that express MHCII was widely express myostatin and with minor extend myonuclei express MHCI (Artaza et al., 2002). It could be concluded that block myostatin signalling by injection

sActRIIB in *Ercc1*$^{+/+}$ mice increased nuclei number that expresses MHCII as a compensatory mechanism for reducing myostatin signalling. MHCs profile shift was accompanied by reducing oxidative statutes in mice lacking myostatin and that what we showed after injection of sActRIIB. A study shows the central role of myostatin in regulating oxidative energy metabolism since its absence leads to muscle fibres switch toward a glycolytic phenotype (Mouisel et al., 2014). A further study showed that use of sActRIIB as antagonise for myostatin signalling resulting in a reduction in the level of molecules that involved in the regulation of skeletal muscle mitochondrial functions and oxidative phosphorylation (Rahimov et al., 2011).

The remarkable increase in skeletal muscle mass through attenuation myostatin signalling was shown to be accompanied by a reduction in skeletal muscle force generation (Amthor et al., 2007). However, in disease mice, mdx mice, the antagonising of myostatin lead to increase of muscle-specific force output (Wagner et al., 2002, Bogdanovich et al., 2002). The reduction in specific force generation and animal activity in *Ercc1*$^{+/+}$ mice after sActRIIB injection could be due to lack of mitochondrial support since the muscle increases in size but reduce in oxidative capacity. Omairi et al. found that there was an enhancement in exercise capacity of animal lack of myostatin after upregulation an *Errγ*, a molecule known of its ability to regulate oxidative metabolism (Omairi et al., 2016). There was also evidence of high mitochondrial content of oxidative fibres (Annex et al., 1998, Cherwek et al., 2000) compared to lower content in glycolytic fibres (Annex et al., 1998, Narkar et al., 2011). The glycolytic profile that we showed after treatment could explain the force generation reduction and reduce animal activity since the glycolytic fibres have low mitochondrial contents, i.e. decrease ATP generation in these fibres.

Increase in skeletal mass achieved by increase fibre number, hyperplasia, or/and increase myofibres size, hypertrophy (Stickland, 1981). Injection of sActRIIB in *Ercc1*$^{+/+}$ lead to increase muscle mass by hypertrophy rather than hyperplasia. Hypertrophy results from recruiting differentiated satellite cells and balance between protein synthesis and degradation (Schiaffino et al., 2013). Since the injection of sActRIIB did not affect satellite cell number and activity in *Ercc1*$^{+/+}$ mice, it could be concluded that the increase in muscle fibre size resulted from remodelling protein synthesis system.

Chapter 8

General discussion and conclusion

General discussion

The main aim of this project was to investigate the potential therapeutic effects of antagonising of myostatin/activin signalling by using sActRIIB on the progression of sarcopenia in progeric *Ercc1*$^{\Delta/-}$ mice. The ageing signs in this mouse model were due to the accumulation of DNA damage because of attenuation of ERCC1 protein that has a central role in DNA damage repair. One of the widely accepted theories of ageing is that DNA damage induces a stress response that shifts cellular resources from growth towards maintenance. By antagonising a negative regulator of muscle growth, we challenge the notion that tissue growth is conflicted with maintaining tissue function. A range of experiments was conducted to address the following: (A) skeletal muscle in the *Ercc1*$^{\Delta/-}$ progeric mouse was profiled by examining a broad range of parameters to provide a basis for subsequence experimentation. (B) Investigating the effect of injection of sActRIIB on body weight and organismal activity and strength in *Ercc1*$^{\Delta/-}$ mice. (C) The therapeutic potential of sActRIIB in quantitative and qualitative improvement in *Ercc1*$^{\Delta/-}$ mice. (D) The efficacy of sActRIIB in the normalisation of *Ercc1*$^{\Delta/-}$ extracellular components and differentiation and self-renewal of its satellite cells. (E) The effect of antagonising myostatin/activin signalling on internal control (*Ercc1*$^{+/+}$) mice.

The main findings in this project are, first that the progeric *Ercc1*$^{\Delta/-}$ mice not only mimicking many features and signs of naturally aged sarcopenic muscle but in some aspect were more severe. Second, the sActRIIB ameliorate many sarcopenic features despite the persistence of DNA damage. Third, the antagonise of myostatin/activin signalling in addition to enhance skeletal muscle in *Ercc1*$^{\Delta/-}$ mice, they reveal many organismal improvements; mice increased locomotor activity; increased specific force and delayed parameters of neurodegeneration. Finally, the effect of introducing the sActRIIB treatment on control (*Ercc1*$^{+/+}$) mice agreed with previous work in term of increasing muscle mass and decrease force generation.

***Ercc1*$^{\Delta/-}$ muscle parallels with natural muscle ageing and pathological muscle diseases.**

Here we value of *Ercc1*$^{\Delta/-}$ mice as a model to study ageing particularly age-related loss of skeletal muscle, sarcopenia. Considering previous work, the *Ercc1*$^{\Delta/-}$ progeroid model not only showed the apparent severity in muscle loss, but also this muscle illustrated many unexpected compositional alterations. At the quantitative level, all muscle groups from

Ercc1$^{\Delta/-}$ mice were much lighter than control mice, which concords with findings in aged humans and mouse models. A study report 40% reduction in human muscle area in ages of the 70s compared to ages of 20s (Rogers and Evans, 1993). Other study reports a decrease in hindlimb muscle mass in mice significantly between 18 and 24 months of age and 15% further decline between 24 and 29 months (Hamrick et al., 2006).

Besides, our results revealed many qualitative differences between progeroid muscle and muscle of aged wild-type mice. The reduction in muscle mass in naturally aged rat was mainly by a decrease in fibres cross-sectional area of fibres express MHCIIB (Larsson et al., 1993) while the reduction of myofibres size in *Ercc1*$^{\Delta/-}$ mice were involved all fibres types. In contrary to naturally aged human and rodent skeletal muscle profile that undergo fast to slow shifting (Holloszy et al., 1991), the *Ercc1*$^{\Delta/-}$ mice skeletal muscle fibres shifted from slow to fast profile. Aged skeletal muscle undergoes fast to slow shifting were also shifted from glycolytic to oxidative metabolism (Ohlendieck, 2011), and we also showed that the progeric mice undergo oxidative to glycolytic metabolism shifting. In both human and rodent, the decrease in muscle mass results from both reduction in muscle fibres size in a decrease in total fibre numbers (Lexell et al., 1988, Carlson et al., 2001). The unexpected increase was discovered in the number of fibres in both EDL and soleus muscles, which seemingly contradicts the finding of overall loss in muscle mass in *Ercc1*$^{\Delta/-}$ mice. The finding that could explain why hyperplasia in *Ercc1*$^{\Delta/-}$ mice did not increase muscle mass is that there was an increase in the proportion of fibres with the small cross-sectional area (Figure 8.1). However, numbers of myopathological conditions, such as Duchenne muscular dystrophy, have shown an increase in fibres number even with atrophic phenotype. (Faber et al., 2014). It seems that the increase in fibres number was not due to a mechanism that enhancing muscle growth but was due to fibres damage. We found there was an increase in the proportion of damaged fibres in *Ercc1*$^{\Delta/-}$ mice especially split fibres. The muscle fibres apoptosis and necrosis have been reported as some of the causes of sarcopenia (Yoo et al., 2018). Indeed, the fibres dying were far more prominent in *Ercc1*$^{\Delta/-}$ progeric muscle than found in aged wild-type mice (Cheema et al., 2015). The evidence of increased caspase activity and reduction in deposition of dystrophin and collagen IV, making the muscle more prone to developed contraction-induce damage could result in the cellular lesion (splitting) and end with fibres death.

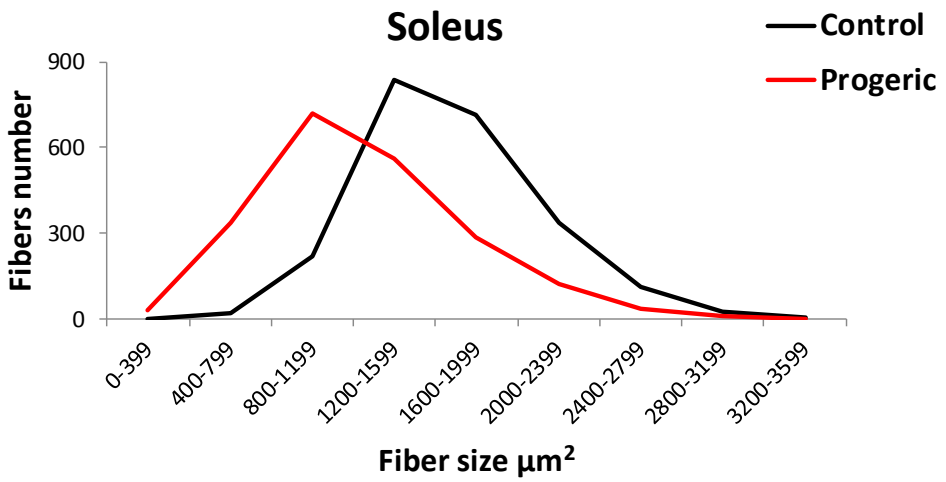

Figure 8.1. Distribution of fibres according to size shows increase number of small size fibres in *Ercc1*$^{\Delta/-}$ mice compared to control.

Number of fibres distributed depend on size intervals from Soleus muscle in both *Ercc1*$^{\Delta/-}$ and control mice. n= 6 each cohorts.

Further analysis of *Ercc1*$^{\Delta/-}$ muscle shows that the fibres have a subcellular aberration even they look healthy and did not show any abnormalities such as tearing or central nucleation. These fibres have both abnormalities in the organisation of the contractile apparatus and the cellular organelles as revealed by ultrastructural examination. Age-related decline in myofibres mitochondrial density (Li et al., 2016) was also shown here within fibres and subsarcolemmal regions were it support contraction and membrane-related activities, respectively (Powers et al., 2012). In addition to this mitochondrial quantitative alteration, there was a qualitative change in *Ercc1*$^{\Delta/-}$ mice. We concluded these alterations were due to either functional deficit or altered fusion (Frank et al., 2001, Terman and Brunk, 2004b) and interpreted as mitochondrial swelling in both within myofibres and subsarcolemmal regions. Mitochondrial abnormalities, due to a mutation in *Ercc1* actively contributed to impaired contractile apparatus and provoked fibres death (Powers et al., 2012). We suggest that the increased level of ROS, gauged by DHE activity (Diaz et al., 2003), resulted from compromised mitochondrial function and ultimately affect fibres performance and viability.

Modulation of Ercc1 gene leads to produce a truncated protein with attenuated excision repair cross-complementation 1 activity, a key component of several DNA repair pathways, including nucleotide excision repair (Sijbers et al., 1996). Attenuation in Ercc1 protein activity results in progeric phenotype due to the accumulation of DNA damage. DNA repair is required for genome integrity and viability of cell (Volkert and Landini, 2001). Persistence of DNA damage leads to the production of an aberrant RNA (Adam and Polo, 2014) and if translated yield a harmful truncated protein (Shyu et al., 2008). These harmful products need to be eliminated by the cell and compensatory produce replacements for them. This could explain the interesting profile shown in *Ercc1*$^{\Delta/-}$ mice in term of anabolic and catabolic vital proteins. The *Ercc1*$^{\Delta/-}$ muscle showed elevates levels of protein synthesis and degradation mechanisms at the same time, and this landscape differs from normal catabolic condition (Sandri, 2008). It showed elevated levels of Akt activity, one of two downstream genes (S6) and the overall rate of protein synthesis.

On the other hand, the muscle of *Ercc1*$^{\Delta/-}$ mice expressed high levels of *MuRF1* and *Atrogin-1* and contained increased levels of ubiquitinated proteins. Although unusual in the context of normal physiology, these results agree with other studies of progeroid models that demonstrate the activation of pathways to limit the effect of the primary lesion (Gregg et

al., 2012). We suggest that in the context of *Ercc1*$^{\Delta/-}$ muscle, the activation of the protein synthesis pathway acts to decrease an extremely high rate of muscle wasting. Nevertheless, the ultimate deregulation of protein synthesis, proteasome and autophagy pathways in *Ercc1*$^{\Delta/-}$ muscle, which parallels many disease conditions, culminates in atrophy (Sandri, 2013, Bonaldo and Sandri, 2013).

Satellite cells (SC) from *Ercc1*$^{\Delta/-}$ mice have shared some but not all features of those from aged fibres. SC from aged mice show lower proportion compare to young animals (Shefer et al., 2006) and the SC from progeric mice do so. However, the aged SC was more prone to activation (Brzeszczynska et al., 2018) whereas the progeric SC display inability to divided after single fibres isolation. Both SC from aged and *Ercc1*$^{\Delta/-}$ mice were did not follow the usual degree of differentiating (Brzeszczynska et al., 2018). However, comparisons of outcomes from different studies are problematic due to the use of different experimental systems.

Effects of soluble activin receptor type IIB on *Ercc1*$^{\Delta/-}$ muscle phenotype

The super-aged phenotype that we showed and related to disruption of Ercc1 were characterised by a significant loss of muscle mass and function. Although the thought of supporting growth was a conflict with the evidence of shifting cell rescores from growth to maintenance, we aim to get a benefit from supporting skeletal muscle growth in *Ercc1*$^{\Delta/-}$ progeric mice by injection sActRIIB. We showed that using a sActRIIB to antagonise myostatin/activin to have a profound effect on the body and muscle mass and function in *Ercc1*$^{\Delta/-}$ mice. This postnatal attenuation of myostatin signalling by using soluble activin receptor ligand trap for eight weeks is worthy to compare to absolute absent of myostatin by prenatal deletion. The EDL was heavier by 60% in *Mstn*$^{-/-}$ mice compared to counterpart wild type mice (Amthor et al., 2007) and hereafter just eight weeks of treatment; it was heaver by 45% in treated mice compared to mock treated.

Furthermore, the plantaris were increased by 62% in sActRIIB treated compared to control. sActRIIB was more efficient even when we compared the muscle that showed lowest increased percentage (TA muscle) that have 30% increment, comparing to using of anti-myostatin antibody used in aged mice and TA shows increase by 6% compared to non-treated mice (Collins-Hooper et al., 2014). These results suggest that the activity of

myostatin and activin in *Ercc1*$^{\Delta/-}$ mice are considerably higher than in aged wild-type mice and an increase in muscle mass was due to suppress signalling through ActRIIB rather than IGF pathway. Indeed, we found that treatment with sActRIIB did not affect the circulating levels of either GH, glucose, insulin, or IGF-1.

The muscle from *Ercc1*$^{\Delta/-}$ mice that show a reduction in muscle mass was also reduced force generation. This is different from what is reported in regular loss of muscle mass, where that contractile force preserved when normalised to weight (Nishio et al., 1992). Here, we see that *Ercc1*$^{\Delta/-}$ mice generated only 50% of normalised grip strength compared with controls. Furthermore, there were an abnormal specific force and relaxation times in the muscle of *Ercc1*$^{\Delta/-}$ muscle, both features of structural alterations (Schwaller et al., 1999). Indeed, using TEM reveal various subcellular and biochemical abnormalities in *Ercc1*$^{\Delta/-}$ muscles. There was clear evidence of sarcomeres and mitochondria abnormalities. Use of sActRIIB treatment was able to largely mitigate the ultrastructure abnormalities and subsequently improve muscle force generation. Reduction in grip strength was significantly improved by sActRIIB treatment. Besides, abnormal specific force and relaxation times in the muscle of *Ercc1*$^{\Delta/-}$ muscle, were improved by sActRIIB treatment. The suggested driver in this enhancement prosses could be the activation of the autophagic programme mediated by members of the FoxO family. Thus, further investigations concluded that blunted autophagic activity in *Ercc1*$^{\Delta/-}$ mice were the leading factor to these deleterious effects. Accumulation of p62 puncta and presumably abnormal mitochondria as well as through hyperactivation of the UPR^{MT} (Haynes and Ron, 2010), elevated levels of genes encoding prohibitins that function to restore organelle function (Merkwirth and Langer, 2009), change in the histone markers profile (down-regulation of H3K9Me3 and upregulation of H4K20me3 that their levels showed an opposite trend in *Ercc1*$^{\Delta/-}$ and naturally aged mice (Ocampo et al., 2016)) as well as ROS superoxide levels, all resulting from abnormal autophagic activity. Consequently, the build-up of ROS causes protein oxidation ultimately compromising the workings of the contractile apparatus and leading to a deficit in specific force (Andersson et al., 2011). Our interpretation of these finding is that sActRIIB treatment of *Ercc1*$^{\Delta/-}$ mice leads to the activation of autophagy (LC3II/I ratio), which prevents the accumulation of p62 puncta and also abnormally functioning mitochondria, thus counteracting the need to activate either the UPR^{MT} or prohibitin programmes, maintains a normal profile of histone modification as well as avoiding the

build-up of high levels of ROS, which ultimately translates in the preservation of organ reserve capacity. We note that the expression of Mul1, a proposed mitochondrion-specific U3 ubiquitin ligase, was not affected by the progeroid condition or following treatment with sActRIIB compared with controls. However, it is worth bearing in mind that numerous mitochondria targeting U3 ubiquitin ligases have been identified including PARKIN and that these non-investigated molecules could be executing mitophagy in our experiments (Rojansky et al., 2016).

However, further investigation is needed to reveal the mechanism that underpins the regulation of both protein synthesis and autophagy in *Ercc1*$^{\Delta/-}$ mice following sActRIIB treatment. These two processes, in normal conditions, are antagonistically driven in large part by FoxO proteins (reviewed in Ronaldo & Sandri (Bonaldo and Sandri, 2013)). However, here in *Ercc1*$^{\Delta/-}$ muscle, we suggest an abnormal landscape evidenced by the hyperactivation of Akt in *Ercc1*$^{\Delta/-}$ muscle. Indeed, there is a growing body of evidence for the dual activation of Akt-mediated pathways and autophagy when the normal conditions of regulation are altered (Chen et al., 2014). Hyper-activation leading to initiation of novel signalling pathways and cellular outcomes is quite a common outcome and has been extensively studied mainly in scenarios of uncontrolled cell division that underpin the development of many cancers (McCubrey et al., 2007, Steelman et al., 2011). Future studies, beyond the scope of the present investigation, combining gene expression and proteomic platforms are planned to identify the pathways susceptible to hyperactivation of Akt. Nevertheless, Omairi et al. proposed that the role of autophagy is in maintaining cellular homeostasis rather than anabolism (Omairi et al., 2016).

Effects of soluble activin receptor type IIB treatment on muscle stem cells and the extracellular matrix

The mechanical performance of skeletal muscle relies on both muscle fibres integrity and ECM. Contractile force is transmitting through the connective tissue of ECM to skeleton and translate to movement or balance. We showed that the disruption of Ercc1 gene was related to change in the ECM component in progeric mice. The elements of this compartments were largely normalised after sActRIIB treatment and could be one of the

reasons for increased mice activity as presented by using an open cage activity monitor system. ECM contribute directly to skeletal muscle growth and regeneration as being a niche of satellite cells (SC), the resident stem cell population of skeletal muscle (Mauro, 1961). We identify unique features of SC in *Ercc1*$^{\Delta/-}$ mice. We show that the *Ercc1* mutation reduces both the number of SC and its ability to proliferate following single fibre isolation as a gauge of senescent. They were able to become activated, judged by their expression of MyoD (Figure 8.2), and differentiate but did not demonstrate the normal self-renewal/terminal differentiation physiognomies following 72 h of culture (Zammit et al., 2006), features shared by counterparts from geriatric wild-type mice (Garcia-Prat et al., 2016). Our results are consistent with the findings of Lavasani et al., who showed that *Ercc1*$^{\Delta/-}$ mice had attenuated muscle regeneration following cardiotoxin injury (Lavasani et al., 2012). The subsequent experiments reveal features of SC that are plastic about myostatin/activin signalling. First, we show that sActRIIB was unable to influence the number of SC in the muscle of *Ercc1*$^{\Delta/-}$ mutants, which remained abnormally low compared with controls. This is not altogether surprising as the number of SC is established approximately a month after birth in mice (Lepper et al., 2009). However, sActRIIB treatment supported SC division and normal differentiation. We propose that these outcomes are unlikely to be due to a direct attenuation of myostatin/activin signalling in SC by sActRIIB as previous studies have shown that they express very little if any, ActRIIB (Amthor et al., 2009). Instead, we contemplate that sActRIIB-induces change in the *Ercc1*$^{\Delta/-}$ myofibre ECM (shown here by changes in collagen IV expression as well as dystrophin) that influences the behaviour of their SC. This is possibly significant given that recent studies have shown that the behaviour (ability to divide and differentiate) of SC is profoundly influenced by the interaction of collagen molecules and stem cell receptors (Baghdadi et al., 2018).

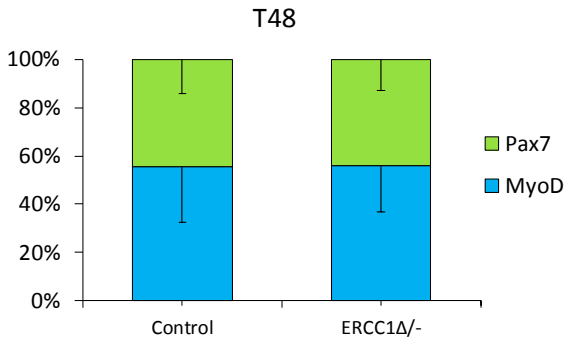

Figure 8.2. Examination of satellite cell status in *Ercc1*$^{\Delta/-}$ in cultured fibres.

Quantification of proportion of stem cells (Pax7+/MyoD-) and activated cells (Pax7-/MyoD+) on EDL fibres after 48h culture. n= 7 for both cohorts. Student's t-test.

Organismal enhancement by soluble activin receptor type IIB treatment

In this study, we show that antagonism of myostatin/activin signalling in *Ercc1*$^{\Delta/-}$ mice attenuated the development of ageing-related changes not only of muscle activity but rather also organismal activity overall. Administration of sActRIIB to *Ercc1*$^{\Delta/-}$ mice increase body weight, improved strength, fitness, and locomotor performance, delayed the onset and importantly, the severity of several age-related neurological abnormalities. We show, surprisingly, even with this lower body weight the *Ercc1*$^{\Delta/-}$ mice, their food consumption was higher than counterpart control mice. One suggested explanation is that the most of nutrients and energy are recruited by protein synthesis/degradation cycles that showed hyperactivated in *Ercc1*$^{\Delta/-}$ muscle. A further metabolic analysis, intestine endothelial integrity and absorption ability and faeces analysis are suggested for more accurate interpretation of this phenomenon. Being underweight consider a health issue and lead to many retaliated health implications. One suggested health implication related to decrease in body weight is decrease bone mineral density and make it more prone to fractures (Lim and Park, 2016) and fall-related fracture consider one of the complications of sarcopenia (Cederholm et al., 2013).

Furthermore, underweight was associated with increased mortality resulting from an accident (Roh et al., 2014). Injection of sActRIIB in *Ercc1*$^{\Delta/-}$ mice significantly increased body weight and the percentage of weight gain was noticed as early as one week after injecting compared to nontreated mice. This increase could result from the direct effect of antagonise myostatin since its level was reported increased in related to decrease in body weight (Motevalli et al., 2015), or indirect by increasing muscle mass, the most abundant tissue in the body. The improved skeletal muscle strength was reported by using anti-myostatin antibody in old age for four weeks, was also reported here by antagonising myostatin/activin signalling. As a result, we have seen that there was an improvement in organismal strength and fitness. Using sActRIIB in R6/2 mice, a model of Huntington's disease, an inherited neurodegenerative disorder, for six weeks was able to reduce muscle atrophy, weakness, contractile abnormalities and loss of functional motor units (Bondulich et al., 2017). We showed here also that the imbalance and severity of tremor as a sign of age-related neurological abnormalities was delayed by using sActRIIB in *Ercc1*$^{\Delta/-}$ progeric mice. Our result showed the persistence of DNA damage in skeletal muscle tissue after

sActRIIB treatment. This evidence suggests that antagonise myostatin/activin signalling is not targeting the primary cause of the condition but consider as symptomatic treatment. However, the enhancement showed by sActRIIB in skeletal muscle of treated *Ercc1*$^{\Delta/-}$ if applied to aged people might have a positive impact on the quality of life by increased mobility and reduction fall-related fractures.

The effects of using sActRIIB in *Ercc1*$^{+/+}$ mice.

The effect of genotype on treatment outcomes has been postulated in early studies. Variation in experimental animal genotype has been suggested to have a significant effect on the mechanism of drug action and how these mice respond to treatment (Meier and Fuller, 1966) and this term as pharmacogenetics (Nebert, 1999) or in broad aspect as pharmacogenomics (Evans and Relling, 1999). In consideration of this fact, we used an inbred control mouse (*Ercc1*$^{+/+}$), to reduce the expected variation in response to treatment related to genetic diversity. Furthermore, to our knowledge, this is the first study investigating the effect of antagonising myostatin/activin in *Ercc1*$^{+/+}$ with FVB/C57Bl6 background mice, as it reported before as normal mice (Dollé et al., 2011).

Injection of sActRIIB to *Ercc1*$^{\Delta/-}$ mice were able to increase body weight, and we suggest it mainly by an increase in muscle mass. Since there was evidence of a decrease in body fat contents in myostatin null mammals (Deng et al., 2017), and a further study shows no change in fat mass after sActRIIB treatment for four weeks (Whittemore et al., 2003, Akpan et al., 2009). We showed that the muscle mass was increased by hypertrophy but not hyperplasia in *Ercc1*$^{+/+}$ treated with sActRIIB. However, it was reported that the increase in muscle mass in myostatin null mice is due to both mechanisms (McPherron et al., 1997). The skeletal muscle hyperplasia mostly related to prenatal deletion of myostatin. For instance, Thomas et al showed that C2C12 muscle cell line treated with Myostatin results in a reduction of myoblast proliferation due to its interaction with the factors that control the progression of the cell cycle from G1 to S-phase through up-regulation of p21 inhibitor and its ability to downregulate Cdk2 (Thomas et al., 2000). We suggest the increase in fibres mass in *Ercc1*$^{+/+}$ mice was due to increase protein synthesis and reduce protein degradation since myostatin mediate inhibition in protein synthesis by reducing Akt and upregulating FoxO activity (Yang et al., 2007). These increases in fibres size were seen in all fibres type

and more pronounce in fibres express MHCIIb. That could be explained, if we consider a study reporting that IIb myofibres express the highest level of activin receptor IIB among other myofibres type (Mendias et al., 1985), therefore reduce inhibitory signal leads them to display the highest increase CSA.

On the other hand, new fibres rely on recruiting satellite cells. We showed that introducing sActRIIB did not affect satellite cell number, the proliferation or even differentiation. This find agrees with previous work that shows no effect of post-natal blocking of myostatin on satellite cell number (Matsakas et al., 2009) and differentiation (Foster et al., 2009). The downregulation of activin receptor in satellite cell could be the reason that these cells have not affected by the level of myostatin after its blocking (Amthor et al., 2007).

We showed that even sActRIIB treatment was able to increase muscle mass; however lead to a partial reduction in muscle force generation. This functional reduction could be explained considering other studies that showed a reduction in specific force and increase fatigability due reduce mitochondrial content, oxidative capacity and capillary density with relation to myostatin null hypertrophic phenotype (Amthor et al., 2007, Mendias et al., 1985, Omairi et al., 2016). Indeed, we find a significant shifting to the glycolytic profile after eight weeks of sActRIIB treatment. Specifically, Rahimov et al. found that injection of sActRIIB resulted in a reduction in the expression of genes that regulate mitochondrial function (Rahimov et al., 2011), and consequently reduce ATP production and muscle force generation. The other reason for reduction specific force that could be concluded from a study that shows an increase in fibres CSA but not myonuclei number after myostatin blocking and that reduce nuclear: cytoplasmic ratio (Matsakas et al., 2009).

Furthermore, another study demonstrated a close relation of myonuclei domain size, the area of cytoplasm served by one nucleus, and maintaining a specific force in hypertrophic condition (Qaisar et al., 2012). In this study the increase of muscle mass in two conditions, IGF overexpression with the addition of new myonuclei and myostatin null with no evidence of increase myonuclei, there was maintaining of a specific force in IGF overexpression but not in *Mstn*$^{-/-}$ mice (Qaisar et al., 2012). The shift that we showed in *Ercc1*$^{+/+}$ mice toward fast MHC profiles after sActRIIB treatment, as IIB fibres well documented to be more susceptible to fatigue because of it lower mitochondrial content, less oxidative enzyme and less blood supply capillary (Armstrong, 1996), did not affect fatigue result by using rotarod.

Further investigation using treadmill needed to ensure this result, because the animals learn how to jump out the rotating shift as they are healthy animal and that not the case with progeric mice. However, the open field result of locomotor activity showed that treated animals travelled, by walking, less than non-treated animals.

In summary, it is antagonising of myostatin/activin by using sActRIIB for eight weeks in *Ercc1*$^{+/+}$ mice significantly increased body and muscle mass. The increase in muscle mass was due to fibres hypertrophy independent of fibres type and did not involve an increase in fibres number. A reduction muscle and animal activity combined this hypertrophic phenotype, and we suggested it could be due to shifting toward a most fatigable fast and glycolytic fibres type.

Conclusion

Our work highlights a novel mechanism that attenuates age-related skeletal muscle tissues alterations. It is well documented that one of the mechanisms that are initiated to slows the signs of ageing is that shift of cellular resources toward maintenance and repair on the expense of growth and proliferation (Niedernhofer et al., 2006, Garinis et al., 2009, Pinkston et al., 2006). Experimentally this mechanism could be achieved by attenuating IGF-1 and GH activity, which controls the somatic growth axis (Hinkal and Donehower, 2008, Guarente and Kenyon, 2000). The other approach that supports this notion is to decrease energy uptake by dietary restriction (DR) (Fontana et al., 2010). Vermeij et al. have shown that DR delays ageing at the organismal level and extends lifespan and healthspan of *Ercc1*$^{\Delta/-}$ mice (Vermeij et al., 2016a). Considering these studies, promoting tissue growth would conflict with the idea of energy expenditure shifting and might be harmful to an ageing model. Our result demonstrates that a mechanism that promoted the growth of skeletal muscle in progeric mice also promotes overall health span as evidenced by activity measurements and tissue structure and function; however it reduces activity in healthy control (*Ercc1*$^{+/+}$). We believe that by examining the defects that underlie the accelerated ageing process in progeroid mice, we can reconcile these apparent discrepancies.

We have shown that the deficiency in repairing DNA leads to the damage that stops transcription at least in postmitotic tissues, which cannot dilute or repair DNA damage through replication related repair pathways. Consequently, a preference loss of long transcripts resulted from the stochastic nature of DNA damage (Vermeij et al., 2016a). Besides, DR is able, by reducing the DNA damage load, to prevent transcription block (Vermeij et al., 2016a). We propose that the transcriptional landscape at least in the skeletal muscle tissue is unaffected by sActRIIB, but that enhanced protein synthesis promoted with sActRIIB may, by increasing the number of polypeptides from each mRNA's molecule, at least partly compensate for a deficit in longer transcripts. In this model, the levels of proteins encoded by long genes in *Ercc1*$^{\Delta/-}$ would be increased by either increased rate of protein synthesis (by sActRIIB) or as previously showed by reduced arrest of gene transcription due to diminished DNA damage induction (by mechanisms induced by DR) (Vermeij et al., 2016a).

Importantly, while many aspects of ageing have been delaying, sActRIIB administration has not increased overall lifespan. This suggests that a model in which myostatin/activin attenuation does not affect the upper limits of lifespan but somewhat reduces morbidity, maintaining health until very old age (Fries, 2002, Dong et al., 2016).

Future work

We are nevertheless mindful that despite promising results in rodent models, translation of therapies based on myostatin/activin antagonists have been, to date, unsuccessful in delivering intended outcomes and others have been curtained due to safety concerns (Golan et al., 2018, Saitoh et al., 2017a) and point to the need to develop a greater understanding of the biological processes controlled by this signalling axis. Although, attenuating of myostatin signalling prevents or ameliorates muscle loss in diseases and physiological conditions such as sarcopenia, using such an approach in wild type and some mouse model had many limitations. One of these limitations represents by reducing muscle specific force, although promoting skeletal muscle growth (Amthor et al., 2007). Another undesirable side effect of antagonising myostatin is that the reduce myostatin signal in skeletal muscle lead to profile shifting from slow to fast MHC and reduce oxidative capacity (Amthor et al., 2007, Hering et al., 2016). Increase the proportion of fast fibres, the most fatigable myofibres, may affect muscle activity.

Furthermore, reduce oxidative status was well document as its combination with the reduction of energy production since the oxidative metabolism relies on mitochondria, the sores of ATP in living tissue (Amthor et al., 2007, Ploquin et al., 2012). However, the use of sActRIIB in progeric *Ercc1*$^{\Delta/-}$ mice was able to increase muscle mass and enhance both muscle and organismal activity. A possible means of alleviating some of the safety issues associated with myostatin/activin antagonists could be through decreasing their dose but at the same time harnessing the benefits of other agents that promote healthy ageing. In line with the thought that fast/glycolytic profile related to myostatin signalling block, we could suggest using a combination of both sActRIIB and approach that enhance oxidative metabolism and facilitate fast to slow shifting, could have more benefit to progeric mice. One of these recommended approaches and most save, and applicable technique is exercise. It is well documented that training leads to increase oxidative metabolism and increase expression of slow MHCs (Röckl et al., 2007, Holloszy, 1967, Gollnick et al., 1973, Holloszy and Booth, 1976). Combination the endurance exercise training with deletion of myostatin results in an increased proportion of SDH positive (oxidative fibres) via increased oxidative enzyme activity and finally resulting in enhance organismal activity (Savage and McPherron, 2010, Matsakas et al., 2010, Matsakas et al., 2012). Training programs that

applied to myostatin-deficient mice in a wild type have been shown an enhancement in oxidative capacity and animal activity. However, progeric mice have a high proportion of damaged fibres with abnormal ECM that the case forces the animal for training may lead to exasperating the condition of the fibre.

Furthermore, the myostatin inhibition itself could lead to muscle damage after moderate exercise (McPherron et al., 1997, Grobet et al., 1997). However, muscle fibres from animal lacking myostatin did not damage in the light period of training (Wagner et al., 2005). In light of these results, we could expect a benefit of the combination of sActRIIB treatment with moderate training in term of enhancing skeletal muscle oxidative capacity in *Ercc1*$^{\Delta/-}$ mice. Furthermore, the training has been shown to enhance the ability of ageing cells to repair DNA damage (Radak et al., 2011) and that would be beneficial in mice lacking DNA repair mechanism.

The other suggested future direction is to use a combination of sActRIIB treatment and dietary restriction (DR). Using rats model, a study show that caloric restriction (CR) was able to modulate the metabolic status to more oxidative by enhancing mitochondrial activity (Chen et al., 2015), and another study demonstrates the ability of caloric restriction to alter the muscle contraction profile by increase slow fibres proportion on expense of fast fibres (De Andrade et al., 2015). The benefits of caloric restriction in aged mammals are well studied. Lee et al. have shown, on expression level, the ability of CR to prevent most of the alteration in gene expression related to ageing that regulates mechanisms including protein turnover and macromolecular damage (Lee et al., 1999). The dietary restriction was reported to reduce the signs of sarcopenia, even in the regime of one-day fasting per week (Cavallini et al., 2008). Most specifically, using DR in *Ercc1*$^{\Delta/-}$ mice were able to delay signs of ageing, reduce DNA damage and increase lifespan (Vermeij et al., 2016a). The increase in muscle mass and muscle enhancements with fast and glycolytic shifting that we have been shown in *Ercc1*$^{\Delta/-}$ mice after sActRIIB treatment, the DR will fit nicely as a combination treatment.

Other attractive proposition could be to use a combination of myostatin/activin antagonists and the deployment of the angiotensin 1–7 hexapeptide. The latter has been shown to block overactive renin-angiotensin signalling, which not only drives muscle dysfunction but also leads to muscle fibrosis (Meneses et al., 2015, Morales et al., 2013). A

recent study showed that angiotensin 1–7 was able to restore age-related muscle weakness in a rodent model (Takeshita et al., 2018). Both the sActRIIB and angiotensin 1–7 are attractive therapeutic molecules because they could be delivered using existing medical devices such as osmotic mini-pumps.

Activin receptor type IIB is the common receptor for TGF-β family members (Shi and Massague, 2003) and using a soluble form of this receptor will neutralise all these molecules. The effects that we have noticed in *Ercc1*$^{\Delta/-}$ mice after injection of sActRIIB might be the effect of antagonising one or more molecules of these family. As the myostatin is a well-defined member of its negative regulator of muscle growth (McPherron et al., 2009), then it will be interesting to compare the effect of the specific blocker of myostatin to sActRIIB in progeric *Ercc1*$^{\Delta/-}$ mice. One of a molecule that specifically inactivates myostatin is the recombinant myostatin propeptide. A study showed its ability to increase muscle mass and enhance repair and regeneration in the mouse model (Hamrick et al., 2010). Furthermore, using myostatin propeptide leads to reverse muscle loss by increase fibres size in aged mice (Arounleut et al., 2013, Flasskamp et al., 2014).

The aged people are more prone to fall-related injury and more susceptible to illness; thus, they subjected to bed rest during the treatment period and recovery. On top of sarcopenia, the involuntary loss of skeletal mass and function, these periods of bed rest could initiate a severe decline in muscle strength and mass (Covinsky et al., 2003, Visser et al., 2000). Considering our result of long-term uses of sActRIIB injection and enhancement of skeletal muscle mass and functional activity in progeric mice, we suggest a future set of experiments to investigate the short-term effect of the sActRIIB injection. Short term treatment of sActRIIB in progeric mice could be mimic the period of bed rest in illness aged people and might preserve muscle mass and functionality in this period.

Appendices

Appendix 1 - Antibodies used

Primary antibodies

Antigen	Species	Dilution	Supplier
Pax7	Mouse	1:1	DSHB
MyoD	Rabbit	1:200	Santa Cruz Biot # sc-760
Myogenin	rabbit	1:200	Santa Cruz sc576
MYHCI	Mouse	1:1	DSHB A4.840
MYHCIIA	Mouse	1:1	DSHB A4.74
MYHCIIB	Mouse	1:1	DSHB BF.F3
CD31	Rat	1:150	AbD serotec MCA2388
Dystrophin	Rabbit	1:200	Abcam 15277
Collagen IV	Rabbit	1:500	Abcam ab6586
Histone H3	Rabbit	1:100	Abcam ab8898
Histone H4	Rabbit	1:200	Abcam ab9052
pSmad2/Smad3	Rabbit	1:200	Cell signalling Technology # 8828
SMA	Mouse	1:300	Sigma A2547
Cleaved Caspase-3	Rabbit	1:200	Cell signalling Technology #9664S
Phospho-S6 Ribosomal Protein (Ser235/236)	Rabbit	1:1000	Cell signalling Technology #4857
Phospho-Akt (Ser473)	Rabbit	1:1000	Cell signalling Technology #4060
LC3	Rabbit	1:1000	Cell signalling Technology #2775
Phospho-4E-BP1 (Thr37/46)	Rabbit	1:1000	Cell signalling Technology #2855
Phospho-4E-BP1 (Ser65)	Rabbit	1:1000	Cell signalling Technology #9451
Anti-p62/SQSTM1	Rabbit	1:1000	Sigma P0067
Phospho-FoxO1 (Ser256)	Rabbit	1:1000	Cell signalling Technology #9461
Anti-Smad3 (phospho S423 + S425)	Rabbit	1:200	Abcam(ab52903)
Nephrin	Goat	1:500	R&D Systems (AF3159)

Secondary antibodies

Antibody	Species	Dilution	supplier
Alexa fluor 633 anti-mouse	Goat	1:200	Life Technologies # A20146
Alexa fluor 488 anti-mouse	Goat	1:200	Life Technologies # A11029
Alexa fluor 488 anti-rabbit	Goat	1:200	Life Technologies # A11034
Alexa fluor 594 anti-rabbit	Goat	1:200	Life Technologies # A11037
Immunoglobulins/HRP anti-Rat	Rabbit	1:200	Dako P0450

Appendix 2 – Materials

Reagents

Substance	supplier
4% Paraformaldehyde	Fisher scientific F/1501/PB08
$CaCl_2$	Fisher scientific 10161800
Chick embryo extract	MP Biomedicals, LLC Cat. No. 2850145
DAPI (2.5 µg/ml)	DakoCytomation DAKO Corp, Carpinteria, California
DMEM	Gibco 31966-021
DPX	Fisher scientific D/5319/05
DHE	Sigma-Aldrich 7008
Glycerol	Sigma-Aldrich G6279-1L
Glutaraldehyde Solution 25%	Merck, Germany 1042390250
Eosin	Sigma-Aldrich 318906-500ML
FBS	Gibco 10270-106
Haematoxylin	Sigma-Aldrich MHS16-500ML
HEPES	Fisher scientific BP410-500
Horse serum	Gibco 16050-122
Isopropanol	Fisher Scientific P/7490/17
Hydro mounting media	Agar scientific R1356
KCl	BDH 101984L
KCN	Fisher scientific 1059938
KH2PO4	BDH 10203
MgSO4	BDH 101514Y
$MgCl_2$	Sigma-Aldrich M2670-500
NaCl	Sigma-Aldrich 71382
OCT	TAAB O023
PBS Tablets	Oxoid BR0014G
Penicillin-streptomycin	Invitrogen 15240-062

Phenazine methosulfate	Sigma P9625-1G
Sodium azide	Fluka
Sodium succinate	Fisher scientific 11418852
Sucrose	Fisher chemical S/8560/53
Triton X-100	Fisher scientific T/3751/08
Type 1 collagenase	Sigma C0130
NaHCO3	Sigma S-8875 NaHCO3 Sigma S-8875
NaOH	Sigma S-5881
NBT	Sigma Aldrich 74032
Na Citrate	BDH # 30128
PBS Tablets	Oxoid BR0014G
Penicillin-streptomycin	Invitrogen 15240-062
PFA	Fisher Scientific P/0840/53
Phenazine methosulphate	Sigma P9625-1G
Protease Inhibitor Cocktail Set l	CALBIOCHEM #539131
RevertAid H Minus First Strand cDNA Synthesis Kit	Life Technologies k1631
RNase-Free DNase Set (50)	QIAGEN 79254
RNeasy Mini Kit	(50) QIAGEN 74104
SDS	Fisher Scientific S/200/53
SYBER Safe DNA gel	Invitrogen S33102
SYBR® Green PCR Master Mix	Applied Biosystems 4309155
Taq 2X Master	Mix New England Biolabs M0270L
Triton X-100	Fisher Scientific T/3751/08
TRIzol	Sigma-Aldrich T9424-100ml
Uranyl acetate	Polysciences, Germany
Urea	BDH, 102908D

Solutions

Phosphate buffer saline (PBS)

PBS tablets were dissolved in distilled water and then autoclaved.

Permeabilization buffer

0.952g Hepes, 0.260g $MgCl_2$, 0.584g NaCl, 0.1g Sodium azide, 20.54g Sucrose and 1ml Triton X-100 were made up to 200ml distilled water. The buffer was stored at 4°C.

Wash buffer

25ml Foetal bovine serum (FBS), 200mg Sodium azide and 250µl Triton X-100 were dissolved in 500ml PBS and stored at 4°C.

Type 1 collagenase

2mg of type 1 collagenase was dissolved in 1ml serum free Dulbecco's Modified Eagle Medium (DMEM) Glutamax^{TM} (0.2% w/v).

Paraformaldehyde (PFA) in PBS

20g of paraformaldehyde powder dissolved in 480 ml PBS by heating to 65°C. Volume was then made to 500ml with PBS and stored at room temperature.

Single Fibre Culture Medium (SFCM)

45ml of DMEM Glutamax^{TM} was supplemented with 250µl of chick embryo extract, 5ml 10% horse serum, 500 µl penicillin-streptomycin. The medium was stored at 4°C.

Nitro blue tetrazolium (NBT)

Phosphate buffer (100mM, pH 7.6) was prepared from two solutions; 12ml solution A (1.36g KH_2PO_4 /100ml), and 88ml solution B (1.42g Na_2HPO_4/100ml). Then 6.5mg KCN, 185mg EDTA, and 100mg Nitroblue tetrazolium (NBT) were dissolved in 100ml Phosphate buffer. The mixture was stored as aliquots of 2 ml at -20°C.

Succinate stocks

2.7g Sodium succinate was dissolved in 20ml distilled water. Then aliquots of 2ml were stored at -20°C.

Formal calcium

100ml 10% $CaCl_2$, 100ml 4% Formaldehyde and 800ml distilled water. The solution was stored at room temperature.

Taq 2X Master Mix

10 mM Tris-HCl, 50 mM KCl, 1.5 mM MgCl2, 0.2 mM dNTPs, 5% Glycerol, 0.08% IGEPAL® CA-630, 0.05% Tween® 20, 25 units/ml Taq DNA Polymerase pH 8.6 at 25°C. The solution was stored at -20°C.

Krebs solution

124 mM NaCl, 3 mM KCl, 1.25 mM KH2PO4, 36 mM NaHCO3, 1 mM MgSO4, 2 mM CaCl2, and Glucose. The solution was stored at 4°C.

Fixative solution for TEM samples

10 ml Glutaraldehyde 25% was added to 50 ml 0.2 M Na- cacodylate buffer pH 7.4, volume was then made to 100 ml with distilled water. The fixative solution was prepared freshly and kept in ice during work.

Appendix 3 – RT-PCR Primer sequences

Oligo Name	Sequence
MuRF1.F	ACCTGCTGGTGGAAAACATC
MuRF1.R	CTTCGTGTTCCTTGCACATC
Atrogin.1F	GCAAACACTGCCACATTCTCTC
Atrogin.1R	CTTGAGGGGAAAGTGAGACG
R_mVEGFA189.F	TGCAGGCTGCTGTAACGATG
R_mVEGFA189.R	CTCCAGGATTTAAACCGGGAT T
R_mFGF1.F	GAAGCATGCGGAGAAGAACTG
R_mFGF1.R	CGAGGACCGCGCTTACAG
R_mVEGFB.F	TGCCATGGATAGACGTTTATG C
R_mVEGFB.R	TGCTCAGAGGCACCACCAC
m Ndufb5.F	CTTCGAACTTCCTGCTCCTT
m Ndufb6.R	GGCCCTGAAAAGAACTACG
m Sdha.F	GGAACACTCCAAAAACAGACCT
m Sdha.R	CCACCACTGGGTATTGAGTAGAA
m Sdhc.F	GCTGCGTTCTTGCTGAGACA
m Sdhc.R	ATCTCCTCCTTAGCTGTGGTT
m Cox5b.F	AAGTGCATCTGCTTGTCTCG
m Cox5b.R	GTCTTCCTTGGTGCCTGAAG
m Atp5b.F	GGTTCATCCTGCCAGAGACTA
m Atp5b.R	AATCCCTCATCGAACTGGACG
m Mdh2.F	TTGGGCAACCCCTTTCACTC
m Mdh3.R	GCCTTTCACATTTGCTCTGGTC
m Idh2.F	GGAGAAGCCGGTAGTGGAGAT
m Idh3.R	GGTCTGGTCACGGTTTGGAA
m Idh3a.F	CCCATCCCAGTTTGATGTTC
m Idh3a.R	ACCGATTCAAAGATGGCAAC
R.mPGC1A.F	AACCACACCCACAGGATCAGA
R.mPGC1A.R	TCTTCGCTTTATTGCTCCATGA
m Mvk.F	GGGACGATGTCTTCCTTGAA
m Mvk.R	GAACTTGGTCAGCCTGCTTC
m Srebf1.F	GATCAAAGAGGAGCCAGTGC
m Srebf1.R	TAGATGGTGGCTGCTGAGTG
m Srebf2.F	GGATCCTCCCAAAGAAGGAG
m Srebf2.R	TTCCTCAGAACGCCAGACTT
R_mCD36.F	AGATGACGTGGCAAAGAACAG
R_mCD36.R	CCTTGGCTAGATAACGAACTCTG
R_mSlc25a20.F	CAACCACCAAGTTTGTCTGGA
R_mSlc25a20.R	CCCTCTCTCATAAGAGTCTTCCG
R_mACADL.F	TGCCCTATATTGCGAATTACGG
R_mACADL.R	CTATGGCACCGATACACTTGC
R_mFabp3.F	ACCTGGAAGCTAGTGGACAG

R_mFabp3.R	TGATGGTAGTAGGCTTGGTCAT
R_mDmd.F	ACTCAGCCACCCAAAGACTG(20)
R_mDmd.R	TGTCTGGATAAGTGGTAGCAACA
R_mCol4a1.F	GGCCCCAAAGGTGTTGATG(19)
R_mCol4a1.R	CAGGTAAGCCGTTAAATCCAGG
m Hsp10.F	CTGACAGGTTCAATCTCTCCAC
m Hsp10.R	AGGTGGCATTATGCTTCCAG
m Clpp.F	CACACCAAGCAGAGCCTACA
m Clpp.R	TCCAAGATGCCAAACTCTTG
m IL6.F	GGTGACAACCACGGCCTTCCC
m IL6.R	AAGCCTCCGACTTGTGAAGTGGT
m IL18.F	GTGAACCCCAGACCAGACTG
m IL18.R	CCTGGAACACGTTTCTGAAAGA
m Phb.F	TCGGGAAGGAGTTCACAGAG
m Phb.R	CAGCCTTTTCCACCACAAAT
m Phb2.F	CAAGGACTTCAGCCTCATCC
m Phb2.R	GCCACTTGCTTGGCTTCTAC

References

AAMANN, M. D., MUFTUOGLU, M., BOHR, V. A. & STEVNSNER, T. 2013. Multiple interaction partners for Cockayne syndrome proteins: implications for genome and transcriptome maintenance. *Mech Ageing Dev,* 134**,** 212-24.

ABBEY, C. K., BOROWSKY, A. D., MCGOLDRICK, E. T., GREGG, J. P., MAGLIONE, J. E., CARDIFF, R. D. & CHERRY, S. R. 2004. In vivo positron-emission tomography imaging of progression and transformation in a mouse model of mammary neoplasia. *Proc Natl Acad Sci U S A,* 101**,** 11438-43.

ABOUSSEKHRA, A., BIGGERSTAFF, M., SHIVJI, M. K., VILPO, J. A., MONCOLLIN, V., PODUST, V. N., PROTIĆ, M., HÜBSCHER, U., EGLY, J. M. & WOOD, R. D. 1995. Mammalian DNA nucleotide excision repair reconstituted with purified protein components. *Cell,* 80**,** 859-68.

ADAM, S. & POLO, S. E. 2014. Blurring the line between the DNA damage response and transcription: the importance of chromatin dynamics. *Experimental cell research,* 329**,** 148-153.

ADAMS, G. R. 2006. Satellite cell proliferation and skeletal muscle hypertrophy. *Appl Physiol Nutr Metab,* 31**,** 782-90.

ADELMAN, R., SAUL, R. L. & AMES, B. N. 1988. Oxidative damage to DNA: relation to species metabolic rate and life span. *Proc Natl Acad Sci U S A,* 85**,** 2706-8.

AGARWAL, A. K., FRYNS, J. P., AUCHUS, R. J. & GARG, A. 2003. Zinc metalloproteinase, ZMPSTE24, is mutated in mandibuloacral dysplasia. *Hum Mol Genet,* 12**,** 1995-2001.

AHMAD, A., ROBINSON, A. R., DUENSING, A., VAN DRUNEN, E., BEVERLOO, H. B., WEISBERG, D. B., HASTY, P., HOEIJMAKERS, J. H. J. & NIEDERNHOFER, L. J. 2008. ERCC1-XPF endonuclease facilitates DNA double-strand break repair. *Mol Cell Biol,* 28**,** 5082-92.

AKPAN, I., GONCALVES, M. D., DHIR, R., YIN, X., PISTILLI, E. E., BOGDANOVICH, S., KHURANA, T. S., UCRAN, J., LACHEY, J. & AHIMA, R. S. 2009. The effects of a soluble activin type IIB receptor on obesity and insulin sensitivity. *Int J Obes,* 33**,** 1265-73.

ALLAMAND, V., BRINAS, L., RICHARD, P., STOJKOVIC, T., QUIJANO-ROY, S. & BONNE, G. 2011. ColVI myopathies: where do we stand, where do we go? *Skelet Muscle,* 1**,** 2044-5040.

ALMEIDA, C. F., FERNANDES, S. A., RIBEIRO JUNIOR, A. F., KEITH OKAMOTO, O. & VAINZOF, M. 2016. Muscle Satellite Cells: Exploring the Basic Biology to Rule Them. *Stem cells international,* 2016**,** 1078686-1078686.

AMTHOR, H., CHRIST, B. & PATEL, K. 1999. A molecular mechanism enabling continuous embryonic muscle growth - a balance between proliferation and differentiation. *Development,* 126**,** 1041-53.

AMTHOR, H., MACHARIA, R., NAVARRETE, R., SCHUELKE, M., BROWN, S. C., OTTO, A., VOIT, T., MUNTONI, F., VRBÓVA, G., PARTRIDGE, T., ZAMMIT, P., BUNGER, L. & PATEL, K. 2007. Lack of myostatin results in excessive muscle growth but impaired force generation. *Proceedings of the National Academy of Sciences,* 104**,** 1835-1840.

AMTHOR, H., OTTO, A., VULIN, A., ROCHAT, A., DUMONCEAUX, J., GARCIA, L., MOUISEL, E., HOURDE, C., MACHARIA, R., FRIEDRICHS, M., RELAIX, F., ZAMMIT, P. S., MATSAKAS, A., PATEL, K. & PARTRIDGE, T. 2009. Muscle hypertrophy driven by myostatin blockade does not require stem/precursor-cell activity. *Proc Natl Acad Sci U S A,* 106**,** 7479-84.

ANDERSEN, J. L. 2003. Muscle fibre type adaptation in the elderly human muscle. *Scand J Med Sci Sports,* 13**,** 40-7.

ANDERSEN, P. & HENRIKSSON, J. 1977. Training induced changes in the subgroups of human type II skeletal muscle fibres. *Acta Physiol Scand,* 99**,** 123-5.

ANDERSSON, D. C., BETZENHAUSER, M. J., REIKEN, S., MELI, A. C., UMANSKAYA, A., XIE, W., SHIOMI, T., ZALK, R., LACAMPAGNE, A. & MARKS, A. R. 2011. Ryanodine receptor oxidation causes intracellular calcium leak and muscle weakness in aging. *Cell Metab,* 14**,** 196-207.

ANNEX, B. H., TORGAN, C. E., LIN, P., TAYLOR, D. A., THOMPSON, M. A., PETERS, K. G. & KRAUS, W. E. 1998. Induction and maintenance of increased VEGF protein by chronic motor nerve stimulation in skeletal muscle. *Am J Physiol,* 274**,** H860-7.

ANSVED, T. & EDSTROM, L. 1991. Effects of age on fibre structure, ultrastructure and expression of desmin and spectrin in fast- and slow-twitch rat muscles. *J Anat,* 174**,** 61-79.

ANTTINEN, A., KOULU, L., NIKOSKELAINEN, E., PORTIN, R., KURKI, T., ERKINJUNTTI, M., JASPERS, N. G., RAAMS, A., GREEN, M. H., LEHMANN, A. R., WING, J. F., ARLETT, C. F. & MARTTILA, R. J. 2008. Neurological symptoms and natural course of xeroderma pigmentosum. *Brain,* 131**,** 1979-89.

ANTUNES, D., PADRAO, A. I., MACIEL, E., SANTINHA, D., OLIVEIRA, P., VITORINO, R., MOREIRA-GONCALVES, D., COLACO, B., PIRES, M. J., NUNES, C., SANTOS, L. L., AMADO, F., DUARTE, J. A., DOMINGUES, M. R. & FERREIRA, R. 2014. Molecular insights into mitochondrial dysfunction in cancer-related muscle wasting. *Biochim Biophys Acta,* 6**,** 896-905.

AOYAGI, Y. & SHEPHARD, R. J. 1992. Aging and muscle function. *Sports Med,* 14**,** 376-96.

ARANY, Z., FOO, S. Y., MA, Y., RUAS, J. L., BOMMI-REDDY, A., GIRNUN, G., COOPER, M., LAZNIK, D., CHINSOMBOON, J., RANGWALA, S. M., BAEK, K. H., ROSENZWEIG, A. & SPIEGELMAN, B. M. 2008. HIF-independent regulation of VEGF and angiogenesis by the transcriptional coactivator PGC-1alpha. *Nature,* 451**,** 1008-12.

ARBOLEDA, G., RAMIREZ, N. & ARBOLEDA, H. 2007. The neonatal progeroid syndrome (Wiedemann-Rautenstrauch): a model for the study of human aging? *Exp Gerontol,* 42**,** 939-43.

ARBOLEDA, H. & ARBOLEDA, G. 2005. Follow-up study of Wiedemann-Rautenstrauch syndrome: long-term survival and comparison with Rautenstrauch's patient "G". *Birth Defects Res A Clin Mol Teratol,* 73**,** 562-8.

ARBOLEDA, H., QUINTERO, L. & YUNIS, E. 1997. Wiedemann-Rautenstrauch neonatal progeroid syndrome: report of three new patients. *J Med Genet,* 34**,** 433-7.

ARIANO, M. A., ARMSTRONG, R. B. & EDGERTON, V. R. 1973. Hindlimb muscle fiber populations of five mammals. *J Histochem Cytochem,* 21**,** 51-5.

ARMSTRONG, R. 1996. Properties, distribution, and functions of mammalian skeletal muscle fibers. *Exercise bioenergetics and gas exchange. Elsevier/North-Holland Biomedical Press, Amsterdam***,** 137-146.

ARMSTRONG, R. B., DELP, M. D., GOLJAN, E. F. & LAUGHLIN, M. H. 1985. Distribution of blood flow in muscles of miniature swine during exercise. *J Appl Physiol,* 62**,** 1285-98.

ARMSTRONG, R. B. & PHELPS, R. O. 1984. Muscle fiber type composition of the rat hindlimb. *Am J Anat,* 171**,** 259-72.

ARMSTRONG, R. B., SAUBERT, C. W. T., SEEHERMAN, H. J. & TAYLOR, C. R. 1982. Distribution of fiber types in locomotory muscles of dogs. *Am J Anat,* 163**,** 87-98.

ARMSTRONG, R. B., WARREN, G. L. & WARREN, J. A. 1991. Mechanisms of exercise-induced muscle fibre injury. *Sports Med,* 12**,** 184-207.

ARNOLD, H. H. & BRAUN, T. 2000. Genetics of muscle determination and development. *Curr Top Dev Biol,* 48**,** 129-64.

AROUNLEUT, P., BIALEK, P., LIANG, L.-F., UPADHYAY, S., FULZELE, S., JOHNSON, M., ELSALANTY, M., ISALES, C. M. & HAMRICK, M. W. 2013. A myostatin inhibitor (propeptide-Fc) increases muscle mass and muscle fiber size in aged mice but does not increase bone density or bone strength. *Experimental gerontology,* 48**,** 898-904.

ARTAZA, J. N., BHASIN, S., MALLIDIS, C., TAYLOR, W., MA, K. & GONZALEZ-CADAVID, N. F. 2002. Endogenous expression and localization of myostatin and its relation to myosin heavy chain distribution in C2C12 skeletal muscle cells. *J Cell Physiol,* 190**,** 170-9.

ATHERTON, P. J. & SMITH, K. 2012. Muscle protein synthesis in response to nutrition and exercise. *J Physiol,* 590**,** 1049-57.

BAGHDADI, M. B., CASTEL, D., MACHADO, L., FUKADA, S. I., BIRK, D. E., RELAIX, F., TAJBAKHSH, S. & MOURIKIS, P. 2018. Reciprocal signalling by Notch-Collagen V-CALCR retains muscle stem cells in their niche. *Nature,* 557**,** 714-718.

BAJANCA, F., LUZ, M., RAYMOND, K., MARTINS, G. G., SONNENBERG, A., TAJBAKHSH, S., BUCKINGHAM, M. & THORSTEINSDOTTIR, S. 2006. Integrin alpha6beta1-laminin interactions regulate early myotome formation in the mouse embryo. *Development,* 133**,** 1635-44.

BAKER, P. B., BABA, N. & BOESEL, C. P. 1981. Cardiovascular abnormalities in progeria. Case report and review of the literature. *Arch Pathol Lab Med,* 105**,** 384-6.

BALIGAND, C., GILSON, H., MENARD, J. C., SCHAKMAN, O., WARY, C., THISSEN, J. P. & CARLIER, P. G. 2010. Functional assessment of skeletal muscle in intact mice lacking myostatin by concurrent NMR imaging and spectroscopy. *Gene Ther,* 17**,** 328-37.

BANI, C., LAGROTA-CANDIDO, J., PINHEIRO, D. F., LEITE, P. E., SALIMENA, M. C., HENRIQUES-PONS, A. & QUIRICO-SANTOS, T. 2008. Pattern of metalloprotease activity and myofiber regeneration in skeletal muscles of mdx mice. *Muscle Nerve,* 37**,** 583-92.

BARATEAU, A., VADROT, N., AGBULUT, O., VICART, P., BATONNET-PICHON, S. & BUENDIA, B. 2017. Distinct Fiber Type Signature in Mouse Muscles Expressing a Mutant Lamin A Responsible for Congenital Muscular Dystrophy in a Patient. *Cells,* 6.

BARTON-DAVIS, E. R., SHOTURMA, D. I., MUSARO, A., ROSENTHAL, N. & SWEENEY, H. L. 1998. Viral mediated expression of insulin-like growth factor I blocks the aging-related loss of skeletal muscle function. *Proc Natl Acad Sci U S A,* 95**,** 15603-7.

BASSEL-DUBY, R. & OLSON, E. N. 2006. Signaling pathways in skeletal muscle remodeling. *Annu Rev Biochem,* 75**,** 19-37.

BATENBURG, N. L., THOMPSON, E. L., HENDRICKSON, E. A. & ZHU, X. D. 2015. Cockayne syndrome group B protein regulates DNA double-strand break repair and checkpoint activation. *Embo j,* 34**,** 1399-416.

BAUMEISTER, W., WALZ, J., ZUHL, F. & SEEMULLER, E. 1998. The proteasome: paradigm of a self-compartmentalizing protease. *Cell,* 92**,** 367-80.

BECHET, D., TASSA, A., TAILLANDIER, D., COMBARET, L. & ATTAIX, D. 2005. Lysosomal proteolysis in skeletal muscle. *Int J Biochem Cell Biol,* 37**,** 2098-114.

BENAYOUN, B. A., POLLINA, E. A. & BRUNET, A. 2015. Epigenetic regulation of ageing: linking environmental inputs to genomic stability. *Nat Rev Mol Cell Biol,* 16**,** 593-610.

BERG, B. R. & SARELIUS, I. H. 1995. Functional capillary organization in striated muscle. *Am J Physiol,* 268**,** H1215-22.

BERGAMINI, E., CAVALLINI, G., DONATI, A. & GORI, Z. 2004. The role of macroautophagy in the ageing process, anti-ageing intervention and age-associated diseases. *Int J Biochem Cell Biol,* 36**,** 2392-404.

BERGMANN, E. & EGLY, J. M. 2001. Trichothiodystrophy, a transcription syndrome. *Trends Genet,* 17**,** 279-86.

BERGO, M. O., GAVINO, B., ROSS, J., SCHMIDT, W. K., HONG, C., KENDALL, L. V., MOHR, A., META, M., GENANT, H., JIANG, Y., WISNER, E. R., VAN BRUGGEN, N., CARANO, R. A., MICHAELIS, S., GRIFFEY, S. M. & YOUNG, S. G. 2002. Zmpste24 deficiency in mice causes spontaneous bone fractures, muscle weakness, and a prelamin A processing defect. *Proc Natl Acad Sci U S A,* 99**,** 13049-54.

BERNARDO, B. L., LEBRASSEUR, N. K., COSGROVE, P. G., LORIA, P. M., SCHELHORN, T. M. & BROWN, T. A. 2009. Myostatin Inhibition Enhances the Effects of Exercise on Performance and Metabolic Outcomes in Aged Mice. *The Journals of Gerontology: Series A,* 64A**,** 940-948.

BINDOKAS, V. P., JORDAN, J., LEE, C. C. & MILLER, R. J. 1996. Superoxide production in rat hippocampal neurons: selective imaging with hydroethidine. *J Neurosci,* 16**,** 1324-36.

BIRESSI, S., MOLINARO, M. & COSSU, G. 2007. Cellular heterogeneity during vertebrate skeletal muscle development. *Dev Biol,* 308**,** 281-93.

BISCHOFF, R. 1990. Interaction between satellite cells and skeletal muscle fibers. *Development,* 109**,** 943-52.

BISCHOFF, R. 1994. The satellite cell and muscle regeneration. *Myology*.

BISCHOFF, R. & HEINTZ, C. 1994. Enhancement of skeletal muscle regeneration. *Dev Dyn,* 201**,** 41-54.

BLACK, J. O. 2016. Xeroderma Pigmentosum. *Head Neck Pathol,* 10**,** 139-44.

BODNAR, A. G., OUELLETTE, M., FROLKIS, M., HOLT, S. E., CHIU, C. P., MORIN, G. B., HARLEY, C. B., SHAY, J. W., LICHTSTEINER, S. & WRIGHT, W. E. 1998. Extension of life-span by introduction of telomerase into normal human cells. *Science,* 279**,** 349-52.

BOGDANOVICH, S., KRAG, T. O., BARTON, E. R., MORRIS, L. D., WHITTEMORE, L. A., AHIMA, R. S. & KHURANA, T. S. 2002. Functional improvement of dystrophic muscle by myostatin blockade. *Nature,* 420**,** 418-21.

BOGDANOVICH, S., PERKINS, K. J., KRAG, T. O., WHITTEMORE, L. A. & KHURANA, T. S. 2005. Myostatin propeptide-mediated amelioration of dystrophic pathophysiology. *Faseb J,* 19**,** 543-9.

BONALDO, P. & SANDRI, M. 2013. Cellular and molecular mechanisms of muscle atrophy. *Dis Model Mech,* 6**,** 25-39.

BONDULICH, M. K., JOLINON, N., OSBORNE, G. F., SMITH, E. J., RATTRAY, I., NEUEDER, A., SATHASIVAM, K., AHMED, M., ALI, N., BENJAMIN, A. C., CHANG, X., DICK, J. R. T., ELLIS, M., FRANKLIN, S. A., GOODWIN, D., INUABASI, L., LAZELL, H., LEHAR, A., RICHARD-LONDT, A., ROSINSKI, J., SMITH, D. L., WOOD, T., TABRIZI, S. J., BRANDNER, S., GREENSMITH, L., HOWLAND, D., MUNOZ-SANJUAN, I., LEE, S.-J. & BATES, G. P. 2017. Myostatin inhibition prevents skeletal muscle pathophysiology in Huntington's disease mice. *Scientific Reports,* 7**,** 14275.

BONNE, G., DI BARLETTA, M. R., VARNOUS, S., BÉCANE, H. M., HAMMOUDA, E. H., MERLINI, L., MUNTONI, F., GREENBERG, C. R., GARY, F., URTIZBEREA, J. A., DUBOC, D., FARDEAU, M., TONIOLO, D. & SCHWARTZ, K. 1999. Mutations in the gene encoding lamin A/C cause autosomal dominant Emery-Dreifuss muscular dystrophy. *Nat Genet,* 21**,** 285-8.

BOPP, D., BURRI, M., BAUMGARTNER, S., FRIGERIO, G. & NOLL, M. 1986. Conservation of a large protein domain in the segmentation gene paired and in functionally related genes of Drosophila. *Cell,* 47**,** 1033-40.

BORISOV, A. B., DEDKOV, E. I. & CARLSON, B. M. 2001. Interrelations of myogenic response, progressive atrophy of muscle fibers, and cell death in denervated skeletal muscle. *Anat Rec,* 264**,** 203-18.

BORYCKI, A. G. & EMERSON, C. P., JR. 2000. Multiple tissue interactions and signal transduction pathways control somite myogenesis. *Curr Top Dev Biol,* 48**,** 165-224.

BOTTA, E., NARDO, T., LEHMANN, A. R., EGLY, J. M., PEDRINI, A. M. & STEFANINI, M. 2002. Reduced level of the repair/transcription factor TFIIH in trichothiodystrophy. *Hum Mol Genet,* 11**,** 2919-28.

BOVERIS, A., OSHINO, N. & CHANCE, B. 1972. The cellular production of hydrogen peroxide. *Biochem J,* 128**,** 617-30.

BOWEN, T. S., SCHULER, G. & ADAMS, V. 2015. Skeletal muscle wasting in cachexia and sarcopenia: molecular pathophysiology and impact of exercise training. *J Cachexia Sarcopenia Muscle,* 6**,** 197-207.

BRAND-SABERI, B. & CHRIST, B. 2000. Evolution and development of distinct cell lineages derived from somites. *Curr Top Dev Biol,* 48**,** 1-42.

BRAND-SABERI, B., KRENN, V., GRIM, M. & CHRIST, B. 1993. Differences in the fibronectin-dependence of migrating cell populations. *Anat Embryol (Berl),* 187**,** 17-26.

BREITBART, A., AUGER-MESSIER, M., MOLKENTIN, J. D. & HEINEKE, J. 2011. Myostatin from the heart: local and systemic actions in cardiac failure and muscle wasting. *Am J Physiol Heart Circ Physiol,* 300**,** 18.

BROSKEY, N. T., GREGGIO, C., BOSS, A., BOUTANT, M., DWYER, A., SCHLUETER, L., HANS, D., GREMION, G., KREIS, R., BOESCH, C., CANTO, C. & AMATI, F. 2014. Skeletal muscle mitochondria in the elderly: effects of physical fitness and exercise training. *J Clin Endocrinol Metab,* 99**,** 1852-61.

BROWN, W. T. 1992. Progeria: a human-disease model of accelerated aging. *Am J Clin Nutr,* 55**,** 1222s-1224s.

BRUGAROLAS, J., LEI, K., HURLEY, R. L., MANNING, B. D., REILING, J. H., HAFEN, E., WITTERS, L. A., ELLISEN, L. W. & KAELIN, W. G., JR. 2004. Regulation of mTOR function in response to hypoxia by REDD1 and the TSC1/TSC2 tumor suppressor complex. *Genes Dev,* 18**,** 2893-904.

BRUUSGAARD, J. C., LIESTOL, K., EKMARK, M., KOLLSTAD, K. & GUNDERSEN, K. 2003. Number and spatial distribution of nuclei in the muscle fibres of normal mice studied in vivo. *J Physiol,* 551**,** 467-78.

BRZESZCZYNSKA, J., JOHNS, N., SCHILB, A., DEGEN, S., DEGEN, M., LANGEN, R., SCHOLS, A., GLASS, D. J., ROUBENOFF, R., GREIG, C. A., JACOBI, C., FEARON, K. & ROSS, J. A. 2016. Loss of oxidative defense and potential blockade of satellite cell maturation in the skeletal muscle of patients with cancer but not in the healthy elderly. *Aging,* 8**,** 1690-702.

BRZESZCZYNSKA, J., MEYER, A., MCGREGOR, R., SCHILB, A., DEGEN, S., TADINI, V., JOHNS, N., LANGEN, R., SCHOLS, A., GLASS, D. J., ROUBENOFF, R., ROSS, J. A., FEARON, K. C. H., GREIG, C. A. & JACOBI, C. 2018. Alterations in the in vitro and in vivo regulation of muscle regeneration in healthy ageing and the influence of sarcopenia. *J Cachexia Sarcopenia Muscle,* 9**,** 93-105.

BUCKINGHAM, M., BAJARD, L., CHANG, T., DAUBAS, P., HADCHOUEL, J., MEILHAC, S., MONTARRAS, D., ROCANCOURT, D. & RELAIX, F. 2003. The formation of skeletal muscle: from somite to limb. *J Anat,* 202**,** 59-68.

BULLER, A. J., ECCLES, J. C. & ECCLES, R. M. 1960a. Differentiation of fast and slow muscles in the cat hind limb. *J Physiol,* 150**,** 399-416.

BULLER, A. J., ECCLES, J. C. & ECCLES, R. M. 1960b. Interactions between motoneurones and muscles in respect of the characteristic speeds of their responses. *The Journal of Physiology,* 150**,** 417-439.

BURKE, B. & STEWART, C. L. 2002. Life at the edge: the nuclear envelope and human disease. *Nat Rev Mol Cell Biol,* 3**,** 575-85.

BURKITT, H. G., YUONG, B., HEATH, J. W. 1993. Wheater's Functional Histology, A Text and colour Atlas. New York, Churchill livingstone.

CADENA, S. M., TOMKINSON, K. N., MONNELL, T. E., SPAITS, M. S., KUMAR, R., UNDERWOOD, K. W., PEARSALL, R. S. & LACHEY, J. L. 1985. Administration of a soluble activin type IIB receptor promotes skeletal muscle growth independent of fiber type. *J Appl Physiol,* 109**,** 635-42.

CADENA, S. M., TOMKINSON, K. N., MONNELL, T. E., SPAITS, M. S., KUMAR, R., UNDERWOOD, K. W., PEARSALL, R. S. & LACHEY, J. L. 2010. Administration of a soluble activin type IIB receptor promotes skeletal muscle growth independent of fiber type. *J Appl Physiol (1985),* 109**,** 635-42.

CADOT, B., GACHE, V., VASYUTINA, E., FALCONE, S., BIRCHMEIER, C. & GOMES, E. R. 2012. Nuclear movement during myotube formation is microtubule and dynein dependent and is regulated by Cdc42, Par6 and Par3. *EMBO Rep,* 13**,** 741-9.

CAIOZZO, V. J., BAKER, M. J. & BALDWIN, K. M. 1985. Novel transitions in MHC isoforms: separate and combined effects of thyroid hormone and mechanical unloading. *J Appl Physiol,* 85**,** 2237-48.

CALVE, S., ODELBERG, S. J. & SIMON, H. G. 2010. A transitional extracellular matrix instructs cell behavior during muscle regeneration. *Dev Biol,* 344**,** 259-71.

CAMPBELL, K. P. & STULL, J. T. 2003. Skeletal muscle basement membrane-sarcolemma-cytoskeleton interaction minireview series. *J Biol Chem,* 278**,** 12599-600.

CAMPBELL, N. A., REECE, J. B., URRY, L. A., CAIN, M. L., WASSERMAN, S. A., MINORSKY, P. V. & JACKSON, R. 2008. *Biology,* San Francisco, Pearson, Benjamin Cummings.

CAMPISI, J., KIM, S. H., LIM, C. S. & RUBIO, M. 2001. Cellular senescence, cancer and aging: the telomere connection. *Exp Gerontol,* 36**,** 1619-37.

CARLSON, B. M., DEDKOV, E. I., BORISOV, A. B. & FAULKNER, J. A. 2001. Skeletal muscle regeneration in very old rats. *J Gerontol A Biol Sci Med Sci,* 56**,** B224-33.

CARNIO, S., LOVERSO, F., BARAIBAR, M. A., LONGA, E., KHAN, M. M., MAFFEI, M., REISCHL, M., CANEPARI, M., LOEFLER, S., KERN, H., BLAAUW, B., FRIGUET, B., BOTTINELLI, R., RUDOLF, R. & SANDRI, M. 2014. Autophagy impairment in muscle induces neuromuscular junction degeneration and precocious aging. *Cell Rep,* 8**,** 1509-21.

CARRARD, G., BULTEAU, A. L., PETROPOULOS, I. & FRIGUET, B. 2002. Impairment of proteasome structure and function in aging. *Int J Biochem Cell Biol,* 34**,** 1461-74.

CASELLAS, J. 2011. Inbred mouse strains and genetic stability: a review. *Animal,* 5**,** 1-7.

CAU, P., NAVARRO, C., HARHOURI, K., ROLL, P., SIGAUDY, S., KASPI, E., PERRIN, S., DE SANDRE-GIOVANNOLI, A. & LÉVY, N. 2014. Nuclear matrix, nuclear envelope and premature aging syndromes in a translational research perspective. *Semin Cell Dev Biol*.

CAVALLINI, G., STRANIERO, S., DONATI, A. & BERGAMINI, E. 2008. Effects of low level and severe dietary restriction on age-related sarcopenia. *BASIC AND APPLIED MYOLOGY,* 18**,** 121-126.

CEDERHOLM, T., CRUZ-JENTOFT, A. J. & MAGGI, S. 2013. Sarcopenia and fragility fractures. *Eur J Phys Rehabil Med,* 49**,** 111-7.

CHEEMA, N., HERBST, A., MCKENZIE, D. & AIKEN, J. M. 2015. Apoptosis and necrosis mediate skeletal muscle fiber loss in age-induced mitochondrial enzymatic abnormalities. *Aging Cell,* 14**,** 1085-93.

CHEN, C. N., LIN, S. Y., LIAO, Y. H., LI, Z. J. & WONG, A. M. 2015. Late-onset caloric restriction alters skeletal muscle metabolism by modulating pyruvate metabolism. *Am J Physiol Endocrinol Metab,* 308**,** 14.

CHEN, J. L., WALTON, K. L., HAGG, A., COLGAN, T. D., JOHNSON, K., QIAN, H., GREGOREVIC, P. & HARRISON, C. A. 2017. Specific targeting of TGF-β family ligands demonstrates distinct roles in the regulation of muscle mass in health and disease. *Proc Natl Acad Sci U S A,* 114**,** E5266-E5275.

CHEN, X. & LI, Y. 2009. Role of matrix metalloproteinases in skeletal muscle: migration, differentiation, regeneration and fibrosis. *Cell Adh Migr,* 3**,** 337-41.

CHEN, Y., WEI, H., LIU, F. & GUAN, J. L. 2014. Hyperactivation of mammalian target of rapamycin complex 1 (mTORC1) promotes breast cancer progression through enhancing glucose starvation-induced autophagy and Akt signaling. *J Biol Chem,* 289**,** 1164-73.

CHERWEK, D. H., HOPKINS, M. B., THOMPSON, M. J., ANNEX, B. H. & TAYLOR, D. A. 2000. Fiber type-specific differential expression of angiogenic factors in response to chronic hindlimb ischemia. *Am J Physiol Heart Circ Physiol,* 279.

CHRIST, B., JACOB, H. J. & JACOB, M. 1977. Experimental analysis of the origin of the wing musculature in avian embryos. *Anat Embryol (Berl),* 150**,** 171-86.

CHRISTOV, C., CHRETIEN, F., ABOU-KHALIL, R., BASSEZ, G., VALLET, G., AUTHIER, F. J., BASSAGLIA, Y., SHININ, V., TAJBAKHSH, S., CHAZAUD, B. & GHERARDI, R. K. 2007. Muscle satellite cells and endothelial cells: close neighbors and privileged partners. *Mol Biol Cell,* 18**,** 1397-409.

CIPOLAT, S., RUDKA, T., HARTMANN, D., COSTA, V., SERNEELS, L., CRAESSAERTS, K., METZGER, K., FREZZA, C., ANNAERT, W., D'ADAMIO, L., DERKS, C., DEJAEGERE, T., PELLEGRINI, L., D'HOOGE, R., SCORRANO, L. & DE STROOPER, B. 2006. Mitochondrial rhomboid PARL regulates cytochrome c release during apoptosis via OPA1-dependent cristae remodeling. *Cell,* 126**,** 163-75.

CIVILETTO, G., VARANITA, T., CERUTTI, R., GORLETTA, T., BARBARO, S., MARCHET, S., LAMPERTI, C., VISCOMI, C., SCORRANO, L. & ZEVIANI, M. 2015. Opa1 overexpression ameliorates the phenotype of two mitochondrial disease mouse models. *Cell Metab,* 21**,** 845-54.

CLARK, R. K. 2005. *Anatomy and Physiology: Understanding the Human Body*, Jones and Bartlett Publishers.

CLEAVER, J. E. 2004. Defective repair replication of DNA in xeroderma pigmentosum. 1968. *DNA Repair (Amst),* 3**,** 183-87.

COCKAYNE, E. A. 1936. Dwarfism with retinal atrophy and deafness. *Arch Dis Child,* 11**,** 1-8.

COLLINS-HOOPER, H., SARTORI, R., MACHARIA, R., VISANUVIMOL, K., FOSTER, K., MATSAKAS, A., FLASSKAMP, H., RAY, S., DASH, P. R., SANDRI, M. & PATEL, K. 2014. Propeptide-mediated inhibition of myostatin increases muscle mass through inhibiting proteolytic pathways in aged mice. *J Gerontol A Biol Sci Med Sci,* 69**,** 1049-59.

COLLINS, C. A., OLSEN, I., ZAMMIT, P. S., HESLOP, L., PETRIE, A., PARTRIDGE, T. A. & MORGAN, J. E. 2005. Stem cell function, self-renewal, and behavioral heterogeneity of cells from the adult muscle satellite cell niche. *Cell,* 122**,** 289-301.

CONTROL, C. F. D. & PREVENTION 2003. Trends in aging--United States and worldwide. *MMWR Morb Mortal Wkly Rep,* 52**,** 101-4, 106.

COOPER, G. M., & HAUSMAN, R. E. 2007. *THE CELL A Molecular Approach,* USA, ASM press and Sinauer Associates.

CORNELISON, D. D. & WOLD, B. J. 1997. Single-cell analysis of regulatory gene expression in quiescent and activated mouse skeletal muscle satellite cells. *Dev Biol,* 191**,** 270-83.

COVINSKY, K. E., PALMER, R. M., FORTINSKY, R. H., COUNSELL, S. R., STEWART, A. L., KRESEVIC, D., BURANT, C. J. & LANDEFELD, C. S. 2003. Loss of independence in activities of daily living in older adults hospitalized with medical illnesses: increased vulnerability with age. *J Am Geriatr Soc,* 51**,** 451-8.

CROALL, D. E. & ERSFELD, K. 2007. The calpains: modular designs and functional diversity. *Genome Biol,* 8**,** 218.

CRUZ-JENTOFT, A. J., BAEYENS, J. P., BAUER, J. M., BOIRIE, Y., CEDERHOLM, T., LANDI, F., MARTIN, F. C., MICHEL, J.-P., ROLLAND, Y., SCHNEIDER, S. M., TOPINKOVÁ, E., VANDEWOUDE, M., ZAMBONI, M. & PEOPLE, E. W. G. O. S. I. O. 2010. Sarcopenia: European consensus on definition and diagnosis: Report of the European Working Group on Sarcopenia in Older People. *Age Ageing,* 39**,** 412-23.

D'ANTONA, G., PELLEGRINO, M. A., ADAMI, R., ROSSI, R., CARLIZZI, C. N., CANEPARI, M., SALTIN, B. & BOTTINELLI, R. 2003. The effect of ageing and immobilization on structure and function of human skeletal muscle fibres. *J Physiol,* 552**,** 499-511.

DAY, K., SHEFER, G., SHEARER, A. & YABLONKA-REUVENI, Z. 2010. The depletion of skeletal muscle satellite cells with age is concomitant with reduced capacity of single progenitors to produce reserve progeny. *Developmental biology,* 340**,** 330-343.

DE ANDRADE, P. B. M., NEFF, L. A., STROSOVA, M. K., ARSENIJEVIC, D., PATTHEY-VUADENS, O., SCAPOZZA, L., MONTANI, J.-P., RUEGG, U. T., DULLOO, A. G. & DORCHIES, O. M. 2015. Caloric restriction induces energy-sparing alterations in skeletal muscle contraction, fiber composition and local thyroid hormone metabolism that persist during catch-up fat upon refeeding. *Frontiers in physiology,* 6**,** 254-254.

DE BOER, J. & HOEIJMAKERS, J. H. 2000. Nucleotide excision repair and human syndromes. *Carcinogenesis,* 21**,** 453-60.

DE ONIS, M. 2015. 4.1 The WHO Child Growth Standards. *World Rev Nutr Diet,* 113**,** 278-94.

DEBUSK, F. L. 1972. The Hutchinson-Gilford progeria syndrome. Report of 4 cases and review of the literature. *J Pediatr,* 80**,** 697-724.

DELFINI, M. C., HIRSINGER, E., POURQUIE, O. & DUPREZ, D. 2000. Delta 1-activated notch inhibits muscle differentiation without affecting Myf5 and Pax3 expression in chick limb myogenesis. *Development,* 127**,** 5213-24.

DELMONICO, M. J., HARRIS, T. B., LEE, J. S., VISSER, M., NEVITT, M., KRITCHEVSKY, S. B., TYLAVSKY, F. A. & NEWMAN, A. B. 2007. Alternative definitions of sarcopenia, lower extremity

performance, and functional impairment with aging in older men and women. *J Am Geriatr Soc,* 55**,** 769-74.

DELP, M. D. & DUAN, C. 1985. Composition and size of type I, IIA, IID/X, and IIB fibers and citrate synthase activity of rat muscle. *J Appl Physiol,* 80**,** 261-70.

DENG, B., ZHANG, F., WEN, J., YE, S., WANG, L., YANG, Y., GONG, P. & JIANG, S. 2017. The function of myostatin in the regulation of fat mass in mammals. *Nutrition & metabolism,* 14**,** 29-29.

DEUTZ, N. E., BAUER, J. M., BARAZZONI, R., BIOLO, G., BOIRIE, Y., BOSY-WESTPHAL, A., CEDERHOLM, T., CRUZ-JENTOFT, A., KRZNARIC, Z., NAIR, K. S., SINGER, P., TETA, D., TIPTON, K. & CALDER, P. C. 2014. Protein intake and exercise for optimal muscle function with aging: recommendations from the ESPEN Expert Group. *Clin Nutr,* 33**,** 929-36.

DEVOS, E. A., LEROY, J. G., FRIJNS, J. P. & VAN DEN BERGHE, H. 1981. The Wiedemann-Rautenstrauch or neonatal progeroid syndrome. Report of a patient with consanguineous parents. *Eur J Pediatr,* 136**,** 245-8.

DIAZ, G., LIU, S., ISOLA, R., DIANA, A. & FALCHI, A. M. 2003. Mitochondrial localization of reactive oxygen species by dihydrofluorescein probes. *Histochem Cell Biol,* 120**,** 319-25.

DICKINSON, J. M., FRY, C. S., DRUMMOND, M. J., GUNDERMANN, D. M., WALKER, D. K., GLYNN, E. L., TIMMERMAN, K. L., DHANANI, S., VOLPI, E. & RASMUSSEN, B. B. 2011. Mammalian target of rapamycin complex 1 activation is required for the stimulation of human skeletal muscle protein synthesis by essential amino acids. *J Nutr,* 141**,** 856-62.

DIETRICH, S., ABOU-REBYEH, F., BROHMANN, H., BLADT, F., SONNENBERG-RIETHMACHER, E., YAMAAI, T., LUMSDEN, A., BRAND-SABERI, B. & BIRCHMEIER, C. 1999. The role of SF/HGF and c-Met in the development of skeletal muscle. *Development,* 126**,** 1621-9.

DIGIOVANNA, J. J. & KRAEMER, K. H. 2012. Shining a light on xeroderma pigmentosum. *J Invest Dermatol,* 132**,** 785-96.

DIRKS, A. & LEEUWENBURGH, C. 2002. Apoptosis in skeletal muscle with aging. *Am J Physiol Regul Integr Comp Physiol,* 282.

DODD, S. L., GAGNON, B. J., SENF, S. M., HAIN, B. A. & JUDGE, A. R. 2010. Ros-mediated activation of NF-kappaB and Foxo during muscle disuse. *Muscle Nerve,* 41**,** 110-3.

DOLLE, M. E., KUIPER, R. V., ROODBERGEN, M., ROBINSON, J., DE VLUGT, S., WIJNHOVEN, S. W., BEEMS, R. B., DE LA FONTEYNE, L., DE WITH, P., VAN DER PLUIJM, I., NIEDERNHOFER, L. J., HASTY, P., VIJG, J., HOEIJMAKERS, J. H. & VAN STEEG, H. 2011. Broad segmental progeroid changes in short-lived Ercc1(-/Delta7) mice. *Pathobiol Aging Age Relat Dis,* 1.

DOLLÉ, M. E. T., KUIPER, R. V., ROODBERGEN, M., ROBINSON, J., DE VLUGT, S., WIJNHOVEN, S. W. P., BEEMS, R. B., DE LA FONTEYNE, L., DE WITH, P., VAN DER PLUIJM, I., NIEDERNHOFER, L. J., HASTY, P., VIJG, J., HOEIJMAKERS, J. H. J. & VAN STEEG, H. 2011. Broad segmental progeroid changes in short-lived Ercc1(-/Δ7) mice. *Pathobiology of aging & age related diseases,* 1**,** 10.3402/pba.v1i0.7219.

DONG, X., MILHOLLAND, B. & VIJG, J. 2016. Evidence for a limit to human lifespan. *Nature,* 538**,** 257-259.

DORAN, P., DONOGHUE, P., O'CONNELL, K., GANNON, J. & OHLENDIECK, K. 2009. Proteomics of skeletal muscle aging. *Proteomics,* 9**,** 989-1003.

DRUMMOND, M. J., FRY, C. S., GLYNN, E. L., DREYER, H. C., DHANANI, S., TIMMERMAN, K. L., VOLPI, E. & RASMUSSEN, B. B. 2009. Rapamycin administration in humans blocks the contraction-induced increase in skeletal muscle protein synthesis. *J Physiol,* 587**,** 1535-46.

DUDDY, W., DUGUEZ, S., JOHNSTON, H., COHEN, T. V., PHADKE, A., GORDISH-DRESSMAN, H., NAGARAJU, K., GNOCCHI, V., LOW, S. & PARTRIDGE, T. 2015. Muscular dystrophy in the mdx mouse is a severe myopathy compounded by hypotrophy, hypertrophy and hyperplasia. *Skelet Muscle,* 5**,** 16.

DURIEUX, A. C., AMIROUCHE, A., BANZET, S., KOULMANN, N., BONNEFOY, R., PASDELOUP, M., MOURET, C., BIGARD, X., PEINNEQUIN, A. & FREYSSENET, D. 2007. Ectopic expression of

myostatin induces atrophy of adult skeletal muscle by decreasing muscle gene expression. *Endocrinology,* 148**,** 3140-7.

EDIFIZI, D. & SCHUMACHER, B. 2015. Genome Instability in Development and Aging: Insights from Nucleotide Excision Repair in Humans, Mice, and Worms. *Biomolecules,* 5**,** 1855-69.

EDOM-VOVARD, F., BONNIN, M. A. & DUPREZ, D. 2001. Misexpression of Fgf-4 in the chick limb inhibits myogenesis by down-regulating Frek expression. *Dev Biol,* 233**,** 56-71.

EDSTRÖM, E. & ULFHAKE, B. 2005. Sarcopenia is not due to lack of regenerative drive in senescent skeletal muscle. *Aging Cell,* 4**,** 65-77.

ELLIOTT, B., RENSHAW, D., GETTING, S. & MACKENZIE, R. 2012. The central role of myostatin in skeletal muscle and whole body homeostasis. *Acta Physiol,* 205**,** 324-40.

ELLISEN, L. W., RAMSAYER, K. D., JOHANNESSEN, C. M., YANG, A., BEPPU, H., MINDA, K., OLINER, J. D., MCKEON, F. & HABER, D. A. 2002. REDD1, a developmentally regulated transcriptional target of p63 and p53, links p63 to regulation of reactive oxygen species. *Mol Cell,* 10**,** 995-1005.

ENGLISH, K. L. & PADDON-JONES, D. 2010. Protecting muscle mass and function in older adults during bed rest. *Current opinion in clinical nutrition and metabolic care,* 13**,** 34-39.

EPSTEIN, J. A., SHAPIRO, D. N., CHENG, J., LAM, P. Y. & MAAS, R. L. 1996. Pax3 modulates expression of the c-Met receptor during limb muscle development. *Proc Natl Acad Sci U S A,* 93**,** 4213-8.

ERIKSSON, M., BROWN, W. T., GORDON, L. B., GLYNN, M. W., SINGER, J., SCOTT, L., ERDOS, M. R., ROBBINS, C. M., MOSES, T. Y., BERGLUND, P., DUTRA, A., PAK, E., DURKIN, S., CSOKA, A. B., BOEHNKE, M., GLOVER, T. W. & COLLINS, F. S. 2003. Recurrent de novo point mutations in lamin A cause Hutchinson-Gilford progeria syndrome. *Nature,* 423**,** 293-8.

ERVASTI, J. M. & CAMPBELL, K. P. 1993. A role for the dystrophin-glycoprotein complex as a transmembrane linker between laminin and actin. *J Cell Biol,* 122**,** 809-23.

EVANS, W. E. & RELLING, M. V. 1999. Pharmacogenomics: translating functional genomics into rational therapeutics. *Science,* 286**,** 487-91.

FABER, R. M., HALL, J. K., CHAMBERLAIN, J. S. & BANKS, G. B. 2014. Myofiber branching rather than myofiber hyperplasia contributes to muscle hypertrophy in mdx mice. *Skelet Muscle,* 4**,** 2044-5040.

FAGIOLO, U., COSSARIZZA, A., SCALA, E., FANALES-BELASIO, E., ORTOLANI, C., COZZI, E., MONTI, D., FRANCESCHI, C. & PAGANELLI, R. 1993. Increased cytokine production in mononuclear cells of healthy elderly people. *Eur J Immunol,* 23**,** 2375-8.

FELDMAN, B. J., STREEPER, R. S., FARESE, R. V., JR. & YAMAMOTO, K. R. 2006. Myostatin modulates adipogenesis to generate adipocytes with favorable metabolic effects. *Proc Natl Acad Sci U S A,* 103**,** 15675-80.

FERRINGTON, D. A., HUSOM, A. D. & THOMPSON, L. V. 2005. Altered proteasome structure, function, and oxidation in aged muscle. *Faseb j,* 19**,** 644-6.

FIELDING, R. A., VELLAS, B., EVANS, W. J., BHASIN, S., MORLEY, J. E., NEWMAN, A. B., ABELLAN VAN KAN, G., ANDRIEU, S., BAUER, J., BREUILLE, D., CEDERHOLM, T., CHANDLER, J., DE MEYNARD, C., DONINI, L., HARRIS, T., KANNT, A., KEIME GUIBERT, F., ONDER, G., PAPANICOLAOU, D., ROLLAND, Y., ROOKS, D., SIEBER, C., SOUHAMI, E., VERLAAN, S. & ZAMBONI, M. 2011. Sarcopenia: an undiagnosed condition in older adults. Current consensus definition: prevalence, etiology, and consequences. International working group on sarcopenia. *J Am Med Dir Assoc,* 12**,** 249-56.

FIEMS, L. O. 2012. Double Muscling in Cattle: Genes, Husbandry, Carcasses and Meat. *Animals : an open access journal from MDPI,* 2**,** 472-506.

FLASSKAMP, H., COLLINS-HOOPER, H., FOSTER, K., PATEL, K., VISANUVIMOL, K., DASH, P. R., SANDRI, M., SARTORI, R., MACHARIA, R., MATSAKAS, A. & RAY, S. 2014. Propeptide-Mediated Inhibition of Myostatin Increases Muscle Mass Through Inhibiting Proteolytic Pathways in Aged Mice. *The Journals of Gerontology: Series A,* 69**,** 1049-1059.

FLOSS, T., ARNOLD, H. H. & BRAUN, T. 1997. A role for FGF-6 in skeletal muscle regeneration. *Genes Dev,* 11**,** 2040-51.

FOLKER, E. S. & BAYLIES, M. K. 2013. Nuclear positioning in muscle development and disease. *Front Physiol,* 4**,** 363.

FONTANA, L., PARTRIDGE, L. & LONGO, V. D. 2010. Extending healthy life span--from yeast to humans. *Science,* 328**,** 321-6.

FOSTER, K., GRAHAM, I. R., OTTO, A., FOSTER, H., TROLLET, C., YAWORSKY, P. J., WALSH, F. S., BICKHAM, D., CURTIN, N. A., KAWAR, S. L., PATEL, K. & DICKSON, G. 2009. Adeno-associated virus-8-mediated intravenous transfer of myostatin propeptide leads to systemic functional improvements of slow but not fast muscle. *Rejuvenation Res,* 12**,** 85-94.

FRANK, S., GAUME, B., BERGMANN-LEITNER, E. S., LEITNER, W. W., ROBERT, E. G., CATEZ, F., SMITH, C. L. & YOULE, R. J. 2001. The role of dynamin-related protein 1, a mediator of mitochondrial fission, in apoptosis. *Dev Cell,* 1**,** 515-25.

FRESNO VARA, J. A., CASADO, E., DE CASTRO, J., CEJAS, P., BELDA-INIESTA, C. & GONZÁLEZ-BARÓN, M. 2004. PI3K/Akt signalling pathway and cancer. *Cancer Treat Rev,* 30**,** 193-204.

FRIES, J. F. 2002. Aging, natural death, and the compression of morbidity. 1980. *Bull World Health Organ,* 80**,** 245-50.

FRONTERA, W. R. & OCHALA, J. 2015. Skeletal muscle: a brief review of structure and function. *Calcif Tissue Int,* 96**,** 183-95.

FRY, C. S., LEE, J. D., MULA, J., KIRBY, T. J., JACKSON, J. R., LIU, F., YANG, L., MENDIAS, C. L., DUPONT-VERSTEEGDEN, E. E., MCCARTHY, J. J. & PETERSON, C. A. 2015. Inducible depletion of satellite cells in adult, sedentary mice impairs muscle regenerative capacity without affecting sarcopenia. *Nat Med,* 21**,** 76-80.

FÜCHTBAUER, E.-M. 2002. Inhibition of skeletal muscle development: less differentiation gives more muscle. *Results Probl Cell Differ,* 38**,** 143-61.

FUCHTBAUER, E. M. 1995. Expression of M-twist during postimplantation development of the mouse. *Dev Dyn,* 204**,** 316-22.

FUENTES, I., COBOS, A. R. & SEGADE, L. A. 1998. Muscle fibre types and their distribution in the biceps and triceps brachii of the rat and rabbit. *J Anat,* 192**,** 203-10.

GARCIA-PRAT, L., MARTINEZ-VICENTE, M., PERDIGUERO, E., ORTET, L., RODRIGUEZ-UBREVA, J., REBOLLO, E., RUIZ-BONILLA, V., GUTARRA, S., BALLESTAR, E., SERRANO, A. L., SANDRI, M. & MUNOZ-CANOVES, P. 2016. Autophagy maintains stemness by preventing senescence. *Nature,* 529**,** 37-42.

GARCIA-ROVES, P. M., OSLER, M. E., HOLMSTROM, M. H. & ZIERATH, J. R. 2008. Gain-of-function R225Q mutation in AMP-activated protein kinase gamma3 subunit increases mitochondrial biogenesis in glycolytic skeletal muscle. *J Biol Chem,* 283**,** 35724-34.

GARINIS, G. A., UITTENBOOGAARD, L. M., STACHELSCHEID, H., FOUSTERI, M., VAN IJCKEN, W., BREIT, T. M., VAN STEEG, H., MULLENDERS, L. H., VAN DER HORST, G. T., BRUNING, J. C., NIESSEN, C. M., HOEIJMAKERS, J. H. & SCHUMACHER, B. 2009. Persistent transcription-blocking DNA lesions trigger somatic growth attenuation associated with longevity. *Nat Cell Biol,* 11**,** 604-15.

GATCHALIAN, C. L., SCHACHNER, M. & SANES, J. R. 1989. Fibroblasts that proliferate near denervated synaptic sites in skeletal muscle synthesize the adhesive molecules tenascin(J1), N-CAM, fibronectin, and a heparan sulfate proteoglycan. *J Cell Biol,* 108**,** 1873-90.

GAUDEL, C., SCHWARTZ, C., GIORDANO, C., ABUMRAD, N. A. & GRIMALDI, P. A. 2008. Pharmacological activation of PPARbeta promotes rapid and calcineurin-dependent fiber remodeling and angiogenesis in mouse skeletal muscle. *Am J Physiol Endocrinol Metab,* 295**,** 20.

GELFI, C., VIGANO, A., RIPAMONTI, M., PONTOGLIO, A., BEGUM, S., PELLEGRINO, M. A., GRASSI, B., BOTTINELLI, R., WAIT, R. & CERRETELLI, P. 2006. The human muscle proteome in aging. *J Proteome Res,* 5**,** 1344-53.

GENSLER, H. L. & BERNSTEIN, H. 1981. DNA damage as the primary cause of aging. *Q Rev Biol,* 56**,** 279-303.

GIBSON, M. C. & SCHULTZ, E. 1983. Age-related differences in absolute numbers of skeletal muscle satellite cells. *Muscle Nerve,* 6**,** 574-80.

GILLIES, A. R., BUSHONG, E. A., DEERINCK, T. J., ELLISMAN, M. H. & LIEBER, R. L. 2014. Three-dimensional reconstruction of skeletal muscle extracellular matrix ultrastructure. *Microsc Microanal,* 20**,** 1835-40.

GILLIES, A. R. & LIEBER, R. L. 2011. Structure and function of the skeletal muscle extracellular matrix. *Muscle Nerve,* 44**,** 318-31.

GIRGENRATH, S., SONG, K. & WHITTEMORE, L. A. 2005. Loss of myostatin expression alters fiber-type distribution and expression of myosin heavy chain isoforms in slow- and fast-type skeletal muscle. *Muscle Nerve,* 31**,** 34-40.

GLASS, D. J. 2005. Skeletal muscle hypertrophy and atrophy signaling pathways. *Int J Biochem Cell Biol,* 37**,** 1974-84.

GLICKMAN, M. H. & CIECHANOVER, A. 2002. The ubiquitin-proteasome proteolytic pathway: destruction for the sake of construction. *Physiol Rev,* 82**,** 373-428.

GOLAN, T., GEVA, R., RICHARDS, D., MADHUSUDAN, S., LIN, B. K., WANG, H. T., WALGREN, R. A. & STEMMER, S. M. 2018. LY2495655, an antimyostatin antibody, in pancreatic cancer: a randomized, phase 2 trial. *Journal of cachexia, sarcopenia and muscle,* 9**,** 871-879.

GOLLNICK, P. D., ARMSTRONG, R., SALTIN, B., SAUBERT 4TH, C., SEMBROWICH, W. L. & SHEPHERD, R. E. 1973. Effect of training on enzyme activity and fiber composition of human skeletal muscle. *Journal of applied physiology,* 34**,** 107-111.

GOMES, M. J., MARTINEZ, P. F., PAGAN, L. U., DAMATTO, R. L., CEZAR, M. D. M., LIMA, A. R. R., OKOSHI, K. & OKOSHI, M. P. 2017. Skeletal muscle aging: influence of oxidative stress and physical exercise. *Oncotarget,* 8**,** 20428-20440.

GONZALEZ-CADAVID, N. F., TAYLOR, W. E., YARASHESKI, K., SINHA-HIKIM, I., MA, K., EZZAT, S., SHEN, R., LALANI, R., ASA, S., MAMITA, M., NAIR, G., ARVER, S. & BHASIN, S. 1998. Organization of the human myostatin gene and expression in healthy men and HIV-infected men with muscle wasting. *Proc Natl Acad Sci U S A,* 95**,** 14938-43.

GOULDING, M., LUMSDEN, A. & PAQUETTE, A. J. 1994. Regulation of Pax-3 expression in the dermomyotome and its role in muscle development. *Development,* 120**,** 957-71.

GOULDING, M. D., CHALEPAKIS, G., DEUTSCH, U., ERSELIUS, J. R. & GRUSS, P. 1991. Pax-3, a novel murine DNA binding protein expressed during early neurogenesis. *Embo J,* 10**,** 1135-47.

GRAY, H., WILLIAMS, P. L. & BANNISTER, L. H. 1995. *Gray's Anatomy: The Anatomical Basis of Medicine and Surgery*, Churchill Livingstone.

GRAY, M. D., SHEN, J. C., KAMATH-LOEB, A. S., BLANK, A., SOPHER, B. L., MARTIN, G. M., OSHIMA, J. & LOEB, L. A. 1997. The Werner syndrome protein is a DNA helicase. *Nat Genet,* 17**,** 100-3.

GREEN, H. J., THOMSON, J. A., DAUB, W. D., HOUSTON, M. E. & RANNEY, D. A. 1979. Fiber composition, fiber size and enzyme activities in vastus lateralis of elite athletes involved in high intensity exercise. *Eur J Appl Physiol Occup Physiol,* 41**,** 109-17.

GREGG, S. Q., GUTIERREZ, V., ROBINSON, A. R., WOODELL, T., NAKAO, A., ROSS, M. A., MICHALOPOULOS, G. K., RIGATTI, L., ROTHERMEL, C. E., KAMILERI, I., GARINIS, G. A., STOLZ, D. B. & NIEDERNHOFER, L. J. 2012. A mouse model of accelerated liver aging caused by a defect in DNA repair. *Hepatology,* 55**,** 609-21.

GREISING, S. M., CALL, J. A., LUND, T. C., BLAZAR, B. R., TOLAR, J. & LOWE, D. A. 2012. Skeletal muscle contractile function and neuromuscular performance in Zmpste24 -/- mice, a murine model of human progeria. *Age (Dordr),* 34**,** 805-19.

GRIM, M. & WACHTLER, F. 1991. Muscle morphogenesis in the absence of myogenic cells. *Anat Embryol (Berl),* 183**,** 67-70.

GRINSPOON, S., MULLIGAN, K., HEALTH, D. O., PREVENTION, H. S. W. G. O. T., WASTING, T. O. & LOSS, W. 2003. Weight loss and wasting in patients infected with human immunodeficiency virus. *Clin Infect Dis,* 36**,** S69-78.

GROBET, L., MARTIN, L. J. R., PONCELET, D., PIROTTIN, D., BROUWERS, B., RIQUET, J., SCHOEBERLEIN, A., DUNNER, S., MÉNISSIER, F. & MASSABANDA, J. 1997. A deletion in the bovine myostatin gene causes the double–muscled phenotype in cattle. *Nature genetics,* 17**,** 71.

GROEN, B. B., HAMER, H. M., SNIJDERS, T., VAN KRANENBURG, J., FRIJNS, D., VINK, H. & VAN LOON, L. J. 1985. Skeletal muscle capillary density and microvascular function are compromised with aging and type 2 diabetes. *J Appl Physiol,* 116**,** 998-1005.

GROISMAN, R., KURAOKA, I., CHEVALLIER, O., GAYE, N., MAGNALDO, T., TANAKA, K., KISSELEV, A. F., HAREL-BELLAN, A. & NAKATANI, Y. 2006. CSA-dependent degradation of CSB by the ubiquitin-proteasome pathway establishes a link between complementation factors of the Cockayne syndrome. *Genes Dev,* 20**,** 1429-34.

GROS, J., MANCEAU, M., THOME, V. & MARCELLE, C. 2005. A common somitic origin for embryonic muscle progenitors and satellite cells. *Nature,* 435**,** 954-8.

GUARENTE, L. & KENYON, C. 2000. Genetic pathways that regulate ageing in model organisms. *Nature,* 408**,** 255-62.

GUDBJORNSDOTTIR, S., SJOSTRAND, M., STRINDBERG, L., WAHREN, J. & LONNROTH, P. 2003. Direct measurements of the permeability surface area for insulin and glucose in human skeletal muscle. *J Clin Endocrinol Metab,* 88**,** 4559-64.

GUMERSON, J. D. & MICHELE, D. E. 2011. The dystrophin-glycoprotein complex in the prevention of muscle damage. *J Biomed Biotechnol,* 210797**,** 5.

GUO, W., MILLER, A. D., PENCINA, K., WONG, S., LEE, A., YEE, M., TORALDO, G., JASUJA, R. & BHASIN, S. 2016. Joint dysfunction and functional decline in middle age myostatin null mice. *Bone,* 83**,** 141-148.

GURALNIK, J. M., FERRUCCI, L., PIEPER, C. F., LEVEILLE, S. G., MARKIDES, K. S., OSTIR, G. V., STUDENSKI, S., BERKMAN, L. F. & WALLACE, R. B. 2000. Lower extremity function and subsequent disability: consistency across studies, predictive models, and value of gait speed alone compared with the short physical performance battery. *J Gerontol A Biol Sci Med Sci,* 55**,** M221-31.

GUTMAN, B. & HANZLIKOVA, V. 1972. *Age Changes in the Neuromuscular System,* Bristol, Scientechnica Ltd.

GUTMANN, E. & HANZLIKOVA, V. 1966. Motor unit in old age. *Nature,* 209**,** 921-2.

GUZDER, S. N., SUNG, P., BAILLY, V., PRAKASH, L. & PRAKASH, S. 1994. RAD25 is a DNA helicase required for DNA repair and RNA polymerase II transcription. *Nature,* 369**,** 578-81.

HAIDET, A. M., RIZO, L., HANDY, C., UMAPATHI, P., EAGLE, A., SHILLING, C., BOUE, D., MARTIN, P. T., SAHENK, Z., MENDELL, J. R. & KASPAR, B. K. 2008. Long-term enhancement of skeletal muscle mass and strength by single gene administration of myostatin inhibitors. *Proc Natl Acad Sci U S A,* 105**,** 4318-22.

HAMALAINEN, N. & PETTE, D. 1993. The histochemical profiles of fast fiber types IIB, IID, and IIA in skeletal muscles of mouse, rat, and rabbit. *J Histochem Cytochem,* 41**,** 733-43.

HAMRICK, M. W., AROUNLEUT, P., KELLUM, E., CAIN, M., IMMEL, D. & LIANG, L.-F. 2010. Recombinant myostatin (GDF-8) propeptide enhances the repair and regeneration of both muscle and bone in a model of deep penetrant musculoskeletal injury. *The Journal of trauma,* 69**,** 579-583.

HAMRICK, M. W., DING, K. H., PENNINGTON, C., CHAO, Y. J., WU, Y. D., HOWARD, B., IMMEL, D., BORLONGAN, C., MCNEIL, P. L., BOLLAG, W. B., CURL, W. W., YU, J. & ISALES, C. M. 2006.

Age-related loss of muscle mass and bone strength in mice is associated with a decline in physical activity and serum leptin. *Bone,* 39**,** 845-53.

HAN, D., WILLIAMS, E. & CADENAS, E. 2001. Mitochondrial respiratory chain-dependent generation of superoxide anion and its release into the intermembrane space. *Biochem J,* 353**,** 411-6.

HARDY, S. E., KANG, Y., STUDENSKI, S. A. & DEGENHOLTZ, H. B. 2011. Ability to walk 1/4 mile predicts subsequent disability, mortality, and health care costs. *J Gen Intern Med,* 26**,** 130-5.

HARPER, M. E., BEVILACQUA, L., HAGOPIAN, K., WEINDRUCH, R. & RAMSEY, J. J. 2004. Ageing, oxidative stress, and mitochondrial uncoupling. *Acta Physiol Scand,* 182**,** 321-31.

HASHIMOTO, S. & EGLY, J. M. 2009. Trichothiodystrophy view from the molecular basis of DNA repair/transcription factor TFIIH. *Hum Mol Genet,* 18**,** R224-30.

HASTINGS, K. E. & EMERSON, C. P., JR. 1982. cDNA clone analysis of six co-regulated mRNAs encoding skeletal muscle contractile proteins. *Proc Natl Acad Sci U S A,* 79**,** 1553-7.

HASTY, P., CAMPISI, J., HOEIJMAKERS, J., VAN STEEG, H. & VIJG, J. 2003. Aging and genome maintenance: lessons from the mouse? *Science,* 299**,** 1355-9.

HAUS, J. M., CARRITHERS, J. A., TRAPPE, S. W. & TRAPPE, T. A. 1985. Collagen, cross-linking, and advanced glycation end products in aging human skeletal muscle. *J Appl Physiol,* 103**,** 2068-76.

HAYNES, C. M. & RON, D. 2010. The mitochondrial UPR - protecting organelle protein homeostasis. *J Cell Sci,* 123**,** 3849-55.

HERING, T., BRAUBACH, P., LANDWEHRMEYER, G. B., LINDENBERG, K. S. & MELZER, W. 2016. Fast-to-Slow Transition of Skeletal Muscle Contractile Function and Corresponding Changes in Myosin Heavy and Light Chain Formation in the R6/2 Mouse Model of Huntington's Disease. *PLoS One,* 11.

HICKEY, M. S., CAREY, J. O., AZEVEDO, J. L., HOUMARD, J. A., PORIES, W. J., ISRAEL, R. G. & DOHM, G. L. 1995. Skeletal muscle fiber composition is related to adiposity and in vitro glucose transport rate in humans. *Am J Physiol,* 268.

HIKIDA, R. S. 2011. Aging changes in satellite cells and their functions. *Curr Aging Sci,* 4**,** 279-97.

HINKAL, G. & DONEHOWER, L. A. 2008. How does suppression of IGF-1 signaling by DNA damage affect aging and longevity? *Mech Ageing Dev,* 129**,** 243-53.

HIONA, A. & LEEUWENBURGH, C. 2008. The role of mitochondrial DNA mutations in aging and sarcopenia: implications for the mitochondrial vicious cycle theory of aging. *Exp Gerontol,* 43**,** 24-33.

HOEIJMAKERS, J. H. 2009. DNA damage, aging, and cancer. *N Engl J Med,* 361**,** 1475-85.

HOFFMAN, E. P., BROWN, R. H., JR. & KUNKEL, L. M. 1987. Dystrophin: the protein product of the Duchenne muscular dystrophy locus. *Cell,* 51**,** 919-28.

HOLLOSZY, J. O. 1967. Biochemical adaptations in muscle effects of exercise on mitochondrial oxygen uptake and respiratory enzyme activity in skeletal muscle. *Journal of Biological Chemistry,* 242**,** 2278-2282.

HOLLOSZY, J. O. & BOOTH, F. W. 1976. Biochemical adaptations to endurance exercise in muscle. *Annual review of physiology,* 38**,** 273-291.

HOLLOSZY, J. O., CHEN, M., CARTEE, G. D. & YOUNG, J. C. 1991. Skeletal muscle atrophy in old rats: differential changes in the three fiber types. *Mech Ageing Dev,* 60**,** 199-213.

HOPPELER, H. 2016. Molecular networks in skeletal muscle plasticity. *J Exp Biol,* 219**,** 205-13.

HORTON, M. J., BRANDON, C. A., MORRIS, T. J., BRAUN, T. W., YAW, K. M. & SCIOTE, J. J. 2001. Abundant expression of myosin heavy-chain IIB RNA in a subset of human masseter muscle fibres. *Arch Oral Biol,* 46**,** 1039-50.

HOUZELSTEIN, D., AUDA-BOUCHER, G., CHÉRAUD, Y., ROUAUD, T., BLANC, I., TAJBAKHSH, S., BUCKINGHAM, M. E., FONTAINE-PÉRUS, J. & ROBERT, B. 1999. The homeobox gene Msx1 is expressed in a subset of somites, and in muscle progenitor cells migrating into the forelimb. *Development,* 126**,** 2689-701.

HOWALD, H., HOPPELER, H., CLAASSEN, H., MATHIEU, O. & STRAUB, R. 1985. Influences of endurance training on the ultrastructural composition of the different muscle fiber types in humans. *Pflugers Arch,* 403**,** 369-76.

HUANG, J. & FORSBERG, N. E. 1998. Role of calpain in skeletal-muscle protein degradation. *Proc Natl Acad Sci U S A,* 95**,** 12100-5.

HUANG, S., LI, B., GRAY, M. D., OSHIMA, J., MIAN, I. S. & CAMPISI, J. 1998. The premature ageing syndrome protein, WRN, is a 3'-->5' exonuclease. *Nat Genet,* 20**,** 114-6.

HUDLICKA, O., BROWN, M. & EGGINTON, S. 1992. Angiogenesis in skeletal and cardiac muscle. *Physiol Rev,* 72**,** 369-417.

HUGHES, D. C., MARCOTTE, G. R., MARSHALL, A. G., WEST, D. W. D., BAEHR, L. M., WALLACE, M. A., SALEH, P. M., BODINE, S. C. & BAAR, K. 2017. Age-related Differences in Dystrophin: Impact on Force Transfer Proteins, Membrane Integrity, and Neuromuscular Junction Stability. *The journals of gerontology. Series A, Biological sciences and medical sciences,* 72**,** 640-648.

HULMI, J. J., OLIVEIRA, B. M., SILVENNOINEN, M., HOOGAARS, W. M., MA, H., PIERRE, P., PASTERNACK, A., KAINULAINEN, H. & RITVOS, O. 2013. Muscle protein synthesis, mTORC1/MAPK/Hippo signaling, and capillary density are altered by blocking of myostatin and activins. *Am J Physiol Endocrinol Metab,* 304**,** 31.

HUTCHISON, C. J. 2002. Lamins: building blocks or regulators of gene expression? *Nat Rev Mol Cell Biol,* 3**,** 848-58.

HUXLEY, A. F. & NIEDERGERKE, R. 1954. Structural changes in muscle during contraction; interference microscopy of living muscle fibres. *Nature,* 173**,** 971-3.

INBAR, O., KAISER, P. & TESCH, P. 1981. Relationships between leg muscle fiber type distribution and leg exercise performance. *Int J Sports Med,* 2**,** 154-9.

INOKUCHI, S., ISHIKAWA, H., IWAMOTO, S. & KIMURA, T. 1975. Age-related changes in the histological composition of the rectus abdominis muscle of the adult human. *Hum Biol,* 47**,** 231-49.

ISHIDO, M., UDA, M., MASUHARA, M. & KAMI, K. 2006. Alterations of M-cadherin, neural cell adhesion molecule and beta-catenin expression in satellite cells during overload-induced skeletal muscle hypertrophy. *Acta Physiol (Oxf),* 187**,** 407-18.

ITIN, P. H., SARASIN, A. & PITTELKOW, M. R. 2001. Trichothiodystrophy: update on the sulfur-deficient brittle hair syndromes. *J Am Acad Dermatol,* 44**,** 891-920; quiz 921-4.

IYAMA, T., LEE, S. Y., BERQUIST, B. R., GILEADI, O., BOHR, V. A., SEIDMAN, M. M., MCHUGH, P. J. & WILSON, D. M., 3RD 2015. CSB interacts with SNM1A and promotes DNA interstrand crosslink processing. *Nucleic Acids Res,* 43**,** 247-58.

JACKSON, M. J. 2011. Control of reactive oxygen species production in contracting skeletal muscle. *Antioxid Redox Signal,* 15**,** 2477-86.

JANSSEN, I., HEYMSFIELD, S. B., WANG, Z. M. & ROSS, R. 1985. Skeletal muscle mass and distribution in 468 men and women aged 18-88 yr. *J Appl Physiol,* 89**,** 81-8.

JASPERS, N. G., RAAMS, A., SILENGO, M. C., WIJGERS, N., NIEDERNHOFER, L. J., ROBINSON, A. R., GIGLIA-MARI, G., HOOGSTRATEN, D., KLEIJER, W. J., HOEIJMAKERS, J. H. & VERMEULEN, W. 2007. First reported patient with human ERCC1 deficiency has cerebro-oculo-facio-skeletal syndrome with a mild defect in nucleotide excision repair and severe developmental failure. *Am J Hum Genet,* 80**,** 457-66.

JEUKENDRUP, A. E. 2002. Regulation of fat metabolism in skeletal muscle. *Ann N Y Acad Sci,* 967**,** 217-35.

JOHNSON, M. A., POLGAR, J., WEIGHTMAN, D. & APPLETON, D. 1973. Data on the distribution of fibre types in thirty-six human muscles. An autopsy study. *J Neurol Sci,* 18**,** 111-29.

JOULIA, D., BERNARDI, H., GARANDEL, V., RABENOELINA, F., VERNUS, B. & CABELLO, G. 2003. Mechanisms involved in the inhibition of myoblast proliferation and differentiation by myostatin. *Exp Cell Res,* 286**,** 263-75.

KADI, F., CHARIFI, N., DENIS, C. & LEXELL, J. 2004. Satellite cells and myonuclei in young and elderly women and men. *Muscle Nerve,* 29**,** 120-7.

KAMBADUR, R., SHARMA, M., SMITH, T. P. & BASS, J. J. 1997. Mutations in myostatin (GDF8) in double-muscled Belgian Blue and Piedmontese cattle. *Genome Res,* 7**,** 910-6.

KAMMOUN, M., CASSAR-MALEK, I., MEUNIER, B. & PICARD, B. 2014. A simplified immunohistochemical classification of skeletal muscle fibres in mouse. *Eur J Histochem,* 58**,** 2254.

KANG, J. S. & KRAUSS, R. S. 2010. Muscle stem cells in developmental and regenerative myogenesis. *Curr Opin Clin Nutr Metab Care,* 13**,** 243-8.

KARIKKINETH, A. C., SCHEIBYE-KNUDSEN, M., FIVENSON, E., CROTEAU, D. L. & BOHR, V. A. 2016. Cockayne syndrome: Clinical features, model systems and pathways. *Ageing Res Rev*.

KASSAR-DUCHOSSOY, L., GIACONE, E., GAYRAUD-MOREL, B., JORY, A., GOMES, D. & TAJBAKHSH, S. 2005. Pax3/Pax7 mark a novel population of primitive myogenic cells during development. *Genes Dev,* 19**,** 1426-31.

KATSETOS, C. D., KOUTZAKI, S. & MELVIN, J. J. 2013. Mitochondrial dysfunction in neuromuscular disorders. *Semin Pediatr Neurol,* 20**,** 202-15.

KAZEMI-BAJESTANI, S. M. R., MAZURAK, V. C. & BARACOS, V. 2015. Computed tomography-defined muscle and fat wasting are associated with cancer clinical outcomes. *Semin Cell Dev Biol*.

KELLER, K. & ENGELHARDT, M. 2013. Strength and muscle mass loss with aging process. Age and strength loss. *Muscles Ligaments Tendons J,* 3**,** 346-50.

KELLER, K. & ENGELHARDT, M. 2014. Strength and muscle mass loss with aging process. Age and strength loss. *Muscles Ligaments Tendons J,* 3**,** 346-50.

KILLIAN, K. J., LEBLANC, P., MARTIN, D. H., SUMMERS, E., JONES, N. L. & CAMPBELL, E. J. 1992. Exercise capacity and ventilatory, circulatory, and symptom limitation in patients with chronic airflow limitation. *Am Rev Respir Dis,* 146**,** 935-40.

KIM, J. H., CHO, J. J. & PARK, Y. S. 2015. Relationship between sarcopenic obesity and cardiovascular disease risk as estimated by the Framingham risk score. *J Korean Med Sci,* 30**,** 264-71.

KJAER, M. 2004. Role of extracellular matrix in adaptation of tendon and skeletal muscle to mechanical loading. *Physiol Rev,* 84**,** 649-98.

KJAER, M., LANGBERG, H., HEINEMEIER, K., BAYER, M. L., HANSEN, M., HOLM, L., DOESSING, S., KONGSGAARD, M., KROGSGAARD, M. R. & MAGNUSSON, S. P. 2009. From mechanical loading to collagen synthesis, structural changes and function in human tendon. *Scand J Med Sci Sports,* 19**,** 500-10.

KLITGAARD, H., BERGMAN, O., BETTO, R., SALVIATI, G., SCHIAFFINO, S., CLAUSEN, T. & SALTIN, B. 1990. Co-existence of myosin heavy chain I and IIa isoforms in human skeletal muscle fibres with endurance training. *Pflugers Arch,* 416**,** 470-2.

KORTHUIS, R. J. 2011. Integrated Systems Physiology: from Molecule to Function to Disease. *Skeletal Muscle Circulation.* San Rafael (CA): Morgan & Claypool Life Sciences

Copyright (c) 2011 by Morgan & Claypool Life Sciences.

KOVANEN, V., SUOMINEN, H. & HEIKKINEN, E. 1980. Connective tissue of "fast" and "slow" skeletal muscle in rats--effects of endurance training. *Acta Physiol Scand,* 108**,** 173-80.

KOVANEN, V., SUOMINEN, H. & HEIKKINEN, E. 1984. Collagen of slow twitch and fast twitch muscle fibres in different types of rat skeletal muscle. *Eur J Appl Physiol Occup Physiol,* 52**,** 235-42.

KOVANEN, V., SUOMINEN, H., RISTELI, J. & RISTELI, L. 1988. Type IV collagen and laminin in slow and fast skeletal muscle in rats--effects of age and life-time endurance training. *Coll Relat Res,* 8**,** 145-53.

KRAGSTRUP, T. W., KJAER, M. & MACKEY, A. L. 2011. Structural, biochemical, cellular, and functional changes in skeletal muscle extracellular matrix with aging. *Scand J Med Sci Sports,* 21**,** 749-57.

KRIVICKAS, L. S., WALSH, R. & AMATO, A. A. 2009. Single muscle fiber contractile properties in adults with muscular dystrophy treated with MYO-029. *Muscle Nerve,* 39**,** 3-9.

KUANG, S., GILLESPIE, M. A. & RUDNICKI, M. A. 2008. Niche regulation of muscle satellite cell self-renewal and differentiation. *Cell Stem Cell,* 2**,** 22-31.

KUHL, U., OCALAN, M., TIMPL, R., MAYNE, R., HAY, E. & VON DER MARK, K. 1984. Role of muscle fibroblasts in the deposition of type-IV collagen in the basal lamina of myotubes. *Differentiation,* 28**,** 164-72.

KUMAMOTO, T., FUJIMOTO, S., ITO, T., HORINOUCHI, H., UEYAMA, H. & TSUDA, T. 2000. Proteasome expression in the skeletal muscles of patients with muscular dystrophy. *Acta Neuropathol,* 100**,** 595-602.

KUNKEL, L. M., BEGGS, A. H. & HOFFMAN, E. P. 1989. Molecular genetics of Duchenne and Becker muscular dystrophy: emphasis on improved diagnosis. *Clin Chem,* 35**,** B21-4.

KUNKEL, T. A., ROBERTS, J. D. & ZAKOUR, R. A. 1987. Rapid and efficient site-specific mutagenesis without phenotypic selection. *Methods Enzymol,* 154**,** 367-82.

KURAOKA, I., KOBERTZ, W. R., ARIZA, R. R., BIGGERSTAFF, M., ESSIGMANN, J. M. & WOOD, R. D. 2000. Repair of an interstrand DNA cross-link initiated by ERCC1-XPF repair/recombination nuclease. *J Biol Chem,* 275**,** 26632-6.

L'HONORE, A., COMMERE, P. H., OUIMETTE, J. F., MONTARRAS, D., DROUIN, J. & BUCKINGHAM, M. 2014. Redox regulation by Pitx2 and Pitx3 is critical for fetal myogenesis. *Dev Cell,* 29**,** 392-405.

LACH-TRIFILIEFF, E., MINETTI, G. C., SHEPPARD, K., IBEBUNJO, C., FEIGE, J. N., HARTMANN, S., BRACHAT, S., RIVET, H., KOELBING, C., MORVAN, F., HATAKEYAMA, S. & GLASS, D. J. 2014. An antibody blocking activin type II receptors induces strong skeletal muscle hypertrophy and protects from atrophy. *Mol Cell Biol,* 34**,** 606-18.

LARSSON, L., BIRAL, D., CAMPIONE, M. & SCHIAFFINO, S. 1993. An age-related type IIB to IIX myosin heavy chain switching in rat skeletal muscle. *Acta Physiol Scand,* 147**,** 227-34.

LARSSON, L., YU, F., HÖÖK, P., RAMAMURTHY, B., MARX, J. O. & PIRCHER, P. 2001. Effects of aging on regulation of muscle contraction at the motor unit, muscle cell, and molecular levels. *Int J Sport Nutr Exerc Metab,* 11 Suppl**,** S28-43.

LAUGEL, V. 2013. Cockayne syndrome: the expanding clinical and mutational spectrum. *Mech Ageing Dev,* 134**,** 161-70.

LAVASANI, M., ROBINSON, A. R., LU, A., SONG, M., FEDUSKA, J. M., AHANI, B., TILSTRA, J. S., FELDMAN, C. H., ROBBINS, P. D., NIEDERNHOFER, L. J. & HUARD, J. 2012. Muscle-derived stem/progenitor cell dysfunction limits healthspan and lifespan in a murine progeria model. *Nat Commun,* 3.

LEBRASSEUR, N. K., SCHELHORN, T. M., BERNARDO, B. L., COSGROVE, P. G., LORIA, P. M. & BROWN, T. A. 2009. Myostatin inhibition enhances the effects of exercise on performance and metabolic outcomes in aged mice. *J Gerontol A Biol Sci Med Sci,* 64**,** 940-8.

LECKER, S. H., GOLDBERG, A. L. & MITCH, W. E. 2006. Protein degradation by the ubiquitin-proteasome pathway in normal and disease states. *J Am Soc Nephrol,* 17**,** 1807-19.

LEE, C. K., KLOPP, R. G., WEINDRUCH, R. & PROLLA, T. A. 1999. Gene expression profile of aging and its retardation by caloric restriction. *Science,* 285**,** 1390-3.

LEE, S. J. & MCPHERRON, A. C. 2001. Regulation of myostatin activity and muscle growth. *Proc Natl Acad Sci U S A,* 98**,** 9306-11.

LEE, S. J., REED, L. A., DAVIES, M. V., GIRGENRATH, S., GOAD, M. E., TOMKINSON, K. N., WRIGHT, J. F., BARKER, C., EHRMANTRAUT, G., HOLMSTROM, J., TROWELL, B., GERTZ, B., JIANG, M. S., SEBALD, S. M., MATZUK, M., LI, E., LIANG, L. F., QUATTLEBAUM, E., STOTISH, R. L. & WOLFMAN, N. M. 2005. Regulation of muscle growth by multiple ligands signaling through activin type II receptors. *Proc Natl Acad Sci U S A,* 102**,** 18117-22.

LEE, W. S., CHEUNG, W. H., QIN, L., TANG, N. & LEUNG, K. S. 2006. Age-associated decrease of type IIA/B human skeletal muscle fibers. *Clin Orthop Relat Res,* 450**,** 231-7.

LEHMANN, A. R. 2003. DNA repair-deficient diseases, xeroderma pigmentosum, Cockayne syndrome and trichothiodystrophy. *Biochimie,* 85**,** 1101-11.

LEPPER, C., CONWAY, S. J. & FAN, C. M. 2009. Adult satellite cells and embryonic muscle progenitors have distinct genetic requirements. *Nature,* 460**,** 627-31.

LEVINE, B. & KROEMER, G. 2008. Autophagy in the pathogenesis of disease. *Cell,* 132**,** 27-42.

LEXELL, J. 1993. Ageing and human muscle: observations from Sweden. *Can J Appl Physiol,* 18**,** 2-18.

LEXELL, J., HENRIKSSON-LARSEN, K., WINBLAD, B. & SJOSTROM, M. 1983. Distribution of different fiber types in human skeletal muscles: effects of aging studied in whole muscle cross sections. *Muscle Nerve,* 6**,** 588-95.

LEXELL, J., TAYLOR, C. C. & SJOSTROM, M. 1988. What is the cause of the ageing atrophy? Total number, size and proportion of different fiber types studied in whole vastus lateralis muscle from 15- to 83-year-old men. *J Neurol Sci,* 84**,** 275-94.

LI, C., WHITE, S. H., WARREN, L. K. & WOHLGEMUTH, S. E. 2016. Effects of aging on mitochondrial function in skeletal muscle of American American Quarter Horses. *Journal of applied physiology (Bethesda, Md. : 1985),* 121**,** 299-311.

LI, N., RAGHEB, K., LAWLER, G., STURGIS, J., RAJWA, B., MELENDEZ, J. A. & ROBINSON, J. P. 2003. Mitochondrial complex I inhibitor rotenone induces apoptosis through enhancing mitochondrial reactive oxygen species production. *J Biol Chem,* 278**,** 8516-25.

LI, Z. B., KOLLIAS, H. D. & WAGNER, K. R. 2008. Myostatin directly regulates skeletal muscle fibrosis. *J Biol Chem,* 283**,** 19371-8.

LIGHT, N. & CHAMPION, A. E. 1984. Characterization of muscle epimysium, perimysium and endomysium collagens. *Biochem J,* 219**,** 1017-26.

LIM, J. & PARK, H. S. 2016. Relationship between underweight, bone mineral density and skeletal muscle index in premenopausal Korean women. *Int J Clin Pract,* 70**,** 462-8.

LIN, J., WU, H., TARR, P. T., ZHANG, C. Y., WU, Z., BOSS, O., MICHAEL, L. F., PUIGSERVER, P., ISOTANI, E., OLSON, E. N., LOWELL, B. B., BASSEL-DUBY, R. & SPIEGELMAN, B. M. 2002. Transcriptional co-activator PGC-1 alpha drives the formation of slow-twitch muscle fibres. *Nature,* 418**,** 797-801.

LIPINA, C., KENDALL, H., MCPHERRON, A. C., TAYLOR, P. M. & HUNDAL, H. S. 2010. Mechanisms involved in the enhancement of mammalian target of rapamycin signalling and hypertrophy in skeletal muscle of myostatin-deficient mice. *FEBS Lett,* 584**,** 2403-8.

LIPTON, B. H. 1977. Collagen synthesis by normal and bromodeoxyuridine-modulated cells in myogenic culture. *Dev Biol,* 61**,** 153-65.

LIU, B., WANG, Z., ZHANG, L., GHOSH, S., ZHENG, H. & ZHOU, Z. 2013. Depleting the methyltransferase Suv39h1 improves DNA repair and extends lifespan in a progeria mouse model. *Nat Commun,* 4.

LIU, M., HAMMERS, D. W., BARTON, E. R. & SWEENEY, H. L. 2016. Activin Receptor Type IIB Inhibition Improves Muscle Phenotype and Function in a Mouse Model of Spinal Muscular Atrophy. *PLoS One,* 11.

LJUBICIC, V., JOSEPH, A. M., SALEEM, A., UGUCCIONI, G., COLLU-MARCHESE, M., LAI, R. Y., NGUYEN, L. M. & HOOD, D. A. 2010. Transcriptional and post-transcriptional regulation of mitochondrial biogenesis in skeletal muscle: effects of exercise and aging. *Biochim Biophys Acta,* 3**,** 223-34.

LOKIREDDY, S., WIJESOMA, I. W., TENG, S., BONALA, S., GLUCKMAN, P. D., MCFARLANE, C., SHARMA, M. & KAMBADUR, R. 2012. The ubiquitin ligase Mul1 induces mitophagy in skeletal muscle in response to muscle-wasting stimuli. *Cell Metab,* 16**,** 613-24.

LOMO, T., WESTGAARD, R. H. & DAHL, H. A. 1974. Contractile properties of muscle: control by pattern of muscle activity in the rat. *Proc R Soc Lond B Biol Sci,* 187**,** 99-103.

LONDHE, P. & GUTTRIDGE, D. C. 2015. Inflammation induced loss of skeletal muscle. *Bone,* 80**,** 131-142.

LUKAS, J. R., BLUMER, R., DENK, M., BAUMGARTNER, I., NEUHUBER, W. & MAYR, R. 2000. Innervated myotendinous cylinders in human extraocular muscles. *Invest Ophthalmol Vis Sci,* 41**,** 2422-31.

LUND, N., DAMON, D. H., DAMON, D. N. & DULING, B. R. 1987. Capillary grouping in hamster tibials anterior muscles: flow patterns, and physiological significance. *Int J Microcirc Clin Exp,* 5**,** 359-72.

MACINTOSH, B. R., GARDINER, P. F. & MCCOMAS, A. J. 2006. *Skeletal Muscle: Form and Function*, Human Kinetics.

MAMMUCARI, C., SCHIAFFINO, S. & SANDRI, M. 2008. Downstream of Akt: FoxO3 and mTOR in the regulation of autophagy in skeletal muscle. *Autophagy,* 4**,** 524-6.

MANCEAU, M., MARCELLE, C. & GROS, J. 2005. Une source unique de progéniteurs musculaires. *Med Sci (Paris),* 21**,** 915-917.

MANTA, P., VASSILOPOULOS, D. & SPENGOS, M. 1987. Nucleo-cytoplasmic ratio in ageing skeletal muscle. *Eur Arch Psychiatry Neurol Sci,* 236**,** 235-6.

MARSHALL, P. A., WILLIAMS, P. E. & GOLDSPINK, G. 1989. Accumulation of collagen and altered fiber-type ratios as indicators of abnormal muscle gene expression in the mdx dystrophic mouse. *Muscle Nerve,* 12**,** 528-37.

MARTIN, G. M. 1978. Genetic syndromes in man with potential relevance to the pathobiology of aging. *Birth Defects Orig Artic Ser,* 14**,** 5-39.

MARTIN, S. J., O'BRIEN, G. A., NISHIOKA, W. K., MCGAHON, A. J., MAHBOUBI, A., SAIDO, T. C. & GREEN, D. R. 1995. Proteolysis of fodrin (non-erythroid spectrin) during apoptosis. *J Biol Chem,* 270**,** 6425-8.

MARTINEZ-VICENTE, M., SOVAK, G. & CUERVO, A. M. 2005. Protein degradation and aging. *Exp Gerontol,* 40**,** 622-33.

MARTINI, F. H., NATH, J. L. & BARTHOLOMEW, E. F. 2018. *Fundamentals of Anatomy & Physiology, Global Edition*, Pearson.

MARTYN, J. K., BASS, J. J. & OLDHAM, J. M. 2004. Skeletal muscle development in normal and double-muscled cattle. *Anat Rec A Discov Mol Cell Evol Biol,* 281**,** 1363-71.

MARZETTI, E., CALVANI, R., CESARI, M., BUFORD, T. W., LORENZI, M., BEHNKE, B. J. & LEEUWENBURGH, C. 2013. Mitochondrial dysfunction and sarcopenia of aging: from signaling pathways to clinical trials. *Int J Biochem Cell Biol,* 45**,** 2288-301.

MATEOS-AIERDI, A. J., GOICOECHEA, M., AIASTUI, A., FERNÁNDEZ-TORRÓN, R., GARCIA-PUGA, M., MATHEU, A. & LÓPEZ DE MUNAIN, A. 2015. Muscle wasting in myotonic dystrophies: a model of premature aging. *Front Aging Neurosci,* 7**,** 125.

MATSAKAS, A., FOSTER, K., OTTO, A., MACHARIA, R., ELASHRY, M. I., FEIST, S., GRAHAM, I., FOSTER, H., YAWORSKY, P., WALSH, F., DICKSON, G. & PATEL, K. 2009. Molecular, cellular and physiological investigation of myostatin propeptide-mediated muscle growth in adult mice. *Neuromuscul Disord,* 19**,** 489-99.

MATSAKAS, A., MACHARIA, R., OTTO, A., ELASHRY, M. I., MOUISEL, E., ROMANELLO, V., SARTORI, R., AMTHOR, H., SANDRI, M., NARKAR, V. & PATEL, K. 2012. Exercise training attenuates the hypermuscular phenotype and restores skeletal muscle function in the myostatin null mouse. *Exp Physiol,* 97**,** 125-40.

MATSAKAS, A., MOUISEL, E., AMTHOR, H. & PATEL, K. 2010. Myostatin knockout mice increase oxidative muscle phenotype as an adaptive response to exercise. *J Muscle Res Cell Motil,* 31**,** 111-25.

MATSAKAS, A. & PATEL, K. 2009. Skeletal muscle fibre plasticity in response to selected environmental and physiological stimuli. *Histol Histopathol,* 24**,** 611-29.

MATSUMURA, K., TOME, F. M., IONASESCU, V., ERVASTI, J. M., ANDERSON, R. D., ROMERO, N. B., SIMON, D., RECAN, D., KAPLAN, J. C., FARDEAU, M. & ET AL. 1993. Deficiency of dystrophin-associated proteins in Duchenne muscular dystrophy patients lacking COOH-terminal domains of dystrophin. *J Clin Invest,* 92**,** 866-71.

MAURO, A. 1961. Satellite cell of skeletal muscle fibers. *J Biophys Biochem Cytol,* 9**,** 493-5.

MCCLUNG, J. M., JUDGE, A. R., TALBERT, E. E. & POWERS, S. K. 2009. Calpain-1 is required for hydrogen peroxide-induced myotube atrophy. *Am J Physiol Cell Physiol,* 296**,** 24.

MCCORD, J. M. 2000. The evolution of free radicals and oxidative stress. *Am J Med,* 108**,** 652-9.

MCCORMICK, R. & VASILAKI, A. 2018. Age-related changes in skeletal muscle: changes to life-style as a therapy. *Biogerontology,* 19**,** 519-536.

MCCROSKERY, S., THOMAS, M., MAXWELL, L., SHARMA, M. & KAMBADUR, R. 2003. Myostatin negatively regulates satellite cell activation and self-renewal. *J Cell Biol,* 162**,** 1135-47.

MCCUBREY, J. A., STEELMAN, L. S., CHAPPELL, W. H., ABRAMS, S. L., WONG, E. W., CHANG, F., LEHMANN, B., TERRIAN, D. M., MILELLA, M., TAFURI, A., STIVALA, F., LIBRA, M., BASECKE, J., EVANGELISTI, C., MARTELLI, A. M. & FRANKLIN, R. A. 2007. Roles of the Raf/MEK/ERK pathway in cell growth, malignant transformation and drug resistance. *Biochim Biophys Acta,* 8**,** 7.

MCLEOD, M., BREEN, L., HAMILTON, D. L. & PHILP, A. 2016. Live strong and prosper: the importance of skeletal muscle strength for healthy ageing. *Biogerontology,* 17**,** 497-510.

MCPHERRON, A. C., HUYNH, T. V. & LEE, S. J. 2009. Redundancy of myostatin and growth/differentiation factor 11 function. *BMC Dev Biol,* 9**,** 9-24.

MCPHERRON, A. C., LAWLER, A. M. & LEE, S. J. 1997. Regulation of skeletal muscle mass in mice by a new TGF-beta superfamily member. *Nature,* 387**,** 83-90.

MCPHERRON, A. C. & LEE, S. J. 1997. Double muscling in cattle due to mutations in the myostatin gene. *Proc Natl Acad Sci U S A,* 94**,** 12457-61.

MCWHIR, J., SELFRIDGE, J., HARRISON, D. J., SQUIRES, S. & MELTON, D. W. 1993. Mice with DNA repair gene (ERCC-1) deficiency have elevated levels of p53, liver nuclear abnormalities and die before weaning. *Nat Genet,* 5**,** 217-24.

MEIER, H. & FULLER, J. 1966. Responses to drugs.

MENDIAS, C. L., MARCIN, J. E., CALERDON, D. R. & FAULKNER, J. A. 1985. Contractile properties of EDL and soleus muscles of myostatin-deficient mice. *J Appl Physiol,* 101**,** 898-905.

MENESES, C., MORALES, M. G., ABRIGO, J., SIMON, F., BRANDAN, E. & CABELLO-VERRUGIO, C. 2015. The angiotensin-(1-7)/Mas axis reduces myonuclear apoptosis during recovery from angiotensin II-induced skeletal muscle atrophy in mice. *Pflugers Arch,* 467**,** 1975-84.

MERKWIRTH, C. & LANGER, T. 2009. Prohibitin function within mitochondria: essential roles for cell proliferation and cristae morphogenesis. *Biochim Biophys Acta,* 1**,** 27-32.

MESCHER, A. L. & JUNQUEIRA, L. C. U. 2013. *Junqueira's Basic Histology: Text and Atlas*, McGraw-Hill Medical.

MESHER, A. 2010. *Basic Histology,* New York, McGraw Hill.

MILLAY, D. P., O'ROURKE, J. R., SUTHERLAND, L. B., BEZPROZVANNAYA, S., SHELTON, J. M., BASSEL-DUBY, R. & OLSON, E. N. 2013. Myomaker is a membrane activator of myoblast fusion and muscle formation. *Nature,* 499**,** 301-5.

MILLER, M. S. & TOTH, M. J. 2013. Myofilament protein alterations promote physical disability in aging and disease. *Exerc Sport Sci Rev,* 41**,** 93-9.

MILMAN, S., HUFFMAN, D. M. & BARZILAI, N. 2016. The Somatotropic Axis in Human Aging: Framework for the Current State of Knowledge and Future Research. *Cell Metab,* 23**,** 980-989.

MOEN, R. J., KLEIN, J. C. & THOMAS, D. D. 2014. Electron paramagnetic resonance resolves effects of oxidative stress on muscle proteins. *Exerc Sport Sci Rev,* 42**,** 30-6.

MORALES, M. G., CABRERA, D., CESPEDES, C., VIO, C. P., VAZQUEZ, Y., BRANDAN, E. & CABELLO-VERRUGIO, C. 2013. Inhibition of the angiotensin-converting enzyme decreases skeletal muscle fibrosis in dystrophic mice by a diminution in the expression and activity of connective tissue growth factor (CTGF/CCN-2). *Cell Tissue Res,* 353**,** 173-87.

MORGAN, J. E. & PARTRIDGE, T. A. 2003. Muscle satellite cells. *Int J Biochem Cell Biol,* 35**,** 1151-6.

MORINE, K. J., BISH, L. T., SELSBY, J. T., GAZZARA, J. A., PENDRAK, K., SLEEPER, M. M., BARTON, E. R., LEE, S. J. & SWEENEY, H. L. 2010. Activin IIB receptor blockade attenuates dystrophic pathology in a mouse model of Duchenne muscular dystrophy. *Muscle Nerve,* 42**,** 722-30.

MORTENSEN, S. P. & SALTIN, B. 2014. Regulation of the skeletal muscle blood flow in humans. *Exp Physiol,* 99**,** 1552-8.

MOSHER, D. S., QUIGNON, P., BUSTAMANTE, C. D., SUTTER, N. B., MELLERSH, C. S., PARKER, H. G. & OSTRANDER, E. A. 2007. A mutation in the myostatin gene increases muscle mass and enhances racing performance in heterozygote dogs. *PLoS Genet,* 3**,** 30.

MOSKALEV, A. A., SHAPOSHNIKOV, M. V., PLYUSNINA, E. N., ZHAVORONKOV, A., BUDOVSKY, A., YANAI, H. & FRAIFELD, V. E. 2013. The role of DNA damage and repair in aging through the prism of Koch-like criteria. *Ageing Res Rev,* 12**,** 661-84.

MOSS, F. P. & LEBLOND, C. P. 1971. Satellite cells as the source of nuclei in muscles of growing rats. *Anat Rec,* 170**,** 421-35.

MOTEVALLI, M. S., DALBO, V. J., ATTARZADEH, R. S., RASHIDLAMIR, A., TUCKER, P. S. & SCANLAN, A. T. 2015. The effect of rate of weight reduction on serum myostatin and follistatin concentrations in competitive wrestlers. *Int J Sports Physiol Perform,* 10**,** 139-46.

MOUISEL, E., RELIZANI, K., MILLE-HAMARD, L., DENIS, R., HOURDE, C., AGBULUT, O., PATEL, K., ARANDEL, L., MORALES-GONZALEZ, S., VIGNAUD, A., GARCIA, L., FERRY, A., LUQUET, S., BILLAT, V., VENTURA-CLAPIER, R., SCHUELKE, M. & AMTHOR, H. 2014. Myostatin is a key mediator between energy metabolism and endurance capacity of skeletal muscle. *Am J Physiol Regul Integr Comp Physiol,* 307**,** 25.

MOUNKES, L. C., KOZLOV, S., HERNANDEZ, L., SULLIVAN, T. & STEWART, C. L. 2003. A progeroid syndrome in mice is caused by defects in A-type lamins. *Nature,* 423**,** 298-301.

MURRAY, J., AUWERX, J. & HUSS, J. M. 2013. Impaired myogenesis in estrogen-related receptor gamma (ERRgamma)-deficient skeletal myocytes due to oxidative stress. *Faseb J,* 27**,** 135-50.

NADER, G. A. 2005. Molecular determinants of skeletal muscle mass: getting the "AKT" together. *Int J Biochem Cell Biol,* 37**,** 1985-96.

NAIR, K. S. 2005. Aging muscle. *Am J Clin Nutr,* 81**,** 953-63.

NAJJAR, S. S., SALEM, G. M. & IDRISS, Z. H. 1975. Congenital generalized lipodystrophy. *Acta Paediatr Scand,* 64**,** 273-9.

NAKANISHI, R., HIRAYAMA, Y., TANAKA, M., MAESHIGE, N., KONDO, H., ISHIHARA, A., ROY, R. R. & FUJINO, H. 2016. Nucleoprotein supplementation enhances the recovery of rat soleus mass with reloading after hindlimb unloading-induced atrophy via myonuclei accretion and increased protein synthesis. *Nutr Res,* 36**,** 1335-1344.

NAKATANI, M., TAKEHARA, Y., SUGINO, H., MATSUMOTO, M., HASHIMOTO, O., HASEGAWA, Y., MURAKAMI, T., UEZUMI, A., TAKEDA, S., NOJI, S., SUNADA, Y. & TSUCHIDA, K. 2008. Transgenic expression of a myostatin inhibitor derived from follistatin increases skeletal muscle mass and ameliorates dystrophic pathology in mdx mice. *Faseb J,* 22**,** 477-87.

NARICI, M. V. & MAFFULLI, N. 2010. Sarcopenia: characteristics, mechanisms and functional significance. *British Medical Bulletin,* 95**,** 139-159.

NARKAR, V. A., DOWNES, M., YU, R. T., EMBLER, E., WANG, Y. X., BANAYO, E., MIHAYLOVA, M. M., NELSON, M. C., ZOU, Y., JUGUILON, H., KANG, H., SHAW, R. J. & EVANS, R. M. 2008. AMPK and PPARdelta agonists are exercise mimetics. *Cell,* 134**,** 405-15.

NARKAR, V. A., FAN, W., DOWNES, M., YU, R. T., JONKER, J. W., ALAYNICK, W. A., BANAYO, E., KARUNASIRI, M. S., LORCA, S. & EVANS, R. M. 2011. Exercise and PGC-1alpha-independent synchronization of type I muscle metabolism and vasculature by ERRgamma. *Cell Metab,* 13**,** 283-93.

NATALE, V. 2011. A comprehensive description of the severity groups in Cockayne syndrome. *Am J Med Genet A,* 155a**,** 1081-95.

NEBERT, D. W. 1999. Pharmacogenetics and pharmacogenomics: why is this relevant to the clinical geneticist? *Clin Genet,* 56**,** 247-58.

NELSON, W. B., SMUDER, A. J., HUDSON, M. B., TALBERT, E. E. & POWERS, S. K. 2012. Cross-talk between the calpain and caspase-3 proteolytic systems in the diaphragm during prolonged mechanical ventilation. *Crit Care Med,* 40**,** 1857-63.

NIEDERNHOFER, L. J., GARINIS, G. A., RAAMS, A., LALAI, A. S., ROBINSON, A. R., APPELDOORN, E., ODIJK, H., OOSTENDORP, R., AHMAD, A., VAN LEEUWEN, W., THEIL, A. F., VERMEULEN, W., VAN DER HORST, G. T., MEINECKE, P., KLEIJER, W. J., VIJG, J., JASPERS, N. G. & HOEIJMAKERS, J. H. 2006. A new progeroid syndrome reveals that genotoxic stress suppresses the somatotroph axis. *Nature,* 444**,** 1038-43.

NILWIK, R., SNIJDERS, T., LEENDERS, M., GROEN, B. B., VAN KRANENBURG, J., VERDIJK, L. B. & VAN LOON, L. J. 2013. The decline in skeletal muscle mass with aging is mainly attributed to a reduction in type II muscle fiber size. *Exp Gerontol,* 48**,** 492-8.

NISHIO, M. L., MADAPALLIMATTAM, A. G. & JEEJEEBHOY, K. N. 1992. Comparison of six methods for force normalization in muscles from malnourished rats. *Med Sci Sports Exerc,* 24**,** 259-64.

NWOYE, L. & MOMMAERTS, W. F. 1981. The effects of thyroid status on some properties of rat fast-twitch muscle. *J Muscle Res Cell Motil,* 2**,** 307-20.

OCAMPO, A., REDDY, P., MARTINEZ-REDONDO, P., PLATERO-LUENGO, A., HATANAKA, F., HISHIDA, T., LI, M., LAM, D., KURITA, M., BEYRET, E., ARAOKA, T., VAZQUEZ-FERRER, E., DONOSO, D., ROMAN, J. L., XU, J., RODRIGUEZ ESTEBAN, C., NUNEZ, G., NUNEZ DELICADO, E., CAMPISTOL, J. M., GUILLEN, I., GUILLEN, P. & IZPISUA BELMONTE, J. C. 2016. In Vivo Amelioration of Age-Associated Hallmarks by Partial Reprogramming. *Cell,* 167**,** 1719-1733.

OCHALA, J., FRONTERA, W. R., DORER, D. J., VAN HOECKE, J. & KRIVICKAS, L. S. 2007. Single skeletal muscle fiber elastic and contractile characteristics in young and older men. *J Gerontol A Biol Sci Med Sci,* 62**,** 375-81.

ODELBERG, S. J., KOLLHOFF, A. & KEATING, M. T. 2000. Dedifferentiation of mammalian myotubes induced by msx1. *Cell,* 103**,** 1099-109.

OHIRA, Y., YOSHINAGA, T., OHARA, M., KAWANO, F., WANG, X. D., HIGO, Y., TERADA, M., MATSUOKA, Y., ROY, R. R. & EDGERTON, V. R. 2006. The role of neural and mechanical influences in maintaining normal fast and slow muscle properties. *Cells Tissues Organs,* 182**,** 129-42.

OHLENDIECK, K. 2011. Proteomic Profiling of Fast-To-Slow Muscle Transitions during Aging. *Frontiers in physiology,* 2**,** 105-105.

OHLENDIECK, K., ERVASTI, J. M., SNOOK, J. B. & CAMPBELL, K. P. 1991. Dystrophin-glycoprotein complex is highly enriched in isolated skeletal muscle sarcolemma. *J Cell Biol,* 112**,** 135-48.

OLGUIN, H. C., YANG, Z., TAPSCOTT, S. J. & OLWIN, B. B. 2007. Reciprocal inhibition between Pax7 and muscle regulatory factors modulates myogenic cell fate determination. *J Cell Biol,* 177**,** 769-79.

OMAIRI, S., MATSAKAS, A., DEGENS, H., KRETZ, O., HANSSON, K. A., SOLBRA, A. V., BRUUSGAARD, J. C., JOCH, B., SARTORI, R., GIALLOUROU, N., MITCHELL, R., COLLINS-HOOPER, H., FOSTER, K., PASTERNACK, A., RITVOS, O., SANDRI, M., NARKAR, V., SWANN, J. R., HUBER, T. B. & PATEL, K. 2016. Enhanced exercise and regenerative capacity in a mouse model that violates size constraints of oxidative muscle fibres. *Elife,* 5**,** 16940.

ONTELL, M., ONTELL, M. P., SOPPER, M. M., MALLONGA, R., LYONS, G. & BUCKINGHAM, M. 1993. Contractile protein gene expression in primary myotubes of embryonic mouse hindlimb muscles. *Development,* 117**,** 1435-44.

OPRESKO, P. L., CHENG, W.-H., VON KOBBE, C., HARRIGAN, J. A. & BOHR, V. A. 2003. Werner syndrome and the function of the Werner protein; what they can teach us about the molecular aging process. *Carcinogenesis,* 24**,** 791-802.

OSHIMA, J. 2000. The Werner syndrome protein: an update. *Bioessays,* 22**,** 894-901.

OUSTANINA, S., HAUSE, G. & BRAUN, T. 2004. Pax7 directs postnatal renewal and propagation of myogenic satellite cells but not their specification. *Embo J,* 23**,** 3430-9.

OZDIRIM, E., TOPCU, M., OZON, A. & CILA, A. 1996. Cockayne syndrome: review of 25 cases. *Pediatr Neurol,* 15**,** 312-6.

PALLAFACCHINA, G., BLAAUW, B. & SCHIAFFINO, S. 2013. Role of satellite cells in muscle growth and maintenance of muscle mass. *Nutr Metab Cardiovasc Dis,* 23**,** 22.

PARKER, M. H. 2015. The altered fate of aging satellite cells is determined by signaling and epigenetic changes. *Frontiers in genetics,* 6**,** 59-59.

PARTRIDGE, T. A. & DAVIES, K. E. 1995. Myoblast-based gene therapies. *British Medical Bulletin,* 51**,** 123-137.

PASSERIEUX, E., ROSSIGNOL, R., LETELLIER, T. & DELAGE, J. P. 2007. Physical continuity of the perimysium from myofibers to tendons: involvement in lateral force transmission in skeletal muscle. *J Struct Biol,* 159**,** 19-28.

PATTERSON, M. F., STEPHENSON, G. M. & STEPHENSON, D. G. 2006. Denervation produces different single fiber phenotypes in fast- and slow-twitch hindlimb muscles of the rat. *Am J Physiol Cell Physiol,* 291**,** 12.

PATTISON, J. S., FOLK, L. C., MADSEN, R. W., CHILDS, T. E. & BOOTH, F. W. 2003. Transcriptional profiling identifies extensive downregulation of extracellular matrix gene expression in sarcopenic rat soleus muscle. *Physiol Genomics,* 15**,** 34-43.

PEDERSEN, B. K. & FEBBRAIO, M. A. 2012. Muscles, exercise and obesity: skeletal muscle as a secretory organ. *Nat Rev Endocrinol,* 8**,** 457-65.

PEDERSEN, R. A., SCHATTEN, G. P. & ORDAHL, C. P. 2000. *Somitogenesis*, Elsevier Science.

PENDAS, A. M., ZHOU, Z., CADINANOS, J., FREIJE, J. M., WANG, J., HULTENBY, K., ASTUDILLO, A., WERNERSON, A., RODRIGUEZ, F., TRYGGVASON, K. & LOPEZ-OTIN, C. 2002. Defective prelamin A processing and muscular and adipocyte alterations in Zmpste24 metalloproteinase-deficient mice. *Nat Genet,* 31**,** 94-9.

PETTE, D. 1998. Training effects on the contractile apparatus. *Acta Physiol Scand,* 162**,** 367-76.

PETTE, D. & SPAMER, C. 1986. Metabolic properties of muscle fibers. *Fed Proc,* 45**,** 2910-4.

PETTE, D. & STARON, R. S. 2001. Transitions of muscle fiber phenotypic profiles. *Histochem Cell Biol,* 115**,** 359-72.

PICHIERRI, P., ROSSELLI, F. & FRANCHITTO, A. 2003. Werner's syndrome protein is phosphorylated in an ATR/ATM-dependent manner following replication arrest and DNA damage induced during the S phase of the cell cycle. *Oncogene,* 22**,** 1491-500.

PINKSTON, J. M., GARIGAN, D., HANSEN, M. & KENYON, C. 2006. Mutations that increase the life span of C. elegans inhibit tumor growth. *Science,* 313**,** 971-5.

PIVNICK, E. K., ANGLE, B., KAUFMAN, R. A., HALL, B. D., PITUKCHEEWANONT, P., HERSH, J. H., FOWLKES, J. L., SANDERS, L. P., O'BRIEN, J. M., CARROLL, G. S., GUNTHER, W. M., MORROW, H. G., BURGHEN, G. A. & WARD, J. C. 2000. Neonatal progeroid (Wiedemann-Rautenstrauch) syndrome: report of five new cases and review. *Am J Med Genet,* 90**,** 131-40.

PLOQUIN, C., CHABI, B., FOURET, G., VERNUS, B., FEILLET-COUDRAY, C., COUDRAY, C., BONNIEU, A. & RAMONATXO, C. 2012. Lack of myostatin alters intermyofibrillar mitochondria activity, unbalances redox status, and impairs tolerance to chronic repetitive contractions in muscle. *Am J Physiol Endocrinol Metab,* 302**,** 7.

POCOCK, G., RICHARDS, C. D. & DE BURGH DALY, M. 2004. *Human Physiology: The Basis of Medicine*, Oxford University Press.

POGOZELSKI, A. R., GENG, T., LI, P., YIN, X., LIRA, V. A., ZHANG, M., CHI, J. T. & YAN, Z. 2009. p38gamma mitogen-activated protein kinase is a key regulator in skeletal muscle metabolic adaptation in mice. *PLoS One,* 4**,** 0007934.

POOLE, D. C., BARSTOW, T. J., MCDONOUGH, P. & JONES, A. M. 2008. Control of oxygen uptake during exercise. *Med Sci Sports Exerc,* 40**,** 462-74.

POWERS, S. K., WIGGS, M. P., DUARTE, J. A., ZERGEROGLU, A. M. & DEMIREL, H. A. 2012. Mitochondrial signaling contributes to disuse muscle atrophy. *Am J Physiol Endocrinol Metab,* 303**,** 6.

PRATESI, A., TARANTINI, F. & DI BARI, M. 2013. Skeletal muscle: an endocrine organ. *Clin Cases Miner Bone Metab,* 10**,** 11-4.

PRINCE, F. P., HIKIDA, R. S. & HAGERMAN, F. C. 1976. Human muscle fiber types in power lifters, distance runners and untrained subjects. *Pflugers Arch,* 363**,** 19-26.

PUOLAKKAINEN, T., MA, H., KAINULAINEN, H., PASTERNACK, A., RANTALAINEN, T., RITVOS, O., HEIKINHEIMO, K., HULMI, J. J. & KIVIRANTA, R. 2017. Treatment with soluble activin type IIB-receptor improves bone mass and strength in a mouse model of Duchenne muscular dystrophy. *BMC musculoskeletal disorders,* 18**,** 20-20.

PUTMAN, C. T., DUSTERHOFT, S. & PETTE, D. 1985. Changes in satellite cell content and myosin isoforms in low-frequency-stimulated fast muscle of hypothyroid rat. *J Appl Physiol,* 86**,** 40-51.

QAISAR, R., RENAUD, G., MORINE, K., BARTON, E. R., SWEENEY, H. L. & LARSSON, L. 2012. Is functional hypertrophy and specific force coupled with the addition of myonuclei at the single muscle fiber level? *FASEB journal : official publication of the Federation of American Societies for Experimental Biology,* 26**,** 1077-1085.

RADAK, Z., BORI, Z., KOLTAI, E., FATOUROS, I. G., JAMURTAS, A. Z., DOUROUDOS, I. I., TERZIS, G., NIKOLAIDIS, M. G., CHATZINIKOLAOU, A. & SOVATZIDIS, A. 2011. Age-dependent changes in 8-oxoguanine-DNA glycosylase activity are modulated by adaptive responses to physical exercise in human skeletal muscle. *Free Radical Biology and Medicine,* 51**,** 417-423.

RAHIMOV, F., KING, O. D., WARSING, L. C., POWELL, R. E., EMERSON, C. P., JR., KUNKEL, L. M. & WAGNER, K. R. 2011. Gene expression profiling of skeletal muscles treated with a soluble activin type IIB receptor. *Physiol Genomics,* 43**,** 398-407.

RAMIREZ, C. L., CADINANOS, J., VARELA, I., FREIJE, J. M. & LOPEZ-OTIN, C. 2007. Human progeroid syndromes, aging and cancer: new genetic and epigenetic insights into old questions. *Cell Mol Life Sci,* 64**,** 155-70.

RASMUSSEN, B. B., FUJITA, S., WOLFE, R. R., MITTENDORFER, B., ROY, M., ROWE, V. L. & VOLPI, E. 2006. Insulin resistance of muscle protein metabolism in aging. *Faseb j,* 20**,** 768-9.

RAUTENSTRAUCH, T. & SNIGULA, F. 1977. Progeria: a cell culture study and clinical report of familial incidence. *Eur J Pediatr,* 124**,** 101-11.

REARDON, K. A., DAVIS, J., KAPSA, R. M., CHOONG, P. & BYRNE, E. 2001. Myostatin, insulin-like growth factor-1, and leukemia inhibitory factor mRNAs are upregulated in chronic human disuse muscle atrophy. *Muscle Nerve,* 24**,** 893-9.

REID, M. B., KHAWLI, F. A. & MOODY, M. R. 1993. Reactive oxygen in skeletal muscle. III. Contractility of unfatigued muscle. *Journal of applied physiology,* 75**,** 1081-1087.

RELAIX, F., ROCANCOURT, D., MANSOURI, A. & BUCKINGHAM, M. 2005. A Pax3/Pax7-dependent population of skeletal muscle progenitor cells. *Nature,* 435**,** 948-53.

RELIZANI, K., MOUISEL, E., GIANNESINI, B., HOURDE, C., PATEL, K., MORALES GONZALEZ, S., JULICH, K., VIGNAUD, A., PIETRI-ROUXEL, F., FORTIN, D., GARCIA, L., BLOT, S., RITVOS, O., BENDAHAN, D., FERRY, A., VENTURA-CLAPIER, R., SCHUELKE, M. & AMTHOR, H. 2014. Blockade of ActRIIB signaling triggers muscle fatigability and metabolic myopathy. *Mol Ther,* 22**,** 1423-1433.

REZNIK, M. 1969. Thymidine-3H uptake by satellite cells of regenerating skeletal muscle. *J Cell Biol,* 40**,** 568-71.

RICE, K. M., PRESTON, D. L., NEFF, D., NORTON, M. & BLOUGH, E. R. 2006. Age-related dystrophin-glycoprotein complex structure and function in the rat extensor digitorum longus and soleus muscle. *J Gerontol A Biol Sci Med Sci,* 61**,** 1119-29.

RÖCKL, K. S. C., HIRSHMAN, M. F., BRANDAUER, J., FUJII, N., WITTERS, L. A. & GOODYEAR, L. J. 2007. Skeletal Muscle Adaptation to Exercise Training. *AMP-Activated Protein Kinase Mediates Muscle Fiber Type Shift,* 56**,** 2062-2069.

RODIER, F., CAMPISI, J. & BHAUMIK, D. 2007. Two faces of p53: aging and tumor suppression. *Nucleic Acids Res,* 35**,** 7475-84.

RODRIGUEZ, J., VERNUS, B., CHELH, I., CASSAR-MALEK, I., GABILLARD, J. C., HADJ SASSI, A., SEILIEZ, I., PICARD, B. & BONNIEU, A. 2014. Myostatin and the skeletal muscle atrophy and hypertrophy signaling pathways. *Cell Mol Life Sci,* 71**,** 4361-71.

ROGAKOU, E. P., BOON, C., REDON, C. & BONNER, W. M. 1999. Megabase chromatin domains involved in DNA double-strand breaks in vivo. *J Cell Biol,* 146**,** 905-16.

ROGERS, M. A. & EVANS, W. J. 1993. Changes in skeletal muscle with aging: effects of exercise training. *Exerc Sport Sci Rev,* 21**,** 65-102.

ROH, L., BRAUN, J., CHIOLERO, A., BOPP, M., ROHRMANN, S., FAEH, D. & SWISS NATIONAL COHORT STUDY, G. 2014. Mortality risk associated with underweight: a census-linked cohort of 31,578 individuals with up to 32 years of follow-up. *BMC public health,* 14**,** 371-371.

ROJANSKY, R., CHA, M. Y. & CHAN, D. C. 2016. Elimination of paternal mitochondria in mouse embryos occurs through autophagic degradation dependent on PARKIN and MUL1. *Elife,* 17**,** 17896.

ROMANUL, F. C. A. 1964. Distribution of Capillaries in Relation to Oxidative Metabolism of Skeletal Muscle Fibres. *Nature,* 201**,** 307-308.

ROSENBERG, I. H. 1997. Sarcopenia: origins and clinical relevance. *J Nutr,* 127.

SADEH, M. 1988. Effects of aging on skeletal muscle regeneration. *J Neurol Sci,* 87**,** 67-74.

SAITOH, M., ISHIDA, J., EBNER, N., ANKER, S. D., SPRINGER, J. & HAEHLING, S. V. 2017a. Myostatin inhibitors as pharmacological treatment for muscle wasting and muscular dystrophy. *Journal of Cachexia, Sarcopenia and Muscle-Clinical Reports,* 2.

SAITOH, M., ISHIDA, J., EBNER, N., ANKER, S. D., SPRINGER, J. & HAEHLING, S. V. 2017b. Myostatin inhibitors as pharmacological treatment for muscle wasting and muscular dystrophy. 2.

SALMONS, S. & VRBOVA, G. 1969. The influence of activity on some contractile characteristics of mammalian fast and slow muscles. *J Physiol,* 201**,** 535-49.

SANDRI, M. 2008. Signaling in muscle atrophy and hypertrophy. *Physiology,* 23**,** 160-70.

SANDRI, M. 2013. Protein breakdown in muscle wasting: role of autophagy-lysosome and ubiquitin-proteasome. *Int J Biochem Cell Biol,* 45**,** 2121-9.

SANES, J. R. 2003. The basement membrane/basal lamina of skeletal muscle. *J Biol Chem,* 278**,** 12601-4.

SARKAR, P. K. & SHINTON, R. A. 2001. Hutchinson-Guilford progeria syndrome. *Postgrad Med J,* 77**,** 312-7.

SAUNDERS, M. A., GOOD, J. M., LAWRENCE, E. C., FERRELL, R. E., LI, W.-H. & NACHMAN, M. W. 2006. Human adaptive evolution at Myostatin (GDF8), a regulator of muscle growth. *American journal of human genetics,* 79**,** 1089-1097.

SAVAGE, K. J. & MCPHERRON, A. C. 2010. Endurance exercise training in myostatin null mice. *Muscle Nerve,* 42**,** 355-62.

SCAAL, M., BONAFEDE, A., DATHE, V., SACHS, M., CANN, G., CHRIST, B. & BRAND-SABERI, B. 1999. SF/HGF is a mediator between limb patterning and muscle development. *Development,* 126**,** 4885-93.

SCHÄFER, K. & BRAUN, T. 1999. Early specification of limb muscle precursor cells by the homeobox gene Lbx1h. *Nat Genet,* 23**,** 213-6.

SCHAFER, R., KNAUF, U., ZWEYER, M., HOGEMEIER, O., DE GUARRINI, F., LIU, X., EICHHORN, H. J., KOCH, F. W., MUNDEGAR, R. R., ERZEN, I. & WERNIG, A. 2006. Age dependence of the human skeletal muscle stem cell in forming muscle tissue. *Artif Organs,* 30**,** 130-40.

SCHIAFFINO, S., DYAR, K. A., CICILIOT, S., BLAAUW, B. & SANDRI, M. 2013. Mechanisms regulating skeletal muscle growth and atrophy. *Febs J,* 280**,** 4294-314.

SCHIAFFINO, S. & REGGIANI, C. 2011. Fiber types in mammalian skeletal muscles. *Physiol Rev,* 91**,** 1447-531.

SCHUELKE, M., WAGNER, K. R., STOLZ, L. E., HUBNER, C., RIEBEL, T., KOMEN, W., BRAUN, T., TOBIN, J. F. & LEE, S. J. 2004. Myostatin mutation associated with gross muscle hypertrophy in a child. *N Engl J Med,* 350**,** 2682-8.

SCHULTZ, E. & MCCORMICK, K. M. 1994. Skeletal muscle satellite cells. *Rev Physiol Biochem Pharmacol,* 123**,** 213-57.

SCHWALLER, B., DICK, J., DHOOT, G., CARROLL, S., VRBOVA, G., NICOTERA, P., PETTE, D., WYSS, A., BLUETHMANN, H., HUNZIKER, W. & CELIO, M. R. 1999. Prolonged contraction-relaxation cycle of fast-twitch muscles in parvalbumin knockout mice. *Am J Physiol,* 276.

SEALE, P. & RUDNICKI, M. A. 2000. A new look at the origin, function, and "stem-cell" status of muscle satellite cells. *Dev Biol,* 218**,** 115-24.

SEBASTIAN, D., HERNANDEZ-ALVAREZ, M. I., SEGALES, J., SORIANELLO, E., MUNOZ, J. P., SALA, D., WAGET, A., LIESA, M., PAZ, J. C., GOPALACHARYULU, P., ORESIC, M., PICH, S., BURCELIN, R., PALACIN, M. & ZORZANO, A. 2012. Mitofusin 2 (Mfn2) links mitochondrial and endoplasmic reticulum function with insulin signaling and is essential for normal glucose homeostasis. *Proc Natl Acad Sci U S A,* 109**,** 5523-8.

SEGAL, S. S. 2005. Regulation of blood flow in the microcirculation. *Microcirculation,* 12**,** 33-45.

SHEFER, G., VAN DE MARK, D. P., RICHARDSON, J. B. & YABLONKA-REUVENI, Z. 2006. Satellite-cell pool size does matter: defining the myogenic potency of aging skeletal muscle. *Developmental biology,* 294**,** 50-66.

SHI, Y. & MASSAGUE, J. 2003. Mechanisms of TGF-beta signaling from cell membrane to the nucleus. *Cell,* 113**,** 685-700.

SHYU, A.-B., WILKINSON, M. F. & VAN HOOF, A. 2008. Messenger RNA regulation: to translate or to degrade. *The EMBO journal,* 27**,** 471-481.

SIJBERS, A. M., DE LAAT, W. L., ARIZA, R. R., BIGGERSTAFF, M., WEI, Y. F., MOGGS, J. G., CARTER, K. C., SHELL, B. K., EVANS, E., DE JONG, M. C., RADEMAKERS, S., DE ROOIJ, J., JASPERS, N. G., HOEIJMAKERS, J. H. & WOOD, R. D. 1996. Xeroderma pigmentosum group F caused by a defect in a structure-specific DNA repair endonuclease. *Cell,* 86**,** 811-22.

SINENSKY, M., FANTLE, K., TRUJILLO, M., MCLAIN, T., KUPFER, A. & DALTON, M. 1994. The processing pathway of prelamin A. *J Cell Sci,* 107 (Pt 1)**,** 61-7.

SIRIETT, V., PLATT, L., SALERNO, M. S., LING, N., KAMBADUR, R. & SHARMA, M. 2006. Prolonged absence of myostatin reduces sarcopenia. *J Cell Physiol,* 209**,** 866-73.

SMERDU, V., KARSCH-MIZRACHI, I., CAMPIONE, M., LEINWAND, L. & SCHIAFFINO, S. 1994. Type IIx myosin heavy chain transcripts are expressed in type IIb fibers of human skeletal muscle. *Am J Physiol,* 267.

SMITH, N. T., SORIANO-ARROQUIA, A., GOLJANEK-WHYSALL, K., JACKSON, M. J. & MCDONAGH, B. 2018. Redox responses are preserved across muscle fibres with differential susceptibility to aging. *Journal of Proteomics,* 177**,** 112-123.

SMITH, R. C., CRAMER, M. S., MITCHELL, P. J., CAPEN, A., HUBER, L., WANG, R., MYERS, L., JONES, B. E., EASTWOOD, B. J., BALLARD, D., HANSON, J., CREDILLE, K. M., WROBLEWSKI, V. J., LIN, B. K. & HEUER, J. G. 2015. Myostatin Neutralization Results in Preservation of Muscle Mass and Strength in Preclinical Models of Tumor-Induced Muscle Wasting. *Mol Cancer Ther,* 14**,** 1661-70.

SMUDER, A. J., KAVAZIS, A. N., HUDSON, M. B., NELSON, W. B. & POWERS, S. K. 2010. Oxidation enhances myofibrillar protein degradation via calpain and caspase-3. *Free Radic Biol Med,* 49**,** 1152-60.

SORIMACHI, H., IMAJOH-OHMI, S., EMORI, Y., KAWASAKI, H., OHNO, S., MINAMI, Y. & SUZUKI, K. 1989. Molecular cloning of a novel mammalian calcium-dependent protease distinct from both m- and mu-types. Specific expression of the mRNA in skeletal muscle. *J Biol Chem,* 264**,** 20106-11.

SPANN, T. P., GOLDMAN, A. E., WANG, C., HUANG, S. & GOLDMAN, R. D. 2002. Alteration of nuclear lamin organization inhibits RNA polymerase II-dependent transcription. *J Cell Biol,* 156**,** 603-8.

SRIKANTHAN, P. & KARLAMANGLA, A. S. 2014. Muscle mass index as a predictor of longevity in older adults. *Am J Med,* 127**,** 547-53.

SRIRAM, S., SUBRAMANIAN, S., SATHIAKUMAR, D., VENKATESH, R., SALERNO, M. S., MCFARLANE, C. D., KAMBADUR, R. & SHARMA, M. 2011. Modulation of reactive oxygen species in skeletal muscle by myostatin is mediated through NF-kappaB. *Aging Cell,* 10**,** 931-48.

ST ANDRE, M., JOHNSON, M., BANSAL, P. N., WELLEN, J., ROBERTSON, A., OPSAHL, A., BURCH, P. M., BIALEK, P., MORRIS, C. & OWENS, J. 2017. A mouse anti-myostatin antibody increases muscle mass and improves muscle strength and contractility in the mdx mouse model of Duchenne muscular dystrophy and its humanized equivalent, domagrozumab (PF-06252616), increases muscle volume in cynomolgus monkeys. *Skelet Muscle,* 7**,** 017-0141.

STEELMAN, L. S., CHAPPELL, W. H., ABRAMS, S. L., KEMPF, R. C., LONG, J., LAIDLER, P., MIJATOVIC, S., MAKSIMOVIC-IVANIC, D., STIVALA, F., MAZZARINO, M. C., DONIA, M., FAGONE, P., MALAPONTE, G., NICOLETTI, F., LIBRA, M., MILELLA, M., TAFURI, A., BONATI, A., BASECKE, J., COCCO, L., EVANGELISTI, C., MARTELLI, A. M., MONTALTO, G., CERVELLO, M. & MCCUBREY, J. A. 2011. Roles of the Raf/MEK/ERK and PI3K/PTEN/Akt/mTOR pathways in controlling growth and sensitivity to therapy-implications for cancer and aging. *Aging,* 3**,** 192-222.

STEFANINI, M., LAGOMARSINI, P., ARLETT, C. F., MARINONI, S., BORRONE, C., CROVATO, F., TREVISAN, G., CORDONE, G. & NUZZO, F. 1986. Xeroderma pigmentosum (complementation group D) mutation is present in patients affected by trichothiodystrophy with photosensitivity. *Hum Genet,* 74**,** 107-12.

STEVENSON, E. J., GIRESI, P. G., KONCAREVIC, A. & KANDARIAN, S. C. 2003. Global analysis of gene expression patterns during disuse atrophy in rat skeletal muscle. *The Journal of Physiology,* 551**,** 33-48.

STEVNSNER, T., MUFTUOGLU, M., AAMANN, M. D. & BOHR, V. A. 2008. The role of Cockayne Syndrome group B (CSB) protein in base excision repair and aging. *Mech Ageing Dev,* 129**,** 441-8.

STICKLAND, N. C. 1981. Muscle development in the human fetus as exemplified by m. sartorius: a quantitative study. *J Anat,* 132**,** 557-79.

STOCKDALE, F. E. 1997. Mechanisms of formation of muscle fiber types. *Cell Struct Funct,* 22**,** 37-43.

STOCKDALE, F. E. & HOLTZER, H. 1961. DNA synthesis and myogenesis. *Exp Cell Res,* 24**,** 508-20.

SUN, D. F., CHEN, Y. & RABKIN, R. 2006. Work-induced changes in skeletal muscle IGF-1 and myostatin gene expression in uremia. *Kidney Int,* 70**,** 453-9.

SUZUKI, A. 1995. Differences in distribution of myofiber types between the supraspinatus and infraspinatus muscles of sheep. *Anat Rec,* 242**,** 483-90.

SUZUKI, N., MOTOHASHI, N., UEZUMI, A., FUKADA, S.-I., YOSHIMURA, T., ITOYAMA, Y., AOKI, M., MIYAGOE-SUZUKI, Y. & TAKEDA, S. I. 2007. NO production results in suspension-induced muscle atrophy through dislocation of neuronal NOS. *J Clin Invest,* 117**,** 2468-76.

TAJBAKHSH, S. & BUCKINGHAM, M. 2000. The birth of muscle progenitor cells in the mouse: spatiotemporal considerations. *Curr Top Dev Biol,* 48**,** 225-68.

TAJBAKHSH, S. & BUCKINGHAM, M. E. 1994. Mouse limb muscle is determined in the absence of the earliest myogenic factor myf-5. *Proc Natl Acad Sci U S A,* 91**,** 747-51.

TAJBAKHSH, S., ROCANCOURT, D., COSSU, G. & BUCKINGHAM, M. 1997. Redefining the genetic hierarchies controlling skeletal myogenesis: Pax-3 and Myf-5 act upstream of MyoD. *Cell,* 89**,** 127-38.

TAKESHITA, H., YAMAMOTO, K., NOZATO, S., TAKEDA, M., FUKADA, S. I., INAGAKI, T., TSUCHIMOCHI, H., SHIRAI, M., NOZATO, Y., FUJIMOTO, T., IMAIZUMI, Y., YOKOYAMA, S.,

NAGASAWA, M., HAMANO, G., HONGYO, K., KAWAI, T., HANASAKI-YAMAMOTO, H., TAKEDA, S., TAKAHASHI, T., AKASAKA, H., ITOH, N., TAKAMI, Y., TAKEYA, Y., SUGIMOTO, K., NAKAGAMI, H. & RAKUGI, H. 2018. Angiotensin-converting enzyme 2 deficiency accelerates and angiotensin 1-7 restores age-related muscle weakness in mice. *J Cachexia Sarcopenia Muscle,* 9**,** 975-986.

TALBERT, E. E., SMUDER, A. J., MIN, K., KWON, O. S., SZETO, H. H. & POWERS, S. K. 1985. Immobilization-induced activation of key proteolytic systems in skeletal muscles is prevented by a mitochondria-targeted antioxidant. *J Appl Physiol,* 115**,** 529-38.

TANIMOTO, Y., WATANABE, M., SUN, W., SUGIURA, Y., HAYASHIDA, I., KUSABIRAKI, T. & TAMAKI, J. 2014. Sarcopenia and falls in community-dwelling elderly subjects in Japan: Defining sarcopenia according to criteria of the European Working Group on Sarcopenia in Older People. *Arch Gerontol Geriatr,* 59**,** 295-9.

TANIMOTO, Y., WATANABE, M., SUN, W., SUGIURA, Y., TSUDA, Y., KIMURA, M., HAYASHIDA, I., KUSABIRAKI, T. & KONO, K. 2012. Association between sarcopenia and higher-level functional capacity in daily living in community-dwelling elderly subjects in Japan. *Arch Gerontol Geriatr,* 55**,** e9-13.

TAYLOR, W. E., BHASIN, S., ARTAZA, J., BYHOWER, F., AZAM, M., WILLARD, D. H., JR., KULL, F. C., JR. & GONZALEZ-CADAVID, N. 2001. Myostatin inhibits cell proliferation and protein synthesis in C2C12 muscle cells. *Am J Physiol Endocrinol Metab,* 280.

TERMAN, A. & BRUNK, U. T. 2004a. Lipofuscin. *Int J Biochem Cell Biol,* 36**,** 1400-4.

TERMAN, A. & BRUNK, U. T. 2004b. Myocyte aging and mitochondrial turnover. *Exp Gerontol,* 39**,** 701-5.

THOMAS, K., ENGLER, A. J. & MEYER, G. A. 2015. Extracellular matrix regulation in the muscle satellite cell niche. *Connective tissue research,* 56**,** 1-8.

THOMAS, K. R. & CAPECCHI, M. R. 1987. Site-directed mutagenesis by gene targeting in mouse embryo-derived stem cells. *Cell,* 51**,** 503-12.

THOMAS, M., LANGLEY, B., BERRY, C., SHARMA, M., KIRK, S., BASS, J. & KAMBADUR, R. 2000. Myostatin, a negative regulator of muscle growth, functions by inhibiting myoblast proliferation. *J Biol Chem,* 275**,** 40235-43.

TOWNSON, S. A., MARTINEZ-HACKERT, E., GREPPI, C., LOWDEN, P., SAKO, D., LIU, J., UCRAN, J. A., LIHARSKA, K., UNDERWOOD, K. W., SEEHRA, J., KUMAR, R. & GRINBERG, A. V. 2012. Specificity and structure of a high affinity activin receptor-like kinase 1 (ALK1) signaling complex. *The Journal of biological chemistry,* 287**,** 27313-27325.

TRENDELENBURG, A. U., MEYER, A., ROHNER, D., BOYLE, J., HATAKEYAMA, S. & GLASS, D. J. 2009. Myostatin reduces Akt/TORC1/p70S6K signaling, inhibiting myoblast differentiation and myotube size. *Am J Physiol Cell Physiol,* 296**,** 8.

TRENSZ, F., HAROUN, S., CLOUTIER, A., RICHTER, M. V. & GRENIER, G. 2010. A muscle resident cell population promotes fibrosis in hindlimb skeletal muscles of mdx mice through the Wnt canonical pathway. *Am J Physiol Cell Physiol,* 299**,** 1.

TRIPSIANES, K., FOLKERS, G., AB, E., DAS, D., ODIJK, H., JASPERS, N. G. J., HOEIJMAKERS, J. H. J., KAPTEIN, R. & BOELENS, R. 2005. The structure of the human ERCC1/XPF interaction domains reveals a complementary role for the two proteins in nucleotide excision repair. *Structure,* 13**,** 1849-58.

TROTTER, J. A. & PURSLOW, P. P. 1992. Functional morphology of the endomysium in series fibered muscles. *J Morphol,* 212**,** 109-22.

VAN DER MEER, S. F., JASPERS, R. T., JONES, D. A. & DEGENS, H. 2011. The time course of myonuclear accretion during hypertrophy in young adult and older rat plantaris muscle. *Ann Anat,* 193**,** 56-63.

VAN DER PLUIJM, I., GARINIS, G. A., BRANDT, R. M., GORGELS, T. G., WIJNHOVEN, S. W., DIDERICH, K. E., DE WIT, J., MITCHELL, J. R., VAN OOSTROM, C., BEEMS, R., NIEDERNHOFER, L. J., VELASCO, S., FRIEDBERG, E. C., TANAKA, K., VAN STEEG, H., HOEIJMAKERS, J. H. & VAN DER

HORST, G. T. 2007. Impaired genome maintenance suppresses the growth hormone--insulin-like growth factor 1 axis in mice with Cockayne syndrome. *PLoS Biol,* 5**,** 0050002.

VAN WESSEL, T., DE HAAN, A., VAN DER LAARSE, W. J. & JASPERS, R. T. 2010. The muscle fiber type-fiber size paradox: hypertrophy or oxidative metabolism? *Eur J Appl Physiol,* 110**,** 665-94.

VARELA, I., CADIÑANOS, J., PENDÁS, A. M., GUTIÉRREZ-FERNÁNDEZ, A., FOLGUERAS, A. R., SÁNCHEZ, L. M., ZHOU, Z., RODRÍGUEZ, F. J., STEWART, C. L., VEGA, J. A., TRYGGVASON, K., FREIJE, J. M. P. & LÓPEZ-OTÍN, C. 2005. Accelerated ageing in mice deficient in Zmpste24 protease is linked to p53 signalling activation. *Nature,* 437**,** 564-8.

VELLOSO, C. P. 2008. Regulation of muscle mass by growth hormone and IGF-I. *Br J Pharmacol,* 154**,** 557-68.

VERDIJK, L. B., SNIJDERS, T., DROST, M., DELHAAS, T., KADI, F. & VAN LOON, L. J. 2014. Satellite cells in human skeletal muscle; from birth to old age. *Age,* 36**,** 545-7.

VERMEIJ, W. P., DOLLE, M. E., REILING, E., JAARSMA, D., PAYAN-GOMEZ, C., BOMBARDIERI, C. R., WU, H., ROKS, A. J., BOTTER, S. M., VAN DER EERDEN, B. C., YOUSSEF, S. A., KUIPER, R. V., NAGARAJAH, B., VAN OOSTROM, C. T., BRANDT, R. M., BARNHOORN, S., IMHOLZ, S., PENNINGS, J. L., DE BRUIN, A., GYENIS, A., POTHOF, J., VIJG, J., VAN STEEG, H. & HOEIJMAKERS, J. H. 2016a. Restricted diet delays accelerated ageing and genomic stress in DNA-repair-deficient mice. *Nature,* 537**,** 427-431.

VERMEIJ, W. P., HOEIJMAKERS, J. H. & POTHOF, J. 2016b. Genome Integrity in Aging: Human Syndromes, Mouse Models, and Therapeutic Options. *Annu Rev Pharmacol Toxicol,* 56**,** 427-45.

VINCIGUERRA, M., MUSARO, A. & ROSENTHAL, N. 2010. Regulation of muscle atrophy in aging and disease. *Adv Exp Med Biol,* 694**,** 211-33.

VISSER, M., HARRIS, T. B., FOX, K. M., HAWKES, W., HEBEL, J. R., YAHIRO, J. Y., MICHAEL, R., ZIMMERMAN, S. I. & MAGAZINER, J. 2000. Change in muscle mass and muscle strength after a hip fracture: relationship to mobility recovery. *J Gerontol A Biol Sci Med Sci,* 55**,** M434-40.

VOLKERT, M. R. & LANDINI, P. 2001. Transcriptional responses to DNA damage. *Curr Opin Microbiol,* 4**,** 178-85.

VOLPI, E., MITTENDORFER, B., RASMUSSEN, B. B. & WOLFE, R. R. 2000. The response of muscle protein anabolism to combined hyperaminoacidemia and glucose-induced hyperinsulinemia is impaired in the elderly. *J Clin Endocrinol Metab,* 85**,** 4481-90.

WAGNER, K. R., FLECKENSTEIN, J. L., AMATO, A. A., BAROHN, R. J., BUSHBY, K., ESCOLAR, D. M., FLANIGAN, K. M., PESTRONK, A., TAWIL, R., WOLFE, G. I., EAGLE, M., FLORENCE, J. M., KING, W. M., PANDYA, S., STRAUB, V., JUNEAU, P., MEYERS, K., CSIMMA, C., ARAUJO, T., ALLEN, R., PARSONS, S. A., WOZNEY, J. M., LAVALLIE, E. R. & MENDELL, J. R. 2008. A phase I/IItrial of MYO-029 in adult subjects with muscular dystrophy. *Ann Neurol,* 63**,** 561-71.

WAGNER, K. R., LIU, X., CHANG, X. & ALLEN, R. E. 2005. Muscle regeneration in the prolonged absence of myostatin. *Proceedings of the National Academy of Sciences,* 102**,** 2519-2524.

WAGNER, K. R., MCPHERRON, A. C., WINIK, N. & LEE, S. J. 2002. Loss of myostatin attenuates severity of muscular dystrophy in mdx mice. *Ann Neurol,* 52**,** 832-6.

WALSMITH, J. & ROUBENOFF, R. 2002. Cachexia in rheumatoid arthritis. *Int J Cardiol,* 85**,** 89-99.

WANG, L. C. & KERNELL, D. 2001. Fibre type regionalisation in lower hindlimb muscles of rabbit, rat and mouse: a comparative study. *J Anat,* 199**,** 631-43.

WEEDA, G., DONKER, I., DE WIT, J., MORREAU, H., JANSSENS, R., VISSERS, C. J., NIGG, A., VAN STEEG, H., BOOTSMA, D. & HOEIJMAKERS, J. H. 1997. Disruption of mouse ERCC1 results in a novel repair syndrome with growth failure, nuclear abnormalities and senescence. *Curr Biol,* 7**,** 427-39.

WEISS, A. & LEINWAND, L. A. 1996. The mammalian myosin heavy chain gene family. *Annu Rev Cell Dev Biol,* 12**,** 417-39.

WELLE, S., THORNTON, C., JOZEFOWICZ, R. & STATT, M. 1993. Myofibrillar protein synthesis in young and old men. *Am J Physiol,* 264.

WENZ, T., ROSSI, S. G., ROTUNDO, R. L., SPIEGELMAN, B. M. & MORAES, C. T. 2009. Increased muscle PGC-1alpha expression protects from sarcopenia and metabolic disease during aging. *Proc Natl Acad Sci U S A,* 106**,** 20405-10.

WESSNER, B., LIEBENSTEINER, M., NACHBAUER, W. & CSAPO, R. 2019. Age-specific response of skeletal muscle extracellular matrix to acute resistance exercise: A pilot study. *Eur J Sport Sci,* 19**,** 354-364.

WHITTEMORE, L. A., SONG, K., LI, X., AGHAJANIAN, J., DAVIES, M., GIRGENRATH, S., HILL, J. J., JALENAK, M., KELLEY, P., KNIGHT, A., MAYLOR, R., O'HARA, D., PEARSON, A., QUAZI, A., RYERSON, S., TAN, X. Y., TOMKINSON, K. N., VELDMAN, G. M., WIDOM, A., WRIGHT, J. F., WUDYKA, S., ZHAO, L. & WOLFMAN, N. M. 2003. Inhibition of myostatin in adult mice increases skeletal muscle mass and strength. *Biochem Biophys Res Commun,* 300**,** 965-71.

WIEDEMANN, H. R. 1979. An unidentified neonatal progeroid syndrome: follow-up report. *Eur J Pediatr,* 130**,** 65-70.

WOOD, L. K., KAYUPOV, E., GUMUCIO, J. P., MENDIAS, C. L., CLAFLIN, D. R. & BROOKS, S. V. 1985. Intrinsic stiffness of extracellular matrix increases with age in skeletal muscles of mice. *J Appl Physiol,* 117**,** 363-9.

WYLLIE, F. S., JONES, C. J., SKINNER, J. W., HAUGHTON, M. F., WALLIS, C., WYNFORD-THOMAS, D., FARAGHER, R. G. & KIPLING, D. 2000. Telomerase prevents the accelerated cell ageing of Werner syndrome fibroblasts. *Nat Genet,* 24**,** 16-7.

YAMAGA, M., TAKEMOTO, M., SHOJI, M., SAKAMOTO, K., YAMAMOTO, M., ISHIKAWA, T., KOSHIZAKA, M., MAEZAWA, Y., KOBAYASHI, K. & YOKOTE, K. 2017. Werner syndrome: a model for sarcopenia due to accelerated aging. *Aging,* 9**,** 1738-1744.

YAN, Z., OKUTSU, M., AKHTAR, Y. N. & LIRA, V. A. 1985. Regulation of exercise-induced fiber type transformation, mitochondrial biogenesis, and angiogenesis in skeletal muscle. *J Appl Physiol,* 110**,** 264-74.

YANG, H., ALNAQEEB, M., SIMPSON, H. & GOLDSPINK, G. 1997. Changes in muscle fibre type, muscle mass and IGF-I gene expression in rabbit skeletal muscle subjected to stretch. *J Anat,* 190**,** 613-22.

YANG, W., ZHANG, Y., LI, Y., WU, Z. & ZHU, D. 2007. Myostatin induces cyclin D1 degradation to cause cell cycle arrest through a phosphatidylinositol 3-kinase/AKT/GSK-3 beta pathway and is antagonized by insulin-like growth factor 1. *J Biol Chem,* 282**,** 3799-808.

YARASHESKI, K. E., BHASIN, S., SINHA-HIKIM, I., PAK-LODUCA, J. & GONZALEZ-CADAVID, N. F. 2002. Serum myostatin-immunoreactive protein is increased in 60-92 year old women and men with muscle wasting. *J Nutr Health Aging,* 6**,** 343-8.

YASUDA, T., KONDO, S., HOMMA, T. & HARRIS, R. C. 1996. Regulation of extracellular matrix by mechanical stress in rat glomerular mesangial cells. *J Clin Invest,* 98**,** 1991-2000.

YIN, F. C., SPURGEON, H. A., RAKUSAN, K., WEISFELDT, M. L. & LAKATTA, E. G. 1982. Use of tibial length to quantify cardiac hypertrophy: application in the aging rat. *Am J Physiol,* 243**,** H941-7.

YOO, S.-Z., NO, M.-H., HEO, J.-W., PARK, D.-H., KANG, J.-H., KIM, S. H. & KWAK, H.-B. 2018. Role of exercise in age-related sarcopenia. *J Exerc Rehabil,* 14**,** 551-558.

YU, C. E., OSHIMA, J., FU, Y. H., WIJSMAN, E. M., HISAMA, F., ALISCH, R., MATTHEWS, S., NAKURA, J., MIKI, T., OUAIS, S., MARTIN, G. M., MULLIGAN, J. & SCHELLENBERG, G. D. 1996. Positional cloning of the Werner's syndrome gene. *Science,* 272**,** 258-62.

ZACHWIEJA, J. J., SMITH, S. R., SINHA-HIKIM, I., GONZALEZ-CADAVID, N. & BHASIN, S. 1999. Plasma myostatin-immunoreactive protein is increased after prolonged bed rest with low-dose T3 administration. *J Gravit Physiol,* 6**,** 11-5.

ZAMMIT, P. & BEAUCHAMP, J. 2001. The skeletal muscle satellite cell: stem cell or son of stem cell? *Differentiation,* 68**,** 193-204.

ZAMMIT, P. S., GOLDING, J. P., NAGATA, Y., HUDON, V., PARTRIDGE, T. A. & BEAUCHAMP, J. R. 2004. Muscle satellite cells adopt divergent fates: a mechanism for self-renewal? *J Cell Biol,* 166**,** 347-57.

ZAMMIT, P. S., RELAIX, F., NAGATA, Y., RUIZ, A. P., COLLINS, C. A., PARTRIDGE, T. A. & BEAUCHAMP, J. R. 2006. Pax7 and myogenic progression in skeletal muscle satellite cells. *J Cell Sci,* 119**,** 1824-32.

ZHU, X., HADHAZY, M., WEHLING, M., TIDBALL, J. G. & MCNALLY, E. M. 2000. Dominant negative myostatin produces hypertrophy without hyperplasia in muscle. *FEBS Lett,* 474**,** 71-5.

ZHU, X. D., NIEDERNHOFER, L., KUSTER, B., MANN, M., HOEIJMAKERS, J. H. & DE LANGE, T. 2003. ERCC1/XPF removes the 3' overhang from uncapped telomeres and represses formation of telomeric DNA-containing double minute chromosomes. *Mol Cell,* 12**,** 1489-98.

ZIMMERMAN, S. D., MCCORMICK, R. J., VADLAMUDI, R. K. & THOMAS, D. P. 1985. Age and training alter collagen characteristics in fast- and slow-twitch rat limb muscle. *J Appl Physiol,* 75**,** 1670-4.

Publications

ORIGINAL ARTICLE

Journal of Cachexia, Sarcopenia and Muscle 2019; **10**: 662–686
Published online 27 March 2019 in Wiley Online Library (wileyonlinelibrary.com) **DOI:** 10.1002/jcsm.12404

Compression of morbidity in a progeroid mouse model through the attenuation of myostatin/activin signalling

Khalid Alyodawi[1,2†], Wilbert P. Vermeij[3,4†], Saleh Omairi[1,2], Oliver Kretz[5,6,7], Mark Hopkinson[8], Francesca Solagna[6], Barbara Joch[7], Renata M.C. Brandt[3], Sander Barnhoorn[3], Nicole van Vliet[3], Yanto Ridwan[3,9], Jeroen Essers[3,10,11], Robert Mitchell[1], Taryn Morash[1], Arja Pasternack[12], Olli Ritvos[12,13], Antonios Matsakas[14], Henry Collins-Hooper[1], Tobias B. Huber[5,6,15,16], Jan H.J. Hoeijmakers[3,4,17] & Ketan Patel[1,16*]

[1]*School of Biological Sciences, University of Reading, Reading, UK,* [2]*College of Medicine, Wasit University, Kut, Iraq,* [3]*Department of Molecular Genetics, Erasmus University Medical Center, Rotterdam, The Netherlands,* [4]*Princess Máxima Center, Oncode Institute, Utrecht, The Netherlands,* [5]*Medizinische Klinik, Universitätsklinikum Hamburg-Eppendorf, Hamburg, Germany,* [6]*Department of Medicine IV, Faculty of Medicine, University of Freiburg, Freiburg, Germany,* [7]*Department of Neuroanatomy, Faculty of Medicine, University of Freiburg, Freiburg, Germany,* [8]*Royal Veterinary College, London, UK,* [9]*Department of Radiology and Nuclear Medicine, Erasmus MC, Rotterdam, The Netherlands,* [10]*Department of Radiation Oncology, Erasmus MC, Rotterdam, The Netherlands,* [11]*Department of Vascular Surgery, Erasmus MC, Rotterdam, The Netherlands,* [12]*Department of Bacteriology and Immunology, University of Helsinki, Helsinki, Finland,* [13]*Institute of Molecular Medicine, University of Health Science Center, Houston, TX, USA,* [14]*Molecular Physiology Laboratory, Hull York Medical School, Hull, UK,* [15]*BIOSS Center for Biological Signalling Studies, University of Freiburg, Freiburg, Germany,* [16]*Freiburg Institute for Advanced Studies and Center for Biological System Analysis, Freiburg, Germany,* [17]*CECAD Forschungszentrum, Universität zu Köln, Cologne, Germany*

Abstract

Background One of the principles underpinning our understanding of ageing is that DNA damage induces a stress response that shifts cellular resources from growth towards maintenance. A contrasting and seemingly irreconcilable view is that prompting growth of, for example, skeletal muscle confers systemic benefit.

Methods To investigate the robustness of these axioms, we induced muscle growth in a murine progeroid model through the use of activin receptor IIB ligand trap that dampens myostatin/activin signalling. Progeric mice were then investigated for neurological and muscle function as well as cellular profiling of the muscle, kidney, liver, and bone.

Results We show that muscle of *Ercc1*$^{\Delta/-}$ progeroid mice undergoes severe wasting (decreases in hind limb muscle mass of 40–60% compared with normal mass), which is largely protected by attenuating myostatin/activin signalling using soluble activin receptor type IIB (sActRIIB) (increase of 30–62% compared with untreated progeric). sActRIIB-treated progeroid mice maintained muscle activity (distance travel per hour: 5.6 m in untreated mice vs. 13.7 m in treated) and increased specific force (19.3 mN/mg in untreated vs. 24.0 mN/mg in treated). sActRIIb treatment of progeroid mice also improved satellite cell function especially their ability to proliferate on their native substrate (2.5 cells per fibre in untreated progeroids vs. 5.4 in sActRIIB-treated progeroids after 72 h in culture). Besides direct protective effects on muscle, we show systemic improvements to other organs including the structure and function of the kidneys; there was a major decrease in the protein content in urine (albumin/creatinine of 4.9 sActRIIB treated vs. 15.7 in untreated), which is likely to be a result in the normalization of podocyte foot processes, which constitute the filtration apparatus (glomerular basement membrane thickness reduced from 224 to 177 nm following sActRIIB treatment). Treatment of the progeric mice with the activin ligand trap protected against the development of liver abnormalities including polyploidy (18.3% untreated vs. 8.1% treated) and osteoporosis (trabecular bone volume; 0.30 mm^3 in treated progeroid mice vs. 0.14 mm^3 in untreated mice, cortical bone volume; 0.30 mm^3 in treated progeroid mice vs. 0.22 mm^3 in untreated mice). The onset of neurological abnormalities was delayed (by ~5 weeks) and their severity reduced, overall sustaining health without affecting lifespan.

Conclusions This study questions the notion that tissue growth and maintaining tissue function during ageing are incompatible mechanisms. It highlights the need for future investigations to assess the potential of therapies based on myostatin/activin blockade to compress morbidity and promote healthy ageing.

Keywords Compression; Morbidity; Progeroid; Ageing; Skeletal muscle; Myostatin; Liver; Kidney; Bone; Neurological

Received: 17 August 2018; Revised: 17 December 2018; Accepted: 9 January 2019
**Correspondence to: Ketan Patel, School of Biological Sciences, University of Reading, Reading RG6 6UB, UK. Tel: +44 118 378 8079, Email: ketan.patel@reading.ac.uk*

Introduction

Ageing can be defined as the time-dependent decline in molecular, cellular, tissue, and organismal function increasing risk for morbidity and mortality. It is the major risk factor for numerous diseases including neurodegeneration, cardiovascular disease, and cancer.[1] Progress into understanding the mechanisms underlying the ageing process offers the prospect of slowing its progression and maintaining biological systems enabling a healthier life in old age.

Current models of ageing imply interplay between stochastic and genetic components.[2,3] Random damage in DNA represents a stochastic element. Accumulation of DNA damage-induced mutations is considered a significant mediator of cancer whereas DNA damage-induced cellular functional decline, senescence, and death contribute to ageing.[4] The case for a genetic component comes from numerous studies that have defined the growth hormone/insulin-like growth factor-1 (GH/IGF-1) as a central genetic axis that controls ageing. A spectrum of mutations that attenuate components of the GH/IGF-1 signalling cascade results in extended lifespan.[5] The apparently disparate stochastic and genetic components have been reconciled into a unified model of ageing by proposing that accumulation of DNA damage, and thereafter failure of DNA to properly replicate or be transcribed, leads to activation of a survival response programme that attenuates the GH/IGF-1 activity. The ultimate purpose of dampening GH/IGF-1 signalling is the prioritization of maintenance mechanisms over those that promote growth.[2,3,6]

Ageing results in the progressive decline of the function of essentially all organ systems. One of the most apparent signs of ageing in humans is sarcopenia, the involuntary loss of skeletal muscle mass and function over time.[7] It becomes evident at middle age in humans with a loss of 0.5–1% of mass per year, which increases in the seventh decade.[8] Age-related muscle loss leads to a disproportionate decrease in strength (1.5–5%/year) relative to the change in its mass, implying a reduction in both the quality and quantity of the tissue.[9] Sarcopenia invariably leads to a reduced quality of life by impacting on mobility and stability, which leads to increase incidence of fall-related injury. More importantly, sarcopenia predisposes individuals to adverse disease outcomes (cardiovascular and metabolic diseases) and mortality.[10,11]

Skeletal muscle is a highly adaptable tissue and can be induced to undergo changes in mass as well as composition through numerous interventions including exercise and diet.[12] Numerous non-genetic molecular interventions that increase muscle mass have also been designed.[13,14] One of the most potent reagents is the soluble activin receptor type IIB (sActRIIB) molecule, which acts to neutralize the muscle growth inhibitory properties of myostatin and activin. It induces significant increases in body mass in less than 4 weeks in wild-type and muscle disease model mice.[15]

A number of investigations using rodents models suggest that maintaining muscle mass and function not only guards against sarcopenia but also promotes longevity, implying that the entire multi-organ ageing process can be attenuated by such intervention.[16] However, a mechanism that promotes muscle hypertrophy as an anti-ageing regime would seemingly conflict with the intended outcome of the adaptive changes mediated through decreased GH/IGF-1 signalling that focus a body's reserves on tissue maintenance at the expense of growth. Although studies in humans have shown an association between maintaining muscle mass/function and attenuating the impact of sarcopenia (e.g. Duetz *et al*.[17]) and evidence that mass is a predictor for longevity,[10] there is, to our knowledge, no direct evidence that it directly extends lifespan.

Here, we challenge the notion that tissue growth, specifically in muscle, is incompatible with the systemic maintenance of tissue structure and function during ageing. We have used the progeroid *Ercc1*$^{\Delta/-}$ mutant mouse line as an experimental platform for our studies. It harbours attenuated excision repair cross-complementation 1 activity, a key component of several DNA repair pathways including nucleotide excision repair.[18] The stochastic increased accumulation of various types of DNA adducts, which normally are repaired by these pathways, explains why ERCC1 mutations in humans cause a complex of clinical features called xeroderma pigmentosum type F-ERCC1 (XFE) syndrome[2] combining symptoms of Cockayne Syndrome, a progeroid condition[19] associated with a transcription-replication conflicts (TCR) defect as well as Fanconi's anaemia, a cross-link repair disorder. *Ercc1*$^{\Delta/-}$ hypomorphic mutant mice progressively show signs of ageing in all organs from about 8 weeks of age, which are much more severe than in geriatric wild-type mice[20,21] (and see Vermeij *et al*. for overview[22]). *Ercc1*$^{\Delta/-}$ mutant mice die at 4–6 months of age.[20,23]

Based on the concept that DNA damage induces a survival response that promotes maintenance programmes at the expense of growth, one would predict that augmenting muscle growth would in the long run exacerbate the pathological features in a progeroid model. What we find is something quite different; sActRIIB treatment prior to the onset of progeria can support the growth of skeletal muscle, notwithstanding nucleotide excision repair defects. Importantly, the muscle is free of the numerous ultrastructural abnormalities found in untreated *Ercc1*$^{\Delta/-}$ littermates, nor does it build up elevated levels of reactive oxygen species (ROS). We show that these qualitative changes in the muscle are underpinned by an active autophagic programme. At the organismal level, sActRIIB protects *Ercc1*$^{\Delta/-}$ mice from age-related decline in muscle strength and locomotor activity. It also protects kidney function from developing proteinuria, the liver from nuclear abnormalities and metabolic shift, and the skeletal system from osteoporosis and delays the development and severity of neurological abnormalities like tremors. However, lifespan was not increased. We believe that this work highlights the need for future investigations

focusing on assessing the therapeutic potential of antagonism of the myostatin/activin signalling cascade in sustaining health and quality of life until old age.

Methods

Ethical approval

'The authors certify that they comply with the ethical guidelines for publishing in the Journal of Cachexia, Sarcopenia and Muscle: update 2017'.[24] The experiments were performed under a project licence from the United Kingdom Home Office in agreement with the Animals (Scientific Procedures) Act 1986. The University of Reading Animal Care and Ethical Review Committee approved all procedures. Animals were humanely sacrificed via Schedule 1 killing. The Erasmus MC study was in strict accordance with the Guide for the Care and Use of Laboratory Animals of the National Institutes of Health and was approved by the Dutch Ethical Committee (permit # 139-12-13), in full accordance with European legislation.

Animal maintenance

Control (*Ercc1*$^{+/+}$) and transgenic (*Ercc1*$^{\Delta/-}$) mice were bred as previously described[20,25] and maintained in accordance to the Animals (Scientific Procedures) Act 1986 (UK) and approved by the Biological Resource Unit of Reading University or the Dutch Ethical Committee at Erasmus MC. Mice were housed in individual ventilated cages under specific pathogen-free conditions (20–22°C, 12–12 hr light–dark cycle) and provided food and water *ad libitum*. Because the *Ercc1*$^{\Delta/-}$ mice were smaller, food was administered within the cages, and water bottles with long nozzles were used from around 2 weeks of age. Animals were bred and maintained (for the lifespan cohort) on AIN93G synthetic pellets (Research Diet Services B. V.; gross energy content 4.9 kcal/g dry mass, digestible energy 3.97 kcal/g). Post-natal myostatin/activin block was induced in 7-week-old male mice, through intraperitoneal (IP) injection with 10 mg/kg of sActRIIB-Fc every week, two times till week 16.[26] Each experimental group consisted of a minimum of five male mice. The University of Reading experiments were performed on 12 controls, 9 *Ercc1*$^{\Delta/-}$, and 14 sActRIIB-treated *Ercc1*$^{\Delta/-}$ mice (all male mice). Lifespan experiments were performed on both genders, with five male and five female *Ercc1*$^{\Delta/-}$ mice per treatment condition and four males and four female littermate wild-type controls. End-of-life *Ercc1*$^{\Delta/-}$ animals, both sActRIIB and mock treated, were post-mortem investigated and scored negative for visible tumours, signs of internal bleedings, enlarged spleen size, or abnormally coloured heart or enlarged heart size.

Phenotype scoring

The mice were weighed and visually inspected at least weekly and were scored in a blinded manner by experienced research technicians for the onset of various phenotypical parameters. The onset of body weight was counted as the first week. A decline in body weight was noted after their maximal body weight was reached. Whole-body tremor was scored if mice were trembling for a combined total of at least 10 s when put on a flat surface for 20 s. Impaired balance was determined by observing the mice walking on a flat surface for 20 s. Mice that had difficulties in maintaining an upright orientation during this period were scored as having imbalance. If mice showed a partial loss of function of the hind limbs, they were scored as having paresis.

Open-field activity cages monitoring system

Open-field cages (Linton Instrumentation AM548) with an array of invisible infrared light beams and multiple photocell receptors were used. Beams scan activity at two levels from front to back and left to right was performed to determine movement with data captured using AMON software, running on Windows PCs. The lower grid measured normal X, Y movement, whilst the upper grid measured rearing movement. Mice (14 weeks of age) were acclimatized for 30 min before recording. Data were measured on three occasions at 1 day intervals.

Rotarod

Rotarod machine (Panlab Harvard Apparatus LE8500; or Ugo Basile for Erasmus MC cohort) was used for motor activity and fatigue characterization. Mice were held manually by the tail and placed on the central rod that rotated at the minimum speed for acclimatization for 1 min. Thereafter, the rotation rate of the central rod was increased to a maximum of 40 rpm. The rotation rate and time mice stayed on the central rod was recorded.

Grip strength

In vivo assessment of forelimb muscle maximum force was performed using a force transducer (Chatillon DFM-2, Ontario, Canada). Mice were held by the tail base, lowered towards the bar, and allowed to grip. The mouse was pulled backwards, and the force applied to the bar just before loss of grip was recorded.

Muscle tension measurements

Dissection of the hind limb was carried out under oxygenated Krebs solution (95% O_2 and 5% CO_2). Under circulating oxygenated Krebs solution, one end of a silk suture was attached to the distal tendon of the extensor digitorum longus (EDL) and the other to a force transducer (FT03). The proximal tendon remained attached to the tibial bone. The leg was secured in the experimental chamber. Silver electrodes were positioned on either side of the EDL. A constant voltage stimulator was used to directly stimulate the EDL, which was stretched to attain the optimal muscle length to produce maximum twitch tension (P_t). Tetanic contractions were invoked by stimulus trains of 500 ms duration at 20, 50, 100, and 200 Hz. The maximum tetanic tension (P_o) was determined from the plateau of the frequency–tension curve.

Protein synthesis measure

The relative rate of protein synthesis was measured using the surface sensing of translation method (SUnSET).[27] Briefly, mice were injected exactly 30 min before tissue collection with 0.04 μmol/g body mass puromycin into the peritoneal cavity and then returned to their cages. After tissue collection, muscles were solubilized as for western blotting and then pulled through a slot blotting chamber facilitating the transfer of protein onto a nylon membrane. Thereafter, the membrane was processed identically to a western blot.

Histological analysis and immunohistochemistry

Following dissection, the muscle was immediately frozen in liquid nitrogen-cooled isopentane and mounted in optimal cutting temperature compound (TAAB O023) cooled by dry ice/ethanol. Immunohistochemistry was performed on 10 μm cryosections that were air-dried at room temperature (RT) for 30 min before the application of block wash buffer [PBS with 5% foetal calf serum (v/v), 0.05% Triton X-100]. Antibodies were diluted in wash buffer 30 min before using. Fluorescence-based secondary antibodies were used to detect all primary antibodies except for CD-31 where the Vectastain ABC-HRP kit was deployed (Vector PK-6100) with an avidin/biotin-based peroxidase system and DAB peroxidase (HRP) substrate (Vector SK-4100). Morphometric analysis of muscle fibre size was performed as previously described.[28] Details of primary and secondary antibodies are given in *Table* 1.

Dihydroethidium staining

Sectioned slides were dried for 30 min at RT. The sections were rehydrated with PBS then incubated with dihydroethidium (DHE) (50 μmol/L in PBS Sigma D7008) for 30 min at 37°C in the dark. Counterstain for nuclei was DAPI-containing fluorescent mounting medium.

Haematoxylin and eosin

Muscle and liver sections were dewaxed in xylene and rehydration in ethanol prior to incubation with Harris' haematoxylin solution (Sigma HHS16) for 30 s and thereafter in eosin solution (Sigma-Aldrich 318906) for 2 min.

Succinate dehydrogenase staining

Muscle cyro-sections were incubated for 3 min at RT in a sodium phosphate buffer containing 75 mM sodium succinate, 1.1 mM Nitroblue Tetrazolium (Sigma-Aldrich), and 1.03 mM Phenazine Methosulphate (Sigma-Aldrich). Samples were then fixed in 10% formal-calcium, dehydrated and cleared in xylene prior to mounting with DPX mounting medium (Fisher).

Transmission electron microscopy

Biceps muscle and the kidney were briefly fixed with 4% paraformaldehyde and 2.5% glutaraldehyde in 0.1 M cacodylate buffer pH 7.4 *in situ* at RT then dissected, removed, and cut into pieces of 1 mm^3 and fixed for 48 h in same solution at 4°C. Tissue blocks were contrasted using 0.5% OsO_4 (Roth, Germany; RT, 1.5 hr) and 1% uranyl acetate (Polysciences, Germany) in 70% ethanol (RT, 1 hr). After dehydration, tissue blocks were embedded in epoxy resin (Durcopan, Roth, Germany), and ultrathin sections of 40 nm thickness were cut using a Leica UC6 ultramicrotome (Leica, Wetzlar, Germany). Sections were imaged using a Zeiss 906 TEM (Zeiss, Oberkochen, Germany) and analysed using ITEM software (Olympus, Germany).[26]

Blood glucose, growth hormone, insulin, and insulin-like growth factor-1 levels

Glucose levels were measured using a freestyle mini blood glucose metre. GH, insulin, and IGF-1 levels were measured in serum using a rat/mouse growth hormone ELISA (Merck Millipore), ultrasensitive mouse insulin ELISA (Mercodia), or mouse IGF-1 ELISA (Abcam), respectively.

Micro-computed tomography imaging

Computed tomography imaging was performed using a high-speed *in vivo* micro-computed tomography (μCT) scanner (Quantum FX, PerkinElmer, Hopkinton, MA, USA).

Table 1. Primer and antibody details

Primary antibodies Antigen	Species	Dilution	Supplier
Pax7	Mouse	1:1	DSHB
MyoD	Rabbit	1:200	Santa Cruz Biot # sc-760
Myogenin	Rabbit	1:200	Santa Cruz sc576
MYHCI	Mouse	1:1	DSHB A4.840
MYHCIIA	Mouse	1:1	DSHB A4.74
MYHCIIB	Mouse	1:1	DSHB BF.F3
CD31	Rat	1:150	AbD serotec MCA2388
Dystrophin	Rabbit	1:200	Abcam 15277
Collagen IV	Rabbit	1:500	Abcam ab6586
Histone H3	Rabbit	1:100	Abcam ab8898
Histone H4	Rabbit	1:200	Abcam ab9052
pSmad2/Smad3	Rabbit	1:200	Cell signalling Technology # 8828
SMA	Mouse	1:300	Sigma A2547
Caspase-3	Rabbit	1:200	Cell signalling Technology #9664S
Phospho-S6 Ribosomal Protein (Ser235/236)	Rabbit	1:1000	Cell signalling Technology #4857
Phospho-Akt (Ser473)	Rabbit	1:1000	Cell signalling Technology #4060
LC3	Rabbit	1:1000	Cell signalling Technology #2775
Phospho-4E-BP1 (Thr37/46)	Rabbit	1:1000	Cell signalling Technology #2855
Phospho-4E-BP1 (Ser65)	Rabbit	1:1000	Cell signalling Technology #9451
Anti-p62/SQSTM1	Rabbit	1:1000	Sigma P0067
Phospho-FoxO1 (Ser256)	Rabbit	1:1000	Cell signalling Technology #9461
Anti-Smad3 (phospho S423 + S425)	Rabbit	1:200	Abcam (ab52903)
Nephrin	Goat	1:500	R&D Systems (AF3159)
PFoxO3a (Ser253)	Rabbit	1:1000	Cell signalling Technology #9466
Anti-gamma H2A.X (phospho S139)	Rabbit	1:1000	Abcam 11174

Secondary antibodies Antibody	Species	Dilution	Supplier
Alexa fluor 633 anti-mouse	Goat	1:200	Life Technologies # A20146
Alexa fluor 488 anti-mouse	Goat	1:200	Life Technologies # A11029
Alexa fluor 488 anti-rabbit	Goat	1:200	Life Technologies # A11034
Alexa fluor 594 anti-rabbit	Goat	1:200	Life Technologies # A11037
Immunoglobulins/HRP anti-Rat	Rabbit	1:200	Dako P0450

qPCR primers sequence Oligo name	Sequence
MuRF1.F	ACCTGCTGGTGGAAAACATC
MuRF1.R	CTTCGTGTTCCTTGCACATC
Atrogin.1F	GCAAACACTGCCACATTCTCTC
Atrogin.1R	CTTGAGGGGAAAGTGAGACG
R_mVEGFA189.F	TGCAGGCTGCTGTAACGATG
R_mVEGFA189.R	CTCCAGGATTTAAACCGGGAT T
R_mFGF1.F	GAAGCATGCGGAGAAGAACTG
R_mFGF1.R	CGAGGACCGCGCTTACAG
R_mVEGFB.F	TGCCATGGATAGACGTTTATG C
R_mVEGFB.R	TGCTCAGAGGCACCACCAC
m Ndufb5.F	CTTCGAACTTCCTGCTCCTT
m Ndufb6.R	GGCCCTGAAAAGAACTACG
m Sdha.F	GGAACACTCCAAAAACAGACCT
m Sdha.R	CCACCACTGGGTATTGAGTAGAA
m Sdhc.F	GCTGCGTTCTTGCTGAGACA
m Sdhc.R	ATCTCCTCCTTAGCTGTGGTT
m Cox5b.F	AAGTGCATCTGCTTGTCTCG
m Cox5b.R	GTCTTCCTTGGTGCCTGAAG
m Atp5b.F	GGTTCATCCTGCCAGAGACTA
m Atp5b.R	AATCCCTCATCGAACTGGACG
m Mdh2.F	TTGGGCAACCCCTTTCACTC
m Mdh3.R	GCCTTTCACATTTGCTCTGGTC
m Idh2.F	GGAGAAGCCGGTAGTGGAGAT
m Idh3.R	GGTCTGGTCACGGTTTGGAA
m Idh3a.F	CCCATCCCAGTTTGATGTTC

(*Continues*)

Table 1 (continued)

qPCR primers sequence	
Oligo name	Sequence
m Idh3a.R	ACCGATTCAAAGATGGCAAC
R.mPGC1A.F	AACCACACCCACAGGATCAGA
R.mPGC1A.R	TCTTCGCTTTATTGCTCCATGA
m Mvk. F	GGGACGATGTCTTCCTTGAA
m Mvk.R	GAACTTGGTCAGCCTGCTTC
m Srebf1.F	GATCAAAGAGGAGCCAGTGC
m Srebf1.R	TAGATGGTGGCTGCTGAGTG
m Srebf2.F	GGATCCTCCCAAAGAAGGAG
m Srebf2.R	TTCCTCAGAACGCCAGACTT
R_mCD36.F	AGATGACGTGGCAAAGAACAG
R_mCD36.R	CCTTGGCTAGATAACGAACTCTG
R_mSlc25a20.F	CAACCACCAAGTTTGTCTGGA
R_mSlc25a20.R	CCCTCTCTCATAAGAGTCTTCCG
R_mACADL.F	TGCCCTATATTGCGAATTACGG
R_mACADL.R	CTATGGCACCGATACACTTGC
R_mFabp3.F	ACCTGGAAGCTAGTGGACAG
R_mFabp3.R	TGATGGTAGTAGGCTTGGTCAT
R_mDmd.F	ACTCAGCCACCCAAAGACTG(20)
R_mDmd.R	TGTCTGGATAAGTGGTAGCAACA
R_mCol4a1.F	GGCCCCAAAGGTGTTGATG(19)
R_mCol4a1.R	CAGGTAAGCCGTTAAATCCAGG
m Hsp10.F	CTGACAGGTTCAATCTCTCCAC
m Hsp10.R	AGGTGGCATTATGCTTCCAG
m Clpp.F	CACACCAAGCAGAGCCTACA
m Clpp.R	TCCAAGATGCCAAACTCTTG
m IL6.F	GGTGACAACCACGGCCTTCCC
m IL6.R	AAGCCTCCGACTTGTGAAGTGGT
m IL18.F	GTGAACCCCAGACCAGACTG
m IL18.R	CCTGGAACACGTTTCTGAAAGA
m Phb.F	TCGGGAAGGAGTTCACAGAG
m Phb.R	CAGCCTTTTCCACCACAAAT
m Phb2.F	CAAGGACTTCAGCCTCATCC

The X-ray source was set to a current of 160 μA and a voltage of 90 kVp. The field of view was 30 mm × 30 mm for muscle with a voxel size of 60 μm and 20 mm × 20 mm, and voxel size was 40 μm, for bone. The animals received isoflurane anaesthesia (2.5%) to immobilize them during scanning. Following scanning, image segmentation was performed semi-automatically using the Volume Edit tools within the analysis software package (AnalyzeDirect, Overland Park, KS, USA). Briefly, segmentation masks (object maps) were created using a combination of semi-automatic and manual techniques (object extraction, region growing, and thresholding tools). These segmentation results were then manually modified if necessary and quantified using the ROI tools.

Protein expression by immunoblotting

Frozen muscles were pulverized with pestle and mortar and solubilized in 50 mM Tris, pH 7.5, 150 mM NaCl, 5 mM $MgCl_2$, 1 mM DTT, 10% glycerol, 1% SDS, 1% Triton X-100, 1X Roche Complete Protease Inhibitor Cocktail, and 1X Sigma-Aldrich Phosphatase Inhibitor Cocktails 1 and 3. Proteins were denatured in Laemmli buffer and resolved on 10% SDS-PAGEs prior to immunoblotting and probing with antibodies and the SuperSignal West Pico Chemiluminescent substrate (Pierce). Details of antibodies are given in *Table* 1.

Quantitative polymerase chain reaction

Fifty to 100 mg of tissue was solubilized in TRIzol (Fisher) using a tissue homogenizer. Total RNA was prepared using the RNeasy Mini Kit (Qiagen, Manchester, UK). Five micrograms of RNA were reverse-transcribed to cDNA with SuperScript II Reverse Transcriptase (Invitrogen) and analysed by quantitative real-time RT-PCR on a StepOne Plus cycler, using the Applied Biosystems SYBR-Green PCR Master Mix. Primers were designed using the software Primer Express 3.0 (Applied Biosystems). Relative expression was calculated using the ΔΔCt method and normalized to cyclophilin-B and hypoxanthine-guanine phosphoribosyltransferase. Primer sequences are given in *Table* 1.

Satellite cell culture

Single fibres from EDL were isolated using 0.2% collagenase I in Dulbecco's modified Eagle's medium and either fixed in 2% paraformaldehyde or cultured for 24, 48, and 72 hr as previously described.[29]

Bone scanning

Tibial samples were scanned and analysed by μCT; 180° scans were performed on a Skyscan 1172F μCT scanner (Skyscan, Kontich, Belgium); the X-ray source was operated at 50 kV and 200 uA, a 0.5 aluminium filter was used with a 1650 ms exposure time and a pixel size of 5 μm. Projection images were reconstructed into tomograms using NRecon (Skyscan, Kontich, Belgium), and regions of interest were analysed using CTAn (Skyscan, Kontich, Belgium).

Trabecular analysis

The reconstructed datasets were re-oriented in Dataviewer (Skyscan, Kontich, Belgium) so that the long axis of the bone ran along the Y-axis, which allowed the tibial length to be measured in CTAn. The reference point for trabecular analysis was the disappearance of primary spongiosa bone and the appearance of the secondary trabecular bone in the centre and subjacent to the epiphyseal growth plate. The volume of interest for trabecular analysis was set as 5% of the tibial length from this reference point down the diaphysis. This volume of trabecular bone was selected using CTAn and then analysed using CTAn BatMan software.

Cortical analysis

The reference point for cortical analysis was set as the midpoint of the diaphysis, and then a volume of interest was selected 0.25 mm in either side of this point, ensuring to remove any trabecular bone within the tomograms. Cortical regions were selected using CTAn and then analysed using CTAn BatMan software.

Statistical analysis

Data are presented as mean ± SE. Data normal distribution were checked by the D'Agostino-Pearson omnibus test. Significant differences between two groups were performed by the Student's *t*-test for independent variables. Differences among groups were analysed by one-way analysis of variance followed by Bonferroni's multiple comparison tests or the non-parametric Kruskal–Wallis test followed by the Dunn's multiple comparisons as appropriate. Statistical analysis was performed on GraphPad Prism 5 (La Jolla, USA). Lifespan, onset of neurological phenotypes, and body weight decline were statistically analysed with the survival curve analysis using the product limit method of Kaplan and Meier with Log-rank Mantel-Cox test in GraphPad Prism. Differences were considered statistically significant at $P < 0.05$.

Results

Characterization of skeletal muscle in the *Ercc1*$^{\Delta/-}$ progeroid mouse

We first characterized the muscle phenotype of *Ercc1*$^{\Delta/-}$ progeroid mice. It is important to mention that a number of studies have established that the initial development of *Ercc1*$^{\Delta/-}$ mice in a uniform FVB/C57Bl6 F1 hybrid genetic background is normal.[20] After birth, mice are progressively affected leading to accelerated appearance of numerous features of ageing.[22] Therefore, we decided to investigate muscle from *Ercc1*$^{\Delta/-}$ male mice at the age of 16 weeks, when mice show numerous signs of ageing, but before the onset of premature mortality.[20] At this time, all muscles examined from *Ercc1*$^{\Delta/-}$ mice were significantly smaller compared with control animals (ranging from 40% to 60% of normal mass; Supporting Information *Figure* S1A). Surprisingly, even though the muscle mass was decreased, the number of fibres was increased in *Ercc1*$^{\Delta/-}$ EDL (significantly) and soleus muscles (not-significant) (*Figure* S1B). The muscle from the progeric mice had significantly more fibres with centrally located nuclei than controls (*Figure* S1C). Fibre size analysis showed decreases in the cross-sectional area across most myosin heavy chain (MHC) isoforms in muscles with differing contraction properties [EDL, soleus and tibialis anterior (TA)] of *Ercc1*$^{\Delta/-}$ mutants (*Figure* S1D–S1G). There was no evident trend for changes in size in relation to the MHC isoform. Every muscle examined displayed a decrease in the number of fibres expressing the slower forms of MHC and a concomitant increase in the fast fibre population, except for MHCIIa and MHCIIb in the superficial portion of the TA (*Figure* S1H–S1J). We examined the whole muscle for its metabolic status by profiling the proportion of fibres displaying high levels of succinate dehydrogenase (SDH) activity, an indicator of oxidative phosphorylation. These experiments revealed that *Ercc1*$^{\Delta/-}$ EDL and soleus muscles contained a lower proportion of oxidative fibres compared with controls (*Figure* S1K).

We next examined features of individual fibres. The number of satellite cells (SC) on EDL fibres from *Ercc1*$^{\Delta/-}$ animals was reduced to 50% or less of the normal value (*Figure* S1L). Furthermore, *Ercc1*$^{\Delta/-}$ SC were unable to follow the normal proliferation and differentiation programmes and displayed a deficit in the proportion of myogenin-positive cells and an increase in the number of cells expressing Pax7 (*Figure* S1M). These results show that both the muscle fibre and satellites cells show quantitative and qualitative features associated with extreme ageing.

Figure 1 sActRIIB treatment mitigates body, whole animal activity, grip strength, losses, and specific force loss in *Ercc1*$^{\Delta/-}$ mice. (A) Relative changes in body mass over time. Intraperitoneal injection of *Ercc1*$^{\Delta/-}$ with sActRIIB started at week 7 and tissues collected at the end of week 15. Organismal activity measurements through activity cages. Measurements in (B–E) made at the end of week 14. (F) Rotarod activity. (G) Muscle contraction measurement through assessment of grip strength. (H) *Ex vivo* assessment of EDL-specific force. (I) Half relaxation time for the EDL. Levels of (J) growth hormone, (K) glucose, (L) insulin, and (M) insulin-like growth factor-1 at beginning of week 15. (N) Food intake and (O) relative food intake at the end of week 15. n = 6 control male mice, n = 5 *Ercc1*$^{\Delta/-}$ untreated male mice, and n = 5 *Ercc1*$^{\Delta/-}$ treated male mice. All analysis performed using non-parametric Kruskal–Wallis test followed by the Dunn's multiple comparisons except (J) where one-way analysis of variance followed by Bonferroni's multiple comparison tests was used. *$P < 0.05$, **$P < 0.01$, ***$P < 0.001$. EDL, extensor digitorum longus; IGF-1, insulin-like growth factor-1; sActRIIB, soluble activin receptor type IIB.

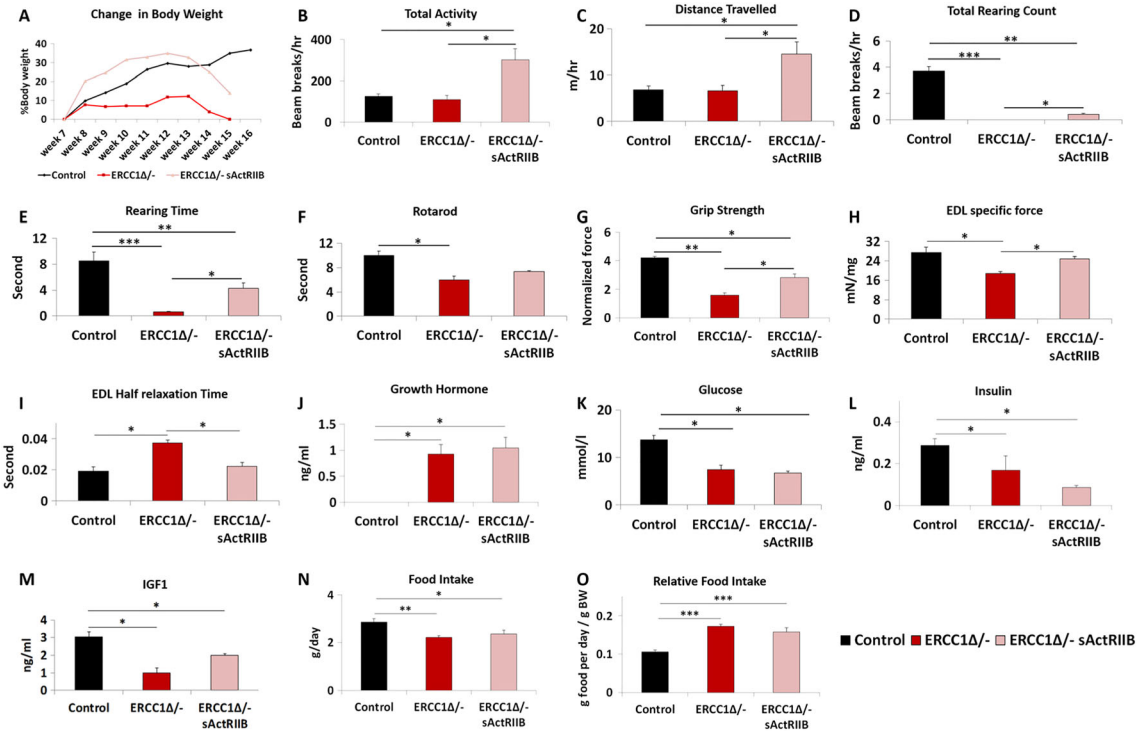

The activin ligand trap increases body organismal activity and strength

We determined whether the age-related reduced muscle mass in *Ercc1*$^{\Delta/-}$ mutants could be prevented by the sActRIIB protein, which we have shown to antagonize signalling mediated by myostatin and related proteins.[26] To that end, male *Ercc1*$^{\Delta/-}$ mice were IP injected twice a week with sActRIIB from 7 weeks of age till week 16. Mock-treated *Ercc1*$^{\Delta/-}$ mutants showed no overall body mass gain in 8 weeks, whereas both control and *Ercc1*$^{\Delta/-}$ animals treated with sActRIIB displayed weight increases of 37% and 18%, respectively (*Figures* 1A, S2A, and S2B).

Using activity cages, we found that sActRIIB-treated *Ercc1*$^{\Delta/-}$ mice were more active than both their mock-treated counterparts and control mice (*Figure* 1B and *Movie* S1). Treatment of *Ercc1*$^{\Delta/-}$ mice with sActRIIB increased the distance travelled compared not only with untreated mice but also with control animals (*Figure* 1C and *Movie* S1). Total rearing counts and rearing time, measures of locomotor activity as well as exploration and anxiety, were highest in control mice and significantly reduced in *Ercc1*$^{\Delta/-}$ mice. sActRIIB treatment increased these values compared with *Ercc1*$^{\Delta/-}$ but not to normal levels (*Figure* 1D–1E). Motor coordination, measured using the Rotarod, showed that *Ercc1*$^{\Delta/-}$ mice at the age of 16 weeks have significant deficit in this skill, which was improved, albeit not to normal levels, by sActRIIB (*Figure* 1F). Muscle function, as assessed using a grip metre, revealed that progeric mice had reduced strength compared with control mice. This parameter was significantly improved in *Ercc1*$^{\Delta/-}$ mutants by sActRIIB (*Figure* 1G). *Ex vivo* measure of specific force revealed a significant deficit in this parameter in *Ercc1*$^{\Delta/-}$ mutants that was significantly increased by sActRIIB treatment (*Figure* 1H). Half-relaxation time was increased in *Ercc1*$^{\Delta/-}$ mutants compared with controls but reduced by sActRIIB treatment (*Figure* 1I).

We determined the circulatory levels of molecules known to regulate organismal growth and found elevated levels of

DOI: 10.1002/jcsm.12404

Figure 2 Quantitative and qualitative improvements to *Ercc1*$^{\Delta/-}$ skeletal muscle through sActRIIB treatment. (A) Muscle weight at end of week 15. (B) Muscle mass normalized to tibial length. (C) Micro-computed tomography scan of hind limb to visualize the increase in muscle upon sActRIIB treatment in *Ercc1*$^{\Delta/-}$ mice. (D–G) Cross-sectional fibre areas assigned to specific myosin heavy chain isoforms. (H) Fibre number increased in EDL and soleus of *Ercc1*$^{\Delta/-}$ mice and further increased following treatment. (I) Incidence of damaged fibres following single fibre isolation. (J) Example of micro-tear (arrows) in an *Ercc1*$^{\Delta/-}$ EDL fibre. (K) Fibres containing caspase 3 epitope as a percentage of all EDL and soleus fibres. (L) Percentage of fibres with centrally located nuclei in the EDL and soleus. (M) Quantification of hyper-stained SDH fibres. (N) SDH in control muscle and (O) *Ercc1*$^{\Delta/-}$ muscle showing hyper-stained fibres (arrows). (P) Quantification of DHE fluorescence in TA muscle fibres. (Q) Control TA fibres with little DHE fluorescence in the body of control fibres. (R) *Ercc1*$^{\Delta/-}$ TA fibres with elevated DHE fluorescence in the body of control fibres. (S) Treated *Ercc1*$^{\Delta/-}$ TA fibres with little DHE fluorescence in the body of fibres. n = 9 control male mice, n = 8 *Ercc1*$^{\Delta/-}$ untreated male mice, and n = 8 *Ercc1*$^{\Delta/-}$ treated male mice. Scale for single fibre 50 μm, SDH 100 μm and DHE 20 μm. One-way analysis of variance followed by Bonferroni's multiple comparison tests. *$P < 0.05$, **$P < 0.01$, ***$P < 0.001$. DHE, dihydroethidium; EDL, extensor digitorum longus; sActRIIB, soluble activin receptor type IIB; SDH, succinate dehydrogenase; TA, tibialis anterior.

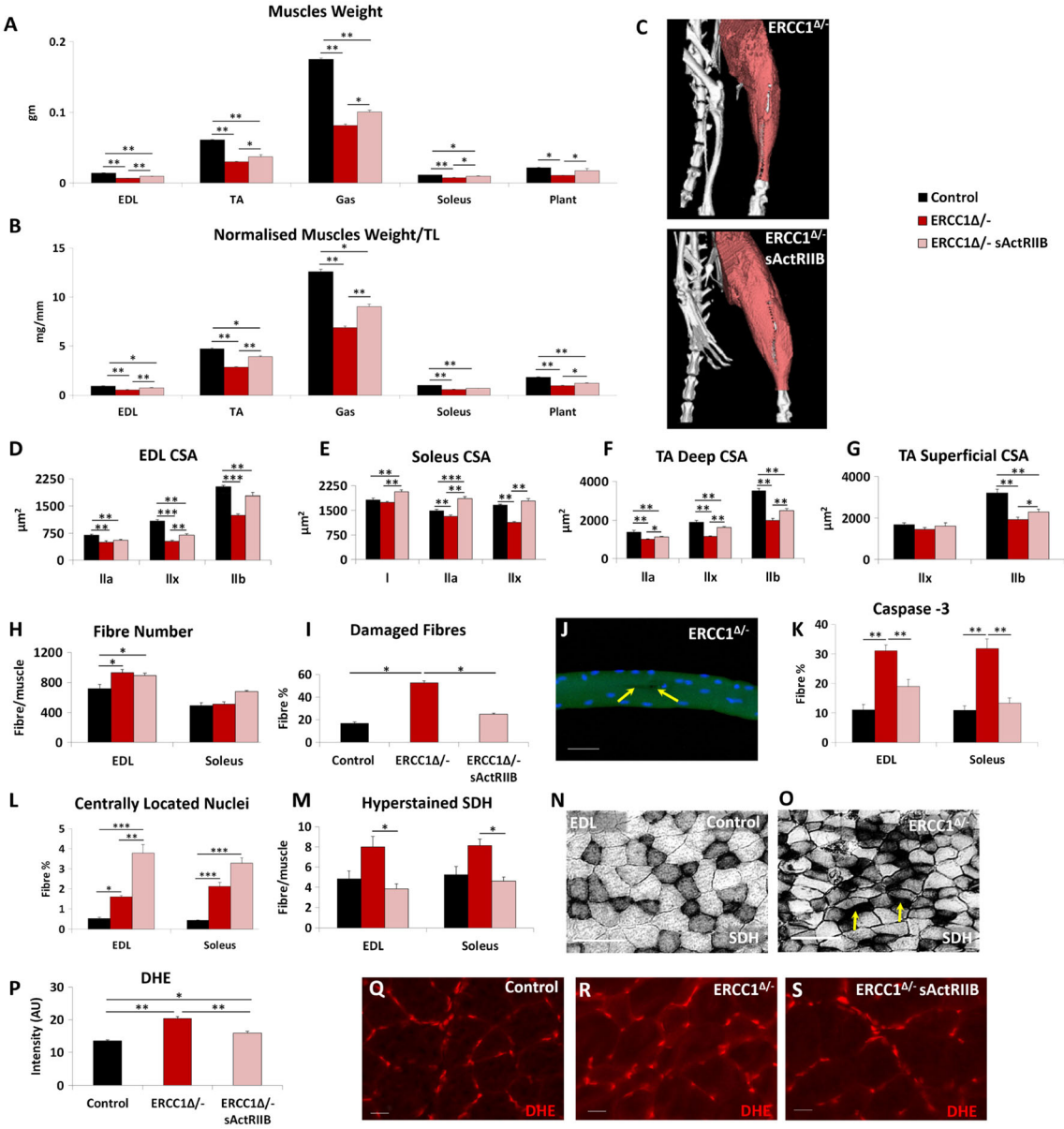

GH in both untreated and sActRIIB treated *Ercc1*$^{\Delta/-}$ mutants (*Figure* 1J), likely as previously noted feedback mechanism in response to prolonged low IGF-1.[2] Indeed, levels of blood glucose, serum insulin, and IGF-1 were decreased in *Ercc1*$^{\Delta/-}$ mutants as compared with controls, and none of these factors were changed in response to sActRIIB treatment (*Figure*

DOI: 10.1002/jcsm.12404

Figure 3 sActRIIB induces fast and glycolytic transformation of *Ercc1*$^{\Delta/-}$ muscle. (A) MHC profile of EDL muscle. (B–D) EDL MHCIIA/IIB fibre distribution in the three cohorts, controls, *Ercc1*$^{\Delta/-}$, and *Ercc1*$^{\Delta/-}$ treated with sActRIIB. (E) SDH-positive and -negative fibre profile of EDL muscle. (F–H) SDH stain in the three cohorts. (I) Quantification of EDL capillary density. (J–L) Identification of EDL capillaries with CD-31 in the three cohorts. Quantitative PCR profiling of (M) angiogenic genes, (N) PGC1α, (O) mitochondrial genes, and (P) regulators of fat metabolism. $n = 8$ for all cohorts. Scale for SDH 100 μm and CD31 50 μm. One-way analysis of variance followed by Bonferroni's multiple comparison tests used in all data sets except (E) where non-parametric Kruskal–Wallis test followed by the Dunn's multiple comparison was used. $^{*}P < 0.05$, $^{**}P < 0.01$, $^{***}P < 0.001$. EDL, extensor digitorum longus; MHC, myosin heavy chain; SDH, succinate dehydrogenase; sActRIIB, soluble activin receptor type IIB.

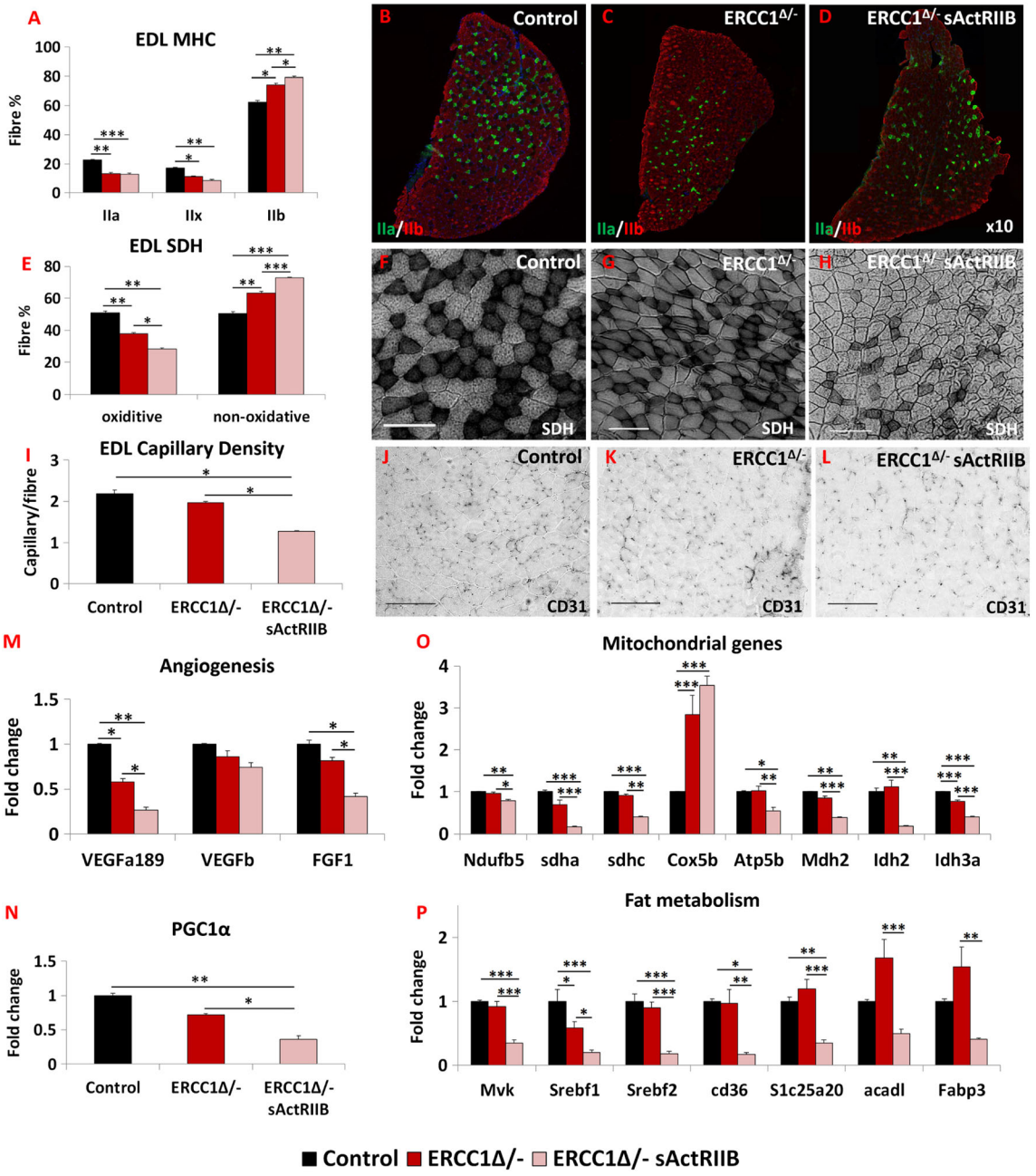

1K–1M). Food intake of *Ercc1*$^{\Delta/-}$ mutants, relative to body weight, was higher than control mice, but unaffected by sActRIIB treatment, excluding indirect effects of diet restriction for which *Ercc1*$^{\Delta/-}$ mice are very sensitive (*Figure* 1N–1O).[23] Water intake was not affected by the treatment (data not shown).

Quantitative and qualitative improvements to skeletal muscle through soluble activin receptor type IIB treatment

Previous work has shown that sActRIIB treatment increases muscle mass. The increased body weight and grip strength of *Ercc1*$^{\Delta/-}$ mice subjected to sActRIIB prompted us to further examine individual muscles. Treated *Ercc1*$^{\Delta/-}$ mice revealed that all five groups showed significant greater mass compared with those from mock-treated *Ercc1*$^{\Delta/-}$ animals with a range of 30–62% (TA and plantaris, respectively; *Figure* 2A–2C). Activation of signalling pathways initiated through ActRIIB and relevant to this study was found to be elevated in the muscle of *Ercc1*$^{\Delta/-}$ mice and decreased by sActRIIB treatment (*Figure* S3A). Importantly, the abundance of DNA breaks was not changed by sActRIIB treatment (*Figure* S3B). Furthermore, sActRIIB failed to increase the mass of any other organ examined including the heart, kidney, and liver (*Figure* S2C and S2D). We explored the mechanisms underlying the increase in muscle mass following sActRIIB treatment of *Ercc1*$^{\Delta/-}$ mice. Introduction of sActRIIB induced fibre hypertrophy irrespective of MHC expression (*Figure* 2D–2G). Of particular note was the finding that some types of fibres in the sActRIIB-treated *Ercc1*$^{\Delta/-}$ muscles were significantly larger than even in controls (see MHCI and IIA in soleus; *Figure* 2E). The total fibre number in EDL was elevated in *Ercc1*$^{\Delta/-}$ mutants and maintained by sActRIIB (*Figure* 2H). A similar trend was found in the soleus (*Figure* 2H). Of particular note was the observation of a large proportion of fibres with micro-lesions (including tears to the membrane) isolated from the EDL muscle from *Ercc1*$^{\Delta/-}$ animals, which appeared largely normalized by sActRIIB (*Figure* 2I and 2J). Caspase-3 activity as a gauge of apoptosis was significantly elevated in muscle of *Ercc1*$^{\Delta/-}$ mice and largely normalized by treatment with sActRIIB (*Figures* 2K and S3C). The number of fibres displaying centrally located nuclei was elevated in both the EDL and soleus muscles from *Ercc1*$^{\Delta/-}$ mice compared with controls and became even more abundant following sActRIIB treatment (*Figures* 2L and S3D). The fibres showing supranormal levels of SDH activity, indicative of abnormal mitochondrial activity that leads to apoptosis,[30] were significantly more frequent in both the EDL and soleus of *Ercc1*$^{\Delta/-}$ mice compared with treated mutants (*Figure* 2M–2O). Assessment of ROS activity through DHE intensity showed elevated levels of superoxide in muscle of *Ercc1*$^{\Delta/-}$ animals, which was lowered by sActRIIB treatment although it did not reach the level of control mice (*Figure* 2P–2S).[31,32]

Myosin heavy chain, oxidative fibre profiling, vascular organization, and molecular metabolic analysis of skeletal muscle

Myosin heavy chain analysis revealed that the progeric muscle displayed a faster profile compared with control muscles (*Figure* S1H–S1J). Treatment of progeric animals with sActRIIB resulted in a shift towards an even faster MHC profile. This was particularly pronounced in the EDL, with an increase in the proportion of type IIB fibres at the expense of both types IIA and IIX (*Figure* 3A–3D).

To examine the metabolic status of the sActRIIB-treated muscle, we determined the SDH activity. In both the EDL and the soleus, the number of SDH-positive fibres was decreased in the progeric mice compared with controls (*Figures* 3E–3H and S3E). Introduction of sActRIIB treatment further decreased the number of SDH^{+} fibres and, at the same time, increased the number of SDH^{-} entities in the EDL (*Figure* 3E–3H). Similar changes were also recorded in the soleus (*Figure* S3E). Therefore, the sActRIIB treatment further reduces the status of the already diminished oxidative character of *Ercc1*$^{\Delta/-}$ muscles. Subsequently, we investigated whether changes in the muscle metabolic profile wrought by sActRIIB also induced a remodelling of the vasculature. The capillary density profile indeed showed that the number of blood vessels serving each fibre was lower in *Ercc1*$^{\Delta/-}$ mice (albeit non-significantly) and further decreased following sActRIIB treatment (*Figure* 3I–3L). These changes were underpinned by decreases in the expression of three genes examined that control the development of blood vessels (*Figure* 3M). Expression of *PGC1α*, a key regulator of oxidative properties in muscle, was slightly lower in muscle from *Ercc1*$^{\Delta/-}$ mice compared with controls and was even more suppressed following sActRIIB treatment (*Figure* 3N). The changes in genes supporting the development of blood vessels were mirrored by mitochondrial transcript levels. qPCR analysis of eight genes important for the mitochondrial metabolism revealed that seven had decreased expression in *Ercc1*$^{\Delta/-}$ muscles induced by sActRIIB treatment (*Figure* 3O). We also investigated genes that control fat metabolism. All seven genes examined were significantly reduced in expression by sActRIIB (*Figure* 3P).

Therefore, the attenuation of signalling through sActRIIB results in the patterning of muscle towards a fast contracting status, which has a paucity of oxidative fibres and supporting blood vessels underpinned by changes in the expression of genes that control capillary development and sustain aerobic metabolism.

Ultrastructure and mitochondrial characterization in muscle

The ultrastructure of skeletal muscle in the three cohorts was examined using transmission electron microscopy. Numerous abnormalities were evident in the muscle from *Ercc1*$^{\Delta/-}$ mice including heterogeneous Z-line lengths, missing Z-lines, misaligned Z-lines, split sarcomeres, and large inter-sarcomeric spaces compared with controls (*Figure* 4A, 4B, 4D, 4E, 4G, and 4H). These abnormalities were largely absent

Figure 4 sActRIIB prevents *Ercc1*$^{\Delta/-}$ muscle ultrastructural abnormalities and supports normal levels of expression of key stress indicators. All Electron microscopy (EM) longitudinal image and quantitative measurements are from the bicep muscle. (A) Low-power image of control muscle. (B) Low-power image of *Ercc1*$^{\Delta/-}$ muscle. Note large spaces (black arrowheads), non-uniform sarcomere width (red arrows), dilated sarcomeric mitochondria (red arrowheads), split sarcomere (black arrow), and disrupted M-Line (blue arrow). (C) Low-power image of sActRIIB-treated *Ercc1*$^{\Delta/-}$ muscle. (D) Higher magnification of sarcomeric region of control muscle showing uniformly sized mitochondria (black arrows). (E) Enlarged mitochondria in sarcomeric region of *Ercc1*$^{\Delta/-}$ muscle (blue arrowhead) and absent (blue arrow) or faint Z-line (black arrow). (F) Higher magnification of sarcomeric region of treated *Ercc1*$^{\Delta/-}$ mice showing smaller sarcomeric mitochondria (black arrows). (G) Sarcolemma region of control muscle showing compact mitochondria (red arrowhead). (H) Dilated (blue arrowhead) and aberrant mitochondria (blue arrow) in sub-sarcolemma region of *Ercc1*$^{\Delta/-}$ muscle. (I) Sarcolemma region of treated *Ercc1*$^{\Delta/-}$ mice showing compact mitochondria (red arrowhead). (J, K) Sarcomeric (intrafusal) and sub-membrane mitochondrial density measurements. (L, M) Sub-membrane and sarcomeric (intrafusal) mitochondrial size measurements. (N) Expression of mitochondria unfolded protein response gene in gastrocnemius muscle. (O) Expression of inflammatory genes in gastrocnemius muscle. (P) Expression of *prohibitin* genes in gastrocnemius muscle. (Q) Quantification of EDL fibres expressing H3K9me3 and (R) H4K20me3. EM studies n = 6–7 for all cohorts. All other measures n = 8–9 for all cohorts. Non-parametric Kruskal–Wallis test followed by the Dunn's multiple comparisons used in (N, O) and the rest with one-way analysis of variance followed by Bonferroni's multiple comparison tests. *$P < 0.05$, **$P < 0.01$. EDL, extensor digitorum longus; sActRIIB, soluble activin receptor type IIB.

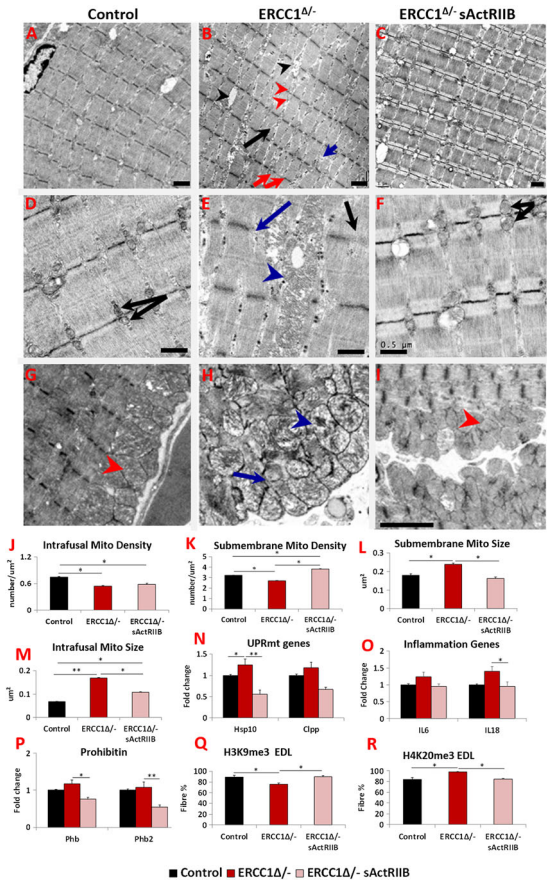

in muscle from *Ercc1*$^{\Delta/-}$ mice treated with sActRIIB (*Figure* 4C, 4F, and 4I). Quantification of mitochondria density revealed a decrease in this parameter both within the fibre (sarcomeric region) and directly under the sarcolemma (*Figure* 4J and 4K). Of special note was the alteration (swelling) of mitochondria both within the fibre and immediately under the sarcolemma (*Figure* 4H). Quantification of mitochondrial size showed enlargement in the muscle from *Ercc1*$^{\Delta/-}$ mutants, which was reduced by the treatment with sActRIIB (*Figure* 4L and 4M). Mitochondrial hypertrophy has been shown to be a protective response to a decrease in mitochondrial function or number or an indicative excessive fusion.[33–35] It is thought to promote mitochondrial survival by up-regulating a stress response programme. Indeed, we found that there was an increase in the expression of key genes involved in the mitochondrial unfolded protein response (UPR^{MT}) pathway in the muscle from *Ercc1*$^{\Delta/-}$ mice (*Figure* 4N). We also examined the levels of inflammatory and prohibitin genes, which support mitochondrial function of ensuring correct folding of the cristae.[36] Expression of *IL6* and *IL18* as well as two key prohibitin genes (*Phb* and *Phb2*) appeared slightly elevated in the muscle of *Ercc1*$^{\Delta/-}$ mice (*Figure* 4O and 4P). Treatment of *Ercc1*$^{\Delta/-}$ mice with sActRIIB generally prevented these changes (*Figure* 4A–4P). Lastly, we examined whether muscle harboured epigenetic modifications involved in the maintenance of heterochromatin that change with age.[37,38] The ageing process causes a decrease in the level of H3K9me3 but an increase in H4K20me3.[39] H3K9me3 was decreased, and H4K20me3 increased in *Ercc1*$^{\Delta/-}$ animals in keeping with an age-related change (*Figure* 4Q and 4R). Both features were normalized following sActRIIB treatment (*Figure* 4Q and 4R).

These results demonstrate subcellular defects in the *Ercc1*$^{\Delta/-}$ muscle and the expression of genes indicative of ongoing stress. sActRIIB treatment prevented the development of many of these abnormal features.

Connective tissue profiling

Skeletal muscle force transmission relies on proteins that link the contractile apparatus to the extra cellular matrix (ECM). We examined two of its components and determined how they were modified by the *Ercc1*$^{\Delta/-}$ genotype and thereafter by sActRIIB treatment. First, we examined the expression of *dystrophin*, a key intercellular component that links the cytoskeleton to the ECM. Its RNA expression was decreased in the *Ercc1*$^{\Delta/-}$ muscle, which was subsequently increased to levels greater than controls by sActRIIB (*Figure* 5A). We measured the amount of dystrophin specifically located between fibres using quantitative immuno-fluorescence and confirmed its reduction specifically at this site in the *Ercc1*$^{\Delta/-}$ muscle compared with controls and was significantly increased by sActRIIB (*Figure* 5B and 5D). Thereafter, we examined

DOI: 10.1002/jcsm.12404

Figure 5 Normalization of *Ercc1*$^{\Delta/-}$ extracellular components by sActRIIB and differentiation and self-renewal of its satellite cells. (A) *Dystrophin* gene expression measured by quantitative PCR (qPCR). (B) Measure of dystrophin in fibre-type-specific manner using quantitative immunofluorescence. (C) Measure of *collagen IV* expression profiling by qPCR. (D) Immunofluorescence image for dystrophin expression in EDL muscle. (E) Immunofluorescence image for collagen IV expression in EDL muscle. $n = 7$ for all cohorts. (F) EDL myonuclei count. (G) Quantification of satellite cells on freshly isolated EDL fibres. (H) Quantification of cells on EDL fibres after 72 h culture. (I) Control, mock-treated *Ercc1*$^{\Delta/-}$, and sActRIIB-treated *Ercc1*$^{\Delta/-}$ fibre examined at 72 h for expression of Myogenin (red) and Pax7 (green). Arrows indicated satellite cell progeny. (J) Quantification of EDL differentiated (Pax7^{-}/Myogenin^{+}) vs. stem cell (Pax7^{+}/Myogenin^{-}) after 72 h in culture. Fibres collected from three mice from each cohort and minimum of 25 fibres examined. Scale 50 μm. Non-parametric Kruskal–Wallis test followed by the Dunn's multiple comparisons used for (A–C). Rest of data was analysed using one-way analysis of variance followed by Bonferroni's multiple comparison tests. $^{*}P < 0.05$, $^{**}P < 0.01$, $^{***}P < 0.001$. EDL, extensor digitorum longus; sActRIIB, soluble activin receptor type IIB.

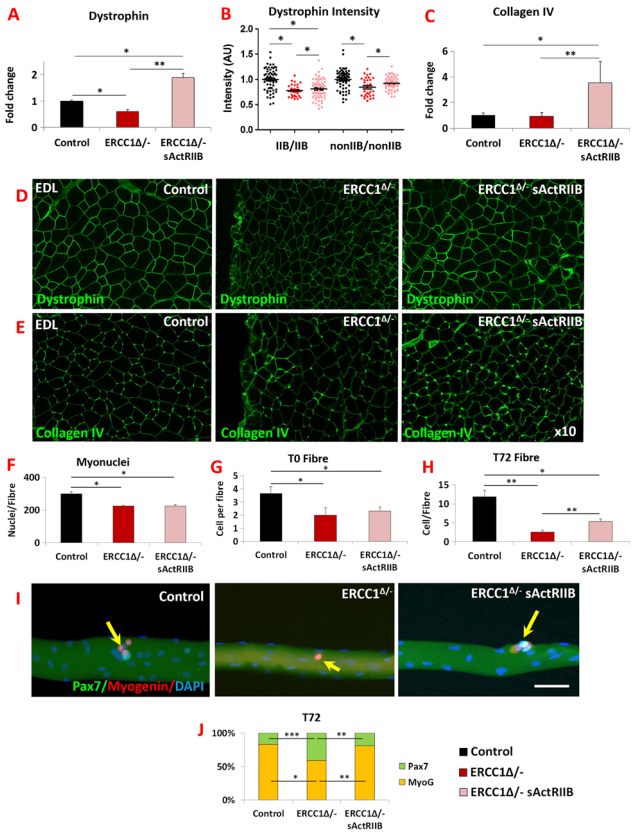

expression of *collagen IV* as basement membrane component important for force transmission. Its expression was slightly decreased albeit not reaching statistical significance in *Ercc1*$^{\Delta/-}$ muscle (*Figure* 5C). However, sActRIIB caused its level to increase over both untreated *Ercc1*$^{\Delta/-}$ and control levels (*Figure* 5C). Collagen IV gene expression levels were reflected at the protein level at the myofibre surface (*Figure* 5E).

Mechanisms underlying fibre size changes

To explore mechanisms regulating muscle mass, we investigated changes in anabolic and catabolic programmes. Surprisingly, levels of phosphorylated Akt (an inducer of anabolism) appeared elevated in the muscle from 16-week-old mock-treated *Ercc1*$^{\Delta/-}$ mice (*Figure* S4A). Next, we examined downstream targets of pAkt and found that there was a slight decrease in the phosphorylation of 4EBP1 at Thr37/46 but none at Ser65 (*Figure* S4B). However, there was an elevated level of phosphorylation at another pAkt target, S6 (*Figure* S4C). The effect of sActRIIB on the anabolic programme of *Ercc1*$^{\Delta/-}$ muscle showed a general increase in the level of pAkt, as well as its two downstream targets, 4EBP1 and S6, relative to both mock-treated *Ercc1*$^{\Delta/-}$ and control groups (*Figure* S4A–S4C). Thereafter, we probed the catabolic programme and found that activity of FoxO1 and FoxO3a, key regulators of both ubiquitin-mediated protein breakdown (FoxO1 significantly, FoxO3a not so), was generally decreased in the muscle from *Ercc1*$^{\Delta/-}$ mice (*Figure* S4D and S4E), even to a level exceeding controls. Expression of both *MuRF1* and *Atrogin-1* downstream targets of FoxO1 and FoxO3a were elevated at the RNA level in the muscle of *Ercc1*$^{\Delta/-}$ mice (*Figure* S4I and S4J). The LC3 autophagy activity was suppressed compared with controls (*Figure* S4F). Treatment with sActRIIB caused an elevation in the levels of inactive FoxO1 and FoxO3a (*Figure* S4D and S4E) and a decrease in the expression of *MuRF1* but, surprisingly, not *Atrogin-1* (*Figure* S4I and S4J). Expression of *Mul1*, a key regulator of mitophagy,[40] did not differ in the three groups (*Figure* S4K). Significantly, we found an increase in the level of autophagy gauged by the LC3II/I ratio and levels of p62 following sActRIIB treatment (*Figure* S4F and S4G). We quantified the presence of p62 puncta, which has been used as an indicator of autophagic flux, with an increase in the numbers of p62 puncta implying a decrease in autophagic activity.[41] The number of p62 puncta per given area were higher in *Ercc1*$^{\Delta/-}$ EDL muscle compared with controls, and their levels were reduced by sActRIIB treatment (*Figure* S4L and S4M). Treatment of *Ercc1*$^{\Delta/-}$ mice with sActRIIB resulted in a non-significant increase in the amount of active eIF2a, a key regulator of the endoplasmic reticulum UPR (UPR^{ER}) programme (*Figure* S4H). At the organismal level, we found that the rate of protein synthesis was elevated (but not to significant levels) in *Ercc1*$^{\Delta/-}$ mice and further elevated by sActRIIB treatment (*Figure* S4N). The abundance of ubiquitinated proteins was elevated in the muscle of *Ercc1*$^{\Delta/-}$ mice but reduced by sActRIIB treatment (*Figure* S4O).

These results reveal novel characteristics considering the changes in muscle mass in the progeric mice. The muscle of *Ercc1*$^{\Delta/-}$ mice activates both its protein synthesis pathway and has elevated gene expression of molecules that control protein breakdown. However, autophagy is blunted. Treatment of *Ercc1*$^{\Delta/-}$ with sActRIIB results in an increase in the

DOI: 10.1002/jcsm.12404

activity of molecules controlling protein synthesis as well as overall rate of protein synthesis, a decrease in the abundance of ubiquitinated proteins E3 as well as an increase in key regulators of autophagy.

Myonuclei and satellite cell profiling

We examined features of individual myofibres to determine the effect of sActRIIB treatment. The number of myonuclei in the fibres from the EDL or the number of SC on them from either PBS- or sActRIIB-treated *Ercc1*$^{\Delta/-}$ mutants was significantly lower than the number in control mice (*Figure* 5F and 5G). We then investigated the proliferative capacity of the SC from the three cohorts and found that, after 72 h of culture, the population from control fibres had undergone a three-fold increase compared with initial numbers. In sharp contrast, the SC from PBS-treated *Ercc1*$^{\Delta/-}$ mice failed to undergo any significant proliferation. Importantly, sActRIIB treatment of *Ercc1*$^{\Delta/-}$ mice resulted in SC being able to undergo a 2.3-fold increase in number (*Figure* 5H). Finally, we found that the attenuated differentiation

Figure 6 The prevention of kidney function abnormalities through the maintenance of the filtration barriers by sActRIIB treatment of *Ercc1*$^{\Delta/-}$ mice. (A) Urine protein measurements at the end of week 14. (B–D) Low and (F–H) high magnification of electron microscopy images of podocytes from control, mock-treated *Ercc1*$^{\Delta/-}$, and sActRIIB-treated *Ercc1*$^{\Delta/-}$ mice. Pod indicates the podocyte. (C) *Ercc1*$^{\Delta/-}$ tissue contains autophagosomes (yellow arrow) and enlarged mitochondria (yellow arrowhead). (D) sActRIIB-treated *Ercc1*$^{\Delta/-}$ mice show some foot process effacement (red arrowheads) but significant number of mature foot processes (red arrow). (E) Quantification of foot process width. (F) Numerous mature foot processes in control sample (red arrows). (G) Very few foot processes in *Ercc1*$^{\Delta/-}$ sample but thickened glomerular basement membrane (red arrowheads). (H) Treated *Ercc1*$^{\Delta/-}$ sample showing numerous mature foot processes (red arrows). (I) Quantification of glomerular basement membrane thickness. (J) Nuclear size measurements in Nephrin-positive domain. (K) pSmad2/3 profile in control mice (red) in relation to podocytes, identified through Nephrin expression. (L) Abundant levels of pSmad2/3 (red arrows) in *Ercc1*$^{\Delta/-}$ podocytes. (M) Few pSmad2/3 puncta in sActRIIB-treated *Ercc1*$^{\Delta/-}$ podocytes (red arrow). n = 8 mice examined for each cohort for (A) and n = 5 mice examined for each cohort for (EM). Analysis performed using non-parametric Kruskal–Wallis test followed by the Dunn's multiple comparisons. *$P < 0.05$, **$P < 0.01$. sActRIIB, soluble activin receptor type IIB.

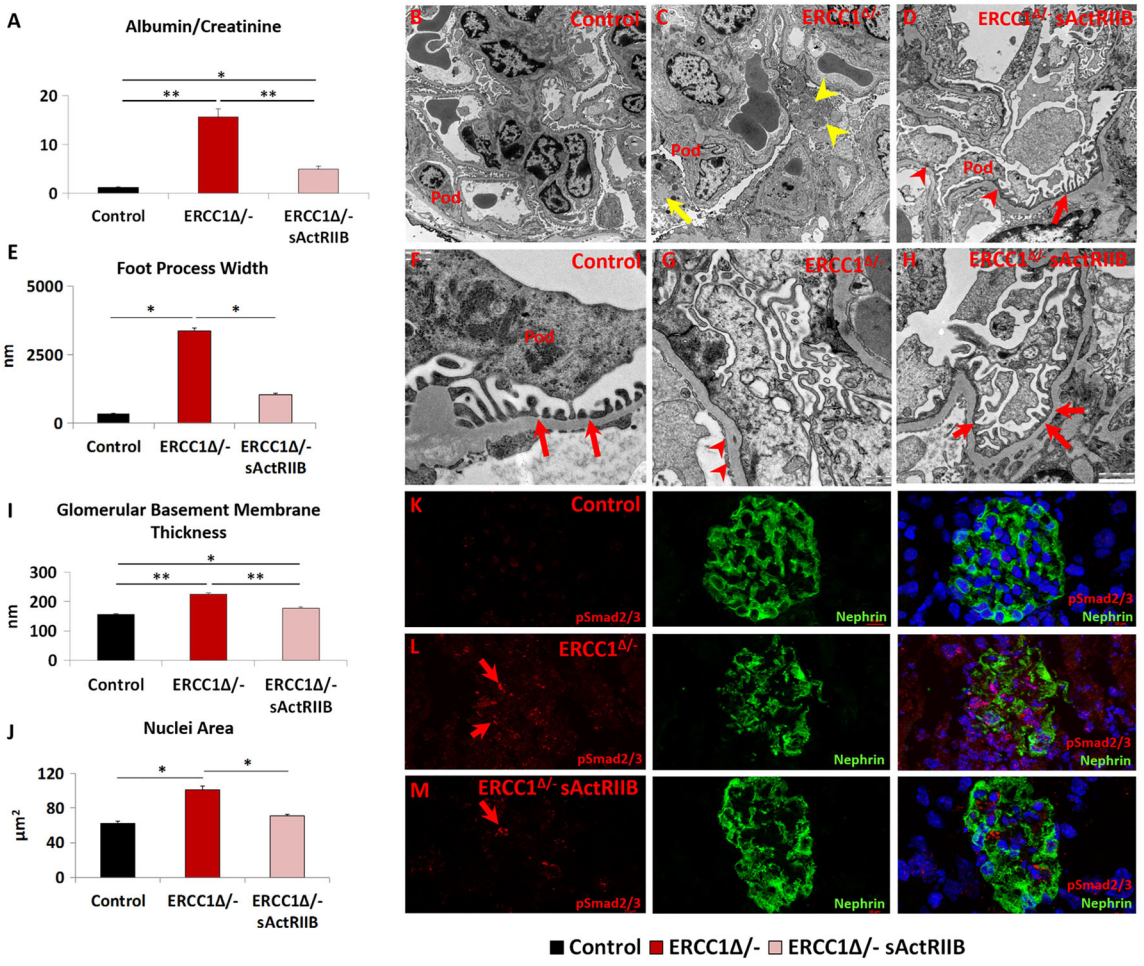

DOI: 10.1002/jcsm.12404

programme of SC from *Ercc1*$^{\Delta/-}$ mice was normalized by sActRIIB treatment (*Figure* 5I–5J).

Therefore, sActRIIB treatment mitigates abnormalities in SC proliferation, differentiation and self-renewal programmes in *Ercc1*$^{\Delta/-}$ animals. However, it did not normalize the low SC number found in mock-treated *Ercc1*$^{\Delta/-}$ mice.

Inhibition of glomerular anomalies in Ercc1$^{\Delta/-}$ mice by soluble activin receptor type IIB

Kidney pathology due to mutations in *ERCC1* has been reported in both human and mice.[2,20] Here, we investigated the impact of sActRIIB on kidney function and structure. Proteinuria analysis showed a 12-fold elevation in the albumin/creatinine ratio in urine from *Ercc1*$^{\Delta/-}$ mutants compared with controls at 16 weeks of age. This measure was reduced to an elevation of 3.7-fold in the urine of sActRIIB-treated *Ercc1*$^{\Delta/-}$ mice (*Figure* 6A). We investigated the mechanism underlying the proteinuria in *Ercc1*$^{\Delta/-}$ mice and how it is influenced by sActRIIB by examining the ultrastructure of the kidney filtration apparatus. Transmission electron microscopy showed the *Ercc1*$^{\Delta/-}$ podocytes hypertrophic, but additionally, they contained numerous abnormalities, including enlarged mitochondria as well as accumulation of autophagosomes (*Figure* 6B, 6C, 6F, and 6G, autophagosomes shown in detail in *Figure* S5A). The most prominent feature was the degree of foot process effacement in the *Ercc1*$^{\Delta/-}$ sample, which contrasted the regular structures found in control samples (*Figure* 6E–6G). When foot processes were present, they are significantly broader in *Ercc1*$^{\Delta/-}$ animals compared with controls (*Figure* 6E–6G). Glomerular basement membrane was also significantly thicker in *Ercc1*$^{\Delta/-}$ kidneys compared with controls (*Figure* 6F, 6G, and I6). All these features were to a greater degree normalized following the treatment with sActRIIB (*Figure* 6B–6I). At the ultrastructural level, enlarged mitochondria area and accumulation of autophagosomes were completely prevented (*Figure* 6D and 6H). Foot processes were evident (*Figure* 6H). It should be noted that in some regions, they appeared normal, whereas in other regions, they are still broader compared with controls (*Figure* 6D and 6H). The thickness of the glomerular basement membrane was significantly reduced by sActRIIB treatment compared with mock-treated progeroid mice but not to normal levels (*Figure* 6I). Nuclear size that was enlarged in the glomeruli of *Ercc1*$^{\Delta/-}$ specimens was maintained at normal dimensions by sActRIIB (*Figure* 6J). Finally, we examined whether the impact of sActRIIB could be through direct antagonism of myostatin/activin signalling by investigating the distribution of pSmad2/3 in podocytes. There was very little pSmad2/3 in control glomeruli (*Figure* 6K). In contrast, abundant pSmad2/3 was found in nuclei of *Ercc1*$^{\Delta/-}$ podocytes (*Figure* 6L). Following sActRIIB treatment, the abundance of pSmad2/3 in *Ercc1*$^{\Delta/-}$ podocytes was reduced compared with untreated progeroid mice (*Figure* 6M). However, it was still more prominent than controls.

These results show that foot process effacement is an underlying cause of proteinuria in *Ercc1*$^{\Delta/}$kidneys. sActRIIB treatment not only improved the ultrastructure of the filtration barrier but significantly also reduced proteinuria.

Impact of soluble activin receptor type IIB on ageing-related liver Ercc1$^{\Delta/-}$ abnormalities

The liver undergoes age-related changes both in humans and rodent models.[21,42,43] The nuclei in the livers of *Ercc1*$^{\Delta/-}$ mice undergo progressive ageing-related changes including enlargement, invaginations, and polyploidy. These features have been interpreted to indicate incomplete cytokinesis.[44] We found that both liver nuclear size and the number of liver multi-nucleated cells were increased in tissue from *Ercc1*$^{\Delta/-}$ mice compared with control tissue (*Figure* 7A and 7B). Treatment of *Ercc1*$^{\Delta/-}$ mice with sActRIIB significantly decreased both measures (*Figure* 7A and 7B). Having shown that age-associated changes in the liver nuclei of *Ercc1*$^{\Delta/-}$ mice were reduced following treatment with sActRIIB, we examined whether this was reflected by changes in epigenetic modification involved in the maintenance of heterochromatin.[37,38] Previous work has shown that levels of H3K9me3 are down-regulated during ageing,[39] and here too, we found such a relationship (*Figure* 7C). In contrast, ageing results in an increase in H4K20me3 marks. Here, we saw extensive levels of H4K20me3 in the liver of *Ercc1*$^{\Delta/-}$ and surprisingly of control mice (*Figure* 7D and 7G). Strikingly, the H4K20me3 marks were essentially absent in livers of *Ercc1*$^{\Delta/-}$ mice treated with sActRIIB (*Figure* 7D and 7G). Oxidative stress is one of the key drivers that induce age-related changes in the liver.[45] Again, we deployed the DHE dye to gauge the level of superoxide.[31,32] Superoxide levels were elevated in the liver samples of both *Ercc1*$^{\Delta/-}$ and control mice, compared with treated *Ercc1*$^{\Delta/-}$ mice (*Figure* 7E and 7H). Next, we profiled the metabolic activity of the liver as it is known to undergo a decrease in the level of oxidative phosphorylation with ageing.[21,46] In agreement with the work by Gregg *et al*. on *Ercc1*$^{\Delta/-}$ livers, we found a decrease in four of the six genes linked to oxidative phosphorylation (*Figure* 7F).[21] Expression of five genes was significantly increased by sActRIIB treatment relative to their levels in mock *Ercc1*$^{\Delta/-}$ animals (*Figure* 7F). Lastly, we determined whether the effects of sActRIIB on the livers of *Ercc1*$^{\Delta/-}$ mice were mediated by direct antagonism of myostatin/activin signalling. Profiling of pSmad2/3 showed that there was no activity in the parenchyma of the livers of the three cohorts (*Figure* S5B). Only a few pSmad2/3-expressing cells were found adjacent to smooth muscle in all three cohorts (*Figure* S5B).

Figure 7 sActRIIB prevents the development age-related liver abnormalities and osteoporotic phenotype in *Ercc1*$^{\Delta/-}$. (A) Measure of liver nuclear size. (B) Profile frequency of multinucleated liver cells. (C) Frequency of H3K9me3-positive liver cells. (D) Frequency of H4K20me3-positive liver cells. (E) Quantification of DHE fluorescence to gauge superoxide levels. (F) Quantitative PCR profiling of mitochondrial gene expression. (G) Immunofluorescence images for H4K20me3 distribution in the three cohorts. (H) DHE intensity levels in the three cohorts. (I) Trabecular bone volume measurements. (J) Trabecular tissue volume measurements. (K) Trabecular bone to tissue volume ratios. (L) Trabecular separation indices. (M) Enumeration of trabeculae. (N) Degrees of trabecular anisotrophy. (O) Trabecular pattern factor as a quantification of bone architecture. (P) Structure model index. (Q) Measure of cortical bone volume. (R) Cortical tissue volume measure. Trabecular bone volume measurements. n = 8 for all animals in (A–H) and n = 6 control male mice, five *Ercc1*$^{\Delta/-}$-untreated male mice, and six *Ercc1*$^{\Delta/-}$-treated male mice in other experiments. One-way analysis of variance followed by Bonferroni's multiple comparison tests used for (A–F) and non-parametric Kruskal–Wallis test followed by the Dunn's multiple comparisons for (I–R). *$P < 0.05$, **$P < 0.01$, ***$P < 0.001$. DHE, dihydroethidium; sActRIIB, soluble activin receptor type IIB.

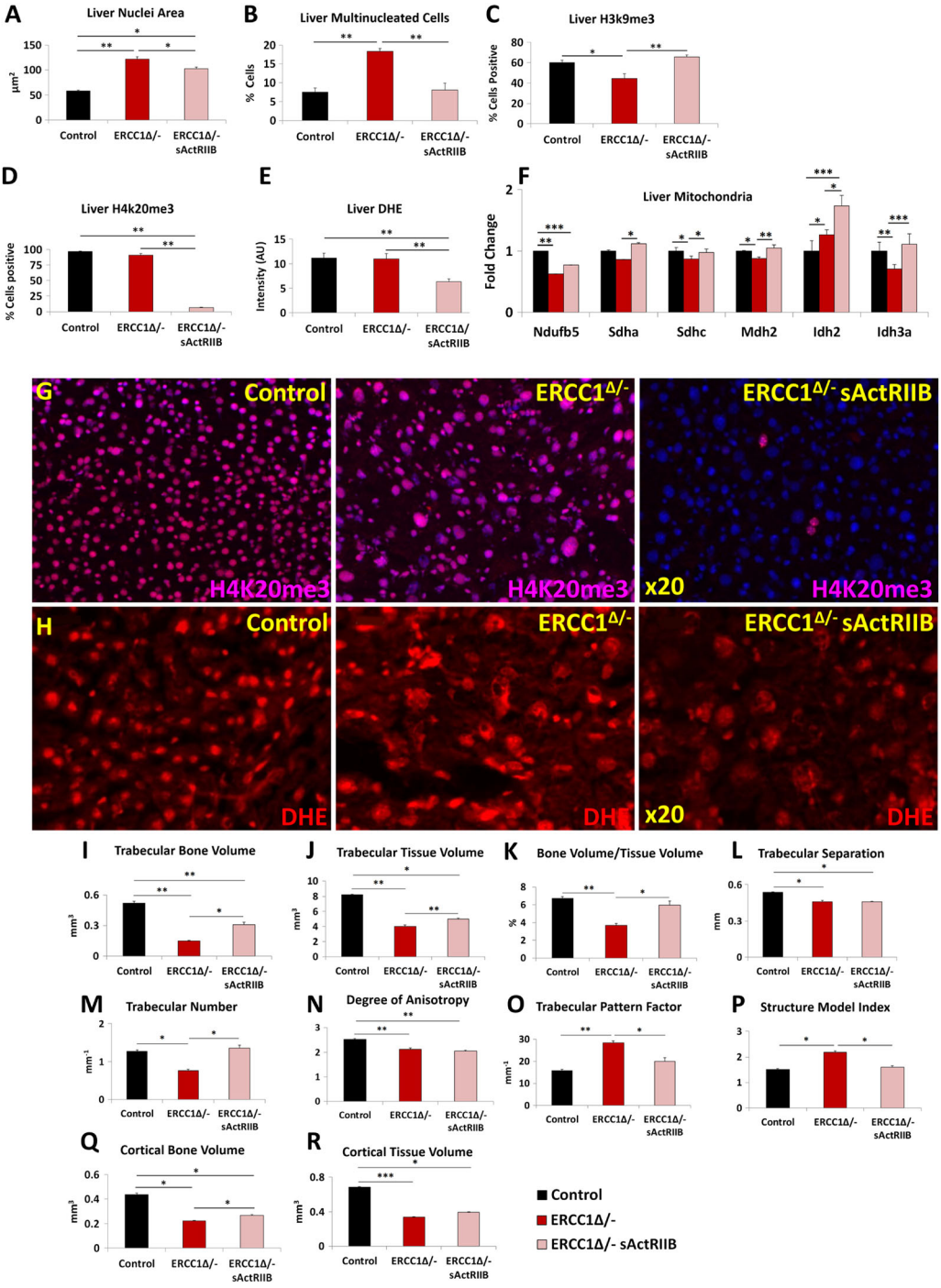

DOI: 10.1002/jcsm.12404

These results show that antagonism of myostatin/activin signalling leads to profound normalization of *Ercc1*$^{\Delta/-}$ liver cell nuclear structure, selective epigenetic modification of DNA and changes in gene expression indicative of increased oxidative phosphorylation and a reduction in superoxide levels.

Prevention of the osteoporotic phenotype in Ercc1$^{\Delta/-}$ mice by soluble activin receptor type IIB

Micro-CT analyses revealed that *Ercc1*$^{\Delta/-}$ mice exhibit a premature ageing-related osteoporotic phenotype with extreme differences in trabecular and cortical bone mass and architecture compared with control mice. In the trabecular compartment, there was a significant reduction in bone volume, tissue volume, bone volume/tissue volume, trabecular separation, trabecular number, and degree of anisotropy, a measure of how highly oriented substructures are within a volume (*Figure* 7I–7N). Significantly higher trabecular pattern factor indicating trabecular connectivity and structure model index a measure of surface convex curvature and an important parameter in measuring the transition of osteoporotic trabecular bone from a plate-like to rod-like architecture were also observed in *Ercc1*$^{\Delta/-}$ mice compared with controls animals (*Figure* 7O). Cortical bone volume and tissue volume were significantly lower, further demonstrating that *Ercc1*$^{\Delta/-}$ mice have an osteoporotic bone phenotype (*Figure* 7Q and 7R).

Analysis of trabecular bone revealed significant increase in bone and tissue volume, bone/tissue volume, and trabecular number in *Ercc1*$^{\Delta/-}$ sActRIIB-treated mice compared with mock-treated animals, indicating treatment prevents a decrease in the size of the trabecular compartment and the amount of bone present (*Figure* 7I–7K). In addition, trabecular pattern factor was significantly lower in the treated group compared with mock-treated with levels close to the control group, showing trabecular connectivity improved upon treatment (*Figure* 7O). Furthermore, the structure model index was significantly lower in the treated group, again with results close to the control group (*Figure* 7P). Cortical bone volume and tissue volume were significantly lower in

Figure 8 sActRIIB delays neurological abnormalities in *Ercc1*$^{\Delta/-}$ mice without affecting lifespan. (A, B) Body weight changes of treated (sActRIIB or mock control) *Ercc1*$^{\Delta/-}$ mice at a second test site ($P = 0.07$). Intraperitoneal injection started at week 7. (C) Average grip strength of the forelimbs and all limbs of 4-month-old *Ercc1*$^{\Delta/-}$ mice under mock and sActRIIB conditions. (D) Average time spent on an accelerating rotarod of *Ercc1*$^{\Delta/-}$ mice on different treatments weekly monitored. (E–G) Onset of neurological abnormalities (F) tremors ($P = 0.28$), (F) severe tremors ($P = 0.0014$), and (G) imbalance ($P = 0.021$) with age. (H) Survival of sActRIIB-treated and mock-treated *Ercc1*$^{\Delta/-}$ mice ($P = 0.27$). $n = 10$ animals per group. Error bars indicate mean ± SE. Log-rank Mantel-Cox test. $^{*}P < 0.05$, $^{**}P < 0.01$, $^{***}P < 0.001$. sActRIIB, soluble activin receptor type IIB.

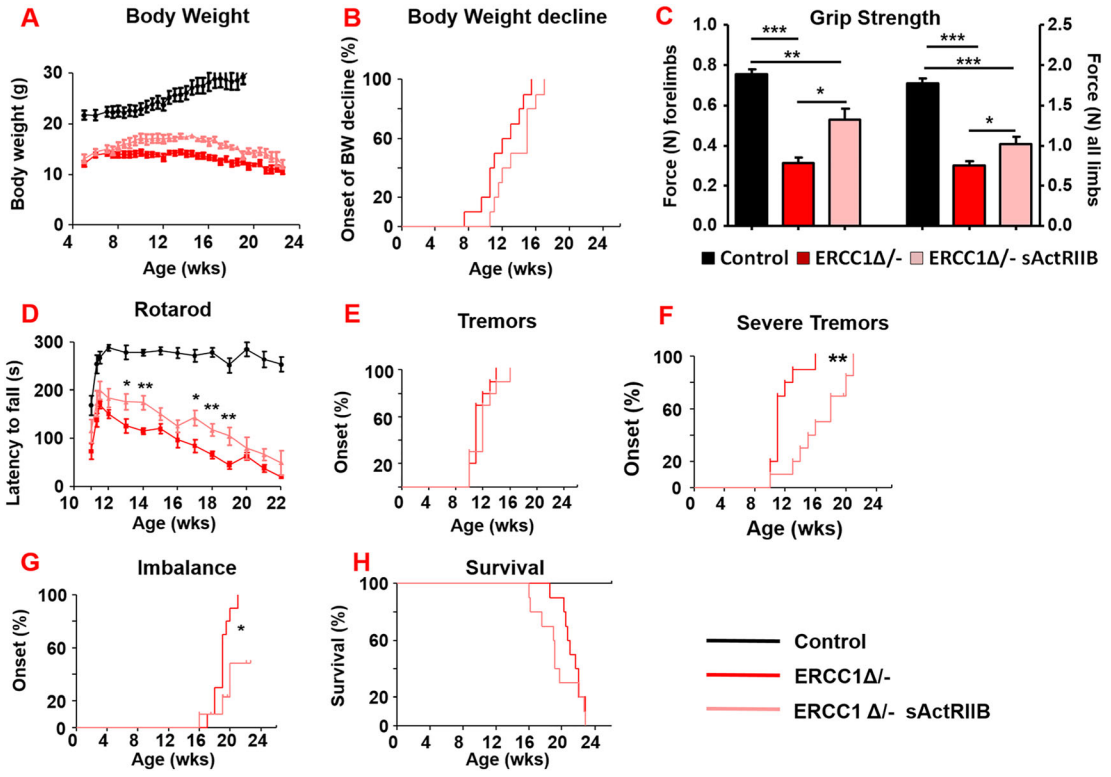

DOI: 10.1002/jcsm.12404

Table 2. sActRIIB administration attenuates progeroid phenotypes of *Ercc1*$^{\Delta/-}$ mice

Symptoms	Age at onset (weeks)		Change of onset (weeks)	# of Ercc1$^{\Delta/-}$ mice (Mock, sActRIIB)
	Mock	sActRIIB		
Clasping	5.00	4.80	−0.20	(10, 10)
Tremors	11.40	12.10	**0.70**	(10, 10)
Severe tremors	11.60	16.11	**4.51**	**(10, 9)**
Body weight decline	11.80	13.60	**1.80**	(10, 10)
Kyphosis	17.75	18.15	0.40	(10, 10)
Imbalance	18.95	18.33	−0.62	**(10, 3)**
Paresis	20.50	18.80	−1.67	**(6, 3)**

The average age at onset of characteristic progeroid phenotypes in treated *Ercc1*$^{\Delta/-}$ mice and the difference between the group averages is shown. The last column indicates the total number of mice out of 10 per group that displays the phenotype before end of life. Phenotypes delayed more than 0.5 weeks on average or absent in mice treated with sActRIIB compared with mock treated *Ercc1* $^{\Delta/-}$ mice are indicated in bold. sActRIIB, soluble activin receptor type IIB.

Ercc1$^{\Delta/-}$ mice compared with the control groups, with treatment significantly lessened the tissue volume and bone volume decline (*Figure* 7Q and 7R).

Together, these analyses reveal that sActRIIB treatment produces tibial architecture changes and prevents a decrease in trabecular and cortical bone mass in *Ercc1*$^{\Delta/-}$ mice, mitigating the premature ageing-related osteoporotic phenotype observed in this and previous studies.

Long-term effects of soluble activin receptor type IIB administration to Ercc1$^{\Delta/-}$ mice

To confirm the previous results and monitor phenotypical age-related changes beyond the age investigated so far, we initiated a second cohort of *Ercc1*$^{\Delta/-}$ mice at another location. Treatment regime, regarding timing, dosage, and frequency, was kept identical. Similarly, *Ercc1*$^{\Delta/-}$ mice reached a higher body weight upon IP injection of sActRIIB as compared with PBS-injected mutant mice (*Figure* 8A). No gender-specific response was found in terms of body weight changes due to sActRIIB treatment of *Ercc1*$^{\Delta/-}$ mice (*Figure* S6B). As a consequence of the ageing-associated deterioration, they all gradually declined with age after reaching their maximal body weight, which was delayed by sActRIIB administration (*Figure* 8B). Simultaneously, *in vivo* imaging showed a substantial increase in both muscle and bone volume (*Figure* S6A) confirming the robustness of sActRIIB treatment.

All animals from the sActRIIB group had a more vigorous and lively appearance and showed an improved grip strength for both the forelimbs and all limbs (*Figure* 8C). Additionally, locomotor function, as measured by Rotarod performance, was significantly improved by sActRIIB over the entire lifespan, but still declined with age parallel to the mock-treated mice (*Figure* 8D).

A prominent ageing feature of these mice is related to neurodegeneration and the onset of several neuro-muscular phenotypic changes.[22] Longitudinal examination of behavioural abnormalities showed that the onset of tremors was not delayed following sActRIIB treatment but was reduced in severity (*Figures* 8E, 8F, and S6C and *Table* 2). The onset of imbalance was greatly postponed and frequently absent as well as the onset of paresis of the hind legs (*Figure* 8G and *Table* 2). Nevertheless, sActRIIB treatment of *Ercc1*$^{\Delta/-}$ mice did not extend survival of the animals (*Figures* 8H and S6D). These results show that attenuating myostatin/activin signalling prolongs health span rather than delaying death.

Discussion

The key findings of this study are, first, that the sarcopenic programme in the *Ercc1*$^{\Delta/-}$ progeroid mouse model not only shows many parallels with naturally aged rodent muscle but also reaches more severe stages and displays several distinctive features. Second, we demonstrate that sarcopenia was attenuated through the antagonism of myostatin/activin signalling despite persistent defective DNA repair. Third, we reveal that inhibition of myostatin/activin signalling induces multi-systemic physiological improvements; mice increased locomotor activity; increased specific force and kidney function; improved key features of liver biology; mitigated the osteoporotic phenotype; and delayed parameters of neurodegeneration.

Ercc1$^{\Delta/-}$ muscle parallels with natural muscle ageing and pathological muscle diseases.

We first defined the characteristics of muscle in the *Ercc1*$^{\Delta/-}$ progeroid model in light of previous work and discovered many unexpected features related to muscle composition rather than in its overall mass. At the quantitative level, all muscle groups from *Ercc1*$^{\Delta/-}$ mice were much lighter than control mice, which concords with findings in aged humans and mouse models.[47,48] In addition, our studies revealed numerous qualitative differences between progeroid muscle and muscle of aged wild-type mice. All MHC fibre types were smaller in *Ercc1*$^{\Delta/-}$ muscle, and most had undergone a slow to fast fibre profile shift. These features differ from wild-type mouse muscle where MHCIIB preferentially undergo aged-related atrophy,[49] and fibres in both humans and rodents undergo a shift from fast to slow.[50] We also discovered that the number of fibres in both EDL and soleus muscles were higher than controls, which seems counter-intuitive given the overall loss in muscle mass in *Ercc1*$^{\Delta/-}$ mice. Parallels are invited between the ostensible hyperplasia in our sarcopenic condition and the increased fibre numbers seen in myo-pathological conditions, such as Duchenne muscular dystrophy.[51] We suggest that the increased fibre number is due to the abundance

DOI: 10.1002/jcsm.12404

of split fibres, a notion supported by our results showing that muscle from *Ercc1*$^{\Delta/-}$ mutants contains a large proportion of damaged fibres. Additional findings including the high level of caspase activity and the decrease in dystrophin and collagen lead us to propose that the muscle fibres from *Ercc1*$^{\Delta/-}$ mice have elevated levels of contraction-induced damage which leads to cellular lesions (splitting) and ultimately results in fibre death. Fibre apoptosis and necrosis are a common feature of age-related muscle wasting but not of disuse atrophy. Indeed, we found that the proportion of dying fibres was far greater in *Ercc1*$^{\Delta/-}$ muscle than found in aged wild-type mice.[30]

The muscle of *Ercc1*$^{\Delta/-}$ mice contains numerous abnormal fibres (identified through central nucleation) and dying fibres, but those that seem normal contain subcellular aberrations. Ultrastructural examination reveals abnormalities in the organization of the contractile apparatus and the cellular organelles. Of note, mitochondria were quantitatively and qualitatively affected by the *Ercc1* mutation in muscle. Their density was decreased both within the fibre as well as under the sarcolemma where they would support contraction and membrane-related activities, respectively.[52] Furthermore *Ercc1*$^{\Delta/-}$ muscle mitochondria at both sites were swollen indicative of response to either functional deficit or altered fusion.[33,34] Our studies show elevated levels of ROS through the profiling of DHE activity.[53] We therefore suggest that the *Ercc1* mutation in muscle leads to ultimately compromised mitochondrial function, resulting in increased ROS production, which may compromise the function of the contractile apparatus as well as ultimately inducing fibre death.[52]

Analysis of key proteins involved in anabolic and catabolic programmes revealed an interesting landscape. Surprisingly, *Ercc1*$^{\Delta/-}$ muscle showed elevated levels of Akt activity, one of two downstream genes (S6) and overall rate of protein synthesis. The muscle of *Ercc1*$^{\Delta/-}$ mice expressed high levels of *MuRF1* and *Atrogin-1* and contained increased levels of ubiquitinated proteins. Hence, the muscle of *Ercc1*$^{\Delta/-}$ animals had initiated a programme of protein synthesis yet, at the same time, was promoting their breakdown, which significantly deviates from normal catabolic conditions.[54] Although unusual in the context of normal physiology, these results agree with other studies of progeroid models that demonstrate the activation of pathways to limit the effect of the primary lesion.[21] We suggest that in the context of *Ercc1*$^{\Delta/-}$ muscle, the activation of the protein synthesis pathway acts to decrease an extremely high rate of muscle wasting. Nevertheless, the ultimate deregulation of protein synthesis, proteasome and autophagy pathways in *Ercc1*$^{\Delta/-}$ muscle, which parallels many disease conditions, culminates in atrophy.[55,56]

We also found changes in the number and behaviour of SC of the *Ercc1*$^{\Delta/-}$ muscle; not only were they fewer in number but they also displayed an inability to divide following the isolation of single muscle fibres as well as an attenuated ability to differentiate. Some but not all these features are shared by SC from sarcopenic human muscle; SC from sarcopenic human muscle were shown to be more prone to activation but not follow through a normal degree of differentiation.[57] However, comparisons of outcomes from different studies are problematic due to use of differing experimental systems.

Effects of soluble activin receptor type IIB on Ercc1$^{\Delta/-}$ muscle phenotype

Our study documents the profound effect of antagonizing myostatin/activin signalling on body and muscle mass as well as function of *Ercc1*$^{\Delta/-}$ mice. Age-related decreases in all three parameters were significantly attenuated in the *Ercc1*$^{\Delta/-}$ mutant by the soluble activin receptor ligand trap. The difference in the muscle mass between treated vs. untreated animals ranged between 30% (TA) and 62% (plantaris). The changes in muscle mass are extremely impressive and worthy of comparison with the *Mstn*$^{-/-}$ mutant. The EDL of the *Mstn*$^{-/-}$ was 60% heavier than the wild-type counterpart.[58] Here, after only 8 weeks of sActRIIB treatment, the EDL was 45% heavier. The differences in muscle mass between treated and untreated mice are of note when compared with outcomes that have previously deployed anti-myostatin/activin, non-genetic approaches in aged mice. One such study showed that the TA of aged mice underwent an increase of 6%, whereas here, even though it was the muscle that displayed the smallest increase nevertheless was 30% heavier than that of mock-treated *Ercc1*$^{\Delta/-}$ mice.[59] These results suggest that activity of myostatin and/or activin in *Ercc1*$^{\Delta/-}$ mice are considerably higher than in aged wild-type mice. Importantly, we show that treatment with sActRIIB did not induce changes in the circulating levels of either GH, glucose, insulin, or IGF-1.

In this study, we show that muscles of *Ercc1*$^{\Delta/-}$ mice not only are smaller but contain numerous subcellular and biochemical abnormalities. It is well documented that contractile force normalized per mass is preserved when muscle undergoes regulated loss in weight.[60] Here, we see that *Ercc1*$^{\Delta/-}$ mice generated only 50% of normalized grip strength compared with controls but that this value was significantly improved by sActRIIB treatment. Abnormal specific force and relaxation times in the muscle of *Ercc1*$^{\Delta/-}$ muscle, both features of structure alterations,[61] were improved by sActRIIB treatment. We therefore suggest that sActRIIB not only prevents muscle from undergoing atrophy but also prevents the subcellular abnormalities. This is clearly evident in the TEM profiles of skeletal muscle, which show that every abnormal feature of *Ercc1*$^{\Delta/-}$ muscle (sarcomeres and mitochondria) was largely prevented by the action of sActRIIB. We suggest that at least one key mechanistic driver in this

process is the activation of the autophagic programme mediated by members of the FoxO family. Thus, we propose that abnormally low autophagic activity displayed in *Ercc1*$^{\Delta/-}$ muscle leads to accumulation of p62 puncta and presumably abnormal mitochondria as well as through hyper-activation of the UPR^{MT},[62] elevated levels of genes encoding *prohibitins* that function to restore organelle function,[36] change in the histone mark profile (down-regulation of H3K9Me3 and up-regulation of H4K20me3) as well as ROS superoxide levels. The build-up of ROS causes protein oxidation ultimately compromising the workings of the contractile apparatus and leading to a deficit in specific force.[63] Our interpretation of these finding is that sActRIIB treatment of *Ercc1*$^{\Delta/-}$ mice leads to the activation of autophagy (LC3II/I ratio), which prevents the accumulation of p62 puncta and also abnormally functioning mitochondria, thus counteracting the need to activate either the UPR^{MT} or prohibitin programmes, maintains a normal profile of histone modification as well as avoiding the build-up of high levels of ROS, which ultimately translates in the preservation of organ reserve capacity. We note that the expression of Mul1, a proposed mitochondrion-specific U3 ubiquitin ligase, was not affected by the progeroid condition or following treatment with sActRIIB compared with controls. However, it is worth bearing in mind that numerous mitochondria targeting U3 ubiquitin ligases have been identified including PARKIN and that these non-investigated molecules could be executing mitophagy in our experiments.[40]

However, the concomitant increase in protein synthesis and autophagy levels in *Ercc1*$^{\Delta/-}$ mice following sActRIIB treatment remains to be further investigated. In a normal setting, the two processes are antagonistically driven in large part by FoxO proteins (reviewed in Bonaldo & Sandri[56]). Here, we suggest that normal parameters do not operate evidenced by the hyper-activation of Akt in *Ercc1*$^{\Delta/-}$ muscle. Indeed, there is a growing body of evidence for dual activation of Akt-mediated pathways and autophagy when the normal landscape of regulation is altered.[64] Hyper-activation leading to initiation of novel signalling pathways and cellular outcomes is quite a common outcome and has been extensively studied especially in scenarios of uncontrolled cell division that underpin the development of many cancers.[65,66] Future studies, beyond the scope of the present investigation, combining gene expression and proteomic platforms are planned to identify the pathways susceptible to hyper-activation of Akt. Nevertheless, we propose that the role of autophagy is in maintaining cellular homeostasis rather than anabolism.[26]

Effects of soluble activin receptor type IIB treatment on muscle stem cells and the extra cellular matrix

Our work identifies novel features of progeroid SC, the resident stem cell population of skeletal muscle.[67] We show that the number of SC is reduced by the *Ercc1* mutation and it renders the cells senescent gauged by their inability to proliferate following single fibre isolation. They were able to become activated, judged by their expression of MyoD (data not shown), and differentiate but did not demonstrate the normal self-renewal/terminal differentiation physiognomies following 72 h of culture,[68] features shared by counterparts from geriatric wild-type mice.[35] Our results are consistent with the findings of Lavasani *et al*. who showed that *Ercc1*$^{\Delta/-}$ mice have attenuated muscle regeneration following cardiotoxin injury.[16] The subsequent experiments reveal features of SC that are plastic with regard to myostatin/activin signalling. First, we show that sActRIIB was unable to influence the number of SC in the muscle of *Ercc1*$^{\Delta/-}$ mutants, which remained abnormally low compared with controls. This is not altogether surprising as the number of SC is established approximately a month after birth in mice.[69] However, sActRIIB treatment supported SC division and normal differentiation. We propose that these outcomes are unlikely to be due to a direct attenuation of myostatin/activin signalling in SC by sActRIIB as previous studies have shown that they express very little, if any, ActRIIB.[70] Rather, we contemplate that sActRIIB-induces change in the *Ercc1*$^{\Delta/-}$ myofibre ECM (shown here by changes in collagen IV expression as well as dystrophin) that influences the behaviour of their SC. This is possibly significant given that recent studies have shown that the behaviour (ability to divide and differentiate) of SC is profoundly influenced by the interaction of collagen molecules and stem cell receptors.[71]

Compression of morbidity by soluble activin receptor type IIB treatment

In this study, we show that antagonism of myostatin/activin signalling in *Ercc1*$^{\Delta/-}$ mice attenuated the development of ageing-related changes not only of muscle but rather also of health overall. Administration of sActRIIB to *Ercc1*$^{\Delta/-}$ mice improved strength, fitness, and locomotor performance, delayed the onset and importantly the severity of several age-related neurological abnormalities, and reduced deterioration of the bones, liver, and kidney.

An issue that needs addressing is how sActRIIB delivers multi-organ protection against ageing. One possibility is that myostatin/activin signalling promotes the age-related changes independently in each organ system examined in this study and that they are attenuated by systemic delivery of sActRIIB. This certainly could be the case for the kidney as we have seen that downstream activation of myostatin/activin pathways, identified through presence of pSmad2/3, in tissue from progeric mice were blocked by sActRIIB. Moreover, numerous studies have shown that activation of TGF-ß signalling, which can result in the Smad2/3 phosphorylation, is able to induce 'podocyte disease

transformation', an atypical form of epithelial mesenchymal transition.[72] However, we were unable to detect significant levels of pSmad2/3 in the liver (concordant with the findings of others[73]), which nevertheless showed signs of being protected from the ageing process by sActRIIB. Therefore, we postulate that sActRIIB may act both directly (e.g. muscle and kidney) or indirect for other organ systems (e.g. the liver). For the indirect actions of sActRIIB, it is possible that the skeletal muscle plays a role promoting the maintenance and homeostasis of other tissues through inter-organ signalling. It is well known that pathology of skeletal muscle leads to failure of other organs. For example, rhabdomyolysis induces acute kidney injury in part by the release of myoglobin.[74] There are also examples where a malfunctioning organ leads to myopathy, which in turn exacerbates the primary lesion. An example has been elegantly assimilated into the 'Muscle Hypothesis' of Chronic Heart Failure.[75] Herein, changes in skeletal muscle structure and function, mediated by a number of factors including tissue hypoxia and inflammation, lead to hyper-responsiveness of the ergoreflex system.[76] This leads to over-activation of the sympathetic nervous system and consequently an increased load on the ventricles.[77] We postulate that severe *Ercc1*$^{\Delta/-}$ muscle wasting results in the release of myokines and/or intracellular molecules, which lead to pathological changes in other organs.[78] Additionally, we speculate that the normalization of aged muscle following treatment with sActRIIB may also impact the ergoreflex system. By protecting the muscle against age-related changes through the action of sActRIIB, we propose a diminution in the release of harmful factors and possibly by changes to afferent activity. Support for our notion for the release of secreted factors comes from an elegant study that demonstrated transplantation of healthy muscle stem cells into a progeroid model led to the secretion of factors, which acted on numerous organs.[16] Nevertheless, it is possible that sActRIIB mediates actions that are independent of skeletal muscle function. Indeed, it was recently reported that the same treatment used in our work attenuated hepatic protein synthesis and splenomegaly in a rodent cachexia model that were independent of changes in muscle phenotype.[79]

We are nevertheless mindful that despite promising results in rodent models, translation of therapies based on myostatin/activin antagonists have been, to date, unsuccessful in delivering intended outcomes and others have been curtained due to safety concerns[80,81] and point to the need to develop a greater understanding of the biological processes controlled by this signalling axis. A possible means of alleviating some of the safety issues associated with myostatin/activin antagonists could be through decreasing their dose but at the same time harnessing the benefits of other agents that promote healthy ageing. One attractive proposition could be to use a combination of myostatin/activin antagonists and the deployment of the angiotensin 1–7 hexapeptide. The latter has been shown to block over active renin-angiotensin signalling, which not only drives muscle dysfunction but also leads to muscle fibrosis.[82,83] A recent study showed that angiotensin 1–7 was able to restore age-related muscle weakness in a rodent model.[84] Both the sActRIIB and angiotensin 1–7 are attractive therapeutic molecules because they could be delivered using existing medical devices such as osmotic mini-pumps.

In conclusion, this dataset highlights a novel mechanism that attenuates age-related tissues changes. Previous findings support the notion that an organism slows ageing by remodelling its cellular activity from growth and proliferation to maintenance and repair.[2,3,85] This can be achieved by attenuating IGF-1 and GH activity, which controls the somatic growth axis[86,87] and by dietary restriction (DR).[88] We have previously shown that DR delays ageing at the organismal level and extends lifespan and health span of *Ercc1*$^{\Delta/-}$ mice.[23] These studies advocate that promoting tissue growth in an ageing model might well be harmful to the organism. However, we show that a mechanism that promoted growth of skeletal muscle also promotes overall health span as evidenced by activity measurements and tissue structure and function. We believe that we can reconcile these apparent discrepancies by examining the defects that underpin the accelerated ageing process in progeroid mice. We have shown that DNA repair deficiency leads to damage that stalls transcription at least in post-mitotic tissues, which cannot dilute DNA damage by replication or repair it by replication-associated repair pathways. As a consequence, the stochastic nature of DNA damage leads to a preferential loss of long transcripts.[23] Furthermore, DR is able to counteract the transcriptional block by reducing the DNA damage load.[23] We propose that, at least in muscle, the transcriptional landscape is unaltered by sActRIIB but that enhanced protein synthesis promoted by sActRIIB can compensate at least in part for the deficit in long transcripts by increasing the number of polypeptides from each mRNA molecule. In this model, the levels of proteins encoded by long genes in *Ercc1*$^{\Delta/-}$ would be increased by either reduced arrest of gene transcription due to diminished DNA damage induction (by mechanisms induced by DR) or increased rate of protein synthesis (by sActRIIB). Future studies again relying on gene expression and proteomic platforms are planned to test this novel hypothesis.

In summary, we believe that attenuating myostatin/activin signalling protects numerous organs including the kidney, bone, liver, and likely nervous system as well as skeletal muscle through a combination of direct and inter-organ signalling processes. Although delaying many aspects of ageing, overall lifespan was not increased by administration of sActRIIB. This implies that a model where attenuation of myostatin/activin signalling does not affect the upper limits of lifespan but rather compresses morbidity, sustaining health until very old ages.[89,90]

Author contributions

K. P., J. H. J. H., W. P. V., and T. B. H. performed conceptualization. K. P, J. H. J. H., and W. P. V. carried out methodology. W. P. V., R. M. C. B., N. v. V., and S. B. performed validation. K. P., W. P. V., K. A., and S. O. carried out formal analysis. K. A., W. P. V., S. O., O. K., M. H., F. S., B. J., R. M., T. M., A. P., O. R., A. M., and H. C.-H. performed investigation. K. P., J. H. J. H., and W. P. V. carried out writing. K. A., S. O., K. P., and W. P. V. performed visualization. K. P., J. H. J. H., and W. P. V. carried out supervision.

Acknowledgements

We thank Y. van Loon, J.J.M. Kouwenberg, K. Smit, Y.M.A. Rijksen, and the animal caretakers for general assistance with mouse experiments. The financial support from the Higher Committee for Education Development in Iraq, Biotechnology and Biological Sciences Research Council, is acknowledged (Grants BB/J016454/1 to H. C. H. and BB/I015787/1 to R. M.); the National Institute of Health (NIH)/National Institute of Ageing (NIA) (PO1 AG017242); European Research Council Advanced Grants DamAge and Dam2Age to J. H. J. H.; the KWO Dutch Cancer Society (5030); the Royal Academy of Arts and Sciences of the Netherlands (academia professorship to J. H. J. H.); the NWO Building Blocks of Life (to W. P. V. and J. H. J. H.); and the ADPS Longevity Research Award (to W. P. V.). T. B. H. was supported by the DFG (CRC1140, CRC 992, HU 1016/8-1); the BMBF (01GM1518C); the European Research Council-ERC (Grant 616891); and the H2020-IMI2 consortium BEAt-DKD. Finally, we thank the anonymous reviewers of our study for their constructive comments that have guided us into improving our manuscript.

Online supplementary material

Additional supporting information may be found online in the Supporting Information section at the end of the article.

Figure S1. Muscle profiling of 16-week old male *Ercc1*$^{\Delta/-}$ mice. (A) Muscle weights and normalized muscle weights to tibia length. (B) EDL and soleus fibre number count. (C) Frequency of centrally located nuclei in the EDL and soleus at 16 weeks. (D-G) Muscle fibre cross sectional area in EDL, soleus and the deep and superficial regions of the TA in relation of MHC isoform expression. (H-J) MHC isoform profile of EDL, deep and superficial regions of the TA. (K) Oxidative fibre number enumeration through histological SDH activity staining of the EDL and soleus. (L) Satellite cell and progeny enumeration on fresh and cultured EDL for 72 h. (M) Quantification of proportion of stem cells (Pax7^{+}/Myogenin^{-}) and differentiated cells (Pax7^{-}/Myogenin^{+}) on EDL fibres after 72 h culture. n = 6 male mice from each cohort for data presented in (A-L). Fibres collected from 3 mice from each cohort and minimum of 25 fibres examined for (M). Students t-test, * $<$ 0.05, ** $<$ 0.01, ***p $<$ 0.001.

Figure S2. (A-B) Body and (C-D) organ weights from male control, untreated and sActRIIB treated Ercc1$^{\Delta/-}$ mice at end of 15 weeks age. One-way ANOVA followed by Bonferronis multiple comparison tests, * $<$ 0.05, ** $<$ 0.01, ***p $<$ 0.001.

Figure S3. Smad2/3 signalling, oxidative fibre number, caspase 3 expression and centrally located nuclei number changes induced by sActRIIB treatment in *Ercc1*$^{\Delta/-}$ soleus without impacting on DNA damage. (A) Immunohistology of pSmad2/3 expression (green) in soleus muscle (yellow arrows). (B) Immunohistology of γH2A.X expression (green) in soleus muscle (yellow arrows). (C) Immunohistology of Caspase 3 expression in EDL and soleus muscle (red arrows). (D) H and E staining for the identification of centrally located nuclei in EDL and soleus muscle (black arrows). Scale for H and E 40 μm. (E) SDH stain in soleus of the three cohorts. Scale for SDH 80 μm. N = 8 male mice from each cohort. One-way ANOVA followed by Bonferronis multiple comparison tests, * $<$ 0.05, ** $<$ 0.01, ***p $<$ 0.001.

Figure S4. Western blotting demonstrating that sActRIIB promotes protein synthesis and autophagy but blunts proteasome protein breakdown in *Ercc1*$^{\Delta/-}$ muscle. Immunoblots and densitometry quantification of (A) pAkt, (B) p4EBPI on Thr37/46 and Ser65, (C) pS6, (D) pFoxO1, (E) pFoxO3a, (F) LC3II/I, and (G) p62. (H) Densitometry quantification of eIF2α. (I-K) qPCR quantification of *Atrogin-1, MuRF1*, *Mul1* expression. (L) Quantification of p62 puncta. (M) Immunohistology of p62 puncta in the EDL muscle (green arrows) (N) Densitometry quantification of total puromycin incorporation (protein synthesis rate). (O) Densitometry quantification protein ubiquitination. n = 5 for all western blots and n = 8 for rest. Non-parametric Kruskal-Wallis test followed by the Dunns multiple comparisons used for (A-H and N-O). One-way ANOVA followed by Bonferronis multiple comparison test used for (I-K). * $<$ 0.05, ** $<$ 0.01, ***p $<$ 0.001.

Figure S5. (A) *Ercc1*$^{\Delta/-}$ kidney showing autophagosome (arrow). (B) Evidence for indirect action of sActRIIB in liver. pSmad2/3 (green) in relation to smooth muscle actin (red) in the three cohorts. Note that pSmad2/3 was very sparse in the three cohorts and when present was located adjacent to smooth muscle (arrow).

Figure S6. (A) μCT was used to locate and visualize the increase in muscle and bone volume in *Ercc1*$^{\Delta/-}$ mice following sActRIIB treatment. Sex specific characterization of (B) body weights, (C) onset of sever tremors and (D) survival in the Dutch cohort. n = 5 for all three cohorts.

Movie S1. Representative film of control, *Ercc1*$^{\Delta/-}$ and sActRIIB treated *Ercc1*$^{\Delta/-}$ mice at 15 weeks of age.

Conflict of interest

The authors declare no competing interests.

Ethical statement

The authors certify that they comply with the ethical guidelines for publishing in the Journal of Cachexia, Sarcopenia and Muscle: update 2017.[24]

References

1. Niccoli T, Partridge L. Ageing as a risk factor for disease. *Curr Biol* 2012;**22**:R741–R752.
2. Niedernhofer LJ, Garinis GA, Raams A, Lalai AS, Robinson AR, Appeldoorn E, et al. A new progeroid syndrome reveals that genotoxic stress suppresses the somatotroph axis. *Nature* 2006;**444**:1038–1043.
3. Garinis GA, Uittenboogaard LM, Stachelscheid H, Fousteri M, Van Ijcken W, Breit TM, et al. Persistent transcription-blocking DNA lesions trigger somatic growth attenuation associated with longevity. *Nat Cell Biol* 2009;**11**:604–615.
4. Hoeijmakers JH. DNA damage, aging, and cancer. *N Engl J Med* 2009;**361**:1475–1485.
5. Milman S, Huffman DM, Barzilai N. The somatotropic axis in human aging: framework for the current state of knowledge and future research. *Cell Metab* 2016;**23**:980–989.
6. van der Pluijm I, Garinis GA, Brandt RM, Gorgels TGF, Wijnhoven SW, Diderich KE, et al. Impaired genome maintenance suppresses the growth hormone--insulin-like growth factor 1 axis in mice with Cockayne syndrome. *PLoS Biol* 2007;**5**:e2.
7. Rosenberg IH. Sarcopenia: origins and clinical relevance. *J Nutr* 1997;**127**:990S–991S.
8. Nair KS. Aging muscle. *Am J Clin Nutr* 2005;**81**:953–963.
9. Keller K, Engelhardt M. Strength and muscle mass loss with aging process. Age and strength loss. *Muscles Ligaments Tendons J* 2013;**3**:346–350.
10. Srikanthan P, Karlamangla AS. Muscle mass index as a predictor of longevity in older adults. *Am J Med* 2014;**127**:547–553.
11. Kim JH, Cho JJ, Park YS. Relationship between sarcopenic obesity and cardiovascular disease risk as estimated by the Framingham risk score. *J Korean Med Sci* 2015;**30**:264–271.
12. Matsakas A, Patel K. Intracellular signalling pathways regulating the adaptation of skeletal muscle to exercise and nutritional changes. *Histol Histopathol* 2009;**24**:209–222.
13. Velloso CP. Regulation of muscle mass by growth hormone and IGF-I. *Br J Pharmacol* 2008;**154**:557–568.
14. Lach-Trifilieff E, Minetti GC, Sheppard K, Ibebunjo C, Feige JN, Hartmann S, et al. An antibody blocking activin type II receptors induces strong skeletal muscle hypertrophy and protects from atrophy. *Mol Cell Biol* 2014;**34**:606–618.
15. Relizani K, Mouisel E, Giannesini B, Hourdé C, Patel K, Gonzalez SM, et al. Blockade of ActRIIB signaling triggers muscle fatigability and metabolic myopathy. *Mol Ther* 2014;**22**:1423–1433.
16. Lavasani M, Robinson AR, Lu A, Song M, Feduska JM, Ahani B, et al. Muscle-derived stem/progenitor cell dysfunction limits healthspan and lifespan in a murine progeria model. *Nat Commun* 2012;**3**:608.
17. Deutz NE, Bauer JM, Barazzoni R, Biolo G, Boirie Y, Bosy-Westphal A, et al. Protein intake and exercise for optimal muscle function with aging: recommendations from the ESPEN Expert Group. *Clin Nutr* 2014;**33**:929–936.
18. Sijbers AM, de Laat WL, Ariza RR, Biggerstaff M, Wei YF, Moggs JG, et al. Xeroderma pigmentosum group F caused by a defect in a structure-specific DNA repair endonuclease. *Cell* 1996;**86**:811–822.
19. Kashiyama K, Nakazawa Y, Pilz DT, Guo C, Shimada M, Sasaki K, et al. Malfunction of nuclease ERCC1-XPF results in diverse clinical manifestations and causes Cockayne syndrome, xeroderma pigmentosum, and Fanconi anemia. *Am J Hum Genet* 2013;**92**:807–819.
20. Dolle ME, Kuiper RV, Roodbergen M, Robinson J, de Vlugt S, Wijnhoven SW, et al. Broad segmental progeroid changes in short-lived Ercc1(−/Delta7) mice. *Pathobiol Aging Age Relat Dis* 2011;**1**.
21. Gregg SQ, Gutiérrez V, Robinson AR, Woodell T, Nakao A, Ross MA, et al. A mouse model of accelerated liver aging caused by a defect in DNA repair. *Hepatology* 2012;**55**:609–621.
22. Vermeij WP, Hoeijmakers JH, Pothof J. Genome integrity in aging: human syndromes, mouse models, and therapeutic options. *Annu Rev Pharmacol Toxicol* 2016;**56**:427–445.
23. Vermeij WP, Dollé MT, Reiling E, Jaarsma D, Payan-Gomez C, Bombardieri CR, et al. Restricted diet delays accelerated ageing and genomic stress in DNA-repair-deficient mice. *Nature* 2016;**537**:427–431.
24. von Haehling S, Morley JE, Coats AJ, Anker SD. Ethical guidelines for publishing in the journal of cachexia, sarcopenia and muscle: update 2017. *J Cachexia Sarcopenia Muscle* 2017;**8**:1081–1083.
25. Weeda G, Donker I, de Wit J, Morreau H, Janssens R, Vissers CJ, et al. Disruption of mouse ERCC1 results in a novel repair syndrome with growth failure, nuclear abnormalities and senescence. *Curr Biol* 1997;**7**:427–439.
26. Omairi S, Matsakas A, Degens H, Kretz O, Hansson KA, Solbrå AV, et al. Enhanced exercise and regenerative capacity in a mouse model that violates size constraints of oxidative muscle fibres. *Elife* 2016;**5**.
27. Schmidt EK, Clavarino G, Ceppi M, Pierre P. SUnSET, a nonradioactive method to monitor protein synthesis. *Nat Methods* 2009;**6**:275–277.
28. Matsakas A, Macharia R, Otto A, Elashry MI, Mouisel E, Romanello V, et al. Exercise training attenuates the hypermuscular phenotype and restores skeletal muscle function in the myostatin null mouse. *Exp Physiol* 2012;**97**:125–140.
29. Otto A, Schmidt C, Luke G, Allen S, Valasek P, Muntoni F, et al. Canonical Wnt signalling induces satellite-cell proliferation during adult skeletal muscle regeneration. *J Cell Sci* 2008;**121**:2939–2950.
30. Cheema N, Herbst A, McKenzie D, Aiken JM. Apoptosis and necrosis mediate skeletal muscle fiber loss in age-induced mitochondrial enzymatic abnormalities. *Aging Cell* 2015;**14**:1085–1093.
31. Bindokas VP, Jordan J, Lee CC, Miller RJ. Superoxide production in rat hippocampal neurons: selective imaging with hydroethidine. *J Neurosci* 1996;**16**:1324–1336.
32. Li N, Ragheb K, Lawler G, Sturgis J, Rajwa B, Melendez JA, et al. Mitochondrial complex I inhibitor rotenone induces apoptosis through enhancing mitochondrial reactive oxygen species production. *J Biol Chem* 2003;**278**:8516–8525.
33. Frank S, Gaume B, Bergmann-Leitner ES, Leitner WW, Robert EG, Catez F, et al. The role of dynamin-related protein 1, a mediator of mitochondrial fission, in apoptosis. *Dev Cell* 2001;**1**:515–525.
34. Terman A, Brunk UT. Myocyte aging and mitochondrial turnover. *Exp Gerontol* 2004;**39**:701–705.
35. Garcia-Prat L, Martínez-Vicente M, Perdiguero E, Ortet L, Rodríguez-Ubreva J, Rebollo E, et al. Autophagy maintains stemness by preventing senescence. *Nature* 2016;**529**:37–42.
36. Merkwirth C, Langer T. Prohibitin function within mitochondria: essential roles for cell proliferation and cristae morphogenesis. *Biochim Biophys Acta* 2009;**1793**:27–32.
37. Benayoun BA, Pollina EA, Brunet A. Epigenetic regulation of ageing: linking

environmental inputs to genomic stability. *Nat Rev Mol Cell Biol* 2015;**16**:593–610.
38. Liu B, Wang Z, Zhang L, Ghosh S, Zheng H, Zhou Z. Depleting the methyltransferase Suv39h1 improves DNA repair and extends lifespan in a progeria mouse model. *Nat Commun* 2013;**4**:1868.
39. Ocampo A, Reddy P, Martinez-Redondo P, Platero-Luengo A, Hatanaka F, Hishida T, et al. In vivo amelioration of age-associated hallmarks by partial reprogramming. *Cell* 2016;**167**:1719–1733, e12.
40. Rojansky R, Cha MY, Chan DC. Elimination of paternal mitochondria in mouse embryos occurs through autophagic degradation dependent on PARKIN and MUL1. *Elife* 2016;**5**.
41. Abbey CK, Borowsky AD, McGoldrick ET, Gregg JP, Maglione JE, Cardiff RD, et al. In vivo positron-emission tomography imaging of progression and transformation in a mouse model of mammary neoplasia. *Proc Natl Acad Sci U S A* 2004;**101**:11438–11443.
42. Wynne HA, Cope LH, Mutch E, Rawlins MD, Woodhouse KW, James OF. The effect of age upon liver volume and apparent liver blood flow in healthy man. *Hepatology* 1989;**9**:297–301.
43. Popper H. Aging and the liver. *Prog Liver Dis* 1986;**8**:659–683.
44. McWhir J, Selfridge J, Harrison DJ, Squires S, Melton DW. Mice with DNA repair gene (ERCC-1) deficiency have elevated levels of p53, liver nuclear abnormalities and die before weaning. *Nat Genet* 1993;**5**:217–224.
45. Serste T, Bourgeois N. Ageing and the liver. *Acta Gastroenterol Belg* 2006;**69**:296–298.
46. Petersen KF, Befroy D, Dufour S, Dziura J, Ariyan C, Rothman DL, et al. Mitochondrial dysfunction in the elderly: possible role in insulin resistance. *Science* 2003;**300**: 1140–1142.
47. Rogers MA, Evans WJ. Changes in skeletal muscle with aging: effects of exercise training. *Exerc Sport Sci Rev* 1993;**21**:65–102.
48. Evans W. Functional and metabolic consequences of sarcopenia. *J Nutr* 1997;**127**: 998S–1003S.
49. Larsson L, Biral D, Campione M, Schiaffino S. An age-related type IIB to IIX myosin heavy chain switching in rat skeletal muscle. *Acta Physiol Scand* 1993;**147**:227–234.
50. Holloszy JO, Chen M, Cartee GD, Young JC. Skeletal muscle atrophy in old rats: differential changes in the three fiber types. *Mech Ageing Dev* 1991;**60**: 199–213.
51. Faber RM, Hall JK, Chamberlain JS, Banks GB. Myofiber branching rather than myofiber hyperplasia contributes to muscle hypertrophy in mdx mice. *Skelet Muscle* 2014;**4**:10.
52. Powers SK, Wiggs MP, Duarte JA, Zergeroglu AM, Demirel HA. Mitochondrial signaling contributes to disuse muscle atrophy. *Am J Physiol Endocrinol Metab* 2012;**303**:E31–E39.
53. Diaz G, Liu S, Isola R, Diana A, Falchi AM. Mitochondrial localization of reactive oxygen species by dihydrofluorescein probes. *Histochem Cell Biol* 2003;**120**:319–325.
54. Sandri M, Sandri C, Gilbert A, Skurk C, Calabria E, Picard A, et al. Foxo transcription factors induce the atrophy-related ubiquitin ligase atrogin-1 and cause skeletal muscle atrophy. *Cell* 2004;**117**:399–412.
55. Sandri M. Protein breakdown in muscle wasting: role of autophagy-lysosome and ubiquitin-proteasome. *Int J Biochem Cell Biol* 2013;**45**:2121–2129.
56. Bonaldo P, Sandri M. Cellular and molecular mechanisms of muscle atrophy. *Dis Model Mech* 2013;**6**:25–39.
57. Brzeszczynska J, Meyer A, McGregor R, Schilb A, Degen S, Tadini V, et al. Alterations in the in vitro and in vivo regulation of muscle regeneration in healthy ageing and the influence of sarcopenia. *J Cachexia Sarcopenia Muscle* 2018;**9**:93–105.
58. Amthor H, Macharia R, Navarrete R, Schuelke M, Brown SC, Otto A, et al. Lack of myostatin results in excessive muscle growth but impaired force generation. *Proc Natl Acad Sci U S A* 2007;**104**:1835–1840.
59. Collins-Hooper H, Sartori R, Macharia R, Visanuvimol K, Foster K, Matsakas A, et al. Propeptide-mediated inhibition of myostatin increases muscle mass through inhibiting proteolytic pathways in aged mice. *J Gerontol A Biol Sci Med Sci* 2014;**69**:1049–1059.
60. Nishio ML, Madapallimattam AG, Jeejeebhoy KN. Comparison of six methods for force normalization in muscles from malnourished rats. *Med Sci Sports Exerc* 1992;**24**:259–264.
61. Schwaller B, Dick J, Dhoot G, Carroll S, Vrbova G, Nicotera P, et al. Prolonged contraction-relaxation cycle of fast-twitch muscles in parvalbumin knockout mice. *Am J Physiol* 1999;**276**:C395–C403.
62. Haynes CM, Ron D. The mitochondrial UPR—protecting organelle protein homeostasis. *J Cell Sci* 2010;**123**:3849–3855.
63. Andersson DC, Betzenhauser MJ, Reiken S, Meli AC, Umanskaya A, Xie W, et al. Ryanodine receptor oxidation causes intracellular calcium leak and muscle weakness in aging. *Cell Metab* 2011;**14**:196–207.
64. Chen Y, Wei H, Liu F, Guan JL. Hyperactivation of mammalian target of rapamycin complex 1 (mTORC1) promotes breast cancer progression through enhancing glucose starvation-induced autophagy and Akt signaling. *J Biol Chem* 2014;**289**: 1164–1173.
65. McCubrey JA, Steelman LS, Chappell WH, Abrams SL, Wong EW, Chang F, et al. Roles of the Raf/MEK/ERK pathway in cell growth, malignant transformation and drug resistance. *Biochim Biophys Acta* 2007;**1773**:1263–1284.
66. Steelman LS, Chappell WH, Abrams SL, Kempf CR, Long J, Laidler P, et al. Roles of the Raf/MEK/ERK and PI3K/PTEN/Akt/mTOR pathways in controlling growth and sensitivity to therapy-implications for cancer and aging. *Aging (Albany NY)* 2011;**3**:192–222.
67. Mauro A. Satellite cell of skeletal muscle fibers. *J Biophys Biochem Cytol* 1961;**9**: 493–495.
68. Zammit PS, Relaix F, Nagata Y, Ruiz AP, Collins CA, Partridge TA, et al. Pax7 and myogenic progression in skeletal muscle satellite cells. *J Cell Sci* 2006;**119**: 1824–1832.
69. Lepper C, Conway SJ, Fan CM. Adult satellite cells and embryonic muscle progenitors have distinct genetic requirements. *Nature* 2009;**460**:627–631.
70. Amthor H, Otto A, Vulin A, Rochat A, Dumonceaux J, Garcia L, et al. Muscle hypertrophy driven by myostatin blockade does not require stem/precursor-cell activity. *Proc Natl Acad Sci U S A* 2009;**106**:7479–7484.
71. Baghdadi MB, Castel D, Machado L, Fukada SI, Birk DE, Relaix F, et al. Reciprocal signalling by Notch-Collagen V-CALCR retains muscle stem cells in their niche. *Nature* 2018;**557**:714–718.
72. May CJ, Saleem M, Welsh GI. Podocyte dedifferentiation: a specialized process for a specialized cell. *Front Endocrinol (Lausanne)* 2014;**5**:148.
73. Perez Aguilar RC, Honoré SM, Genta SB, Sánchez SS. Hepatic fibrogenesis and transforming growth factor/Smad signaling activation in rats chronically exposed to low doses of lead. *J Appl Toxicol* 2014;**34**:1320–1331.
74. Panizo N, Rubio-Navarro A, Amaro-Villalobos JM, Egido J, Moreno JA. Molecular mechanisms and novel therapeutic approaches to rhabdomyolysis-induced acute kidney injury. *Kidney Blood Press Res* 2015;**40**:520–532.
75. Coats AJ. The 'muscle hypothesis' of chronic heart failure. *J Mol Cell Cardiol* 1996;**28**:2255–2262.
76. Piepoli MF, Kaczmarek A, Francis DP, Davies LC, Rauchhaus M, Jankowska EA, et al. Reduced peripheral skeletal muscle mass and abnormal reflex physiology in chronic heart failure. *Circulation* 2006;**114**:126–134.
77. Belli JF, Bacal F, Bocchi EA, Guimarães GV. Ergoreflex activity in heart failure. *Arq Bras Cardiol* 2011;**97**:171–178.
78. Pedersen BK, Febbraio MA. Muscles, exercise and obesity: skeletal muscle as a secretory organ. *Nat Rev Endocrinol* 2012;**8**:457–465.
79. Nissinen TA, Hentilä J, Penna F, Lampinen A, Lautaoja JH, Fachada V, et al. Treating cachexia using soluble ACVR2B improves survival, alters mTOR localization, and attenuates liver and spleen responses. *J Cachexia Sarcopenia Muscle* 2018;**9**:514–529.
80. Golan T, Geva R, Richards D, Madhusudan S, Lin BK, Wang HT, et al. LY2495655, an antimyostatin antibody, in pancreatic cancer: a randomized, phase 2 trial. *J Cachexia Sarcopenia Muscle* 2018;**9**:871–879.
81. Saitoh M, Ishida J, Ebner N, Anker SD, Springer J, von Haehling S. Myostatin inhibitors as pharmacological treatment for muscle wasting and muscular dystrophy. *J Cachexia, Sarcopenia Muscle - Clinic Rep* 2017;**2**:10.
82. Meneses C, Morales MG, Abrigo J, Simon F, Brandan E, Cabello-Verrugio C. The angiotensin-(1-7)/Mas axis reduces

myonuclear apoptosis during recovery from angiotensin II-induced skeletal muscle atrophy in mice. *Pflugers Arch* 2015;**467**:1975–1984.
83. Morales MG, Cabrera D, Céspedes C, Vio CP, Vazquez Y, Brandan E, et al. Inhibition of the angiotensin-converting enzyme decreases skeletal muscle fibrosis in dystrophic mice by a diminution in the expression and activity of connective tissue growth factor (CTGF/CCN-2). *Cell Tissue Res* 2013;**353**:173–187.
84. Takeshita H, Yamamoto K, Nozato S, Takeda M, Fukada SI, Inagaki T, et al. Angiotensin-converting enzyme 2 deficiency accelerates and angiotensin 1-7 restores age-related muscle weakness in mice. *J Cachexia Sarcopenia Muscle* 2018;**9**:975–986.
85. Pinkston JM, Garigan D, Hansen M, Kenyon C. Mutations that increase the life span of C. elegans inhibit tumor growth. *Science* 2006;**313**:971–975.
86. Hinkal G, Donehower LA. How does suppression of IGF-1 signaling by DNA damage affect aging and longevity? *Mech Ageing Dev* 2008;**129**:243–253.
87. Guarente L, Kenyon C. Genetic pathways that regulate ageing in model organisms. *Nature* 2000;**408**:255–262.
88. Fontana L, Partridge L, Longo VD. Extending healthy life span—from yeast to humans. *Science* 2010;**328**:321–326.
89. Fries JF. Aging, natural death, and the compression of morbidity. *N Engl J Med* 1980;**303**:130–135.
90. Dong X, Milholland B, Vijg J. Evidence for a limit to human lifespan. *Nature* 2016;**538**:257–259.